NASA Contractor Report 182288

Oscillating Flow Loss Test Results in Stirling Engine Heat Exchangers

(NASA-CR-182288) OSCILLATING FLOW LOSS TEST RESULTS IN STIRLING ENGINE HEAT EXCHANGERS Final Report (Sunpower) 296 p CSCL 10B N92-24241

306p 515420 Unclas G3/20 0085743

G. Koester, S. Howell, G. Wood, E. Miller

Sunpower, Inc.
Athens, Ohio

and

D. Gedeon

Gedeon Associates
Athens, Ohio

May 1990

Prepared for
Lewis Research Center
Under Contract NAS3-24879

Date for general release May 1992

National Aeronautics and
Space Administration

ERRATA

NASA Contractor Report 182288

OSCILLATING FLOW LOSS TEST RESULTS IN STIRLING ENGINE HEAT EXCHANGERS

by

G. Koester, S. Howell, G. Wood, E. Miller - Sunpower, Inc.
and
D. Gedeon - Gedeon Associates

May 1990

1. All values of the Tidal Amplitude, A_r, as tabulated in Appendix B and plotted in Section 6 should be multiplied by a factor of 2. This will make these values agree with the equation defining A_r given in the Nomenclature and repeated several other places in the report.

Please also note the effect of this change in the A_r values on the discussions of Sections 7 and 8.

2. The denominator of equations 2.3-9 and 6.2-4 (both are equations for TDF) should read:

$$\int ((fL/D_h + K_t)\ g\ |u|)\ u$$

3. The applicable range for equation 6.1-6 should be Re < 2000.

TABLE OF CONTENTS

NOMENCLATURE

A	Surface area
A_c	Test sample frontal flow area
A_f	Frontal area
$A_r = \dfrac{D_h Re_{max}}{2L Re_\omega}$	Tidal Amplitude
C_p, C_v	Gas specific heats
D	Tube inside diameter
D_h	Test sample hydraulic diameter
D_w, d_w	Regenerator wire diameter
f	Fanning friction factor
fi, fr	General linearized friction factors
E	Fluid energy in piston cylinder
$Eu = \dfrac{2\Delta P_{max}}{\rho (u_{max})^2}$	Euler number
F	Spacial-mean core frictional gradient (Force per unit volume due to wall shear stress)
$g = pu$	Mass flow rate per unit area
h	Film heat transfer coeficient
K_t	Total entrance/exit loss coefficient
L	Length of test sample
L/D	Nondimensional tube length
M	Fluid mass in piston cylinder
$\dot{M}$	Fluid mass flow rate
P	Pressure
P_o	Reference Pressure
P_{ratio}	Measured/Predicted pressure drop
ΔP	Static pressure drop
$\Delta P_{\max}$	Maximum measured pressure drop
Q	Gas-wall heat flux in piston cylinder
R	Gas constant
Re	Reynolds number
$Re_{max} = \dfrac{\rho u_{max} D_h}{\mu}$	Peak Reynolds number
$Re_\omega = \dfrac{\rho \omega D_h^2}{4\mu}$	Kinetic Reynolds number
t	Time coordinate
T	Temperature

T_o	Ambient temperature
T_f	Temperature of fluid at cylinder entrance
TDF	Total dissipation factor
u	Velocity
u_m	Amplitude of the section-average velocity
u_{max}	Max velocity amplitude (of first harmonic if non-sinusoidal) based on actual flow area
V	Piston cylinder volume
$\hat{V} = u_{max} \frac{A_c}{A_f}$	Approach velocity in regenerators
x	Axial coordinate
x_{max}	Maximum piston amplitude

Greek

ε	Porosity
δ	Tidal Amplitude
μ	Viscosity
ω	Angular frequency
ρ	Fluid density
σ	Test sample/cylinder area ratio

Operators

Hm	Harmonic operator: Hm(f) = first harmonic in f Fourier series
RSS	Root sum squared
	Time derivative: f = df/dt
$< >$	Spatial-average: $< f > = 1/L \int f \, dx$
~	Error component: f = standard deviation of f considered as a random variable

Section 1

1.0 INTRODUCTION

Very little information is available concerning fluid flow under oscillating conditions such as those which exist in the heat exchangers of Stirling engines. A thorough review of the available information on this topic has been performed by Seume and Simon (1) at the University of Minnesota. The purpose of the program presented in this report is to generate a database of pressure drop information applicable to the operating ranges of a large group of Stirling engines. This work was done under a NASA Phase II SBIR (Small Business Innovative Research) contract.

Analytical solutions for oscillating flow pressure drops exist only for laminar oscillating flow, and these solutions neglect entrance and exit effects. The flow in the heat exchangers of Stirling engines, however, is most often turbulent oscillating flow, and is, of course, subject to entrance and exit effects. Therefore, experimental information is needed which could be applied to the design and optimization of Stirling engines. At present, this experimental information is largely nonexistent.

These kinds of pressure drop measurements are rather difficult to perform in running engines. This is due in part to the high temperatures that exist in some of the spaces where measurements need to be made. Most of the difficulty, however, arises from the use of differential pressure transducers which rely on connecting tubes to sense the pressure differentials. These connecting tubes and the associated volumes at the connections to the transducer are subject to resonance effects and must be carefully designed to avoid erroneous measurements.

Even if this measurement is done correctly in a running engine, the results obtained are only applicable to the heat exchanger configurations which exist in the engine. The flow regimes over which the given piece of hardware can be operated are also usually quite restricted. For these reasons, the information which can be obtained from running engines is limited.

The lack of knowledge concerning oscillating flow pressure drops is more important to the design and operation of a free-piston Stirling engine (FPSE) than for a kinematic (mechanically constrained motion) engine. In kinematic engines, pressure drops generally influence only power output. In FPSEs, however, these effects also influence the motions of the moving components since these parts are not connected to a mechanical linkage. The result is that in FPSEs these pressure drop effects can have a magnified impact on engine performance. A better understanding of oscillating flow pressure drop is needed to design more efficient and higher specific power engines. A review of the need for this information, as well as for information on the other losses in Stirling engines, is presented by Tew (2).

The intended purpose of this test program was to generate a database of pressure drop information for a large group of different sample types and configurations and to do this over a wide range of flow parameters. The analytical tools used to formulate this problem are described in Section 2. The test rig and the test procedures are described in Section 3 with a description of the data acquisition system given in Section 4. The test matrix is given in Section 5 and the test results are presented and discussed in Sections 6 and 7, respectively. Finally, the conclusions and recommendations are presented in Section 8.

The primary test data and calculations are presented in tabular form in Appendix B. The detailed test data are also available on computer disk; these computer disks are described in Appendix D. The computer disks may be obtained from the Stirling Technology Branch of NASA Lewis.

Section 2

2.0 THEORY

The theory governing the analysis of the oscillating flow test results is presented in this section. A detailed presentation of the theory behind the pressure drop analysis and error analysis is found in Appendices A and C.

2.1 THE MOMENTUM EQUATION

The Momentum Equation, which is the basis for the data reduction model, is given in Equation (2.1-1).

$$P - P_0 = \left(F - \frac{\partial g}{\partial t}\right)L - \frac{1}{2}\left(gu\sigma^2 + g\,|u|\,K_t\right) \qquad (2.1\text{-}1)$$

where

P	=	Pressure at cylinder end of sample
P_0	=	Reference pressure at other end of sample
F	=	Spatial-mean core frictional pressure gradient (Force per unit volume due to surface shear stress)
g	=	Representative mass flow rate per unit area
u	=	Representative fluid velocity
t	=	Time
L	=	Sample length
σ	=	Sample/cylinder area ratio
K_t	=	Combined entrance-exit loss coefficient

An exact solution of the Momentum Equation in the case of incompressible laminar sinusoidal parallel flow between flat plates (3) gives us a solution for F. That is, F can be expressed as

$$-F = f_i \left(\frac{u_m}{2\omega D_h}\right)\frac{\partial g}{\partial t} + f_r \left(\frac{u_m}{2D_h}\right) g \tag{2.1-2}$$

In Equation (2.1-2), f_r and f_i are the real and imaginary parts of a constant dimensionless complex friction factor, u_m is the amplitude of the section-average velocity, D_h is hydraulic diameter, and ω is angular frequency. Everything is constant on the right side of the equation except g which is a sinusoidal function of time. The component of wall stress in phase with the velocity is determined by f_r while the component 90 degrees out of phase is determined by f_i. One can show that the second term on the right of Equation (2.1-2) is responsible for energy dissipation while the first term is nondissipative – merely tending to enhance the apparent density of the fluid. For low frequency oscillation, f_i approaches zero while f_r reduces to the ordinary Darcy friction factor for laminar flow evaluated at u_m. In this analysis, both f_r and f_i are functions of the kinetic Reynolds number (or dimensionless frequency) Re_ω, defined by

$$Re_\omega = \frac{\rho \omega D_h^2}{4\mu} \tag{2.1-3}$$

For parallel flows between flat plates (3), both f_i and f_r begin to differ from the steady flow case as Re_ω increases above about 10. For large Re_ω (above about 100), f_i and f_r approach each other in magnitude and are both proportional to $Re_\omega^{0.5}$.

Equation (2.1-2) can possibly serve as a model for the more general case of compressible, turbulent nonsinusoidal oscillating flow.

2.2 ENERGY EQUATION / MASS FLOW EQUATION

The following analysis applies to the case where the test fluid is compressible, that is a gas. The incompressible case is trivial since then density is constant and the volumetric flow rate in the sample is the same as that in the piston cylinder.

The bulk parameter gas Energy Equation for the piston cylinder volume V in Figure 2.2-1 may be written

$$\dot{E} = -P\dot{V} + C_p T_f \dot{M} + Q \tag{2.2-1}$$

where P is pressure, C_p is the specific heat, T_f is the temperature of the fluid at the cylinder entrance, M is the fluid mass, and Q is the gas-wall heat flux in the piston cylinder. E is the internal energy of the assumed ideal gas given by

$$E = C_v MT = (C_v/R)\, PV \tag{2.2-2}$$

Assume heat flux Q is given by

$$Q = hA(T_0 - T) \tag{2.2-3}$$

where h is a film heat transfer coefficient and A is the cylinder surface area. T_0 is a sort of ambient temperature, representing the temperature of sample and cylinder walls as well as that of the surrounding gas in the pressure vessel. The fluid temperature T_f is not measured. Instead, assume it is given by

$$T_f = \begin{matrix} T_0 \text{ for } \dot{M} \geq 0 \\ T \text{ for } \dot{M} < 0 \end{matrix} \tag{2.2-4}$$

See Figure 2.2-1 for definition of the sign conventions for $\dot{M}$ and Q.

After differentiating Equation (2.2-2), substituting into Equation (2.2-1) for $\dot{E}$ and simplifying, the mass flow rate ($\dot{M} = dM/dt$) works out to

$$\dot{M} = \frac{PV}{RT_f}\left[\frac{\dot{V}}{V} + C_v/C_p \frac{\dot{P}}{P} - R/C_p \frac{Q}{PV}\right] \tag{2.2-5}$$

Unfortunately, Equation (2.2-5) cannot be used directly to find $\dot{M}$ since temperature T is not a measured variable and, therefore, Q and T_f are not known in advance. However, it is possible to numerically solve Equation (2.2-5) as a differential equation. *M(t)* is then uniquely determined under the boundary conditions that the solution is periodic, and outside temperature T_0 and pressure P_0 are known. The detailed calculations are described in Appendix A.

2.3 DETERMINATION OF FRICTIONAL PRESSURE DROP

The fluid Momentum Equation is examined to see how one determines the frictional pressure gradient from the total pressure drop across the sample.

For purposes of argument, define four pressures P_0 through P_3, located as shown in Figure 2.3-1. P_3 is the one that is experimentally measured and varies roughly sinusoidally while P_0 is constant. P_1 and P_2 are the pressures just inside either end of the sample after correcting for entrance and exit effects. That is, assume that P_1 - P_0 and P_3 - P_2 are determined by entrance and exit effects while P_2 - P_1 is determined by core friction and acceleration terms according to the Momentum Equation (2.1-1). In reality, entrance and exit effects cannot be separated from core friction so neatly, but the present model makes the analysis tractable. Also, subscripts 0 to 3 are used on other variables, such as u and g to denote values at the locations shown on Figure 2.3-1.

$\underline{P_3 - P_2}$

Bernoulli's law applies to flow in regions such as tube entrances where there is an abrupt change in area. This can be used for oscillating flow, also. Bernoulli's law is

$$\Delta\left(u^2/2\right) = -\int dP/\rho \tag{2.3-1}$$

Assuming density does not change much in the region 2 to 3, Equation (2.3-1) integrates to

$$P_3 - P_2 \approx \frac{1}{2} g_2 u_2 \left(1 - \sigma^2\right) \tag{2.3-2}$$

where

$$\sigma = u_3/u_2 \approx A_2/A_3 \tag{2.3-3}$$

A_2 is the sample flow area and A_3 is the cylinder cross-section area. Adding an entrance and exit loss coefficient K_2 gives

$$P_3 - P_2 \approx \frac{1}{2}\, g_2 u_2 \left(1 - \sigma^2\right) - \frac{1}{2} g_2 \left| u_2 \right| K_2 \tag{2.3-4}$$

Note that even if g and u are sinusoidal, $P_3 - P_2$ will not be. It will have a second harmonic due to the first term on the right of Equation (2.3-4) and a third harmonic due to the second term.

$\underline{P_1 - P_0}$

Bernoulli's law applies in the region 0 - 1 as well. Assume the velocity in region 0 is zero and introduce a loss coefficient K_1 so that

$$P_1 - P_0 \approx -\frac{1}{2} g_1 u_1 - \frac{1}{2} g_1 \left| u_1 \right| K_1 \tag{2.3-5}$$

$\underline{P_2 - P_1}$

Momentum Equation (2.1-1) can be applied in the region 1 - 2 to give

$$P_2 - P_1 = L < F > - L \frac{\partial}{\partial t} <g> + g_1 u_1 - g_2 u_2 \tag{2.3-6}$$

where L is the sample length and $< >$ denotes the sample spatial average.

Total Pressure Drop

Adding Equations (2.3-4), (2.3-5), and (2.3-6) gives an expression for the instantaneous total pressure drop which is measured in the rig tests

$$\begin{aligned} P_3 - P_0 \approx \frac{1}{2} g_2 u_2 \left(-\sigma^2 - 1\right) + \frac{1}{2} g_1 u_1 - L \frac{\partial}{\partial t} < g > + L<F> \\ - \frac{1}{2} g_2 \left| u_2 \right| K_2 - \frac{1}{2} g_1 \left| u_1 \right| K_1 \end{aligned} \tag{2.3-7}$$

Solving for F

We want to use Equation (2.3-7) to correlate $< F >$ and $< g >$. This is reasonably straightforward if F and g are relatively uniform along the sample at any instant of time. That is, assume that the only valid experiment is one where g and u are fairly uniform within the entire sample and approximately equal to their values at the cylinder inlet. These values are, of course, readily obtained from the solution of the $M(t)$ differential equation discussed previously. The errors caused by this assumption are discussed in Appendices A and C. Replacing g_1 and g_2 in Equation (2.3-7) with g, and replacing u_1 and u_2 with u, and then solving for F gives an equation which is useful for isolating the frictional pressure gradient in an experimental data point.

$$F \approx \frac{1}{L}\left(P_3 - P_0\right) + \frac{\sigma^2}{2L} gu + \frac{K_t}{2L} g \left| u \right| + \frac{\partial g}{\partial t} \qquad (2.3\text{-}8)$$

In Equation (2.3-8), K_1 and K_2 have been combined into an overall entrance/exit loss coefficient K_t. The $< >$ notation around F was dropped with the understanding that the value of F on the left is a mean effective value for the entire sample.

Determining f_i and f_r

Equation (2.3-8) yields F as a function of time over the cycle and, as such, cannot be used directly in a Stirling computer simulation. It was desired to determine the oscillating flow friction factor coefficients f_i and f_r for each data point. The approach was to assume a solution of the form of Equation (2.1-2), then use the first harmonics of g, u, and F to solve for f_i and f_r. Then f_i and f_r would be correlated with Re_ω, Re_{max}, and other appropriate dimensionless groups and, thus, could be used in a Stirling simulation. In reality, two problems prevented the resolution of the test data into f_i and f_r. The first was difficulty in determining proper values of entrance and exit coefficients. The second was the presence of higher harmonics on g, u, and F which made the use of only the first harmonic invalid.

Use of the Total Dissipation Factor (TDF)

It was decided that the oscillating test results would be presented in the form of a coefficient or a factor that could be applied to an integrated steady flow analysis to determine the oscillating flow losses. In the oscillating flow data reduction process, this factor is defined as the Total Dissipation Factor (TDF). It is defined as the ratio of pumping dissipation produced by the total measured pressure drop ΔP in oscillating flow to that calculated by using the cycle-integrated steady flow pressure drop determined with steady flow friction factors and entrance/exit loss coefficients. Hence,

$$\mathrm{TDF} = \frac{2\int \Delta P u}{\int\left(\left(f\frac{L}{D_h}K_t\right)g \mid u \mid \right)u} \tag{2.3-9}$$

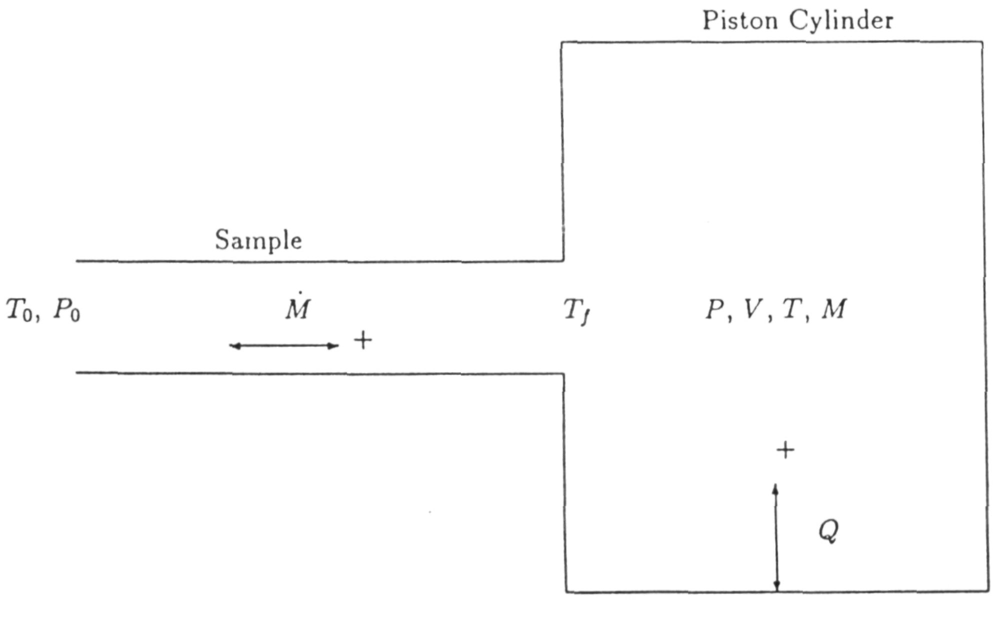

FIGURE 2.2-1 Bulk-Parameter Rig Model

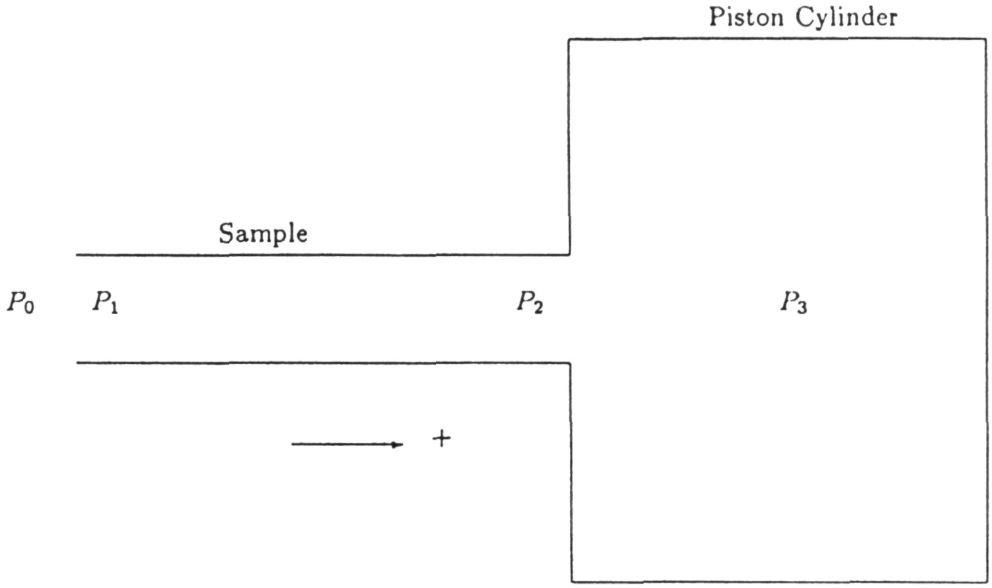

FIGURE 2.3-1 Four Key Pressure Points in the Test Rig

Section 3

3.0 DESCRIPTION OF THE TEST RIGS

This section describes the oscillating and steady flow loss test rigs, their design methodology, and their operational details. The intended purpose of these rigs is to generate a database of pressure drop information for a large group of different sample configurations and to do this over a wide range of flow parameters.

3.1 OSCILLATING FLOW LOSS TEST RIG

Introduction

This section describes the test rig designed to generate heat exchanger pressure drop information under oscillating flow conditions. This oscillating flow rig is based on a variable stroke and variable frequency linear drive motor. A frequency capability of 120 hertz and a mean test pressure up to 15 MPa (2200 psi) allows for testing at flow conditions found in modern high specific power Stirling engines.

An important design feature of this rig is that it utilizes a single close-coupled dynamic pressure transducer to measure the pressure drop across the test sample. This eliminates instrumentation difficulties associated with the pressure sensing lines common to differential pressure transducers. Another feature of the rig is that it utilizes a single displacement piston. This allows for testing of different sample lengths and configurations without hardware modifications. All data acquisition and reduction for the rig is performed with a dedicated personal computer. Thus, the overall system design efficiently integrates the testing and data reduction procedures.

Design Methodology

The approach taken in the design presented here is different from that being pursued in a rig designed by the University of Minnesota (4). The approach of the University of Minnesota rig is to scale the test sample size up several times and reduce frequency and pressure so that measurements can be made within the sample.

The approach taken in the design of the Sunpower oscillating test rig is to test true-size samples at conditions that are as near as possible to the actual operating conditions. Two exceptions to this are made. First, all test samples are run near room temperature; and secondly, mean cyclic pressure variations such as occur in Stirling engines are not included (at least not in the present version of the rig). Since the heat exchangers tested with the test rig usually have small passages, it would be essentially impossible to make measurements within the test sample. Rather than attempt this, the rig is used to measure the pressure drop across the sample.

In order to achieve a wide range of frequencies and piston displacements, the oscillating flow is generated by a linear drive motor. The piston which produces the oscillating flow through the test sample is directly attached to this drive motor. A cross-sectional drawing of the rig is shown in Figure 3.1-1. The individual components of the rig are labeled in the schematic drawing of Figure 3.1-2. This rig is approximately 0.3 meter in diameter and 1 meter in length.

The use of this linear drive motor has several advantages. The stroke of the motor is simply varied by adjusting the driving voltage. Thus, no hardware modifications are required to run tests over the range from zero to the full stroke capability (3 cm) of the rig. The frequency of the linear drive motor is also easily adjusted (within a given range described below) simply by adjusting the frequency of the drive voltage applied to the motor.

Although in theory it would be possible to design a drive motor capable of supplying all the required driving force, this is not practical. A more feasible approach, as used in this Sunpower rig, is to use springs to balance the inertia forces to the reciprocating parts of the rig. The spring-mass combination of the rig is tuned to mechanical resonance near the desired range of testing. How far removed from this frequency the rig can be operated is determined by the electrical current capability and, thus, peak driving force available from the motor.

Mechanical rather than gas springs were chosen for the design. The rig is set up before a run for operation by installing springs to tune the moving mass of the rig to the desired frequency. With a given set of springs installed, the frequency of the rig can still be varied over a range of approximately 10 to 20 hertz. The use of mechanical springs also allows the pressure in the rig to be set as an independent parameter.

From the onset of the project, it was realized that the rig's wide range of operating frequencies would complicate the problems described earlier of using differential transducers with sensing lines. Also, it was recognized that the intended testing of numerous sample lengths and configurations would require many changes to the lengths of these sensing lines. In order to address this instrumentation problem and, thus, reduce the chance of introducing errors, the rig layout shown in Figures 3.1-1 and 3.1-2 was selected. This arrangement surrounds the drive motor, displacement section, and test sample by a pressure enclosure. The volume of this enclosure is much larger than the volume displaced by the piston of the rig, so the pressure in this space is essentially constant during rig operation. Because of this constant pressure, the pressure drop across the test sample can be measured by a single close-coupled pressure transducer in the displacement section.

The pressure transducer used for measuring the dynamic pressure in the displacement section is a silicon diaphragm type which has the back side of the diaphragm ported to the large interior volume of the pressure enclosure. This method allows the use of a sensitive pressure transducer even though the mean test pressure is quite high.

Besides simplifying instrumentation requirements, this arrangement also simplifies the testing of samples. The arrangement requires no hardware modifications to test different sample types and lengths. To change samples, it is only necessary to open the pressure enclosure for access to the sample mounting area.

The rig design requires only two dynamic measurements to be made, these being the pressure in the displacement section and the position of the piston. Static measurements recorded include the mean pressure and temperature within the pressure enclosure as well as gas and metal temperatures at the displacement section. The wall temperature of the test sample is also measured.

Currently the test rig does not perform tests with the significant cycle pressure variations such as exist in Stirling engines. These tests could be performed in the future by installing a second motor and displacement section at what is now the open end of the tube. Considerations have been given to modifying the existing rig so that heat transfer testing could be performed.

3.2 STEADY UNIDIRECTIONAL FLOW TEST RIG

A steady unidirectional flow test rig was also designed under this program. The purpose of this rig for tube type heat exchangers is to verify the unidirectional pressure drop of samples against accepted correlations. This rig is also useful for generating unidirectional flow information for samples for which no reliable information exists, such as in the case of certain types of regenerator samples.

A schematic drawing of this rig is presented in Figure 3.2-1. Physical dimensions of this rig are approximately 1 meter diameter for the main pressure vessel and an overall length of 2 meters. Flow through the loop is provided by means of a piston type

compressor which is driven by a variable speed dc motor. Gas from the compressor flows into an accumulator tank which is provided to suppress pressure pulsations caused by the compressor.

After leaving the accumulator, gas flows first through the element labeled 'filter' in Figure 3.2-1. This element is a dense porous metal plug and is included more as a flow restriction to help eliminate pressure pulsations than for filtering.

After leaving the filter, gas flows through a mass flow sensor and then into the small pressure vessel shown in Figure 3.2-1. Gas then flows through the test sample and into the large pressure reservoir of the main pressure vessel.

Pressure drop across the test sample is measured by a differential pressure transducer with sensing lines. Since the flow in this rig is steady, the response problems mentioned earlier for this type of transducer arrangement do not occur.

The cooling coils and fan shown in the figure were not normally necessary. These were provided only for use if testing of high pumping power samples would result in significant temperature rises of the system.

A photograph of both the oscillating and the steady flow rigs is shown in Figure 3.2-2.

3.3 RANGES OF POSSIBLE OPERATING PARAMETERS

The design philosophy of the oscillating flow rig allows for a wide operating range. This operating range is summarized in Table 3.3-1.

Table 3.3-1

Test Rig Operating Parameters

Oscillating Flow Rig:		
Maximum Mean Pressure	15 MPa	(2200 psi)
Maximum Frequency	120 Hz	
Maximum Stroke *	3 cm	(1.18 in.)
Maximum Sample Length	36 cm	(14.2 in.)

* See Text

The maximum physical stroke of the piston is 3 cm as indicated in the table. However, the rig relies on dry-running Teflon-based bearings for alignment. These bearings inherently have a limiting peak velocity at which they can be run without experiencing excessive wear. This velocity is approximately 5.7 m/sec. Therefore, at frequencies above 60 hertz, the rig is normally run at a reduced stroke. At 120 hertz, for instance, the velocity limit of the bearings requires that the stroke be limited to 1.5 cm. The rig has been sized to account for this; desired flow rates are still obtained at this reduced stroke. For the steady flow test rig, the maximum pressure is 5 mPa (725 psi).

During the testing, it was necessary to avoid certain frequencies for a given test sample and working fluid due to the test rig acting as a Helmholtz resonator. These were encountered primarily at low piston amplitudes and were evident as large values of the harmonics in the measured pressure wave. Avoiding these resonant conditions was not a significant problem in the actual testing.

3.4 OPERATING PARAMETER CONTROL

The charge pressure for both rigs is controlled by manual charge and discharge valves. The other operating parameters for both test rigs are controlled from the instrument rack. For the oscillating flow rig these parameters are piston stroke and frequency, while for the steady flow rig, the single controlled parameter is mass flow rate.

The frequency of the oscillating flow rig is adjusted by means of a potentiometer which controls the switching frequency of a specially developed motor driver. Electrical input to this motor driver is rectified three-phase power. Piston amplitude is controlled by adjusting the voltage of this three-phase power using a Variac.

Mass flow rate for the steady flow rig is also set using the Variac. In this case the rectified three-phase power bypasses the switching electronics and is directly applied to the dc motor.

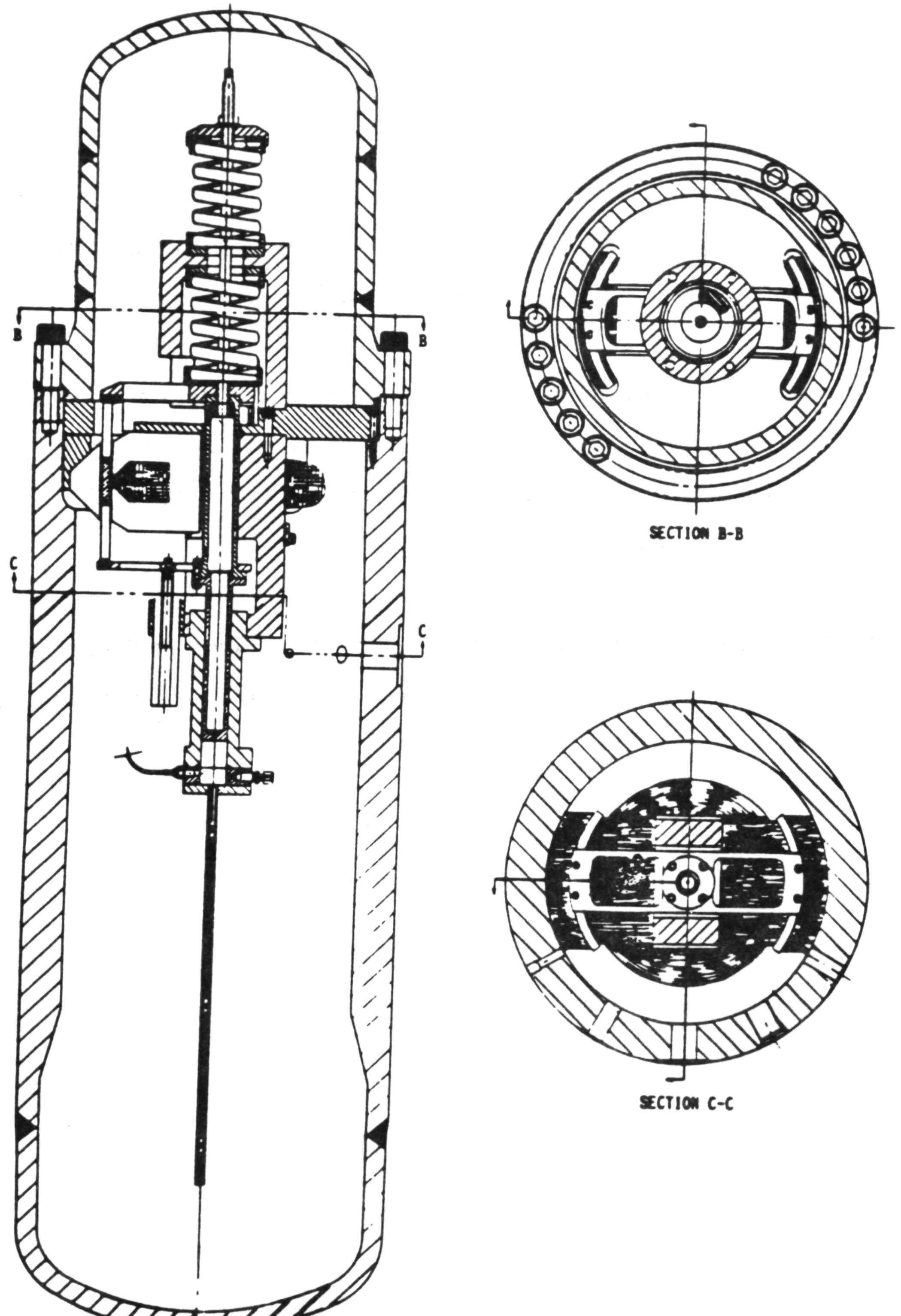

FIGURE 3.1-1 Sunpower Oscillating Flow-Loss Test Rig

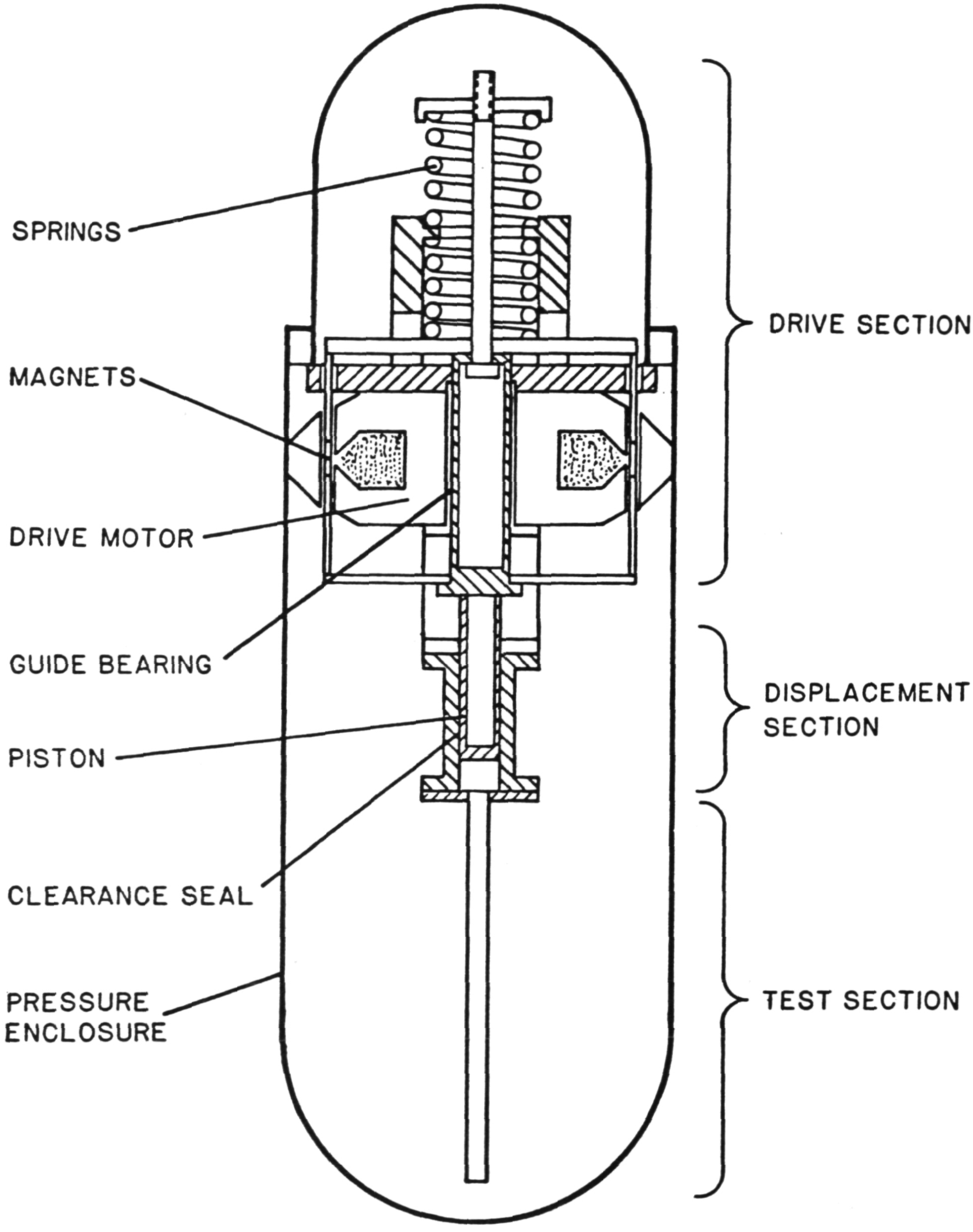

FIGURE 3.1-2 Sunpower Oscillating Flow-Loss Test Rig

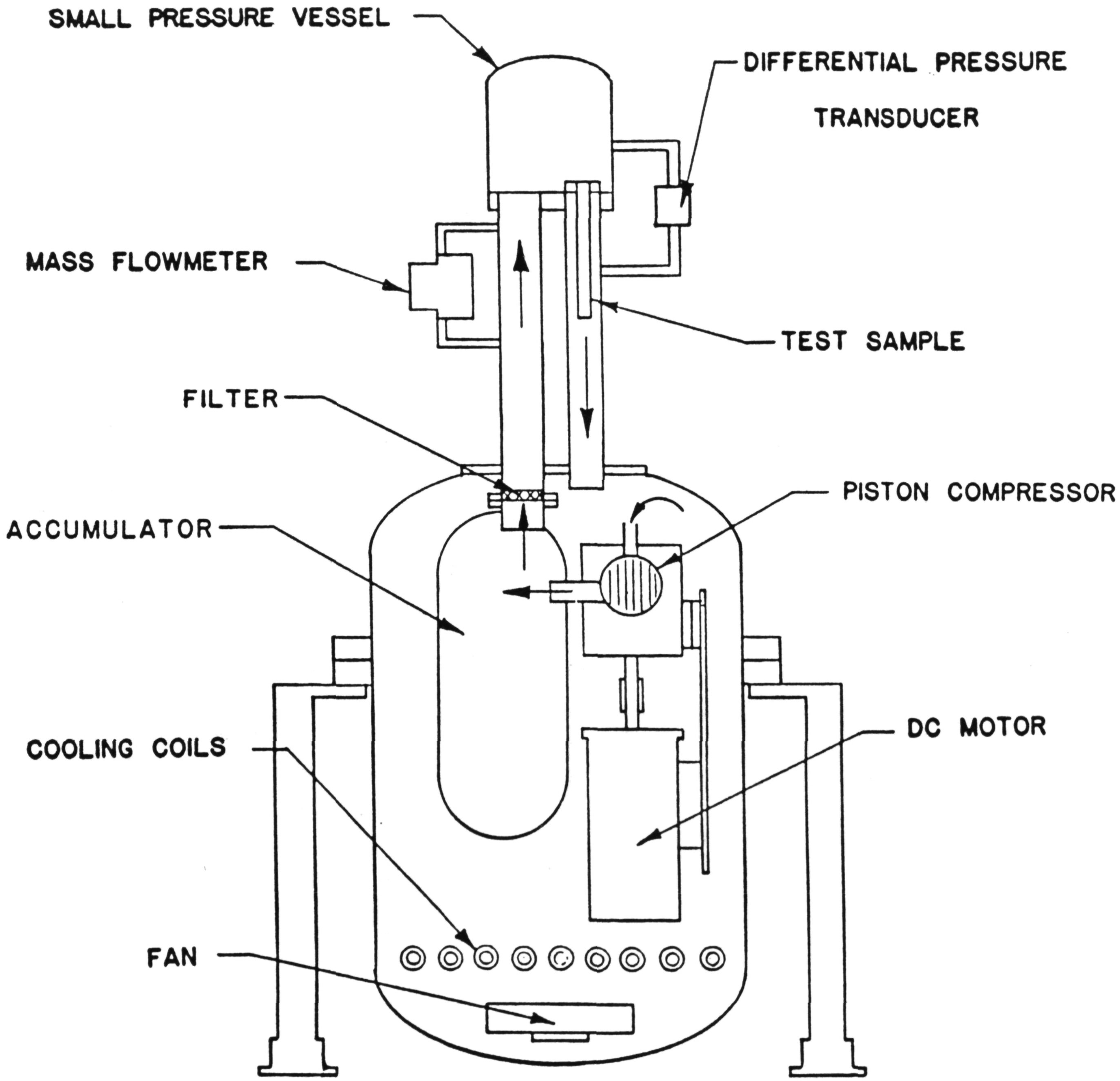

FIGURE 3.2-1 Steady Flow Test Rig

NASA
C-87-11960

ORIGINAL PAGE
BLACK AND WHITE PHOTOGRAPH

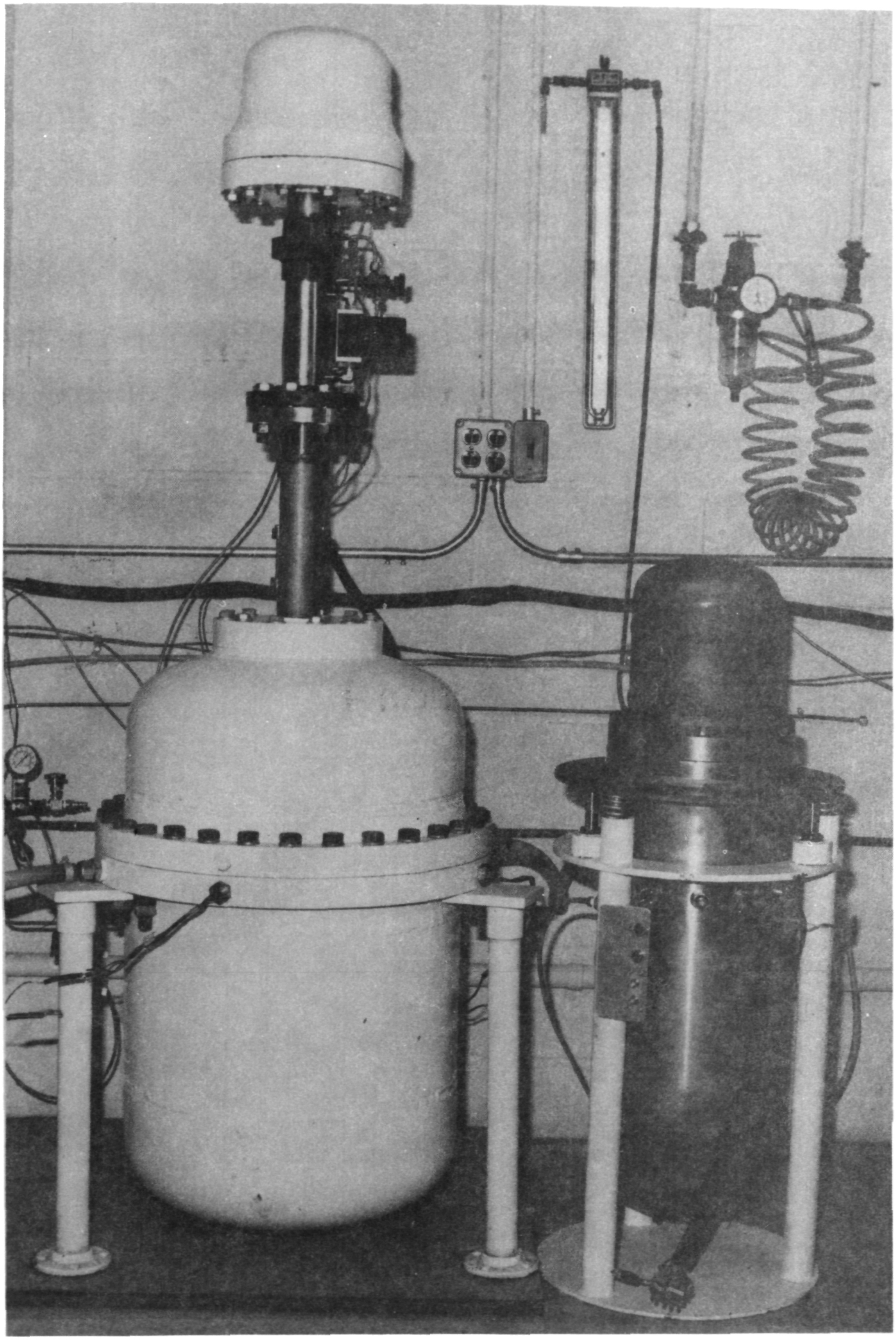

FIGURE 3.2-2 Photograph of Steady and Oscillating Flow Rigs

Section 4

4.0 DATA ACQUISITION

4.1 THE HARDWARE

The same data acquisition system is used for both the steady and oscillating flow test rigs. It is based on a Compaq Deskpro personal computer with a Metrabyte DAS-16 analog/digital conversion board installed. In many of the tests, signals were also recorded on a Kyowa RTP-600B 14-channel data recorder. A photograph of the data acquisition system is shown in Figure 4.1.

During steady flow testing, six static signals were input to the data system. They were from a Hastings STH-750KGP mass flow sensor, a Validyne DP-15 pressure drop transducer, an Omega model PX-621 pressure transducer (for mean pressure), and three type K thermocouples.

For the oscillating tests, there were eight input signals. Two were dynamic signals that had to be sampled many times per cycle; these were signals from an Endevco 8510B pressure transducer (for pressure drop), and a Sunpower TR60 FLDT (for piston position). The other six were static and included outputs from an Omega PX-621 for mean pressure and five type K thermocouples.

All instruments except the thermocouples were connected to the data acquisition system via the amplifiers recommended by the manufacturers. The thermocouple signals were processed by a device using Analog Devices AD-8595CQ monolithic thermocouple amplifiers.

4.2 STEADY FLOW SOFTWARE

The data acquisition software sampled each signal 50 times at a rate of 125 Hz. The mean was found and the instrument calibration curves (best fit polynomials of up to fourth order) were used to determine physical values for each signal. The mass flow rate was used to determine the Reynolds number of the flow through the sample. A theoretical pressure drop at that Reynolds number and mass flow rate was then determined based on the accepted Darcy friction factor correlations used in the Stirling cycle computer simulation GLIMPS. A quantity called *P*ratio was defined as the ratio of the measured to the theoretical pressure drops. Mass flow, pressure drop, Reynolds number, *P*ratio and temperature data were all sampled, calculated, and displayed on the screen about once every second.

When the user determined that the system had settled down to a steady state, data points were taken by depressing a single key. All of the above information for every data point was sent to the printer and the raw data (everything but the Reynolds number and the *P*ratio) were saved in a disk file. The data files were transferred into a database from which information could easily be extracted for graphing and further analysis. Error analysis was done after the run from within the database program (See Appendix C).

A complete list of the software used to run the steady flow rig can be found in Tables 4.2-1 and 4.2-2.

4.3 OSCILLATING FLOW SOFTWARE

Data reduction for the oscillating flow rig was so complex it was impractical to perform all of the calculations during the run. Therefore, the software was split into an acquisition program and a data reduction package. The disk files necessary to run the oscillating rig are tabulated in Table 4.3-1.

The data acquisition program was run during the tests to monitor conditions within the rig and to save selected data points to disk for use by the data reduction package. While running, the program sampled each of the dynamic signals 100 times over approximately two piston cycles, and each of the static voltages 25 times at a rate of 167 Hz. All signals were converted to physical units using quartic curve fits to calibration data (determined either experimentally or from manufacturer's specifications). The dynamic variables were then plotted, either as waveforms or Fourier spectra, and the static variables displayed. In addition, the maximum pressure drop and pV power were calculated and displayed on the screen.

With a single button press, a more extensive data point could be taken, printed, and stored on disk. Static voltages were sampled as above, but dynamic signals were sampled at 2048 Hz for one second. A fast Fourier transform was then performed, and the first seven harmonics were found and saved to disk. This technique allowed data to be averaged over many cycles, giving a clean average signal and effective data compression, but also made it necessary to operate the rig at integral (whole number) frequencies. Data points were taken only when the oscillating frequency was within 0.03 Hz of an integral frequency. The data stored was later used by the data reduction package.

Midway through the testing, the acquisition program was modified to calculate peak Reynolds number and kinetic Reynolds number during runs. The procedure to do this was essentially the same as that used in the data reduction program (see Appendix A), and involved solving a differential equation for the mass flow through the sample. The Reynolds number agreed fairly well with those calculated by the data reduction package, but were not saved on disk or used in the data reduction. They served to allow the experimenters to use Reynolds numbers more effectively as independent variables during data analysis. In addition, control over both Reynolds numbers was necessary to use the version of the data reduction package that simultaneously solved for friction factor and entrance loss (XGRUCE, see Appendix A for details).

The data reduction package took the Fourier coefficients and the static signal information from the disk files generated by the acquisition program, performed the data reduction, and recorded the raw and reduced data in a form that could be read by the database program. The bulk of the package was written by David Gedeon, a consultant to Sunpower, who describes the process in Appendix A. Essentially, it consisted of solving a differential equation to determine the mass flux through the sample, calculating the shear forces on the gas within the sample, and comparing the results to those predicted by steady flow correlations at the same mass flow rates. In addition, an extensive error analysis was performed. After the reduction process, the data was sent to a database program so they could be easily accessible for examination and graphing.

Table 4.2-1
Software Necessary for Both Rigs

SETUP.EXE	A BetterBasic™ program to input information on sample geometry, working fluid, instrumentation used, and calibration curves.
ASYST™	A data acquisition and analysis programming language used for both steady flow and oscillating flow real-time data acquisition.
TRASYST.COM & TRASYST.OVL	Versions of ASYST set up for the hardware in the data acquisition system.
IFILES.SET	Generated by SETUP, this contains names, voltage ranges, and calibration curves for each instrument used in the data acquisition system.
TOPS®	Software for PC-compatible and Macintosh™ computers used to transfer data from the data acquisition system to the database.
REFLEX®	The relational database program used to store, save, and manipulate reduced data from steady and oscillating flow tests.

Table 4.2-2
Files Necessary to Run the Steady Flow Rig

RUNSF.TXT	This text file is the ASYST program that does the data acquisition during a run and saves the results in data files named SFRUN.### where ### is the run number.
SFR.SET	Contains sample geometry and working fluid information from SETUP to be used by RUNSF.
RUN_NUM.SF	Contains the number of the most recent steady flow run. It is used and updated by RUNSF.
FILESF.TXT	Reads SFRUN.### files in ASYST format from RUNSF, reprocesses the data, and rewrites the data as an ASCII text file named SF###.ASC that can be read by REFLEX®.
SSESFdata	The REFLEX® database file containing the results of the steady flow runs.

Table 4.3-1

Files Necessary for the Oscillating Flow Rig

RUNOF.TXT	The ASYST™ program that does the data acquisition and some real-time analysis during oscillating flow tests. Data from a run is saved as a file named OFRUN.### where ### is the test number.
OFR.SET	A file created by SETUP that contains information on working gas and which instrumentation is being used. It is used by RUNOF.
PFILES.SET	Another file generated by SETUP and used by RUNOF. It contains sample geometry and some miscellaneous information.
RUN_NUM.OF	Contains the run number of the most recent oscillating flow test. It is used and updated by RUNOF.
SHTRY.EXE	The primary oscillating flow data reduction package. It takes data files produced by RUNOF (in a directory OFRAWDAT), reduces them, and puts the information into a file named \OFDATA\OF###.OFD. See Appendix A for details of the data reduction process.
SSEOFdata	The REFLEX® database containing raw and reduced data from the oscillating flow tests.
pVpower	A Turbo Pascal® program that finds maximum pressure drop and integrates pressure drop and piston position to get pV power. It takes data exported from the REFLEX® report form pVdataln and returns a text file that can be read by REFLEX®.

ORIGINAL PAGE
BLACK AND WHITE PHOTOGRAPH

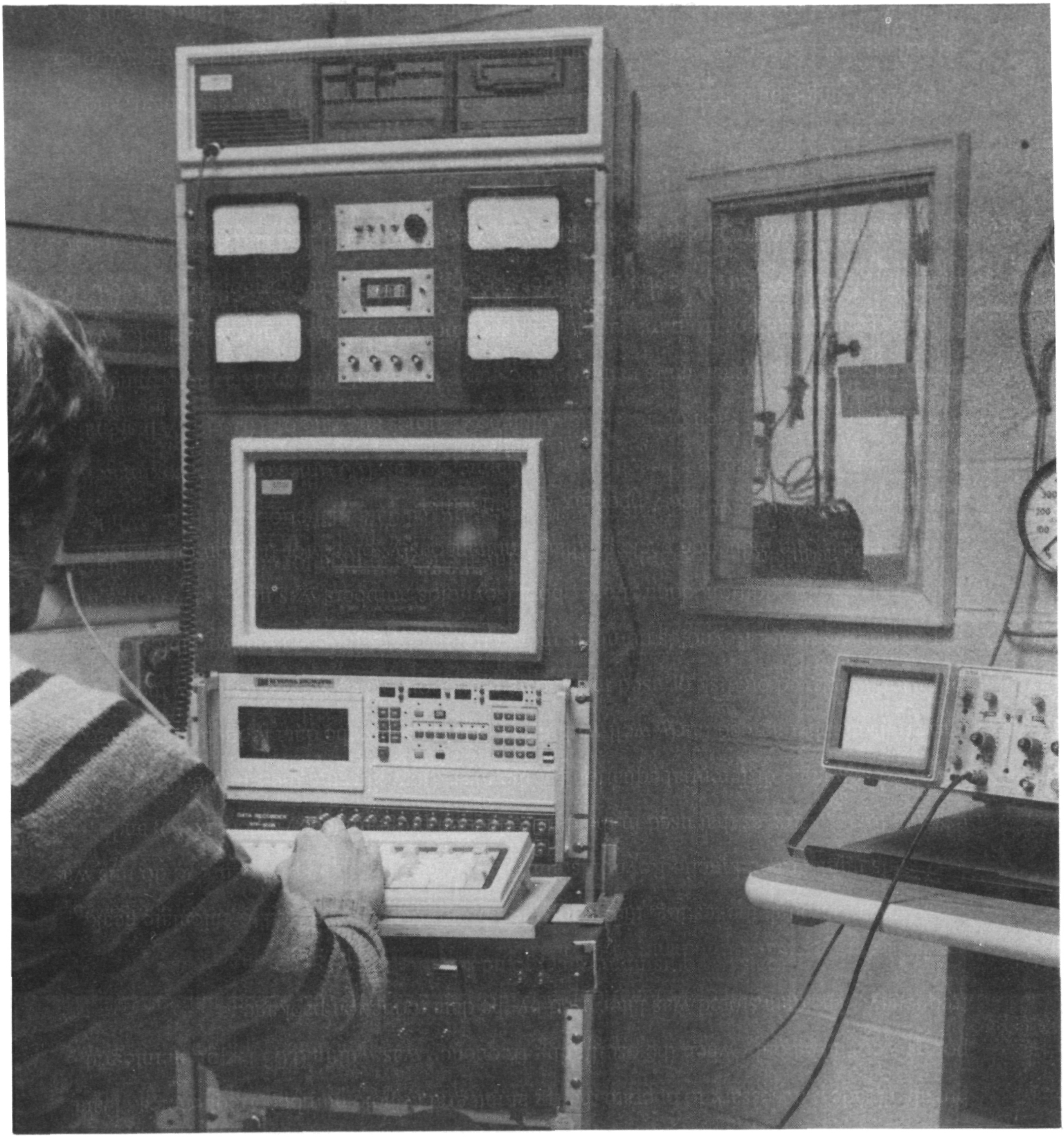

FIGURE 4.1 Photograph of Data Acquisition System

Section 5

5.0 THE TEST MATRIX

Steady flow loss and oscillating flow loss tests were performed on two basic types of Stirling engine heat exchangers. These were heater/cooler tube configurations and a variety of regenerators (stacked and sintered screens, Metex knit wire, and Brunswick felt metal). This section reports on their geometric characteristics and the range of oscillating flow parameters over which the flow loss tests were performed.

5.1 HEATER / COOLER TUBE TEST SAMPLES

The tube test sections constructed for the flow loss tests were fabricated from smooth, constant diameter (I.D. = 2.375 mm) stainless steel tubes of varying lengths. In general, the tube lengths were selected so that the *L/D* ratio was equal to 5.35, 10, 25, 50, 100, and 150. In addition to varying the tube lengths, the tube entrance and exit configurations were also varied. Three combinations of entrance/exit configurations were tested and evaluated. They were:

1. Protruding square entrance and exit on both ends, Figure 5.1-1.
2. Flush square entrance and exit on both ends, Figure 5.1-2.
3. Flush round entrance and exit on both ends, Figure 5.1-3.

Photographs of the tube test sections are shown in Figures 5.1-4 , 5.1-5, and 5.1-6. The geometric characteristics of these tube test sections are presented in Table 5.1-1.

The test matrices for the tube and oscillating flow loss tests are presented in Tables 5.1-2 and 5.1-3, respectively. In addition, the ranges of the operating parameters over which the tests were performed are included in these tables; these parameters include the operating frequency, system mean pressure, Re_{max} , Re_{ω} , A_r , and *L/D*. The significance of these parameters is discussed by Seume and Simon (5).

Figures 5.1-7 and 5.1-8 show the operating ranges of the oscillating flow parameters that were generated in the tube test matrix. Also shown on these figures (by the solid line) is the range of flow parameters found in a wide variety of Stirling engines as reported by Seume and Simon (5). These figures show that the test results presented in this report cover the range of dimensionless parameters appropriate for the NASA Space Power Demonstrator Engine (SPDE) and the Stirling Space Engine (SSE) conceptual design (6,7).

5.2 REGENERATOR TEST SAMPLES

Steady flow and oscillating flow loss tests were performed on three types of Stirling engine regenerators: stacked screens, sintered screens, and random fiber regenerators. Photographs of some of the test samples are shown in Figures 5.2-1, 5.2-2, and 5.2-3. Drawings of the spool that holds the regenerator test sections are shown in Figures 5.2-4 and 5.2-5. The test sections were approximately 19.05 mm in diameter and 12.7 mm to 25.4 mm in length.

Figures 5.2-6 and 5.2-7 show the operating range of the oscillating flow parameters that were included in the test matrix. Also shown on the figures (by the solid line) is the range of flow parameters found in Stirling engine regenerators as reported by Seume and Simon (5). These figures show that the test results cover the range of dimensionless parameters appropriate for the NASA SPDE (6) and the SSE (7) conceptual design.

5.2.1 Stacked Screens

Steady flow and oscillating flow loss tests were performed on four different regenerators composed of stainless steel stacked screens. The screens ranged from 40.6 μm wire diameter at 250 mesh through 191.0 μm wire diameter at 60 mesh. Their porosity was held fairly constant at 66 percent to 68 percent porous. A photograph of a single screen from each of the regenerator test sections is shown in Figure 5.2-1.

In Table 5.2-1, the geometric characteristics of these stacked screen regenerators are presented. The test matrices for the steady and oscillating flow loss tests are presented in Table 5.2-2 and Table 5.2-3, respectively. In addition, the ranges of the operating parameters over which the tests were performed are included in these tables.

5.2.2 Sintered Screens

Steady flow and oscillating flow loss tests were performed on two different regenerators composed of sintered stainless steel stacked screens. The screens were 40.6 μm wire diameter at 250 mesh and 53.0 μm wire diameter at 200 mesh. Their porosity was held fairly constant at 60.4 percent to 61.6 percent. A photograph of one of the sintered stacked screen regenerator test sections is shown in Figure 5.2-2.

In Table 5.2-1, the geometric characteristics of these sintered screen regenerators are presented. The test matrices for the steady and the oscillating flow loss tests are presented in Table 5.2-2 and Table 5.2-3, respectively. In addition, the ranges of the operating parameters over which the tests were performed are included in these tables.

5.2.3 Random Fiber

Steady flow and oscillating flow loss tests were performed on two different random fiber regenerators, Metex knit wire and Brunswick felt metal. The Metex knit wire regenerator was composed of 89.0 μm diameter woven stainless steel wire at 80 percent porosity. The Brunswick felt metal regenerator was composed of 12.7 μm diameter sintered stainless steel wire at 84 percent porosity. A photograph of the random fiber test samples is shown in Figure 5.2-3.

In Table 5.2-1, the geometric characteristics of the random fiber regenerators are presented. The test matrices for the oscillating and the steady flow loss tests are presented in Tables 5.2-2 and 5.2-3, respectively. In addition, the ranges of the operating parameters over which the tests were performed are included in these tables.

Table 5.1-1
Geometric Parameters
of Tube Test Sections

Tube Configuration	D (mm)	A_c (mm^2)	Entrance/Exit Characteristics	L/D
Flush Sq/Sq	2.375	4.430	Flush square edged entrance and exit on both ends	5.35, 10, 25, 50, 75, 100, 150
Flush Rd/Rd	2.375	4.430	Flush rounded entrance and exit on both ends	5.35, 10, 25, 50, 100, 150
Prot Sq/Sq	2.375	4.430	Protruding square edged entrance and exit on both ends	5, 32, 48, 64, 84, 102, 126, 151

Table 5.1-2
Tube Steady Flow Loss Tests
Test Matrix
Dia: 2.375 mm

Tube Entrance/Exit Configuration	L/D	Run Number	Working Gas	Mean Pressure (bar)	Re[1]
Flush	25	50/51	air/N_2	7/18.26	10,000 - 231,000
Rounded	50	52/53	air/N_2	7/18.26	10,000 - 220,000
Entrance	100	56/58	air/N_2	7/18.26	10,000 - 169,000
and Exit -	150	60/61	air/N_2	7/18.26	10,000 - 150,000
Both Ends					
Flush	5.35	47/48	air	7/3.36	11,000 - 102,000
Square	10	49	air	7/3.36	11,000 - 132,000
Entrance	25	44/45	air	7/3.36	11,000 - 104,000
and Exit -	50	42/43	air	7/3.36	10,000 - 103,000
Both Ends	75	40/41	air	7/3.36	10,000 - 90,000
	100	38/39	air	7/3.36	10,000 - 80,000
	150	36/37	air	7/3.36	10,000 - 71,000
Protruding	5	21 - 23	air/N_2	3.36/18/26	9,998 - 211,300
Square	32	18 - 20	air/N_2	3.36/18.26	9,983 - 191,700
Entrance	48	15 - 17	air/N_2	3.36/18.26	8,946 - 177,200
and Exit -	152	7,9,10,11	air/N_2	3.36/18.26	10,000 - 144,700
Both Ends					

1. $Re = \frac{\rho u D_h}{\mu}$

Table 5.1-3
Tube Oscillating Flow Loss Tests
Test Matrix
Dia: 2.375 mm

Tube Entrance/Exit Configuration	L/D	Run Number	Working Gas	f (Hz)	Mean Pressure (bar)	1 Re_{max}	2 Re_{ω}	3 A_r
Flush	5.35	82	He	82	16 - 51	12,000 - 191,000	100 - 300	5.23 - 40.58
Rounded	10	83	He	82	16 - 51	11,700 - 158,000	100 - 300	2.73 - 21.35
Entrance	25	106/107	He	82	16 - 51	10,500 - 121,000	100 - 300	1.04 - 5.96
and Exit -	50	108	He	82	16 - 51	9,800 - 100,800	100 - 300	0.49 - 1.94
Both Ends	100	104	He	82	16 - 51	9,800 - 59,500	100 - 300	0.24 - 1.26
	150	79	He	82	16 - 51	13,500 - 43,800	100 - 300	0.20 - 0.62
	"	103	He	82	16 - 51	9,600 - 38,400	100 - 300	0.14 - 0.33
Flush	5.35	86	He	82	16 - 51	11,500 - 131,500	100 - 300	5.14 - 35.65
Square	10	87	He	82	16 - 51	11,200 - 133,000	100 - 300	2.77 - 18.23
Entrance	"	91	He	82	16 - 51	11,100 - 129,000	100 - 300	2.74 - 18.74
and Exit -	25	92	He	82	16 - 51	11,000 - 82,600	100 - 300	1.07 - 6.16
Both Ends	"	96/97	He	82	16 - 51	10,200 - 105,000	100 - 300	0.81 - 5.86
	50	101	He	82	16 - 51	11,000 - 91,000	100 - 300	0.53 - 2.45
	100	117	He	82	16 - 51	10,000 - 57,000	100 - 300	0.25 - 1.15
	150	102	He	82	16 - 51	16,300 - 40,000	100 - 300	0.16 - 0.58
	"	119	He	82	16 - 51	19,600 - 167,000	100 - 300	0.11 - 0.93

1. $Re_{max} = \dfrac{\rho u_{max} D_h}{\mu}$ 2. $Re_{\omega} = \dfrac{\rho \omega D_h^2}{4\mu}$ 3. $A_r = \dfrac{D_h Re_{max}}{2 L Re_{\omega}}$

Table 5.1-3(Continued)
Tube Oscillating Flow Loss Tests
Test Matrix
Dia: 2.375 mm

Tube Entrance/Exit Configuration	L/D	Run Number	Working Gas	f (Hz)	Mean Pressure (bar)	Re_{max} [1]	Re_{ω} [2]	A_r [3]
Protruding Square Entrance and Exit – Both Ends	5	5	He	80-84	1.44 - 28.9	7,700 - 42,200	100-200	3.67 - 15.12
	32	11	He	94	14.5 - 28.8	7,800 - 41,800	100-200	0.63 - 2.63
	48	13	He	94	14.5	8,800 - 3,200	100	0.43 - 1.69
	64	8	He	94	14.2 - 28.9	8,800 - 44,900	100-200	0.34 - 1.37
	84	12	He	94	14.5 - 28.9	8,700 - 46,500	100-200	0.26 - 1.04
	84	19	N_2	30	6.0 - 12.1	13,400 - 125,400	100-200	0.37 - 2.60
	102	7	He	94	14.4 - 28.9	9,100 - 46,400	100-200	0.23 - 0.89
	102	18	N_2	30	6.0 - 12.1	13,300 - 113,700	100-200	0.32 - 1.93
	126	9/10	He	94	14.5 - 28.6	9,700 - 42,800	100-200	0.19 - 0.64
	126	17	N_2	30	6.0 - 11.8	13,800 - 108,000	100-200	0.27 - 1.71
	151	6	He	94	14.4 - 29.0	10,300 - 47,700	100-185	0.18 - 0.82
	151	14	N_2	30	6.0	10,000 - 63,000	100	0.17 - 1.14
	151	15	He	30	45.6	10,900 - 58,400	100	0.19 - 1.00

1. $Re_{max} = \dfrac{\rho u_{max} D_h}{\mu}$ 2. $Re_{\omega} = \dfrac{\rho \omega D_h^2}{4\mu}$ 3. $A_r = \dfrac{D_h Re_{max}}{2 L Re_{\omega}}$

Table 5.2-1
Regenerator Geometric Parameters

Nominal Regenerator Configuration	Wire Dia. (μm/inches)	Mesh	Porosity (%)	D_h (m)	Cross Sectional Flow Area (m^2)	L (mm)
Stacked Screens						
	40.6/0.0016	250	68.0	0.864E-4	1.938E-4	12.7
	53.0/0.0021	200	66.5	1.059E-4	1.895E-4	12.7/25.4
	94.0/0.0037	120	66.3	1.849E-4	1.890E-4	12.7/25.4
	191.0/0.0075	60	66.5	3.782E-4	1.895E-4	12.7/25.4
Random Fiber						
Metex	89.0/0.0035	NA	80.0	3.556E-4	2.280E-4	12.7/25.4
Brunswick	12.7/0.0005	NA	84.0	0.667E-4	2.394E-4	12.85
Sintered Screens						
	40.6/0.0016	250	61.4	0.864E-4	1.938E-4	25.4
	53.0/0.0021	200	60.6	1.059E-4	1.895E-4	22.3

Table 5.2-2
Regenerator Steady Flow Loss Tests
Test Matrix

Regenerator Configuration	Wire Dia. (μm/inches)	Porosity (%)	Run Number	Working Gas	Mean Pressure (bar)	Re [1]
Stacked Screens						
	40.6/0.0016	68.0	99/100	Air/N_2	7/18.26	16-295
	53.0/0.0021	66.5	95/96	Air/N_2	7/18.26	35 - 380
	94.0/0.0037	66.3	85,88/86,87	Air/N_2	7/18.26	55 - 700
	191.0/0.0075	66.5	89,90/91	Air/N_2	7/18.26	100 - 1200
Random Fiber						
Metex	89.0/0.0035	80.0	92/93,94	Air/N_2	7/18.26	70 - 1100
Brunswick	12.7/0.0005	84.0	97/98	Air/N_2	7/18.26	16 - 190
Sintered Screens						
	40.6/0.0016	61.4	110/112 113/115	Air/N_2	7/18.26	13 - 127
	53.0/0.0021	60.6	108/109	Air/N_2	7/18.26	20 - 238

1. $Re = \frac{\rho u D_h}{\mu}$ (where: $D_h = D_w \frac{\varepsilon}{1-\varepsilon}$, $u = \frac{\dot{M}}{\rho A_c}$, $A_c = A_f \varepsilon$)

Table 5.2-2
Regenerator Oscillating Flow Loss Tests
Test Matrix

Regenerator Configuration	Wire Dia. (μm/inches)	Porosity (%)	Run Number	Working Gas	f (hz)	Mean Pressure (bar)	1 Re_{max}	2 Re_{ω}	3 A_r
Stacked Screens									
	40.6/0.0016	68.0	114	He	90	16 - 53	10 - 190 (3 - 61)	0.15 - 0.45	0.03 - 0.71
	40.6/0.0016	68.0	116	N_2	90	2 - 8	10 - 190 (3 - 61)	0.15 - 0.45	0.11 - 0.74
	53.0/0.0021	66.5	131/132	He	90	16 - 53	6 - 235 (2 - 80)	0.22 - 0.66	0.05 - 0.73
	94.0/0.0037	66.3	130/133 134	He	90	17 - 55	25 - 460 (8 - 156)	0.28 - 1.35	0.13 - 0.90
	191.0/0.0075	66.5	126/127	He	90	17 - 55	79 - 880	2.85 - 8.40	0.10 - 0.48
Random Fiber									
Metex	89.0/0.0035	80.0	122/123	He	90	16 - 53	120 - 630 (41 - 214)	2.50 - 7.50	0.03 - 0.71
Brunswick	12.7/0.0005	84.0	124/125	He	90	16 - 53	6 - 150 (2 - 51)	0.095 - 0.28	0.09 - 0.74
Sintered Screens									
	40.6/0.0016	61.4	135	He	90	18 - 60	11-13	0.10 - 0.20	0.08 - 0.39
	53.0/0.0021	60.6	137/138	He	90	18 - 63	9-219	0.10 - 0.40	0.06 - 0.56

Numbers in parentheses are $Re = \frac{\rho \hat{V} D_w}{\mu}$ (based on regenerator approach velocity and regenerator wire diameter)

1. $Re_{max} = \frac{\rho u_{max} D_h}{\mu}$ (where: $D_h = D_w \frac{\varepsilon}{1-\varepsilon}$, and $A_c = A_f \varepsilon$), $u_{max} = \frac{\dot{M}_{max}}{A_c}$ 2. $Re_{\omega} = \frac{\rho \omega D_h^2}{4\mu}$ 3. $A_r = \frac{D_h Re_{max}}{2 L Re_{\omega}}$

FIGURE 5.1-1 Protruding Square Entrance/Exit Test Sample

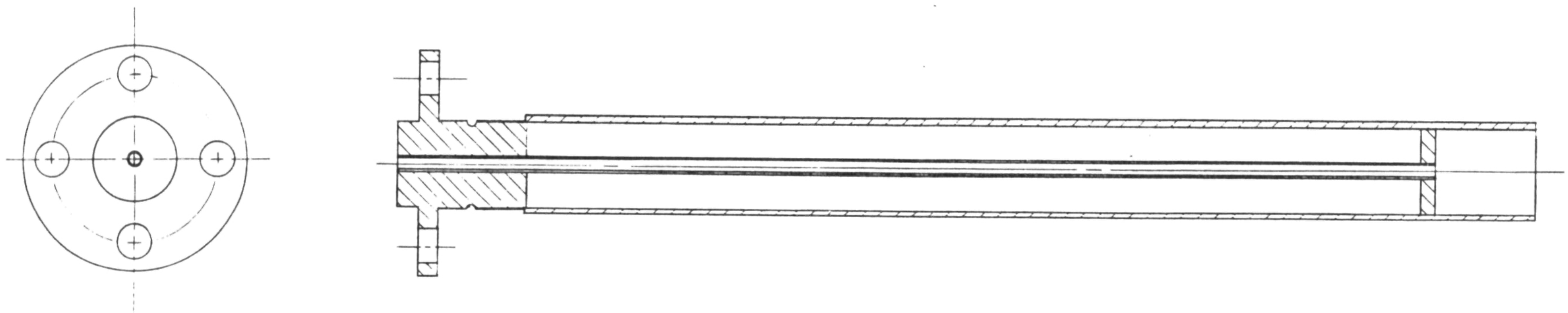

FIGURE 5.1-2 Flush Square Entrance/Exit Test Sample

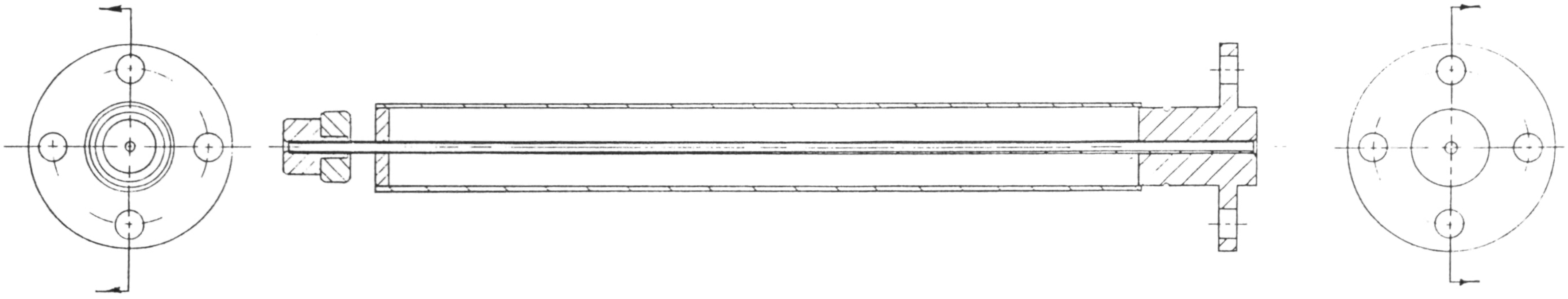

FIGURE 5.1-3 Flush Rounded Entrance/Exit Test Sample

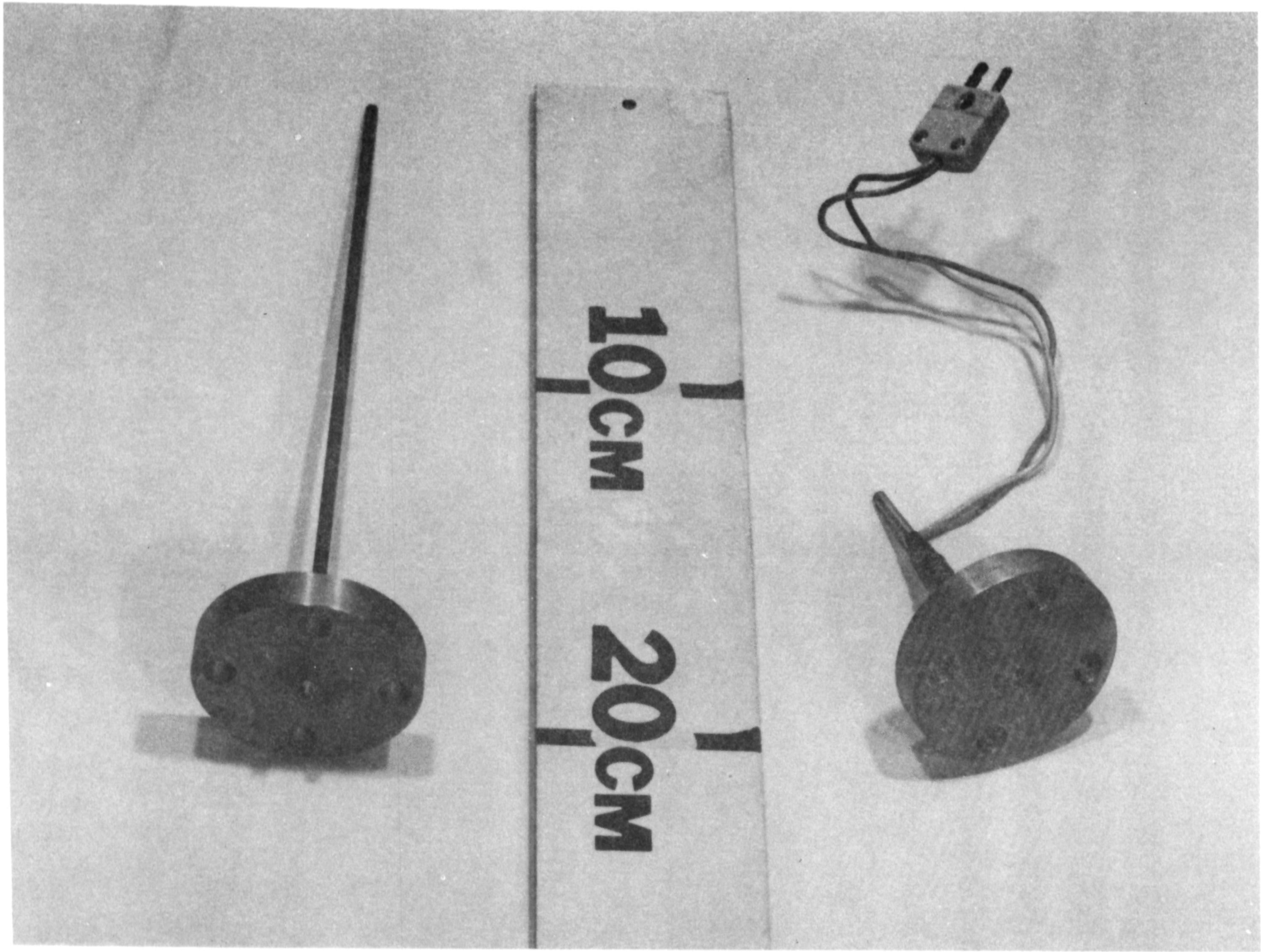

FIGURE 5.1-4 Protruding Square Entrance/Exit Tube Test Sections

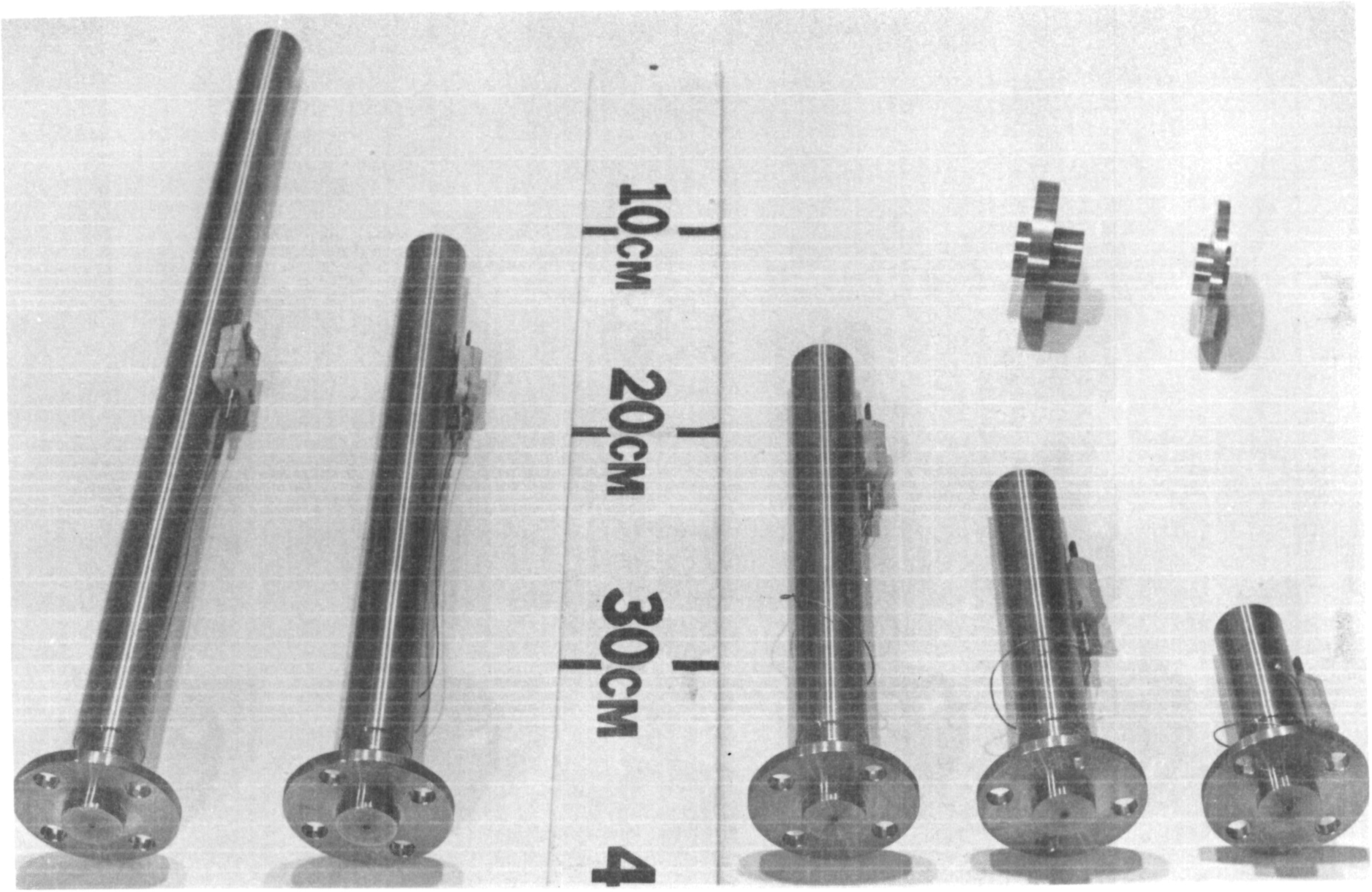

FIGURE 5.1-5 Flush Square Entrance/Exit Tube Test Sections

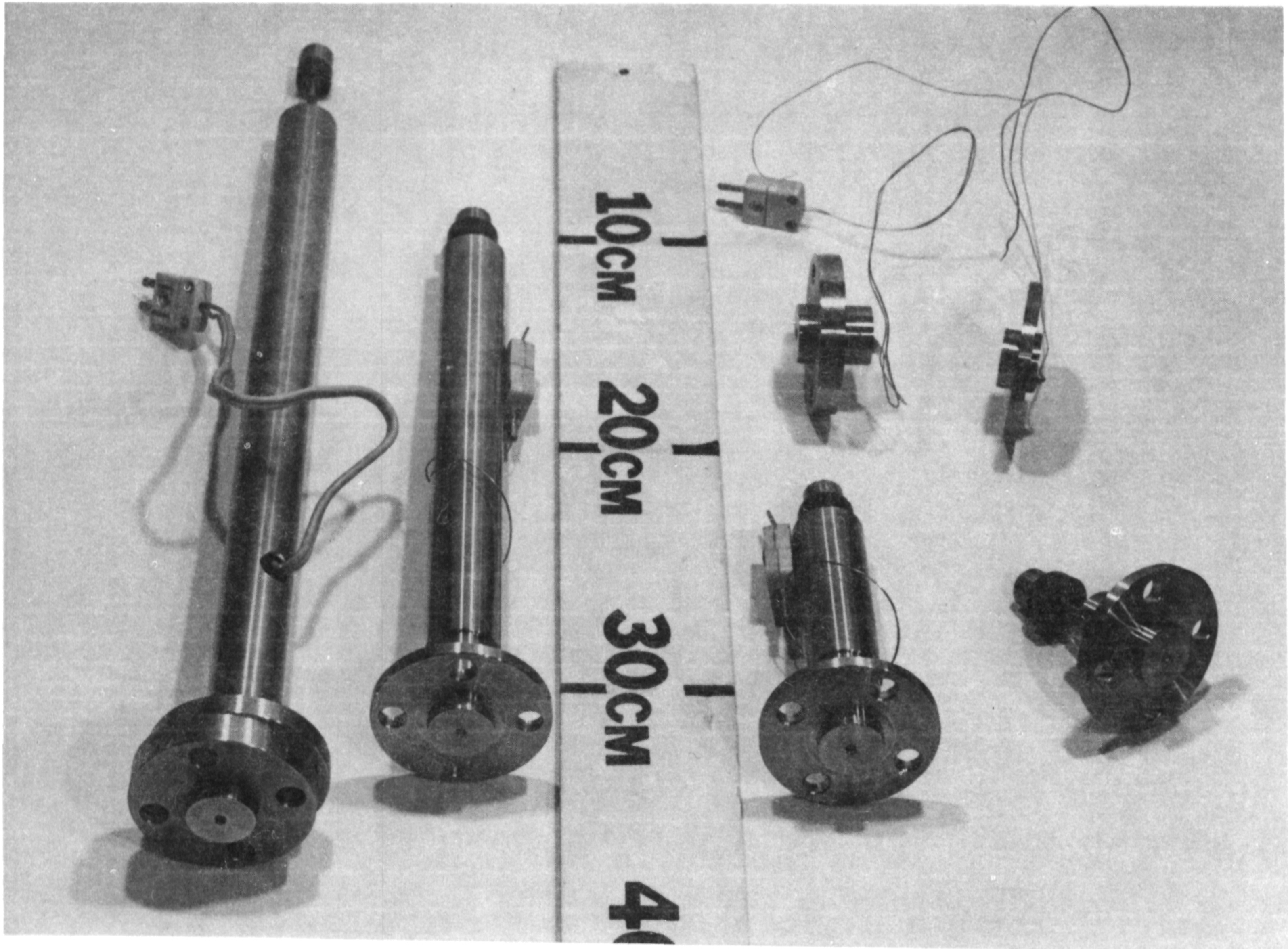

FIGURE 5.1-6 Flush Rounded Entrance/Exit Tube Test Sections

Range of Testing of Re max vs. Re w for Tubes

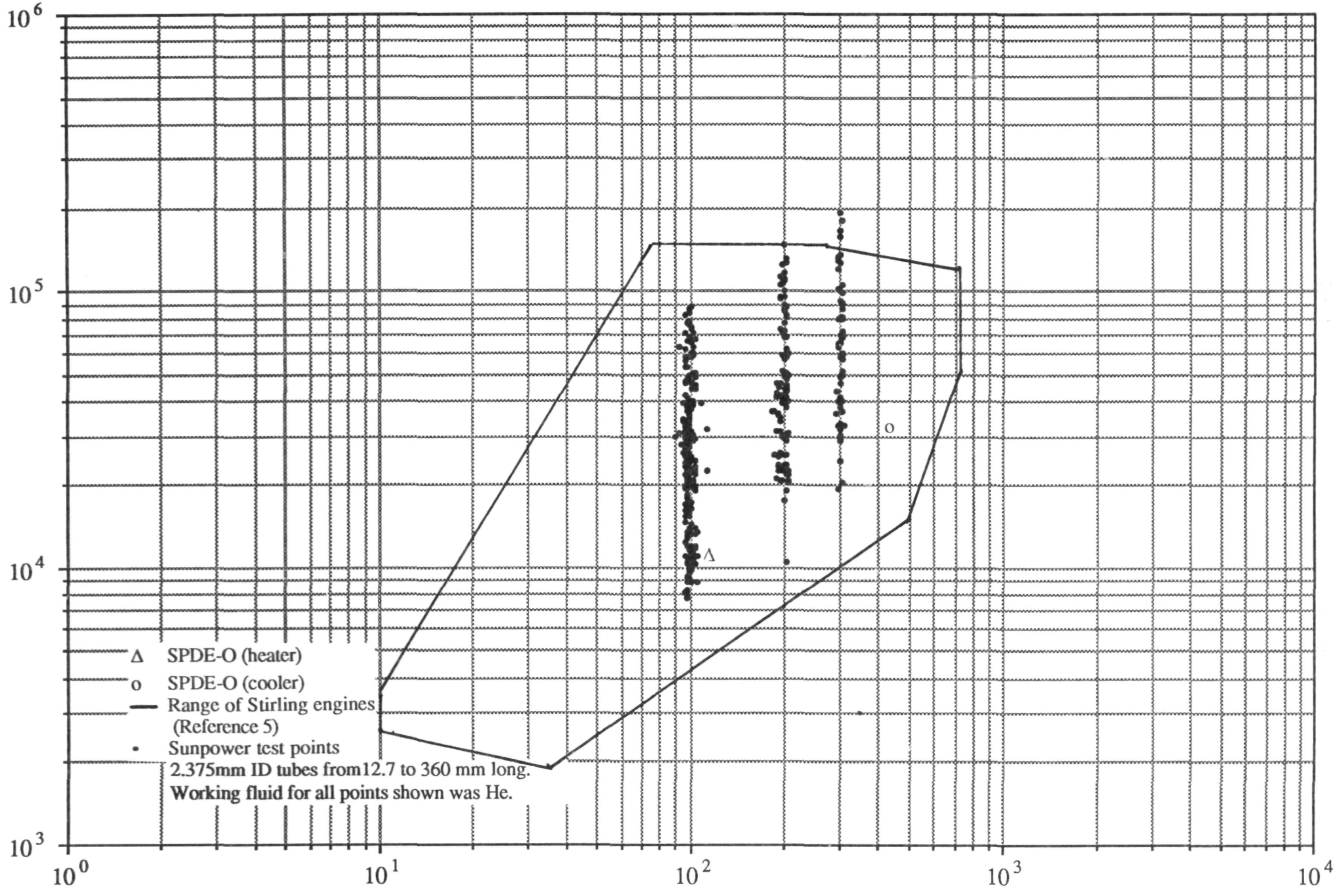

FIGURE 5.1-7

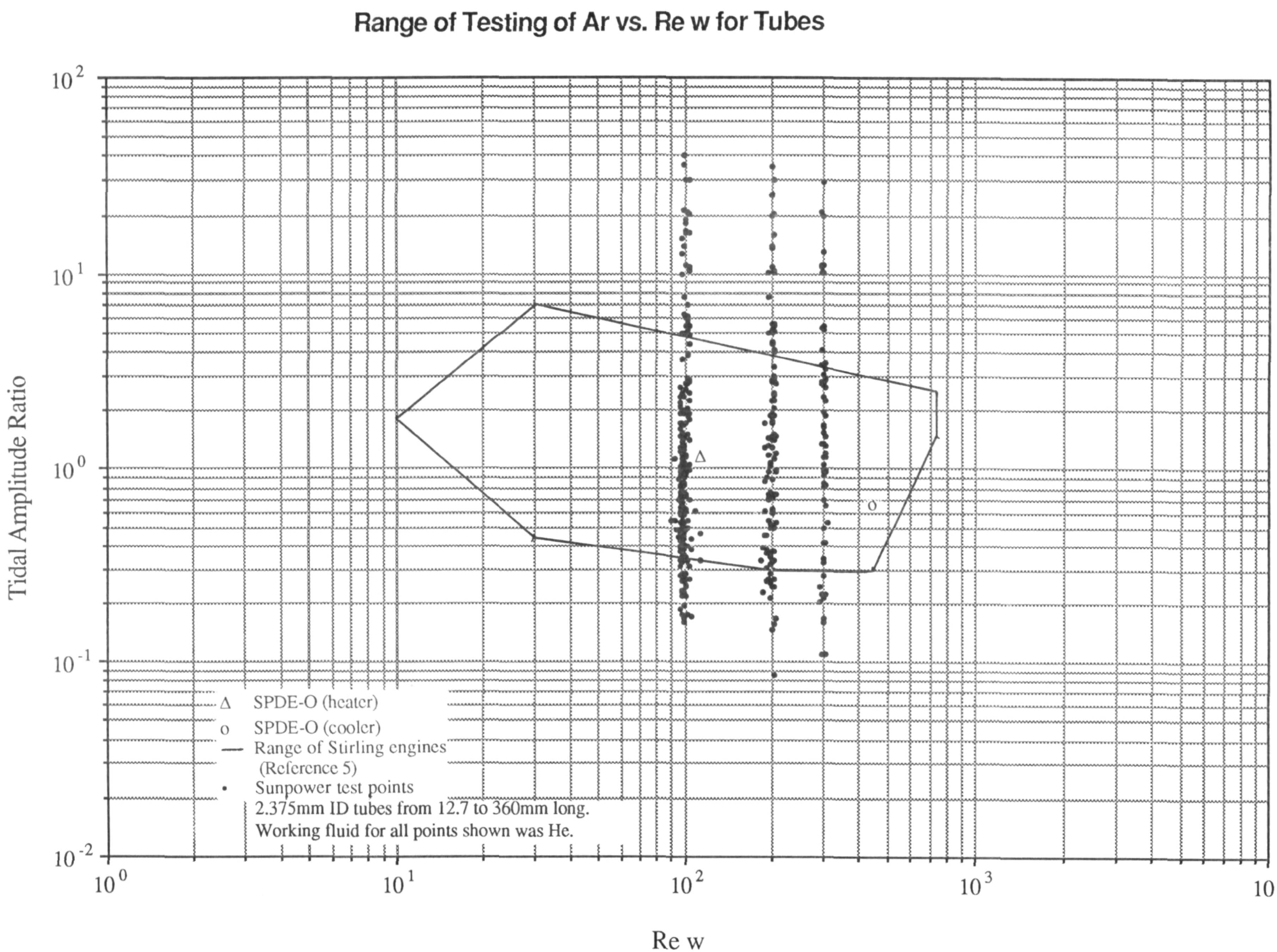

Range of Testing of Ar vs. Re w for Tubes
Tidal Amplitude Ratio
Re w
10^{2}
10^{1}
10^{0}
10^{-1}
10^{-2}
10^{0}
10^{1}
10^{2}
10^{3}
10^{4}
Δ SPDE-O (heater)
o SPDE-O (cooler)
— Range of Stirling engines (Reference 5)
• Sunpower test points
2.375mm ID tubes from 12.7 to 360mm long.
Working fluid for all points shown was He.

FIGURE 5.1-8

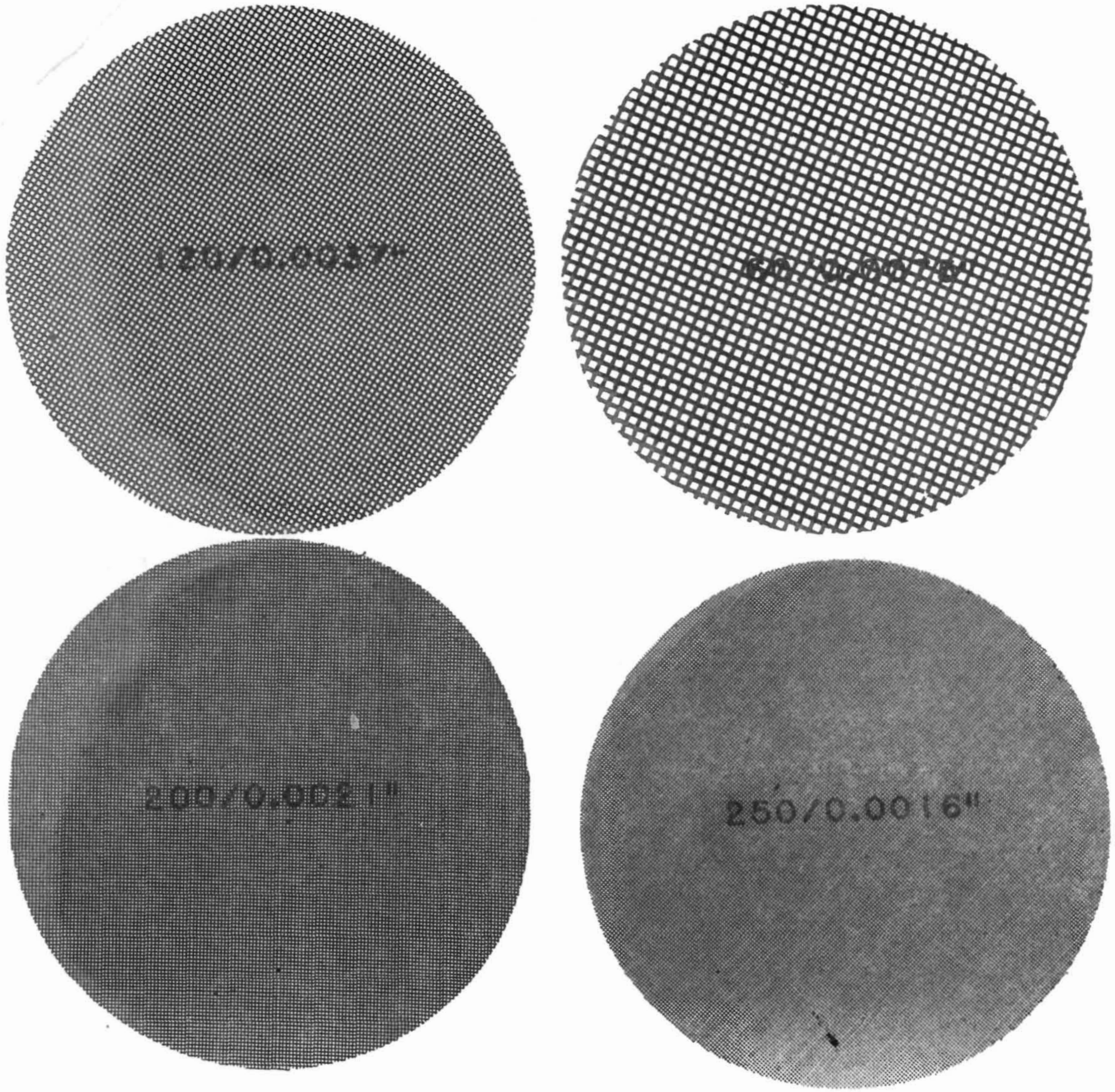

FIGURE 5.2-1 Stacked Regenerator Screen Test Samples (mesh/wire dia. inches)

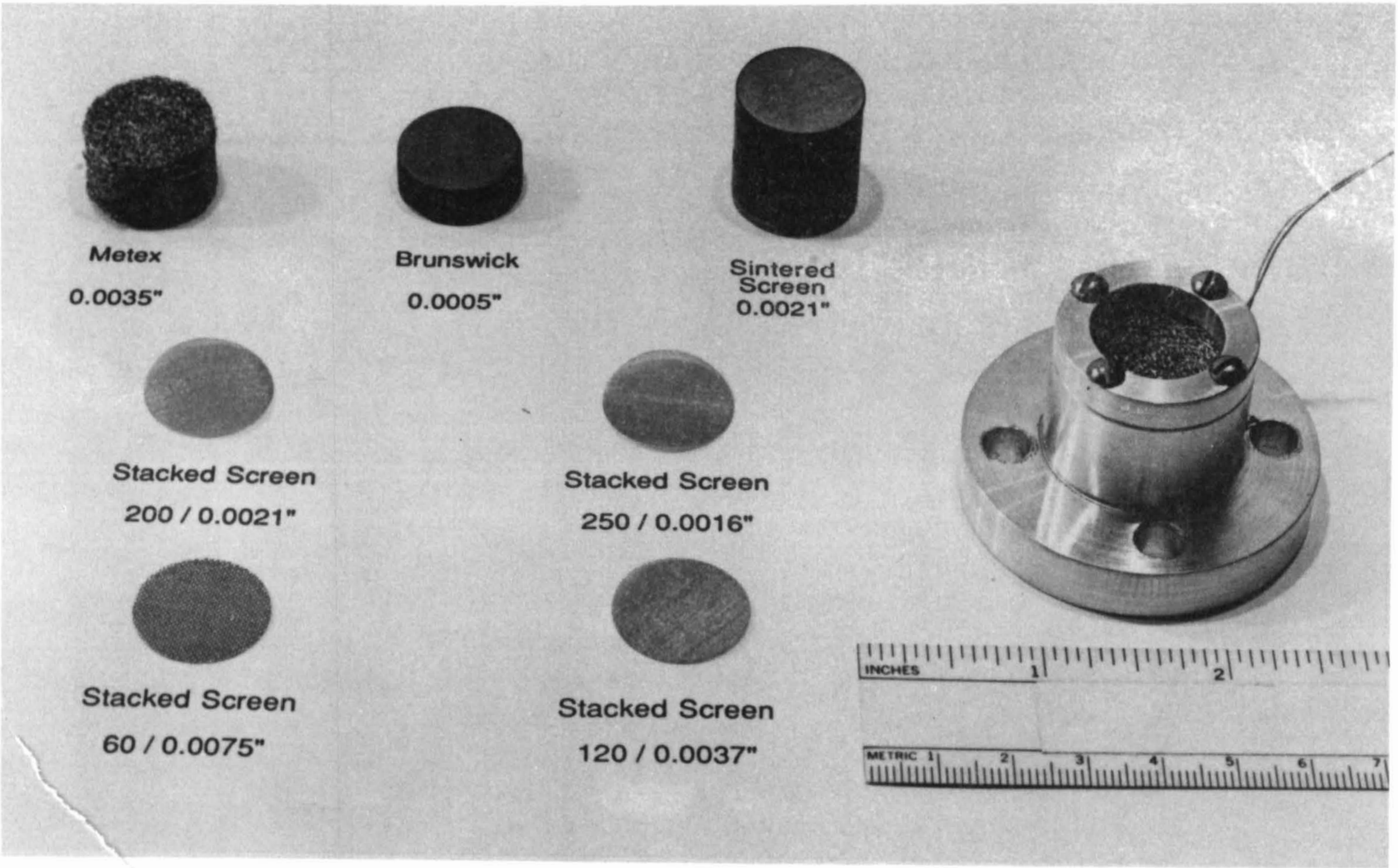

FIGURE 5.2-2 Regenerator Test Samples (mesh/wire dia. inches)

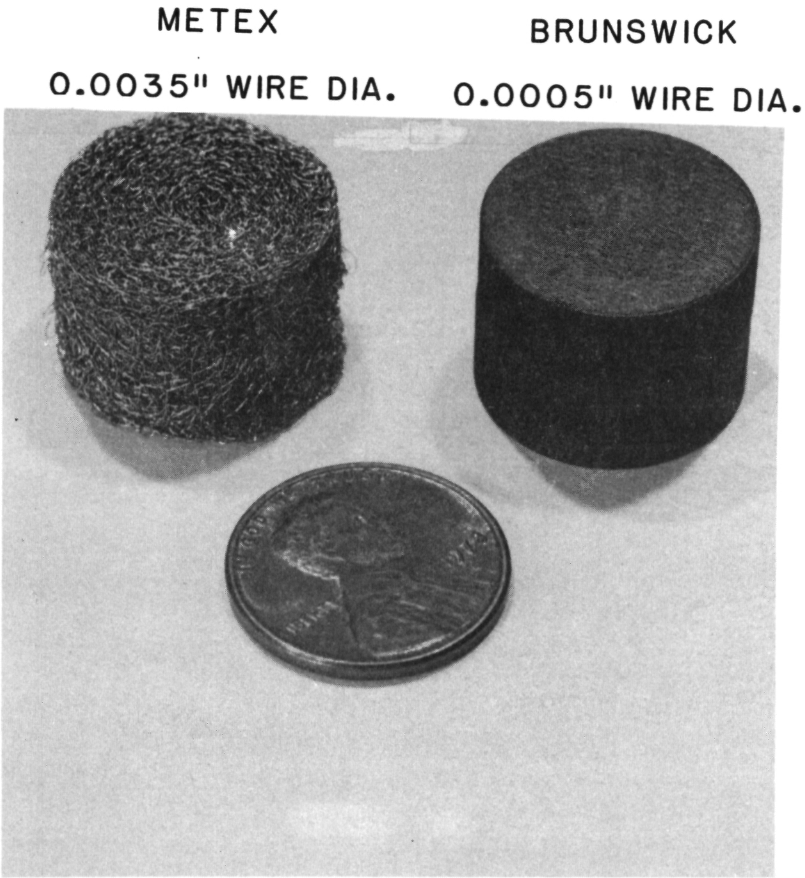

FIGURE 5.2-3 Random Fiber Regenerator Test Samples

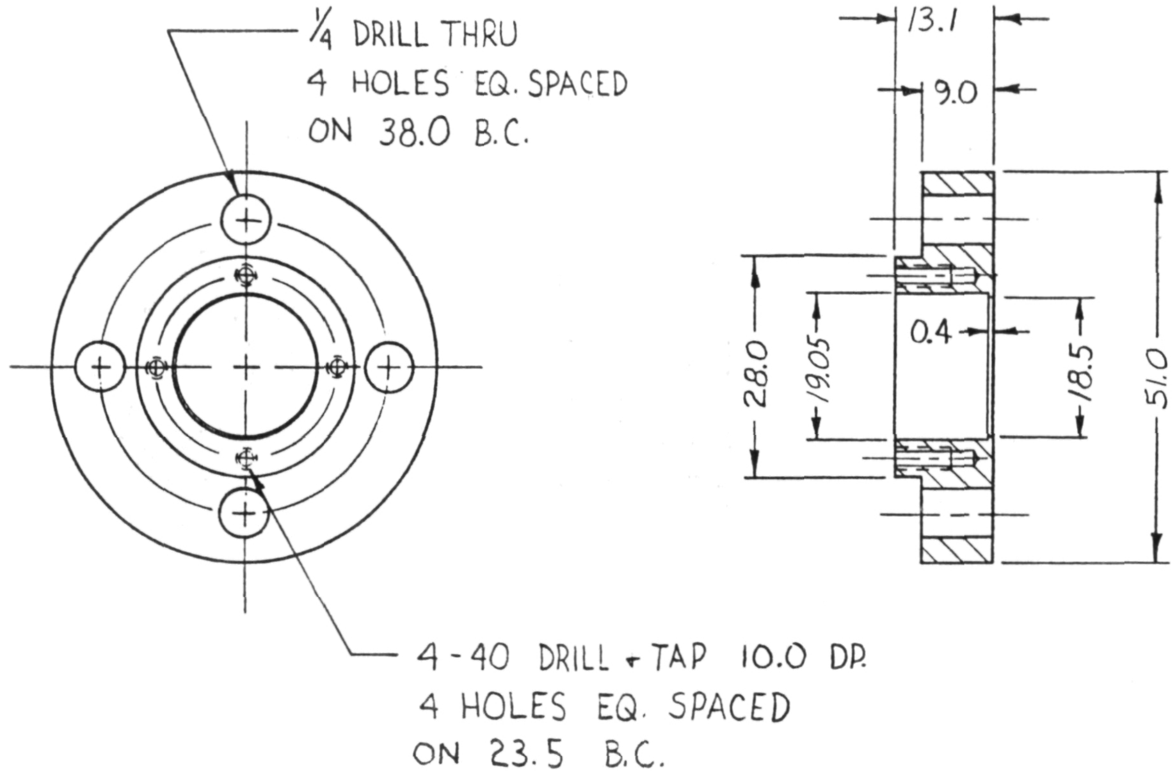

FIGURE 5.2-4 Regenerator Test Section Holder

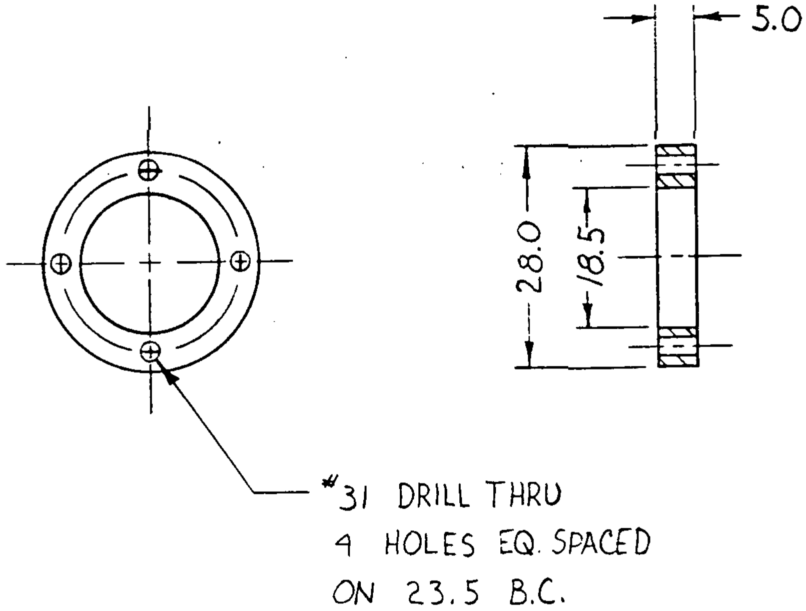

FIGURE 5.2-5 Regenerator Test Holder End Cap

Range of Testing of Re max vs. Re w for Regenerators

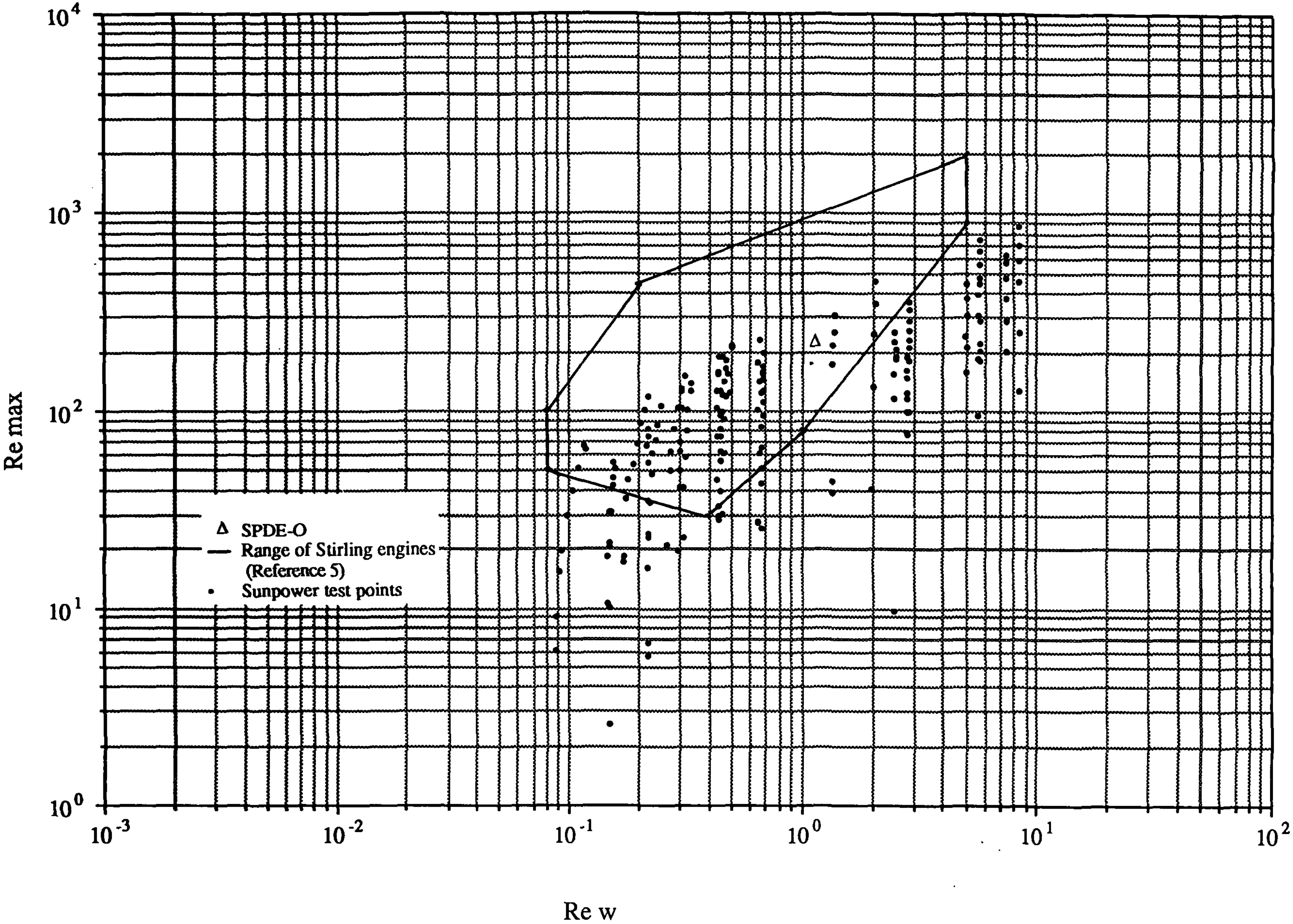

FIGURE 5.2-6

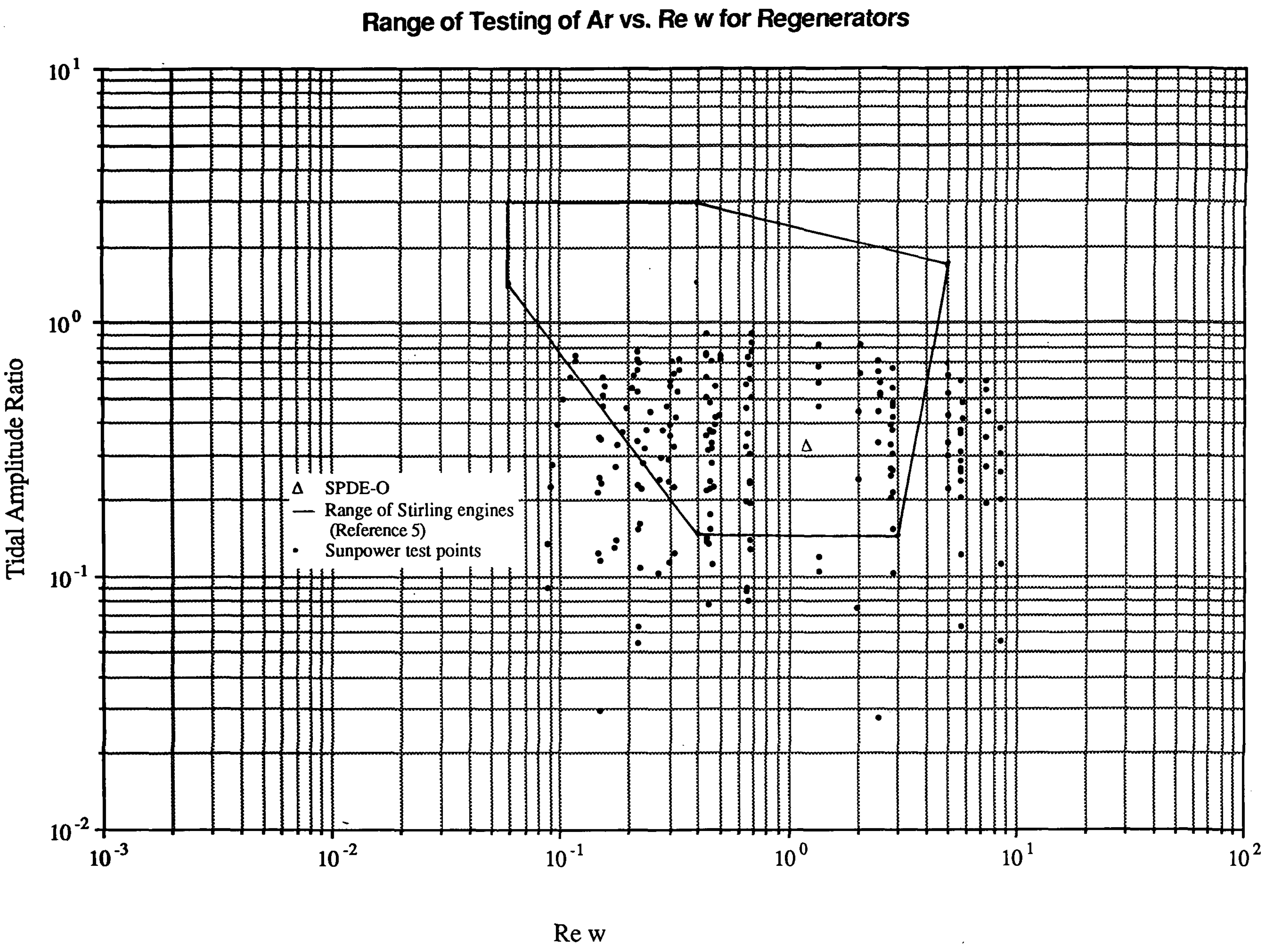

Range of Testing of Ar vs. Re w for Regenerators
10^1
10^0
10^{-1}
10^{-2}
Tidal Amplitude Ratio
Δ SPDE-O
— Range of Stirling engines (Reference 5)
• Sunpower test points
Δ
10^{-3}
10^{-2}
10^{-1}
10^0
10^1
10^2
Re w

FIGURE 5.2-7

Section 6

6.0 GRAPHICAL PRESENTATION OF THE TEST RESULTS

The results of the steady flow and oscillating flow loss tests are graphically presented in this section. The test results and parameters of primary interest are also presented in Appendix B. The oscillating flow database is stored on disks that are available from the Stirling Technology Branch at NASA Lewis; these disks are described in Appendix D.

6.1 STEADY FLOW LOSS TEST RESULTS

The results of the steady flow loss tests for the tube and regenerator heat exchangers outlined in Section 5 are graphically presented in this section and tabulated in Appendix B. The results are presented graphically in Figures 6.1-1 through 6.1-18. These figures are tabulated in Tables 6.1-1 and 6.1-2 for the tubes and regenerators, respectively. In addition, these figures are plotted to reflect the relationships between the following steady flow parameters:

Tubes

ΔP vs. *Re* as a function of *L/D*

Eu vs. *L/D* as a function of *Re*

*P*ratio vs. *Re* as a function of *L/D*

Regenerators

ΔP vs. *Re* as a function of d_w

Measured *f* vs. *Re* as a function of d_w

*P*ratio vs. *Re* as a function of d_w

The significance of the parameters plotted for the steady flow loss tests is discussed below.

Euler Number

The Euler number is the ratio of the static pressure force across the flow to the inertial force of the flow. This parameter is used to characterize momentum energy losses due to sudden flow enlargements or contractions (form losses).

Friction Factor

The friction factor for steady flow comes from the simplified form of Equation (2.3-8), which is:

$$F \approx \frac{1}{L}\left(P_3 - P_0\right) + K_t \frac{g\,|u|}{2L} \qquad (6.1\text{-}1)$$

where

$$F = -f \frac{g\,|u|}{2D_h} \qquad (6.1\text{-}2)$$

$$\Delta P = P_0 - P_3 \qquad (6.1\text{-}3)$$

Hence,

$$f = \left[\frac{2\Delta P}{g\,|u|} - K_t\right]\frac{D_h}{L} \qquad (6.1\text{-}4)$$

Note that in Equation (6.1-4) that

$$\text{Euler number} = \frac{2\Delta P}{g\,|u|}$$

*P*ratio

*P*ratio is the ratio of the measured static pressure drop to the predicted static pressure drop. The predicted pressure drop is calculated from Equation (6.1-1). The entrance/exit loss coefficients (K_t) for the tube tests are standard values obtained from the literature (8,9). For the regenerator tests, K_t was assumed to be zero.

The predicted steady flow pressure drop is also based on friction factor correlations used in GLIMPS. GLIMPS is short for GLobally IMPlicit Simulation, a Stirling cycle simulation based on a sophisticated computational model designed to run on a personal computer (10). These correlations are given in Equations (6.1-5) and (6.1-6) for tube heat exchangers, Equations (6.1-7) and (6.1-8) for stacked and sintered screen regenerators and Equation (6.1-9) for random fiber regenerators. They are as follows:

For tube heat exchangers:

Case: $Re > 4000$

$$f = 0.316\,Re^{-0.25} \tag{6.1-5}$$

Case: $Re < 3000$

$$f = 64/Re \tag{6.1-6}$$

The friction factor in the transition region is determined from an average of Equations (6.1-5) and (6.1-6).

For Stacked and Sintered Screens

Case: $Re > 1$

$$f = b10^{aRe^{-0.33}} \tag{6.1-7}$$

Case: $Re < 1$

$$f = cRe^{-1} \tag{6.1-8}$$

where

β = porosity

$$\sigma = \left(1.27\,\beta - 0.27\right)^2$$

$$a = \frac{1.33}{\beta^2}\left(\left(1 - \beta\right)/\sigma\right)^{-0.33}$$

$$b = 10^{\left(-0.54/\beta\right)}\frac{\beta^3}{2\left(1-\beta\right)\sigma^2}$$

$$c = b10^a$$

For Random Fibers

$$f = (153/Re + 1.5)\,\beta^{-0.6} \tag{6.1-9}$$

6.2 OSCILLATING FLOW LOSS TEST RESULTS

The results of the oscillating flow loss tests outlined in Section 5 are graphically presented in this section. The primary test results are tabulated in Appendix B for the tube and regenerator heat exchangers. These results are herein presented in Figures 6.2-1 through 6.2-68. These figures are tabulated in Tables 6.2-1 and 6.2-2 for tubes and regenerators, respectively, and plotted for the following parameters:

Tubes

ΔP_{max}	vs.	Re_{max} as a function of Re_{ω} and L/D
Total Power Dissipation	vs.	Re_{max} as a function of Re_{ω} and L/D
Eu	vs.	A_r as a function of Re_{ω}
Eu	vs.	Re_{max} as a function of Re_{ω}
TDF	vs.	Re_{max} as a function of L/D
TDF	vs.	A_r as a function of L/D
TDF	vs.	Re_{max} as a function of Re_{ω}

Regenerators

ΔP_{max}	vs.	Re_{max} as a function of Re_{ω} and d_w
Total Power Dissipation	vs.	Re_{max} as a function of Re_{ω} and d_w
TDF	vs.	Re_{max} as a function of d_w
TDF	vs.	Re_{max} as a function of Re_{ω}

The significance of the parameters plotted for the oscillating flow loss tests is discussed below.

Euler Number

The Euler number in cyclic oscillating flow is the ratio of the maximum static pressure force to the maximum inertial forces based on the maximum cycle velocity. The Euler number is useful in characterizing the momentum energy losses due to sudden flow enlargements and contractions and highly turbulent frictional flow. If Equations (2.3-8) and (6.1-2) are combined, where:

$$F \approx \frac{\Delta P}{L} + \frac{\sigma^2}{2L} g u + \frac{K_t}{2L} g \left| u \right| + \frac{\partial g}{\partial t} \tag{2.3-8}$$

and

$$F = -f \frac{g \left| u \right|}{2D_h} \tag{6.1-2}$$

and rearranged, we have

$$\mathrm{Eu} = \frac{2\Delta P}{g \left| u \right|} \approx f \frac{L}{D_h} + \sigma^2 + K_t + \frac{2L}{g \left| u \right|} \frac{\partial g}{\partial t} \tag{6.2-1}$$

Note that as L and σ^2 approach zero, Equation (6.2-1) reduces to

$$\mathrm{Eu} = \frac{2\Delta P}{g \left| u \right|} \approx K_t \tag{6.2-2}$$

where Euler number is calculated at the maximum parameter amplitudes. If instead, L/D_h is held constant in Equation (6.2-1), knowing that σ^2 and K_t are constant, and further noting that:

$$\frac{2L}{g\,|\,u\,|}\frac{\partial g}{\partial t}=\frac{2L\,Re_{\omega}}{D_h Re_{max}}=\frac{1}{A_r} \qquad (6.2\text{-}3)$$

we find that the ratio of static pressure to inertia forces is proportional to the value of the friction factor, f, and inversely proportional to the amplitude of the flow displacement, A_r. We also know that f varies radically as the flow varies from laminar to transitional to turbulent regimes. This will be useful to interpreting the data discussed in Section 7.

Total Dissipation Factor

In the oscillating flow data reduction process, Total Dissipation Factor (TDF) is defined as the ratio of pumping dissipation produced by the total measured pressure drop, ΔP, to the pumping dissipation calculated using cycle-integrated steady flow predicted pressure drop. To wit,

$$\mathrm{TDF}=\frac{2\int \Delta P u}{\int\left(\left(f\frac{L}{D_h}K_t\right)g\,|\,u\,|\right)u} \qquad (6.2\text{-}4)$$

where u is gas velocity calculated from measured parameters, g is mass flow rate per unit area calculated from measured parameters, L is length, D_h is hydraulic diameter, f is Darcy friction factor from steady flow correlations, and K_t is an entrance/exit coefficient obtained from a steady flow correlation; both f and K_t are found at the instantaneous flow conditions.

Table 6.1-1
Listing of Graphs
Tube Steady Flow Test Results

Graph	Test Sample	Figure No.
ΔP vs. Re, function L/D_h	Square Ended Tubes	6.1-1
	Round Ended Tubes	6.1-2
	Protruding Tubes	6.1-3
Eu vs. L/D, function Re		
	Square Ended tubes	6.1-4
	Round Ended Tubes	6.1-5
	Protruding Tubes	6.1-6
Pratio vs. Re, function L/D		
	Square Ended Tubes	6.1-7
	Round Ended Tubes	6.1-8
	Protruding Tubes	6.1-9

Table 6.1-2
Listing of Graphs
Regenerator Steady Flow Test Results

Graph	Test Sample	Figure No.
ΔP vs. Re, function d_w	Stacked Screens	6.1-10
	Random Fibers	6.1-11
	Sintered Screens	6.1-12
f vs. Re, function d_w	Stacked Screens	6.1-13
	Random Fibers	6.1-14
	Sintered Screens	6.1-15
Pratio vs. Re, function d_w	Stacked Screens	6.1-16
	Random Fibers	6.1-17
	Sintered Screens	6.1-18

Table 6.2-1
Listing of Graphs
Tube Oscillating Flow Test Results

Graph	Test Sample	Figure No.
ΔP vs. Re_{max}, function L/D		
@ $Re_{\omega} = 100$	Square Ended Tubes	6.2-1
	Round Ended Tubes	6.2-2
	Protruding Tubes	6.2-3
@ $Re_{\omega} = 200$	Square Ended Tubes	6.2-4
	Round Ended Tubes	6.2-5
@ $Re_{\omega} = 300$	Square Ended Tubes	6.2-6
	Round Ended Tubes	6.2-7
Total Power Dissipation vs. Re_{max}, function L/D		
@ $Re_{\omega} = 100$	Square Ended Tubes	6.2-8
	Round Ended Tubes	6.2-9
	Protruding Tubes	6.2-10

Graph/Test Sample	L/D	Figure No.
Eu vs. A_r, function Re_{ω}		
Square Ended Tubes	@ $L/D = 5.35$	6.2-11
	$L/D = 10$	6.2-12
	$L/D = 25$	6.2-13
	$L/D = 50$	6.2-14
	$L/D = 100$	6.2-15
Round Ended Tubes	@ $L/D = 5.35$	6.2-16
	$L/D = 10$	6.2-17
	$L/D = 25$	6.2-18
	$L/D = 50$	6.2-19
	$L/D = 100$	6.2-20
Protruding Tubes	@ $L/D = 84$	6.2-21

Table 6.2-1(continued)

Graph/Test Sample	***L/D***	**Figure No.**
Eu vs. Re_{max}, function Re_{ω}		
Square Ended Tubes	@ $L/D = 25$	6.2-22
	$L/D = 50$	6.2-23
	$L/D = 100$	6.2-24
Round Ended Tubes	@ $L/D = 25$	6.2-25
	$L/D = 50$	6.2-26
	$L/D = 100$	6.2-27

Graph	**Test Sample**	**Figure No.**
TDF vs. Re_{max}, function L/D		
@ $Re_{\omega} = 100$	Square Ended Tubes	6.2-28
	Round Ended Tubes	6.2-29
	Protruding Tubes	6.2-30
TDF vs. A_r, function L/D		
@ $Re_{\omega} = 100$	Square Ended Tubes	6.2-31
	Round Ended Tubes	6.2-32
	Protruding Tubes	6.2-33

Graph/Test Sample	***L/D***	**Figure No.**
TDF vs. Re_{max}, function Re_{ω}		
Square Ended Tubes	@ $L/D = 5.35$	6.2-34
	$L/D = 10$	6.2-35
	$L/D = 25$	6.2-36
	$L/D = 50$	6.2-37
	$L/D = 100$	6.2-38
	$L/D = 150$	6.2-39
Round Ended Tubes	@ $L/D = 5.35$	6.2-40
	$L/D = 10$	6.2-41
	$L/D = 25$	6.2-42
	$L/D = 50$	6.2-43

Table 6.2-2
Listing of Graphs
Oscillating Flow Regenerator Test Results

Graph	Test Sample	Figure No.
ΔP_{max} vs. Re_{max}, function Re_ω		
	Stacked Screens	6.2-44 through 6.2-47
	Random Fibers	6.2-48 through 6.2-49
	Sintered Screens	6.2-50 through 6.2-51
Total Power Dissipation vs. Re_{max}, function Re_ω		
	Stacked Screens	6.2-52 through 55
	Random Fibers	6.2-56 through 57
	Sintered Screens	6.2-58 through 59
TDF vs. Re_{max}, function d_w		
	Stacked Screens	6.2-60
	Random Fibers	6.2-61
	Sintered Screens	6.2-62
TDF vs. Re_{max}, function Re_ω		
	Stacked Screens	6.2-63 through 64
	Random Fibers	6.2-65 through 66
	Sintered Screens	6.2-67 through 68

<u>TUBE STEADY FLOW TEST RESULTS</u>

FIGURES 6.1-1 through 6.1-9

Steady Flow Test Results for Square Ended Tubes
Pressure Drop vs Re and L/D

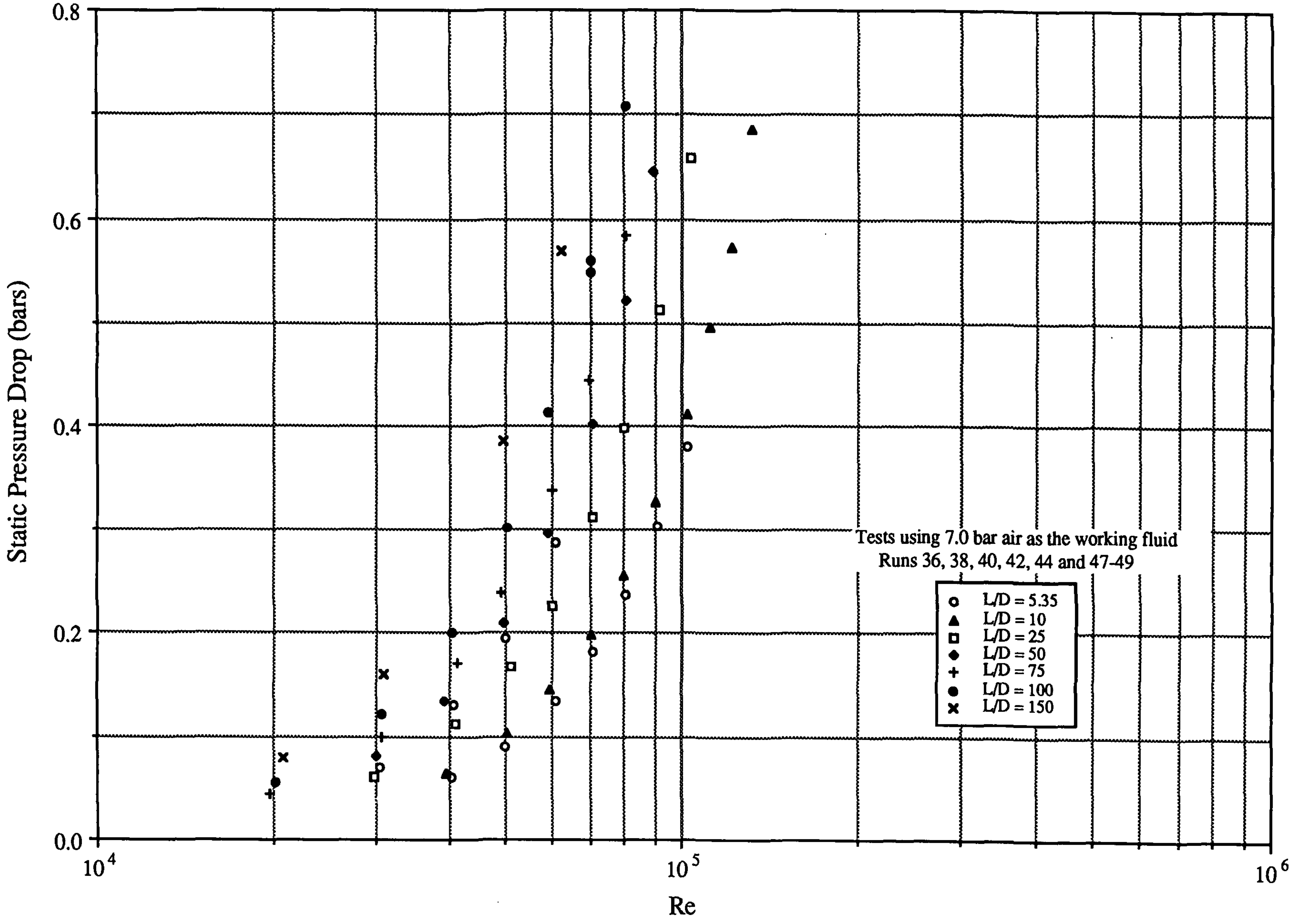

FIGURE 6.1-1

Steady Flow Test Results for Rounded Tubes
Pressure Drop vs Re and L/D

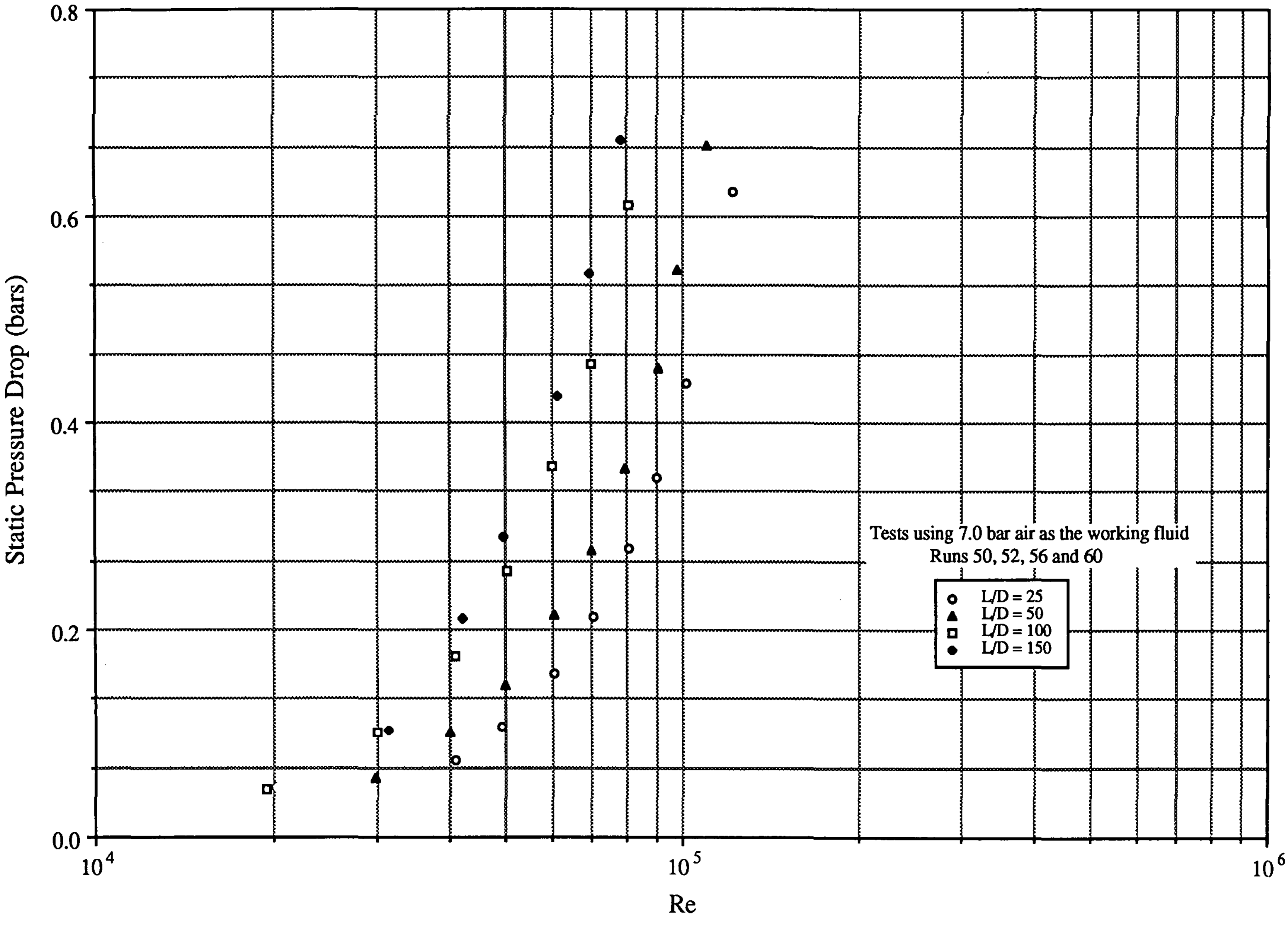

FIGURE 6.1-2

Steady Flow Test Results for Protruding Tubes
Pressure Drop vs Re and L/D

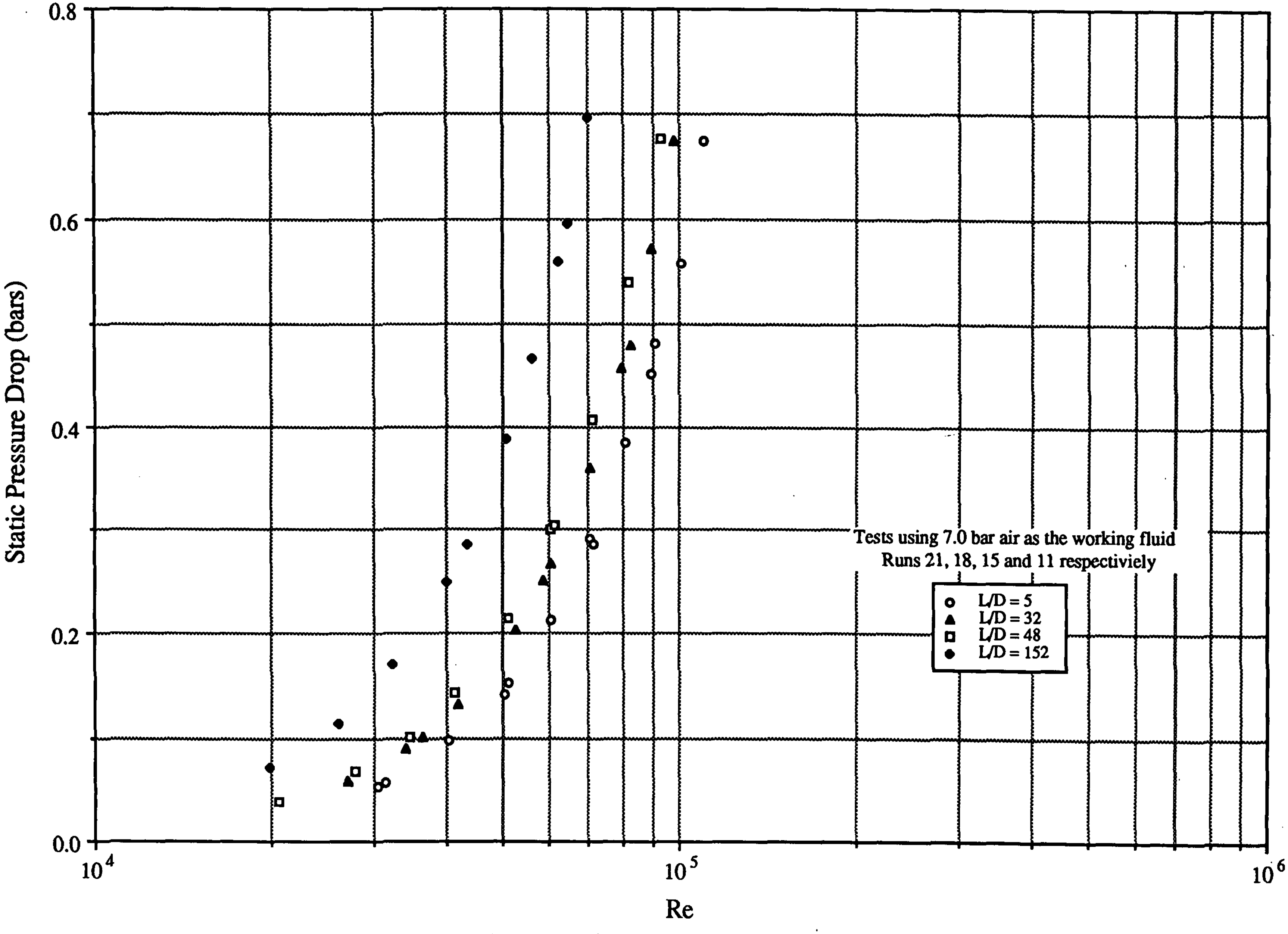

FIGURE 6.1-3

Steady Flow Test Results for Square Ended Tubes
Euler No. vs Re and L/D

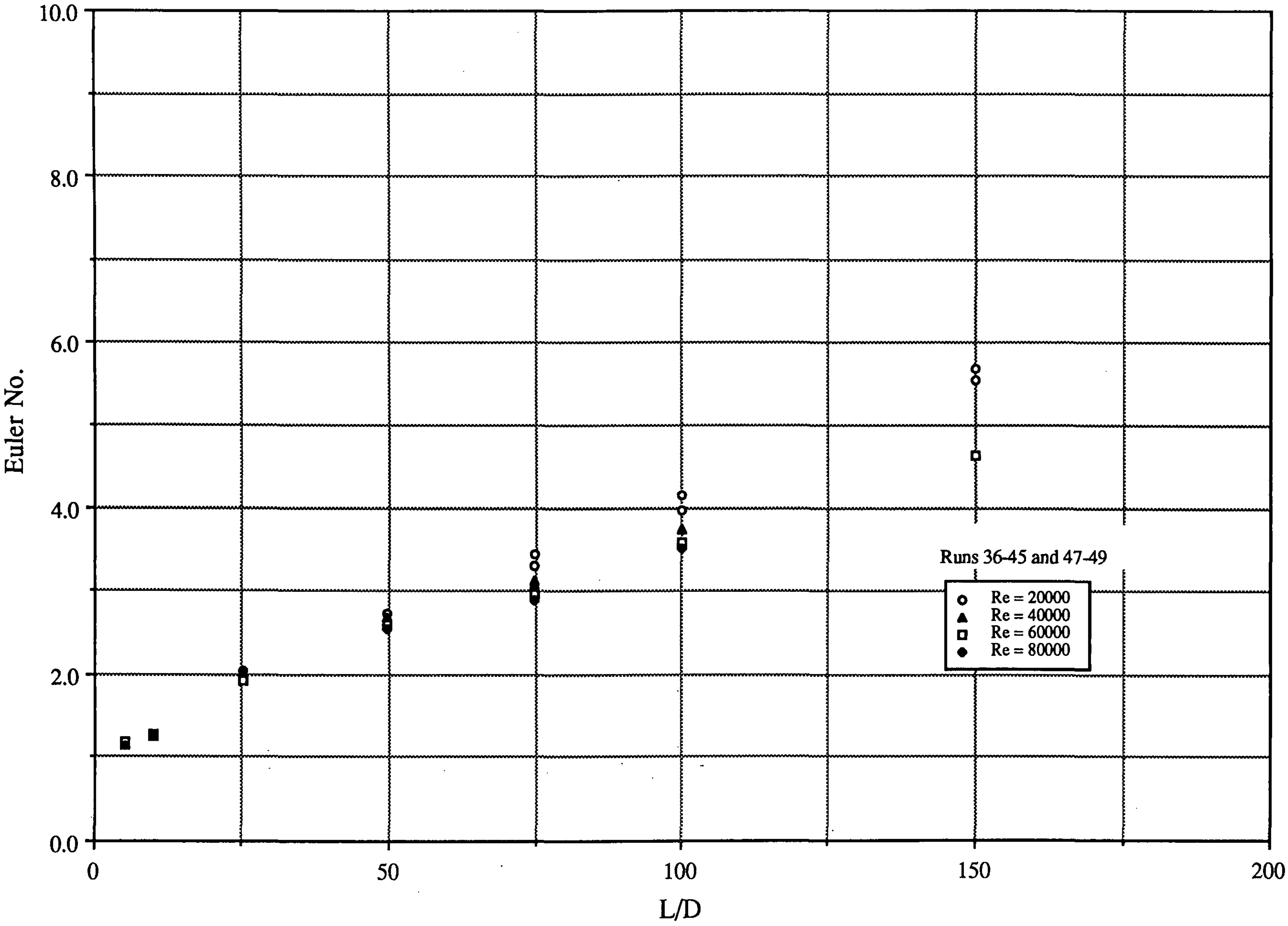

FIGURE 6.1-4

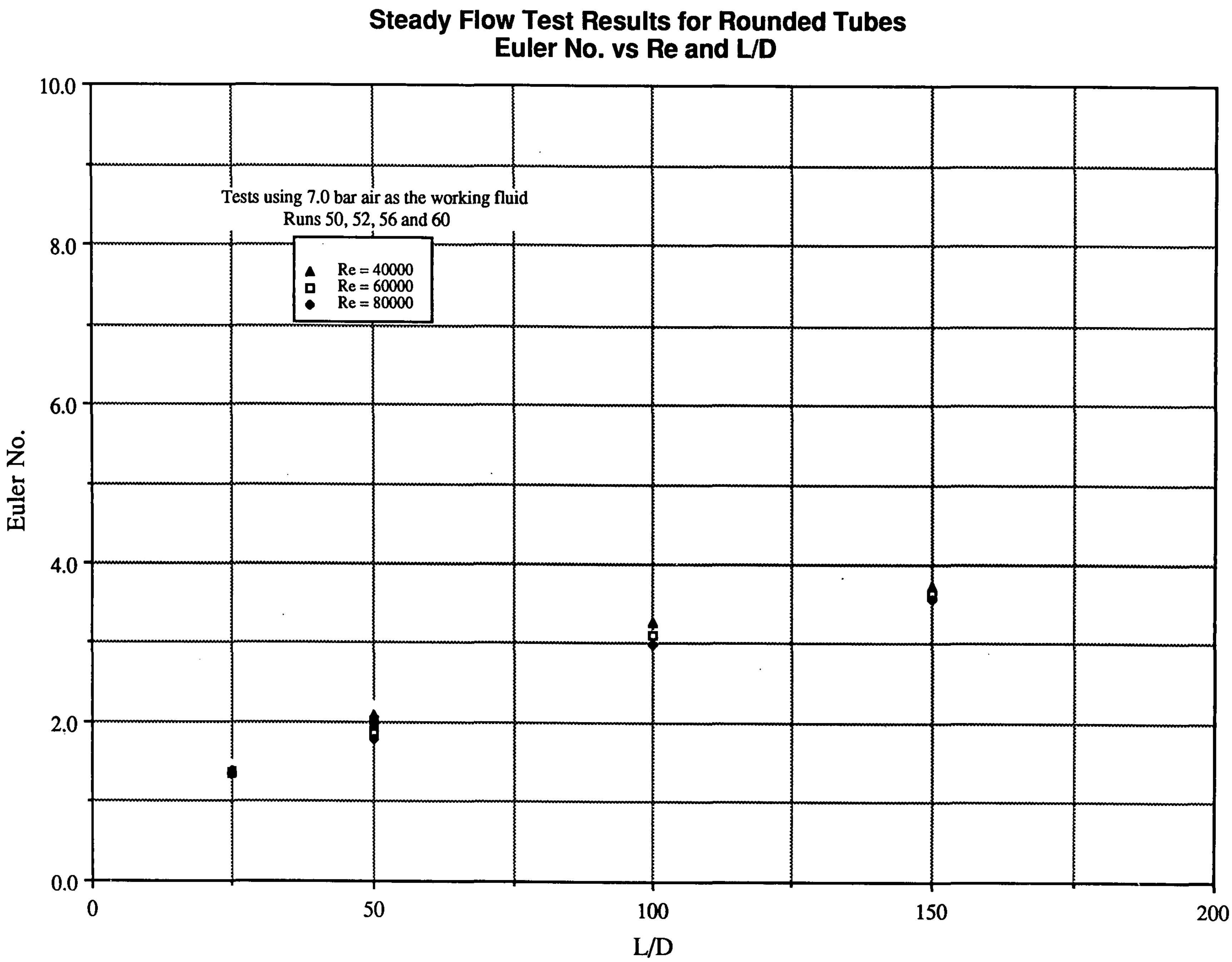
Steady Flow Test Results for Rounded Tubes
Euler No. vs Re and L/D
Tests using 7.0 bar air as the working fluid
Runs 50, 52, 56 and 60
Re = 40000
Re = 60000
Re = 80000
Euler No.
L/D
10.0
8.0
6.0
4.0
2.0
0.0
0
50
100
150
200
FIGURE 6.1-5

Steady Flow Test Results for Protruding Tubes
Euler No. vs Re and L/D

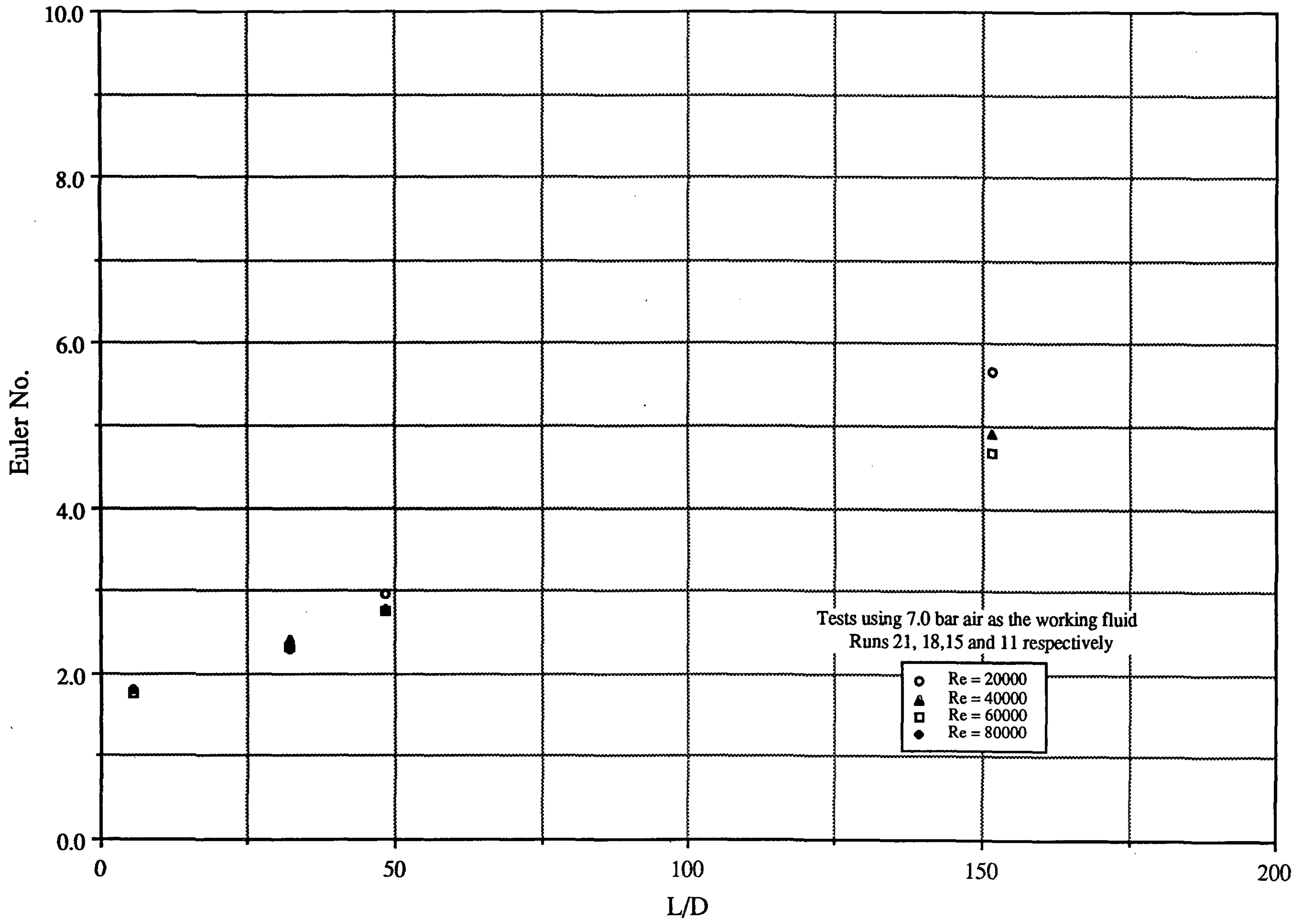

FIGURE 6.1-6

Steady Flow Test Results for Square Ended Tubes
Pratio vs Re and L/D

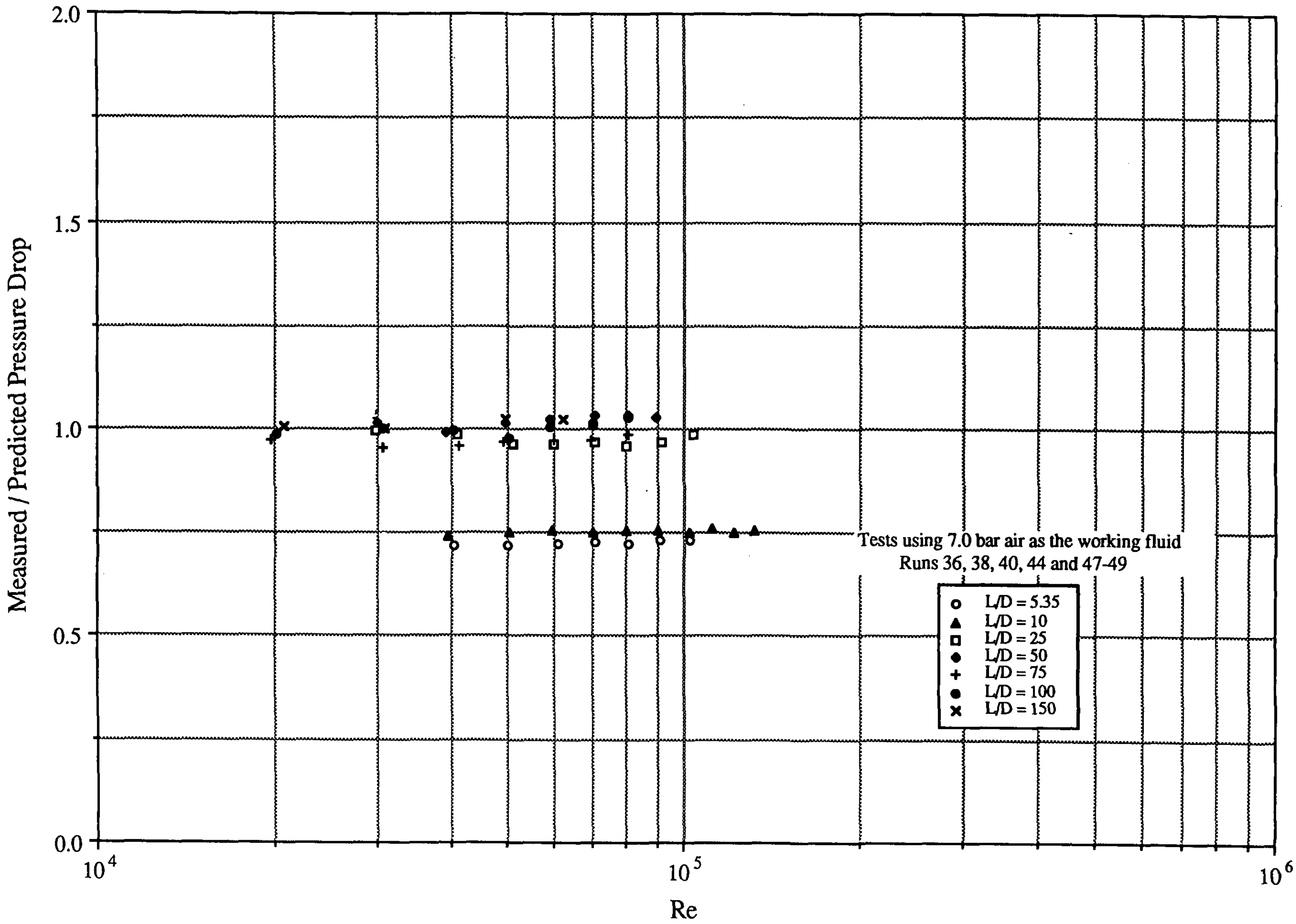

FIGURE 6.1-7

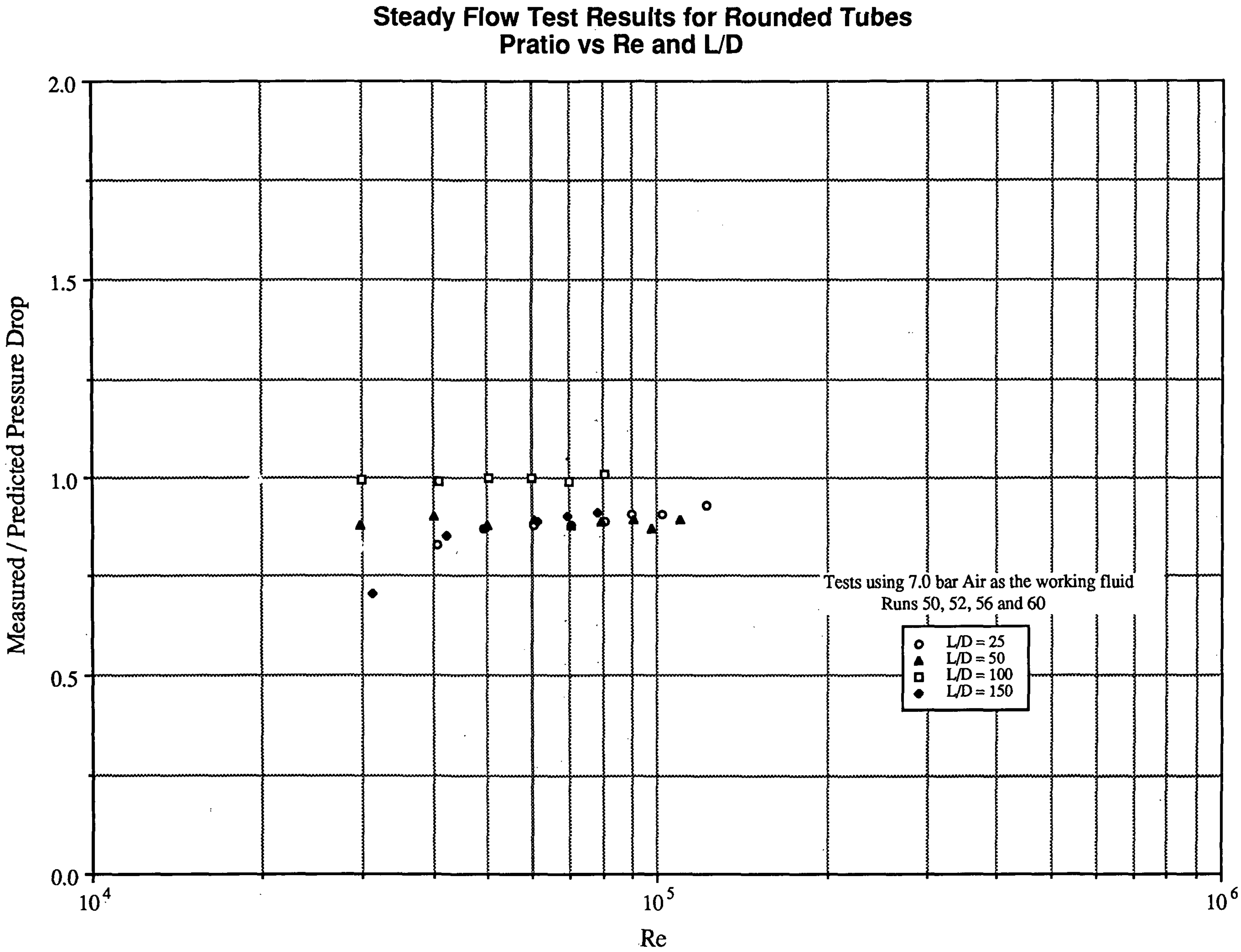
Steady Flow Test Results for Rounded Tubes
Pratio vs Re and L/D
Measured / Predicted Pressure Drop
2.0
1.5
1.0
0.5
0.0
10^4
10^5
10^6
Re
Tests using 7.0 bar Air as the working fluid
Runs 50, 52, 56 and 60
L/D = 25
L/D = 50
L/D = 100
L/D = 150

FIGURE 6.1-8

Steady Flow Test Results for Protruding Tubes
Pratio vs Re and L/D

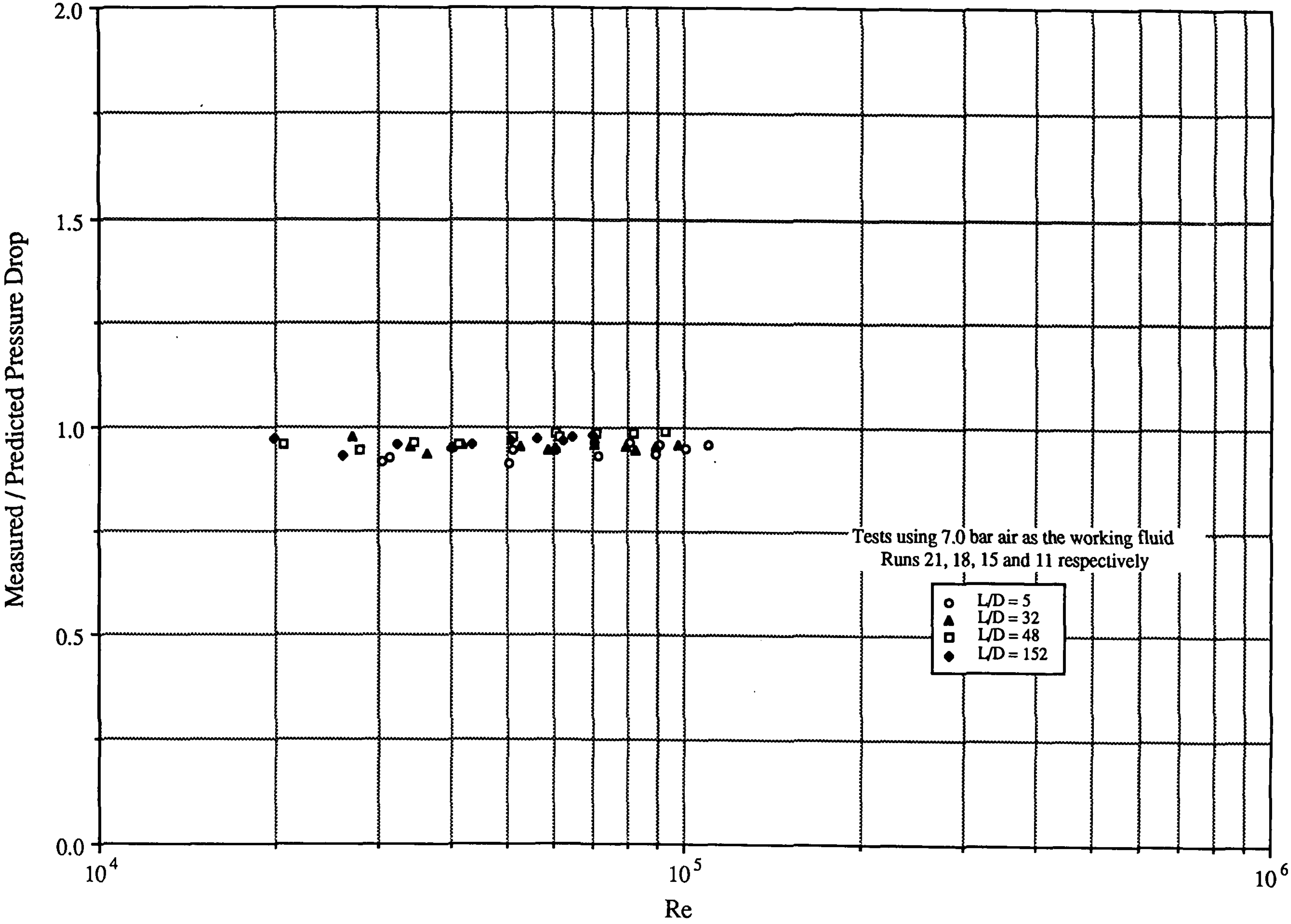

FIGURE 6.1-9

REGENERATOR STEADY FLOW TEST RESULTS

Figures 6.1-10 through 6.1-18

Steady Flow Test Results for Stacked Screen Regenerator
Pressure Drop vs Re and Wire Diameter

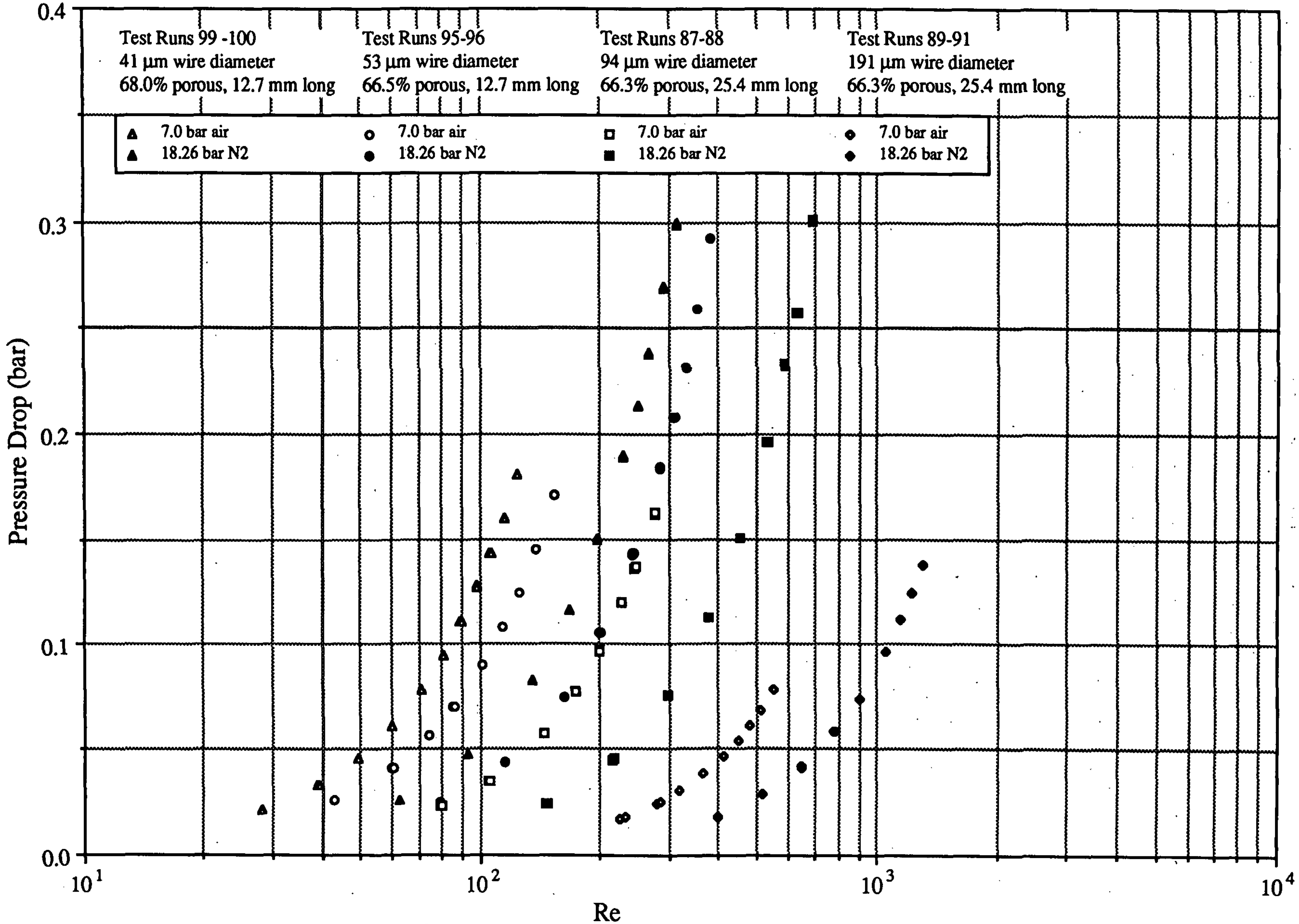

FIGURE 6.1-10

Steady Flow Test Results for Random Fiber Regenerator
Pressure Drop vs Re and Wire Diameter

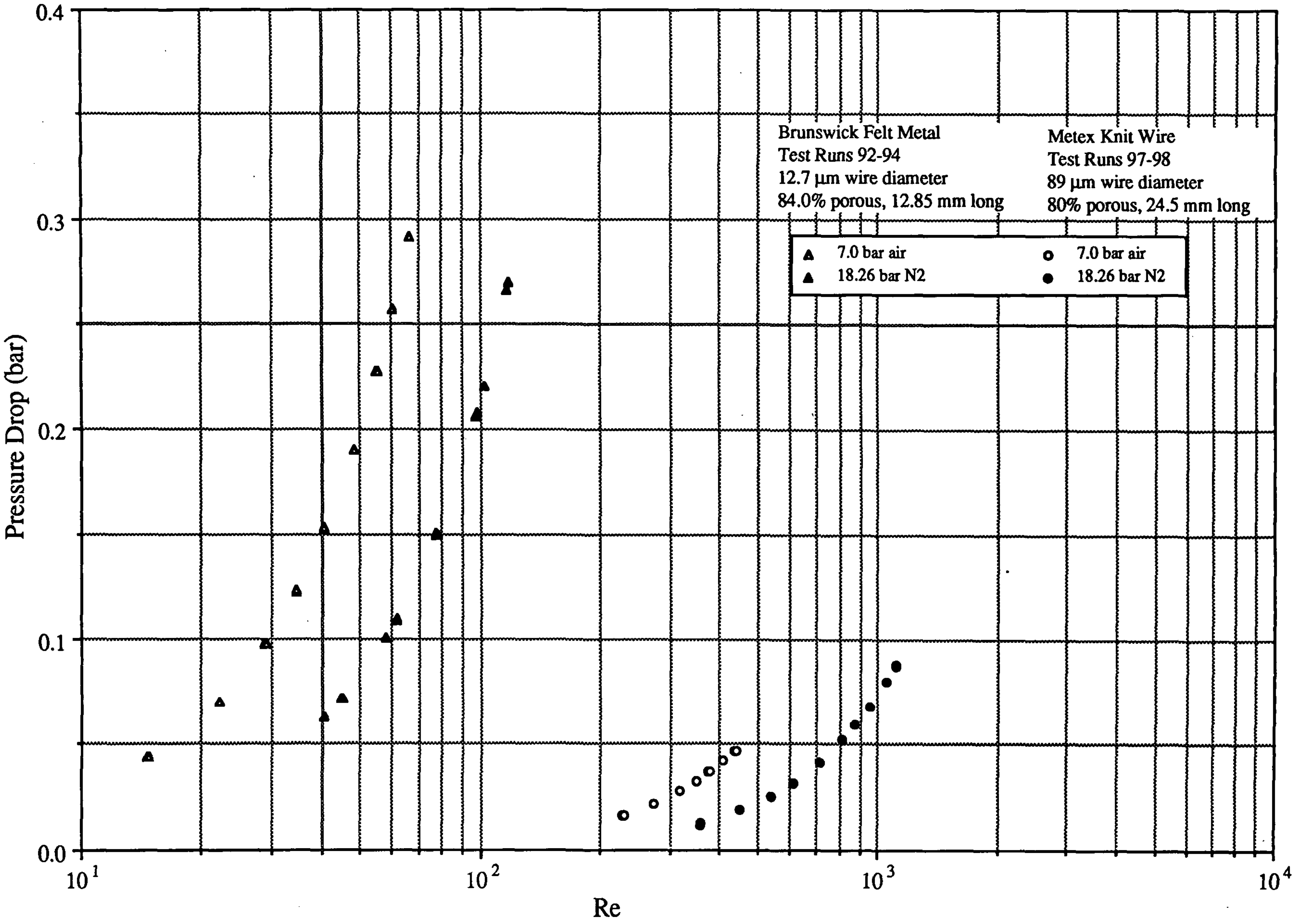

FIGURE 6.1-11

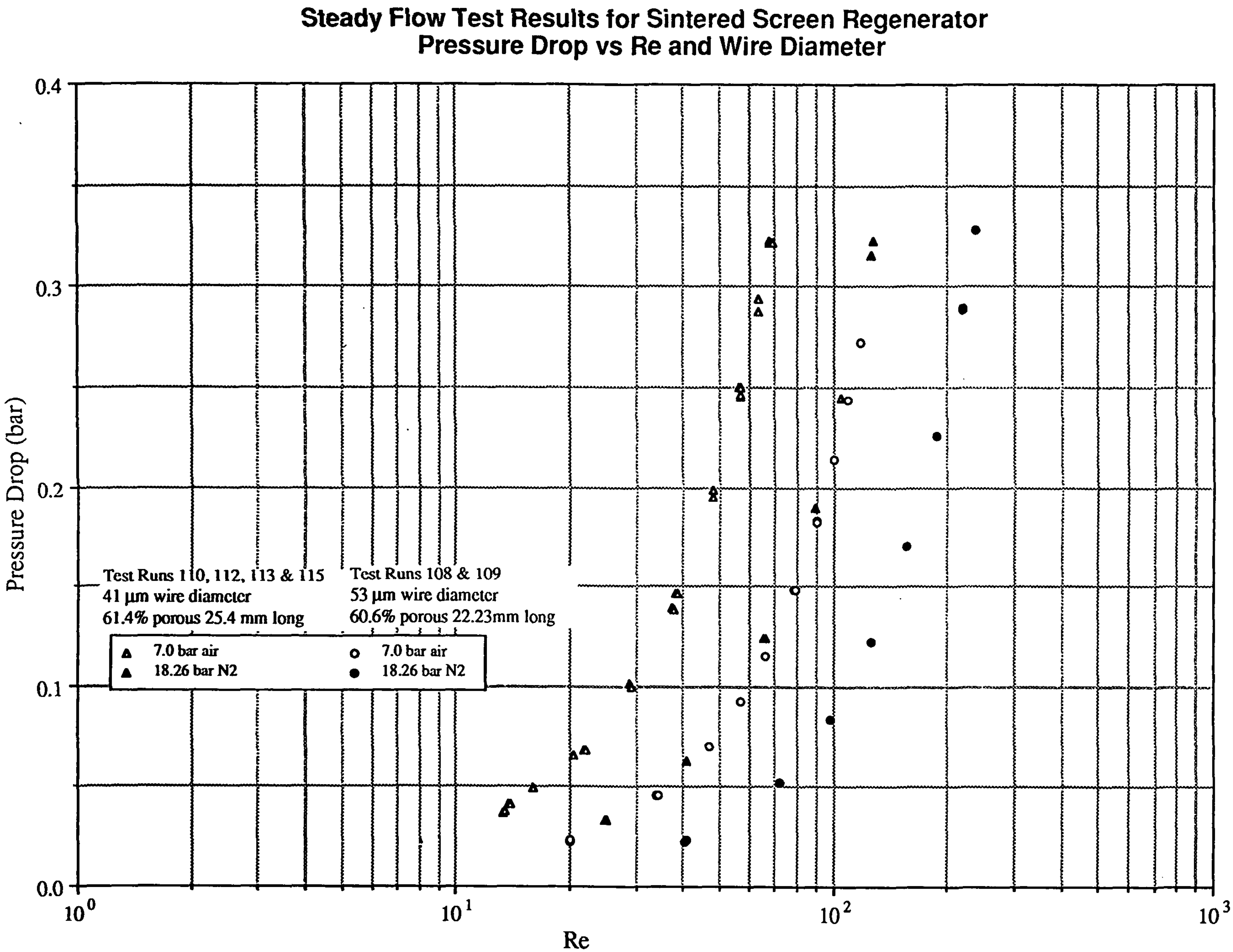
Steady Flow Test Results for Sintered Screen Regenerator
Pressure Drop vs Re and Wire Diameter
Pressure Drop (bar)
0.4
0.3
0.2
0.1
0.0
Test Runs 110, 112, 113 & 115
41 µm wire diameter
61.4% porous 25.4 mm long
Test Runs 108 & 109
53 µm wire diameter
60.6% porous 22.23mm long
7.0 bar air
18.26 bar N2
7.0 bar air
18.26 bar N2
10^0
10^1
10^2
10^3
Re

FIGURE 6.1-12

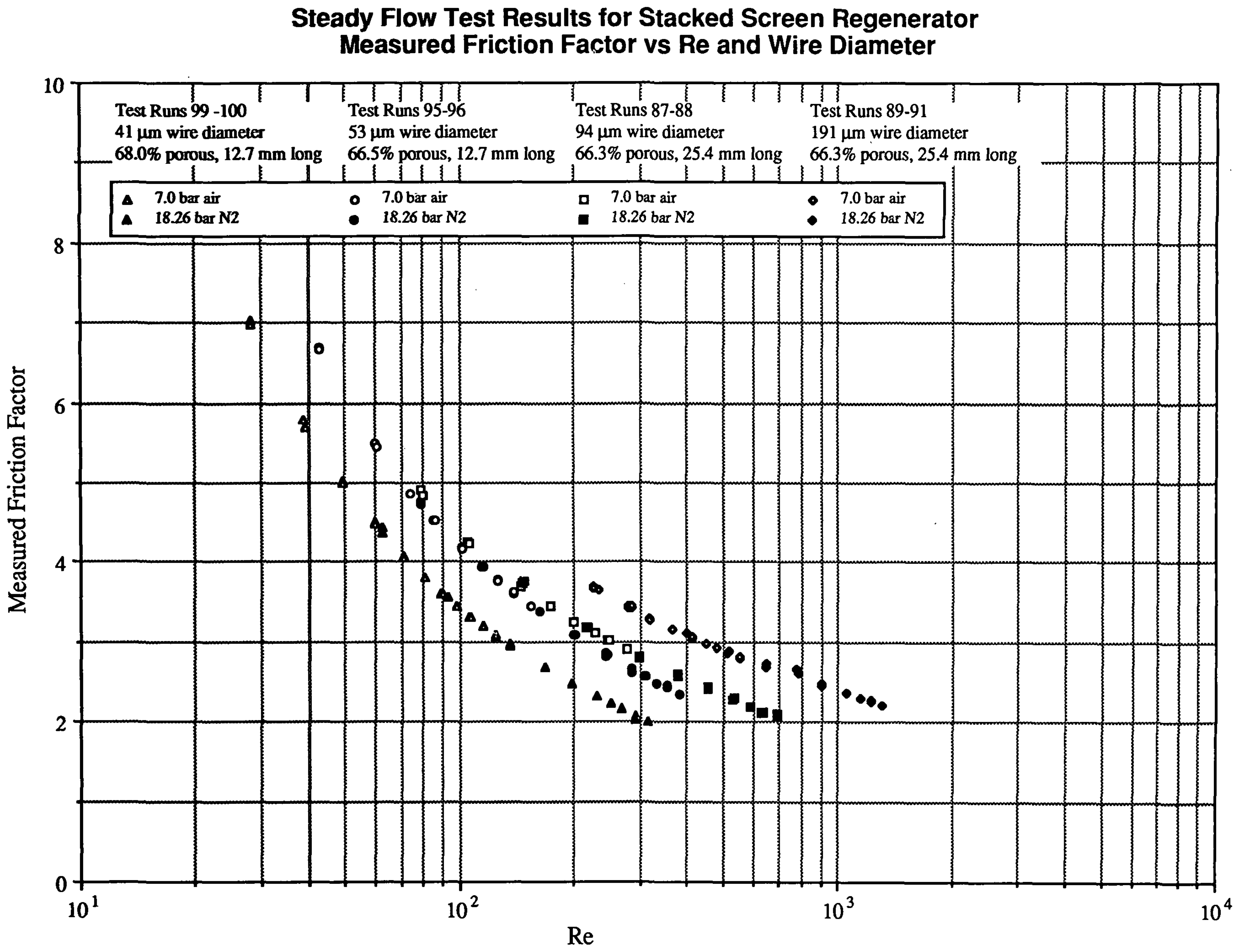

Steady Flow Test Results for Stacked Screen Regenerator
Measured Friction Factor vs Re and Wire Diameter
Test Runs 99 -100
41 μm wire diameter
68.0% porous, 12.7 mm long
Test Runs 95-96
53 μm wire diameter
66.5% porous, 12.7 mm long
Test Runs 87-88
94 μm wire diameter
66.3% porous, 25.4 mm long
Test Runs 89-91
191 μm wire diameter
66.3% porous, 25.4 mm long
7.0 bar air
18.26 bar N2
Measured Friction Factor
Re
10
8
6
4
2
0
10^1
10^2
10^3
10^4

FIGURE 6.1-13

Steady Flow Test Results for Random Fiber Regenerator
Measured Friction Factor vs Re and Wire Diameter

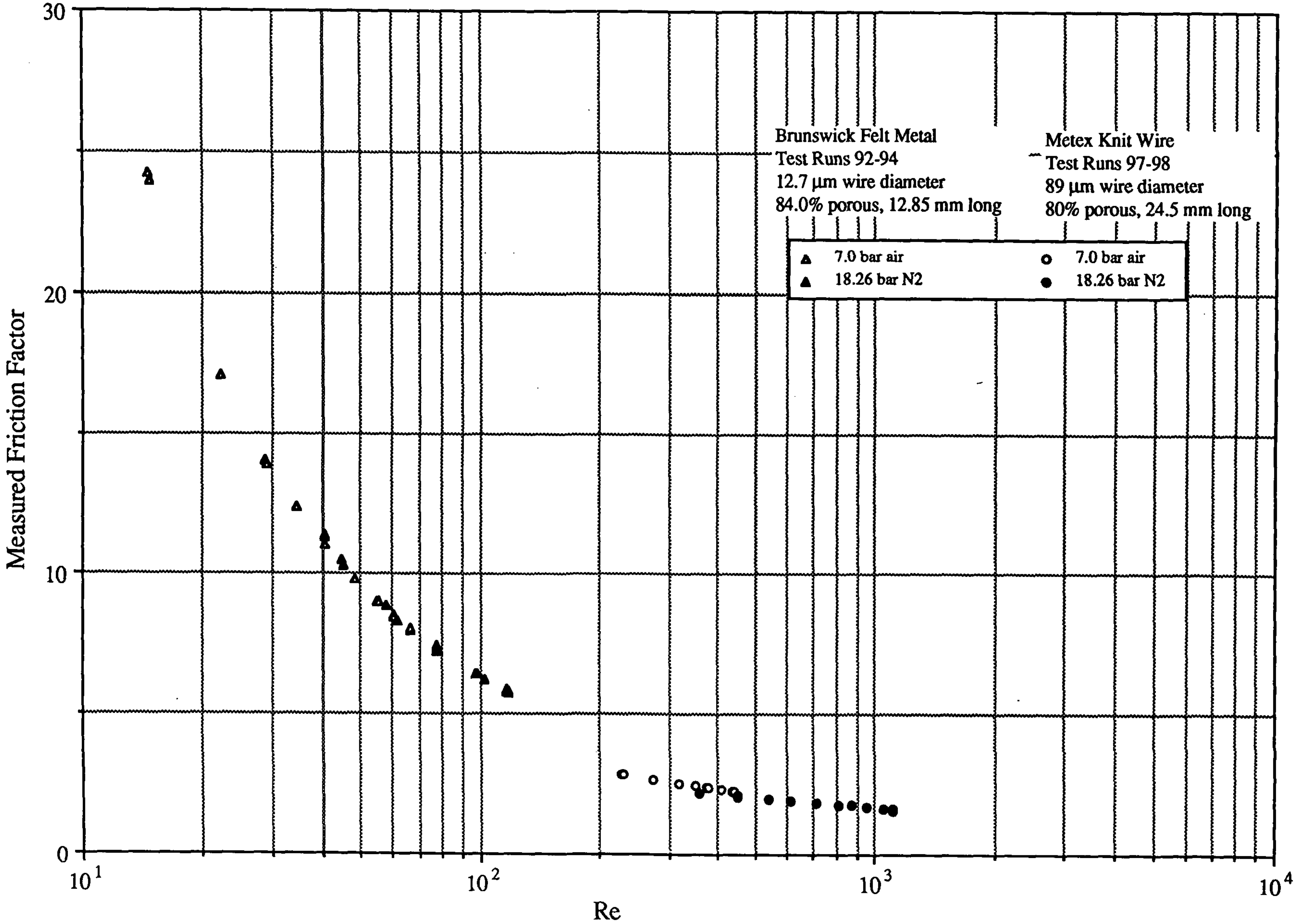

FIGURE 6.1-14

Steady Flow Test Results for Sintered Screen Regenerator
Measured Friction Factor vs Re and Wire Diameter

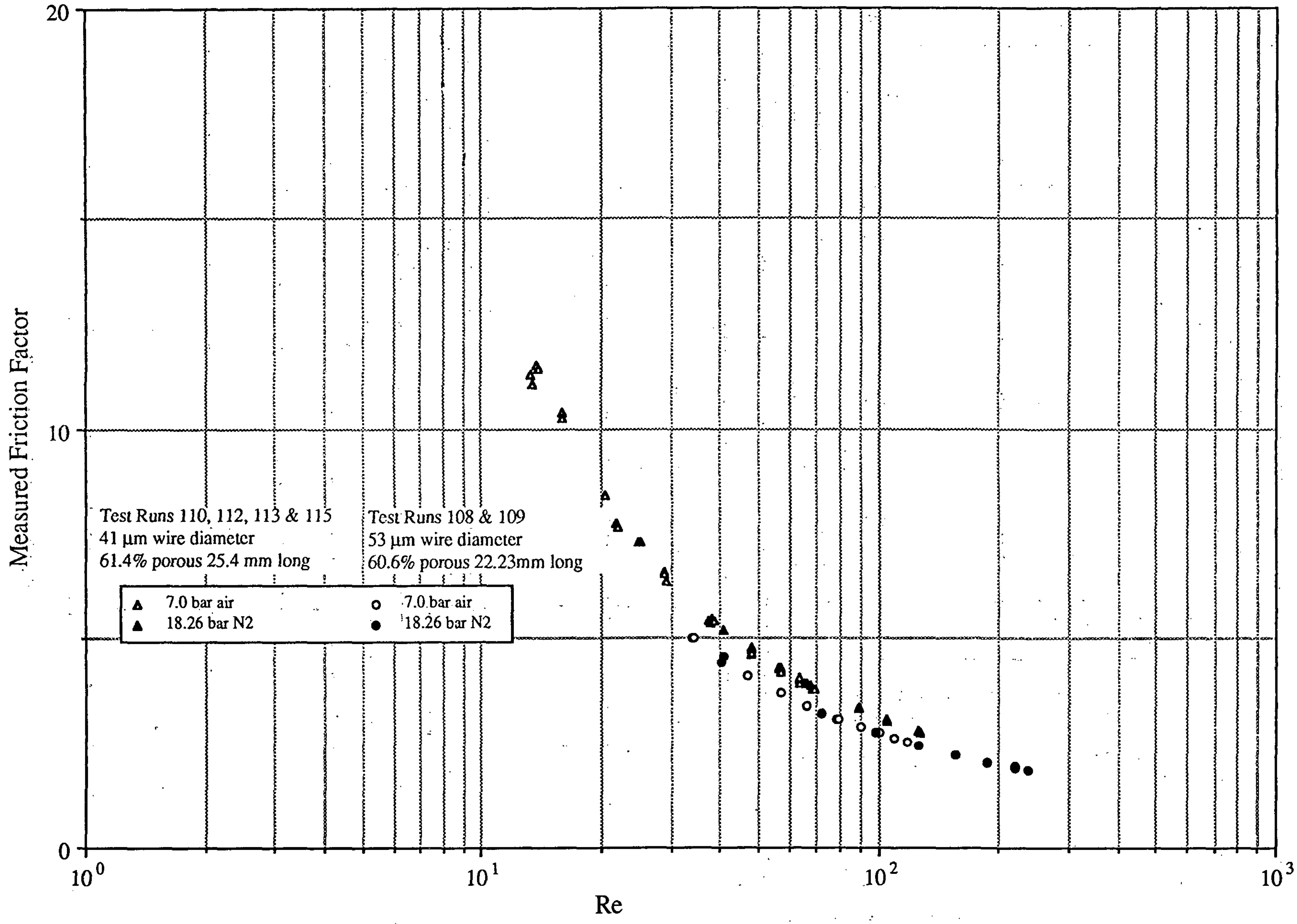

FIGURE 6.1-15

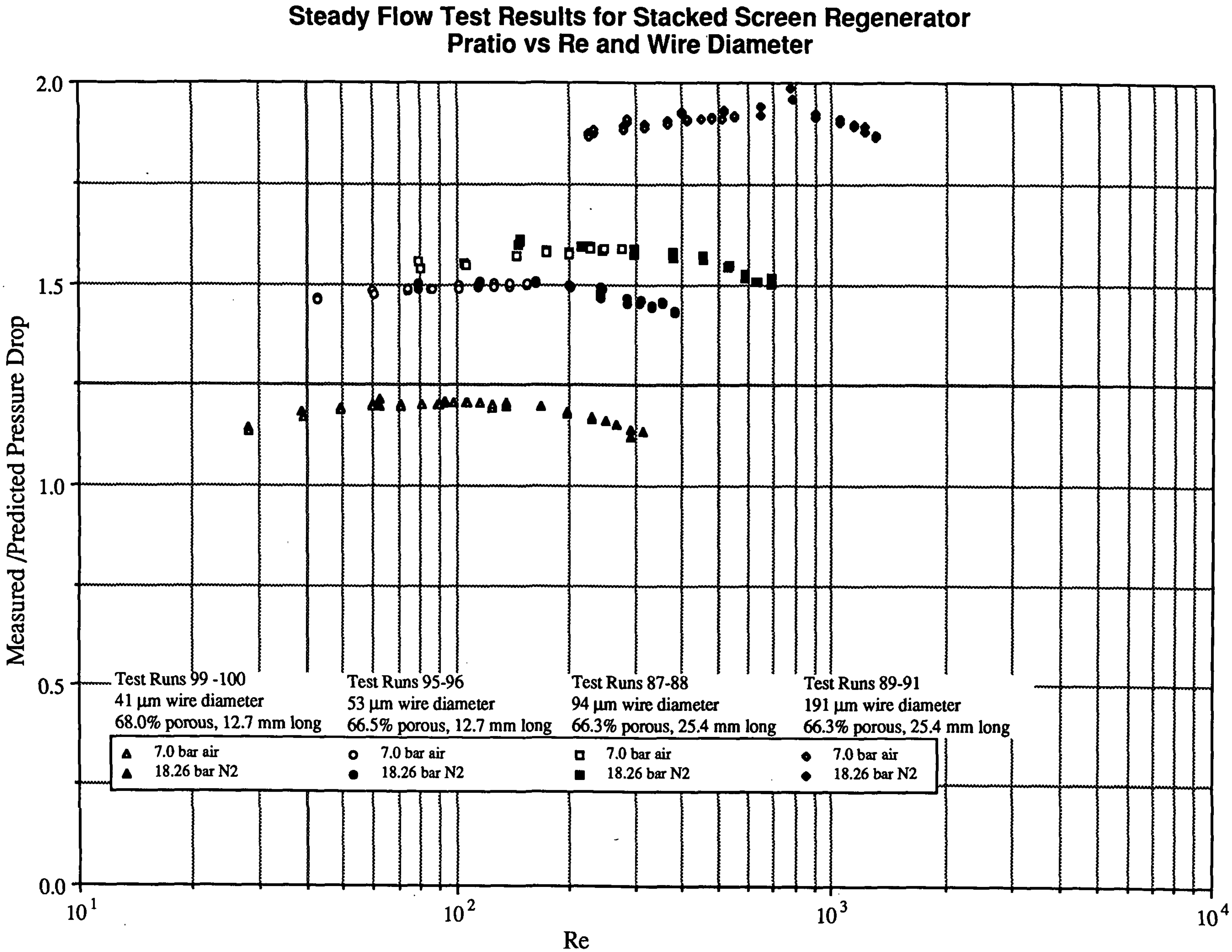

Steady Flow Test Results for Stacked Screen Regenerator
Pratio vs Re and Wire Diameter
Measured /Predicted Pressure Drop
Re
2.0
1.5
1.0
0.5
0.0
10^1
10^2
10^3
10^4
Test Runs 99 -100
41 µm wire diameter
68.0% porous, 12.7 mm long
Test Runs 95-96
53 µm wire diameter
66.5% porous, 12.7 mm long
Test Runs 87-88
94 µm wire diameter
66.3% porous, 25.4 mm long
Test Runs 89-91
191 µm wire diameter
66.3% porous, 25.4 mm long
7.0 bar air
18.26 bar N2
7.0 bar air
18.26 bar N2
7.0 bar air
18.26 bar N2
7.0 bar air
18.26 bar N2

FIGURE 6.1-16

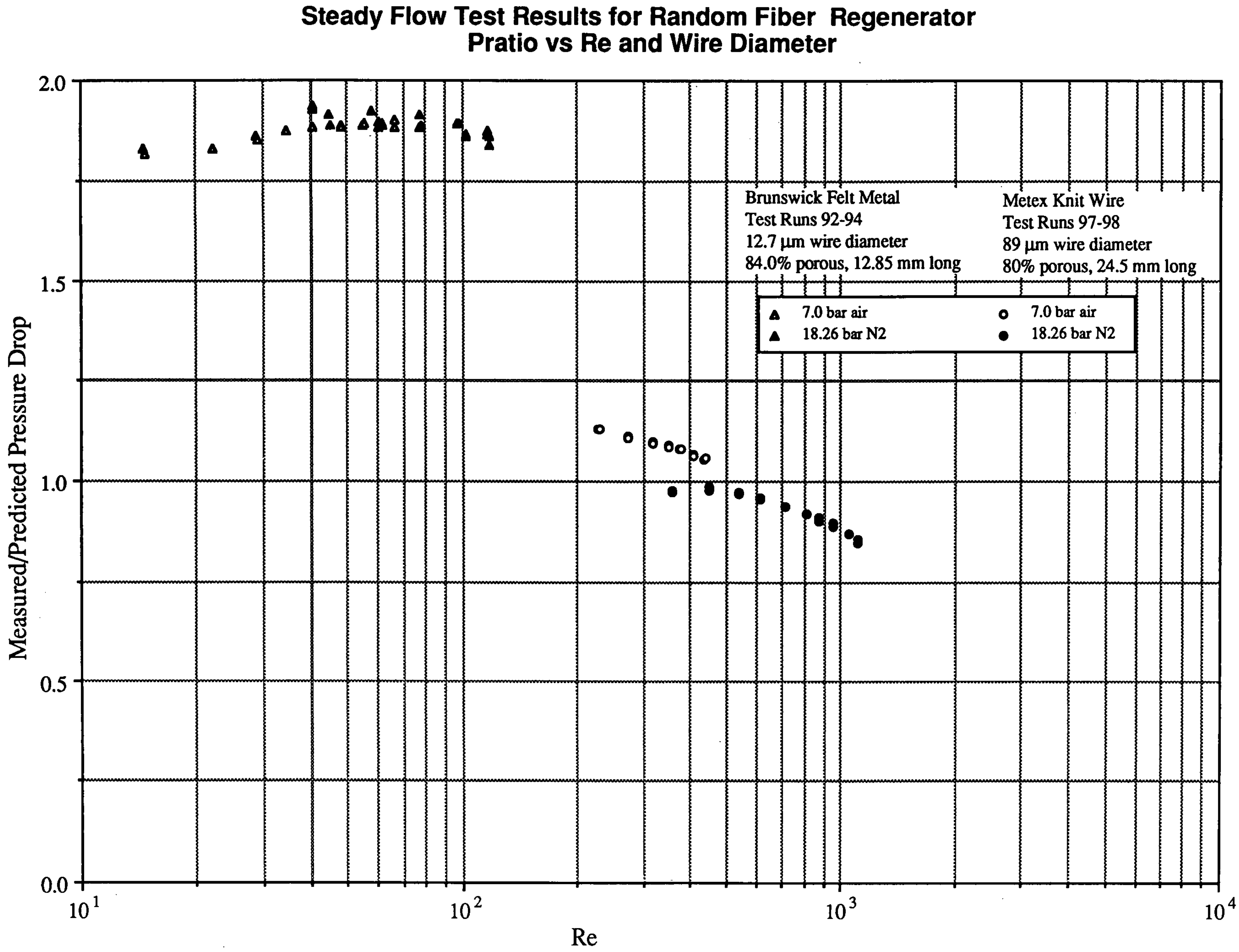
Steady Flow Test Results for Random Fiber Regenerator
Pratio vs Re and Wire Diameter
Measured/Predicted Pressure Drop
2.0
1.5
1.0
0.5
0.0
10^1
10^2
10^3
10^4
Re
Brunswick Felt Metal
Test Runs 92-94
12.7 µm wire diameter
84.0% porous, 12.85 mm long
Metex Knit Wire
Test Runs 97-98
89 µm wire diameter
80% porous, 24.5 mm long
7.0 bar air
18.26 bar N2
7.0 bar air
18.26 bar N2

FIGURE 6.1-17

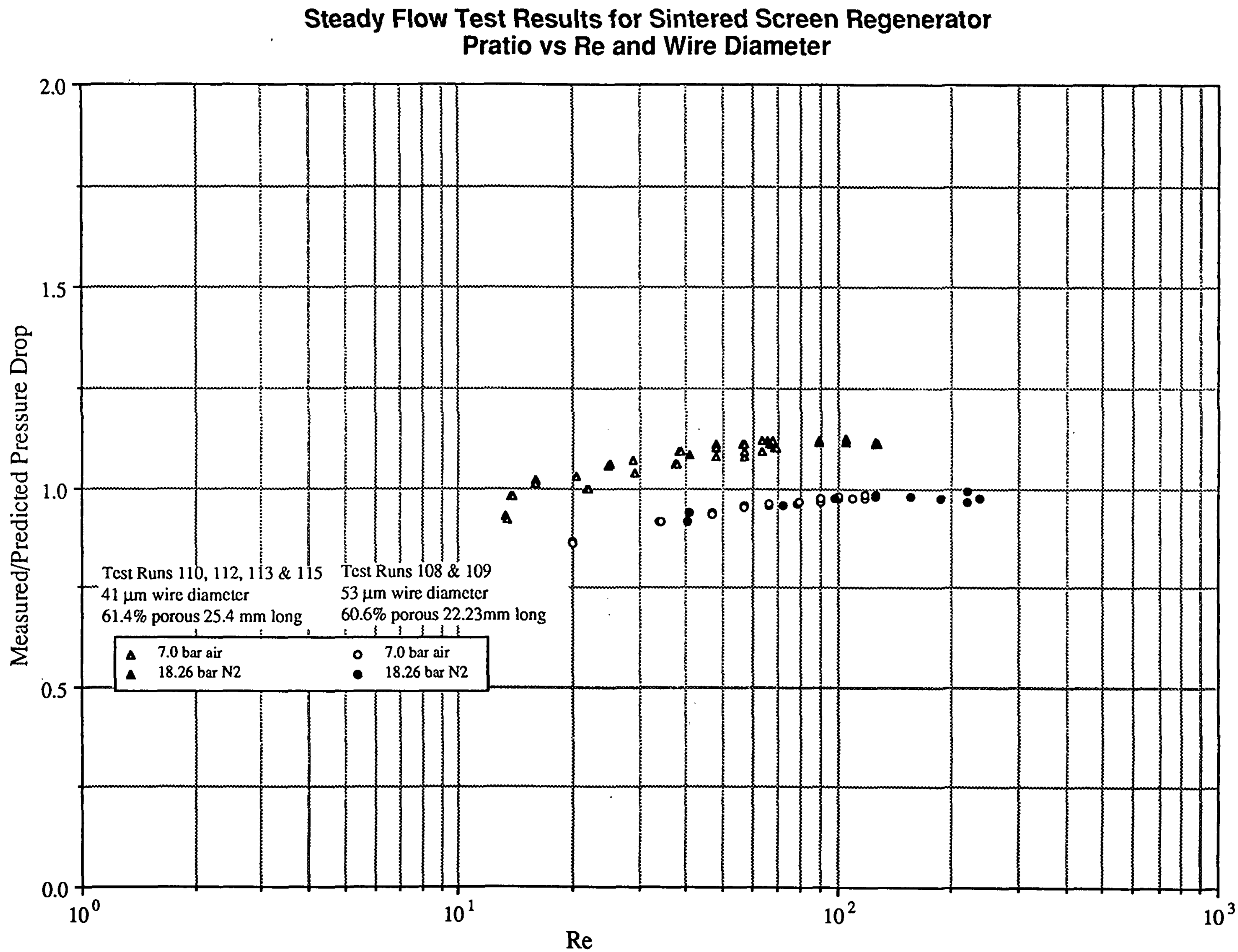

Steady Flow Test Results for Sintered Screen Regenerator
Pratio vs Re and Wire Diameter
Measured/Predicted Pressure Drop
2.0
1.5
1.0
0.5
0.0
10^0
10^1
10^2
10^3
Re
Test Runs 110, 112, 113 & 115
41 µm wire diameter
61.4% porous 25.4 mm long
Test Runs 108 & 109
53 µm wire diameter
60.6% porous 22.23mm long
7.0 bar air
18.26 bar N2
7.0 bar air
18.26 bar N2

FIGURE 6.1-18

TUBE OSCILLATING FLOW TEST RESULTS

Figures 6.2-1 through 6.2-43

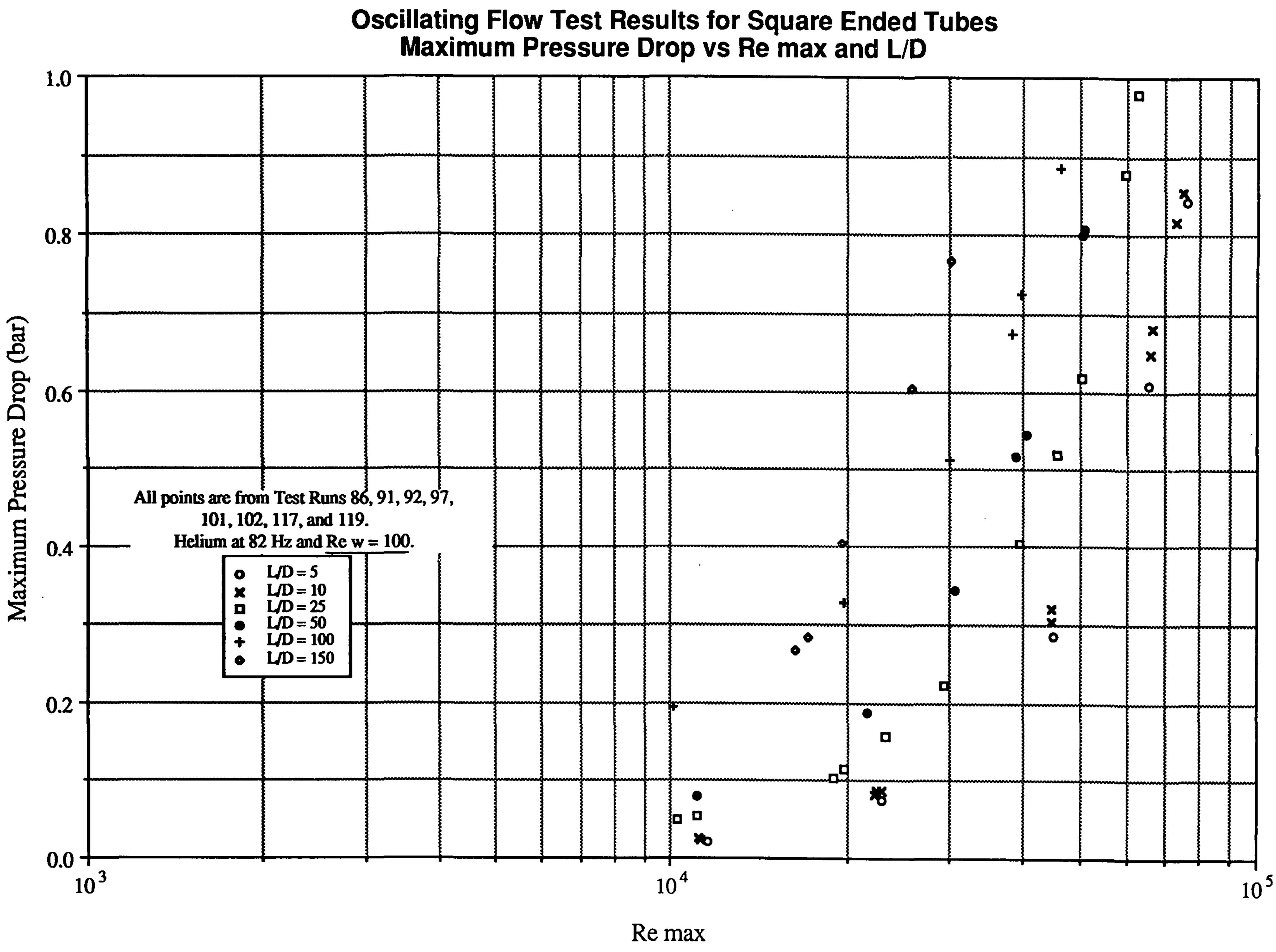

Oscillating Flow Test Results for Square Ended Tubes
Maximum Pressure Drop vs Re max and L/D
Maximum Pressure Drop (bar)
1.0
0.8
0.6
0.4
0.2
0.0
10^3
10^4
10^5
All points are from Test Runs 86, 91, 92, 97, 101, 102, 117, and 119.
Helium at 82 Hz and Re w = 100.
L/D = 5
L/D = 10
L/D = 25
L/D = 50
L/D = 100
L/D = 150
Re max

FIGURE 6.2-1

Oscillating Flow Test Results for Rounded Tubes
Maximum Pressure Drop vs Re max and L/D

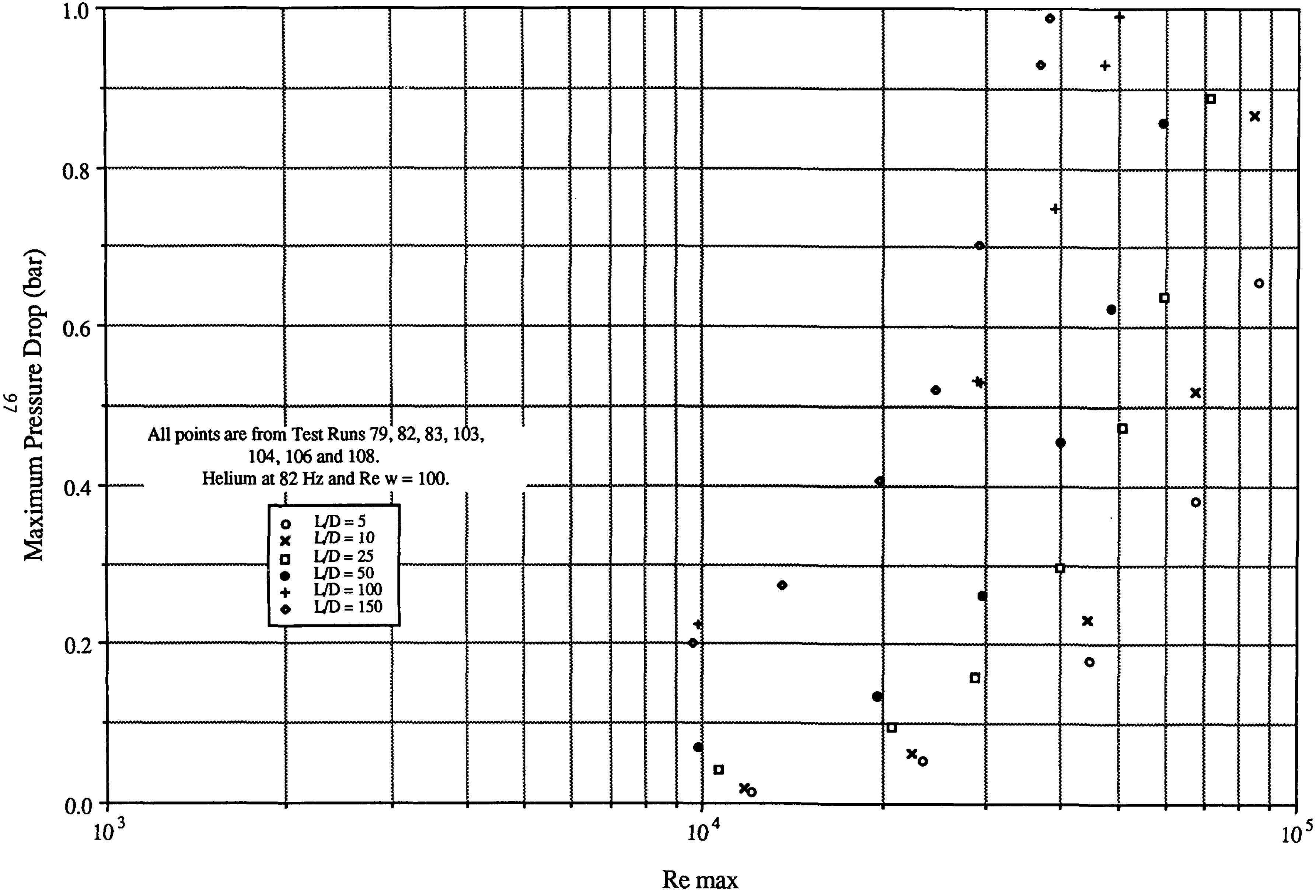

FIGURE 6.2-2

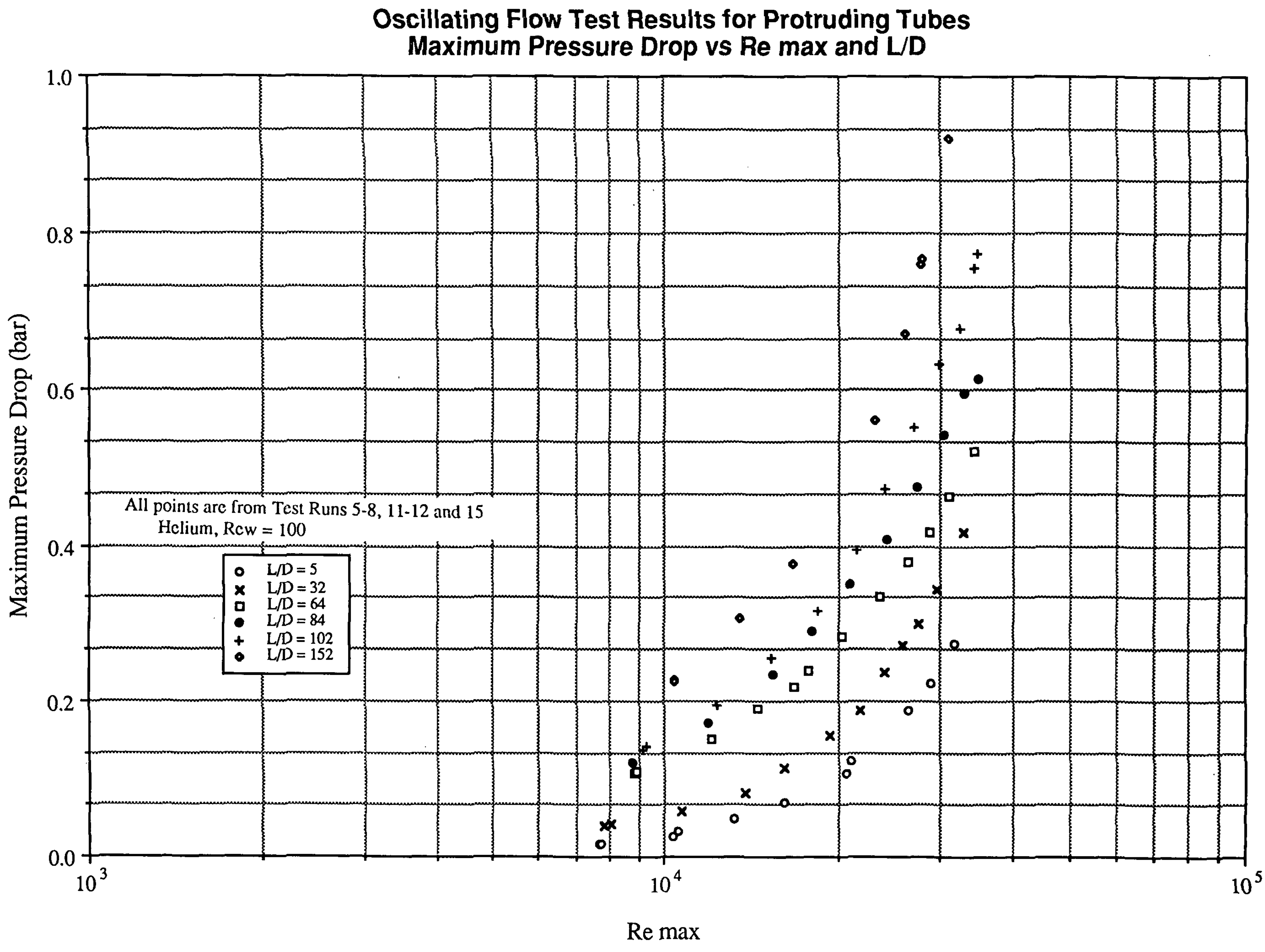

Oscillating Flow Test Results for Protruding Tubes
Maximum Pressure Drop vs Re max and L/D
Maximum Pressure Drop (bar)
1.0
0.8
0.6
0.4
0.2
0.0
All points are from Test Runs 5-8, 11-12 and 15
Helium, Rew = 100
L/D = 5
L/D = 32
L/D = 64
L/D = 84
L/D = 102
L/D = 152
10^3
10^4
10^5
Re max

FIGURE 6.2-3

Oscillating Flow Test Results for Square Ended Tubes
Maximum Pressure Drop vs Re max and L/D

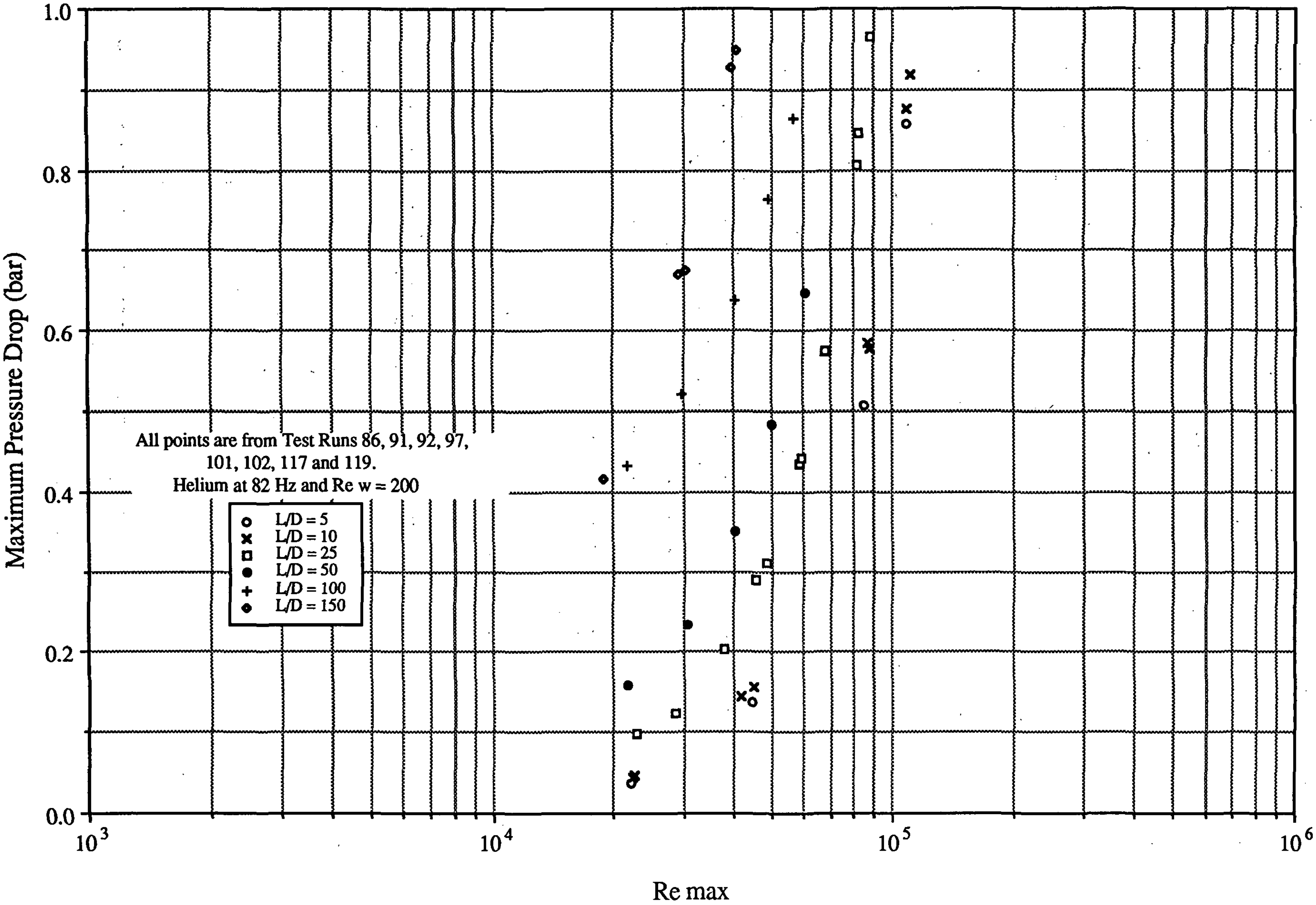

FIGURE 6.2-4

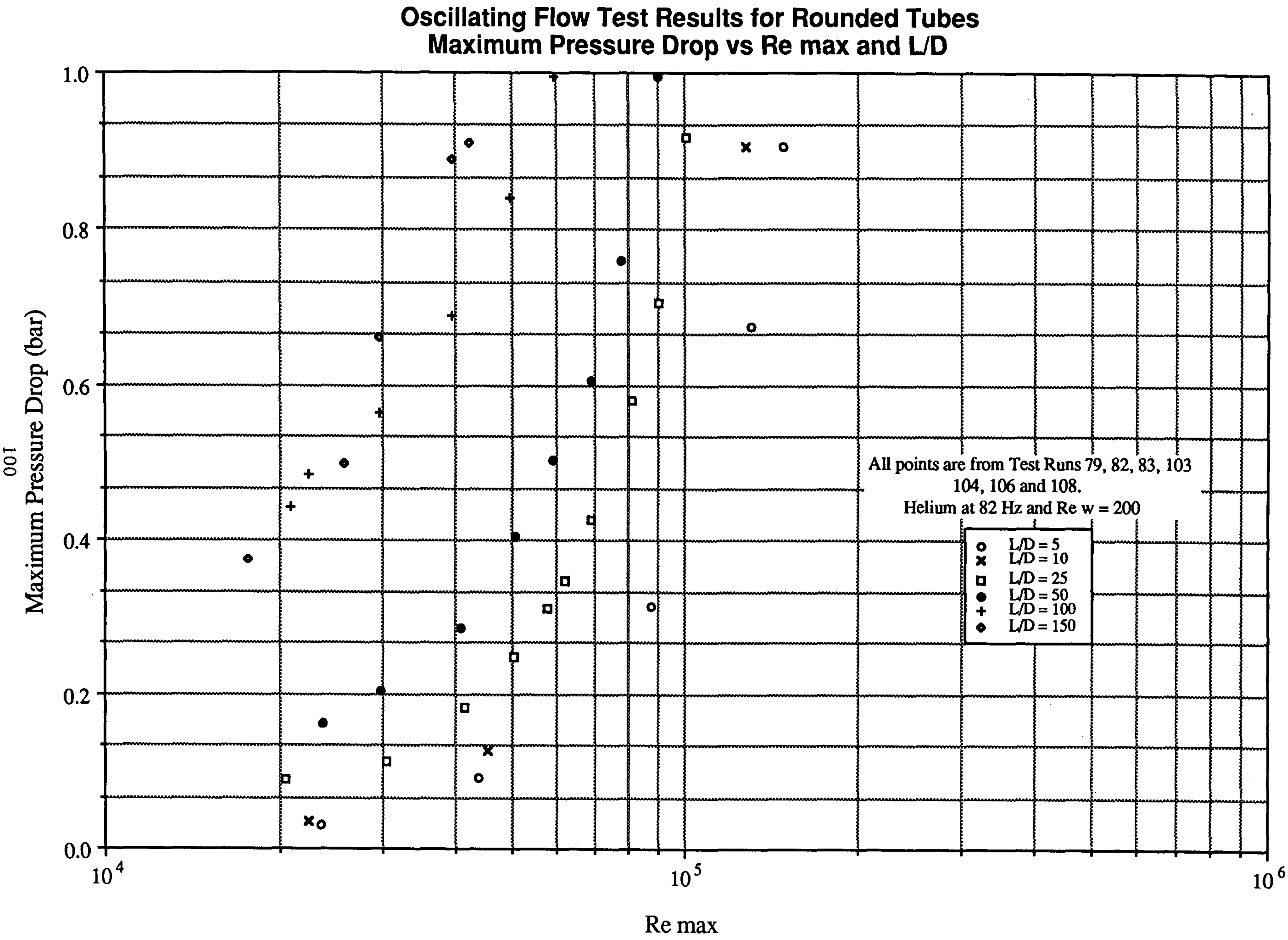

Oscillating Flow Test Results for Rounded Tubes
Maximum Pressure Drop vs Re max and L/D
Maximum Pressure Drop (bar)
1.0
0.8
0.6
0.4
0.2
0.0
10^4
10^5
10^6
Re max
All points are from Test Runs 79, 82, 83, 103
104, 106 and 108.
Helium at 82 Hz and Re w = 200
L/D = 5
L/D = 10
L/D = 25
L/D = 50
L/D = 100
L/D = 150

FIGURE 6.2-5

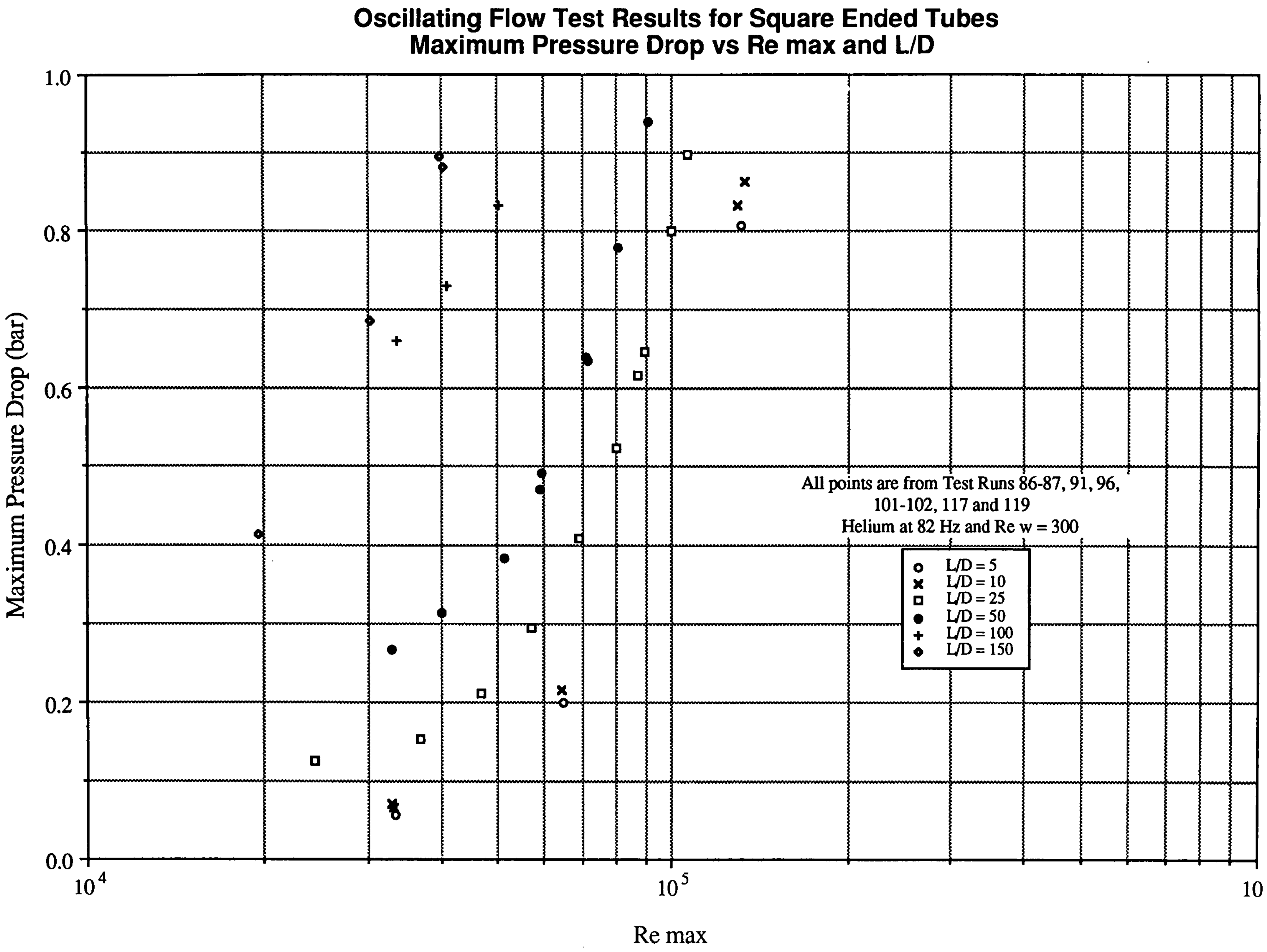
Oscillating Flow Test Results for Square Ended Tubes
Maximum Pressure Drop vs Re max and L/D
Maximum Pressure Drop (bar)
1.0
0.8
0.6
0.4
0.2
0.0
10^4
10^5
10^6
Re max
All points are from Test Runs 86-87, 91, 96, 101-102, 117 and 119
Helium at 82 Hz and Re w = 300
L/D = 5
L/D = 10
L/D = 25
L/D = 50
L/D = 100
L/D = 150

FIGURE 6.2-6

Oscillating Flow Test Results for Rounded Tubes
Maximum Pressure Drop vs Re max and L/D

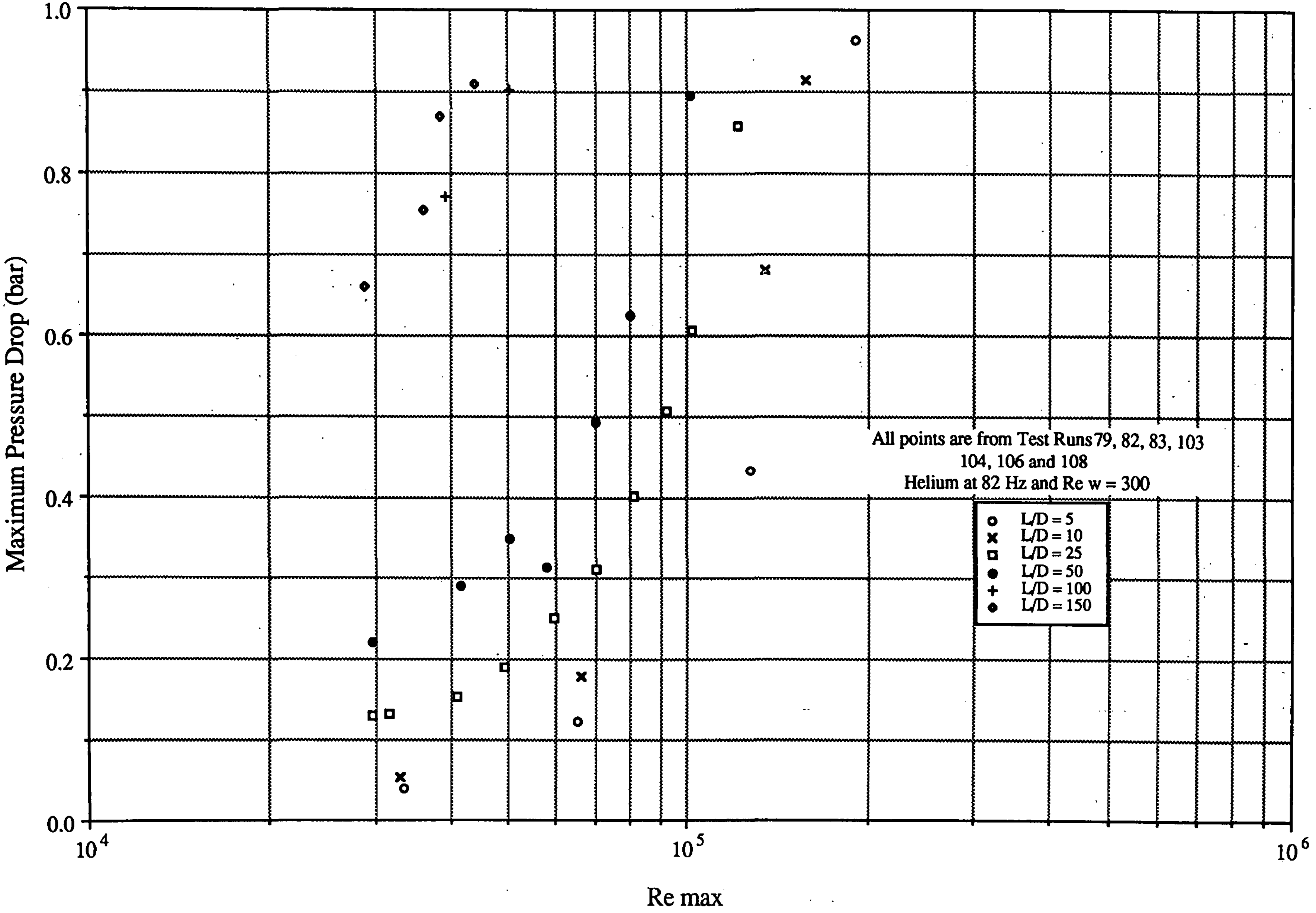

FIGURE 6.2-7

Oscillating Flow Test Results for Square Ended Tubes
Total Power Dissipation vs Re max and L/D

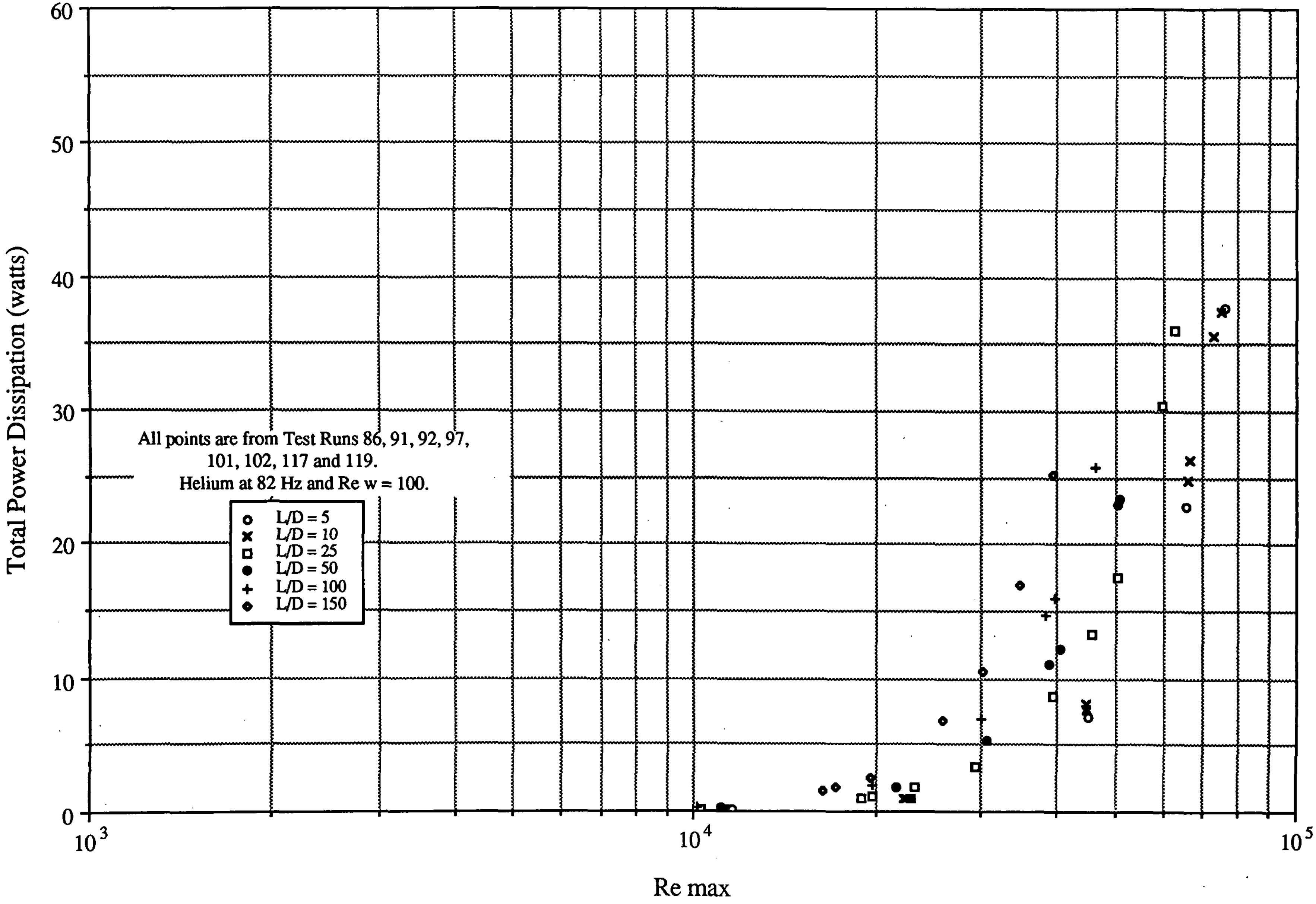

FIGURE 6.2-8

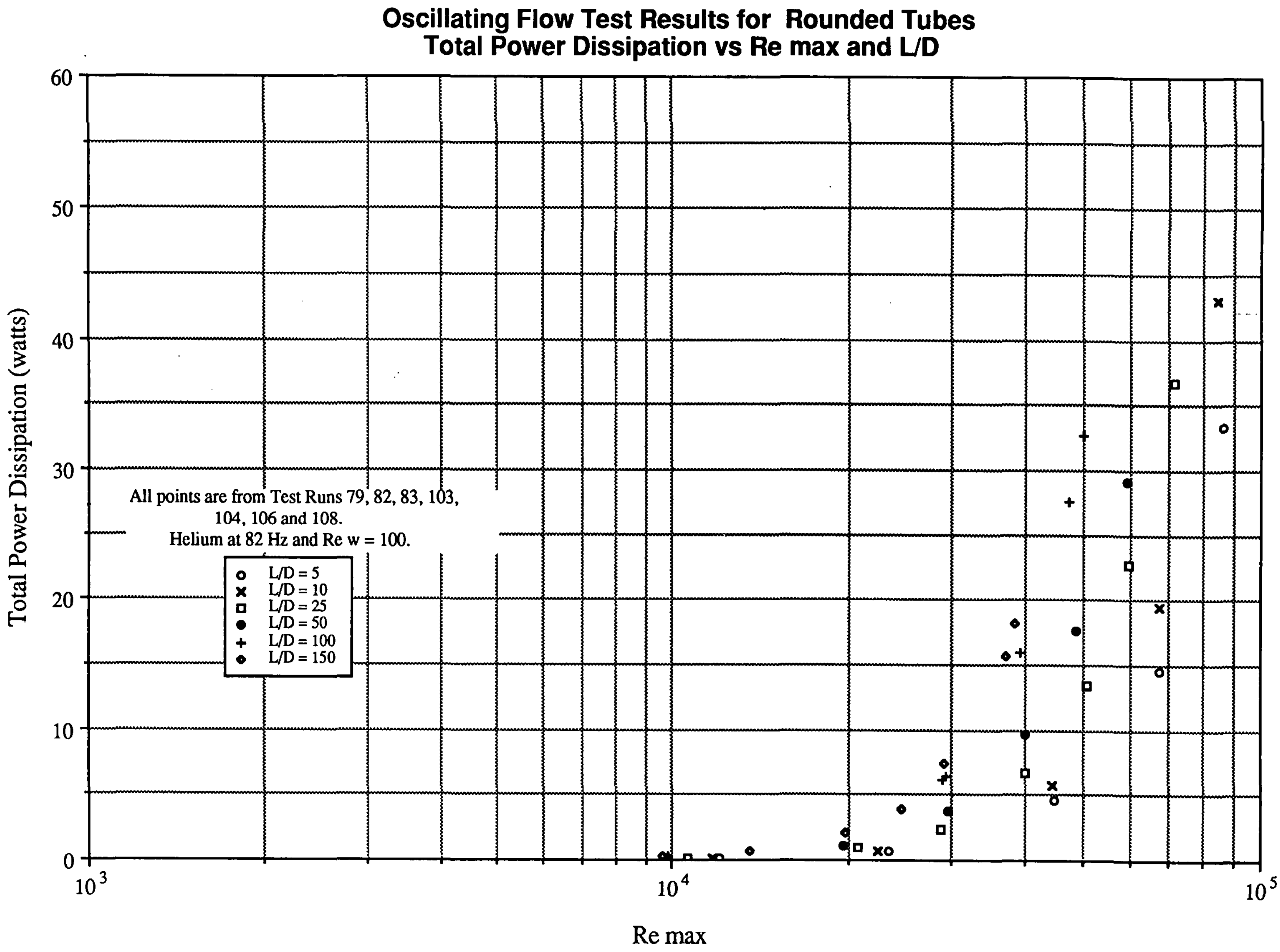
Oscillating Flow Test Results for Rounded Tubes
Total Power Dissipation vs Re max and L/D
Total Power Dissipation (watts)
Re max
60
50
40
30
20
10
0
10^3
10^4
10^5
All points are from Test Runs 79, 82, 83, 103, 104, 106 and 108.
Helium at 82 Hz and Re w = 100.
L/D = 5
L/D = 10
L/D = 25
L/D = 50
L/D = 100
L/D = 150

FIGURE 6.2-9

Oscillating Flow Test Results for Protruding Tubes
Total Power Dissipation vs Re max and L/D

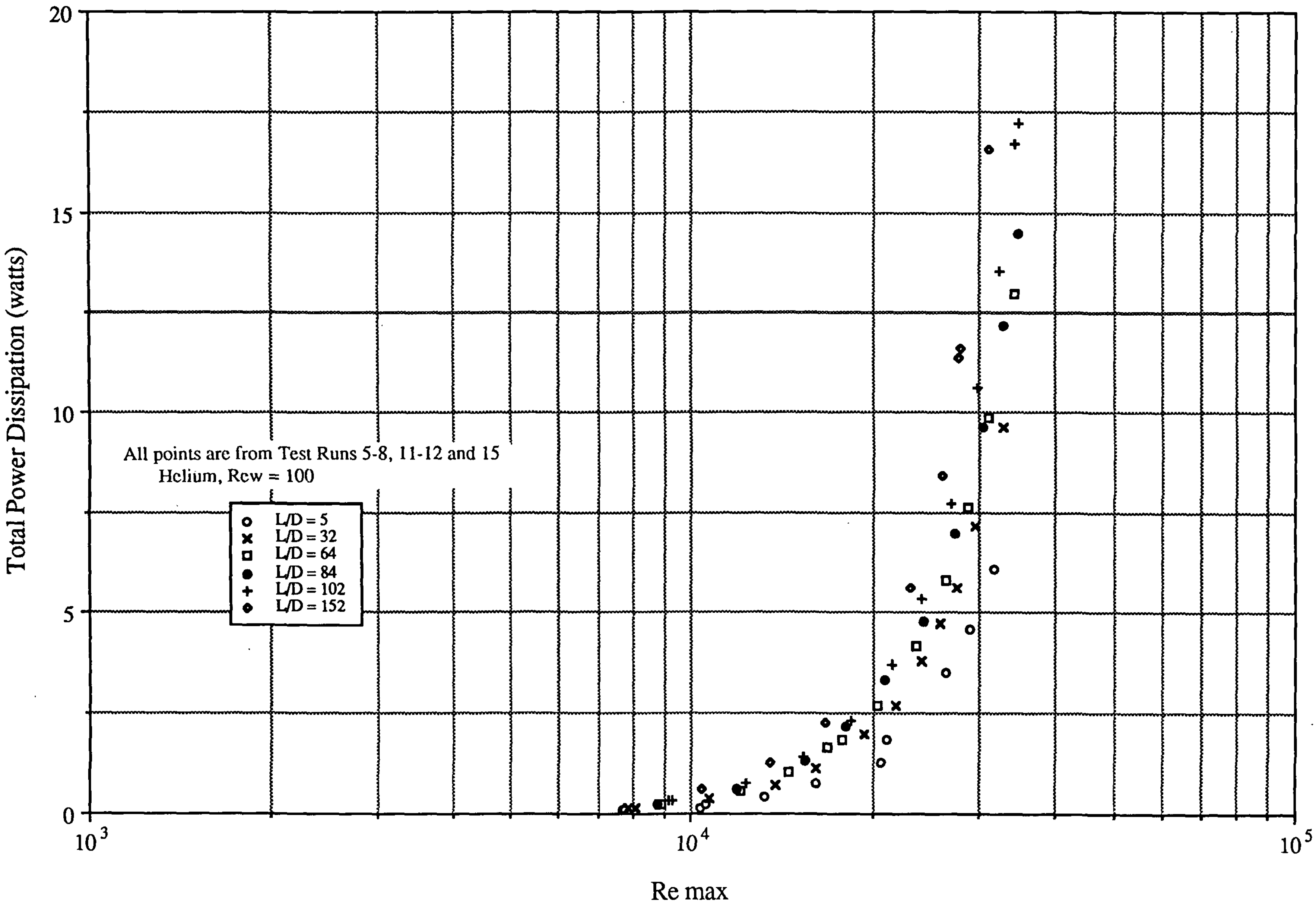

FIGURE 6.2-10

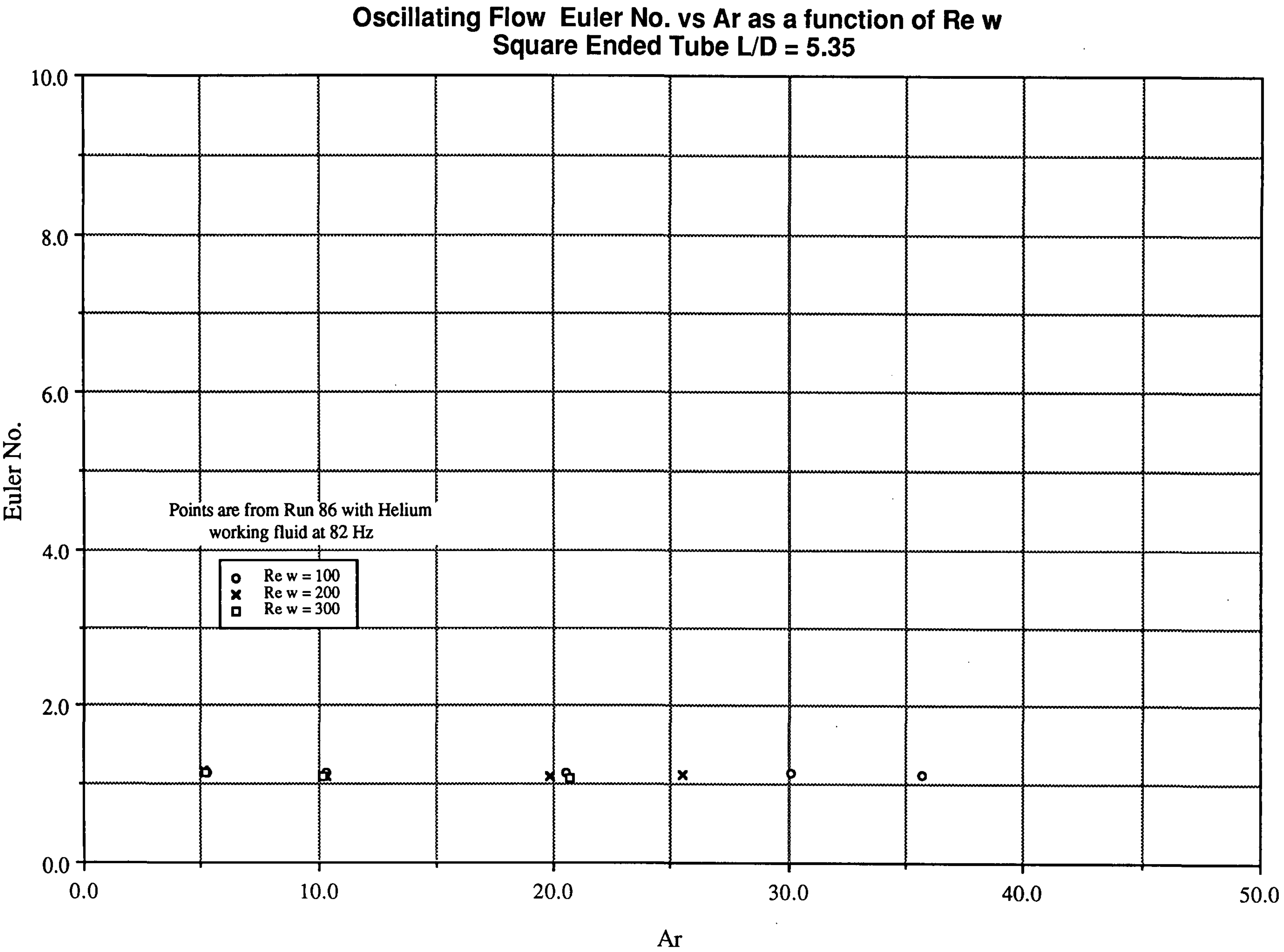

Oscillating Flow Euler No. vs Ar as a function of Re w
Square Ended Tube L/D = 5.35
Euler No.
Ar
Points are from Run 86 with Helium working fluid at 82 Hz
Re w = 100
Re w = 200
Re w = 300
0.0
2.0
4.0
6.0
8.0
10.0
10.0
20.0
30.0
40.0
50.0

FIGURE 6.2-11

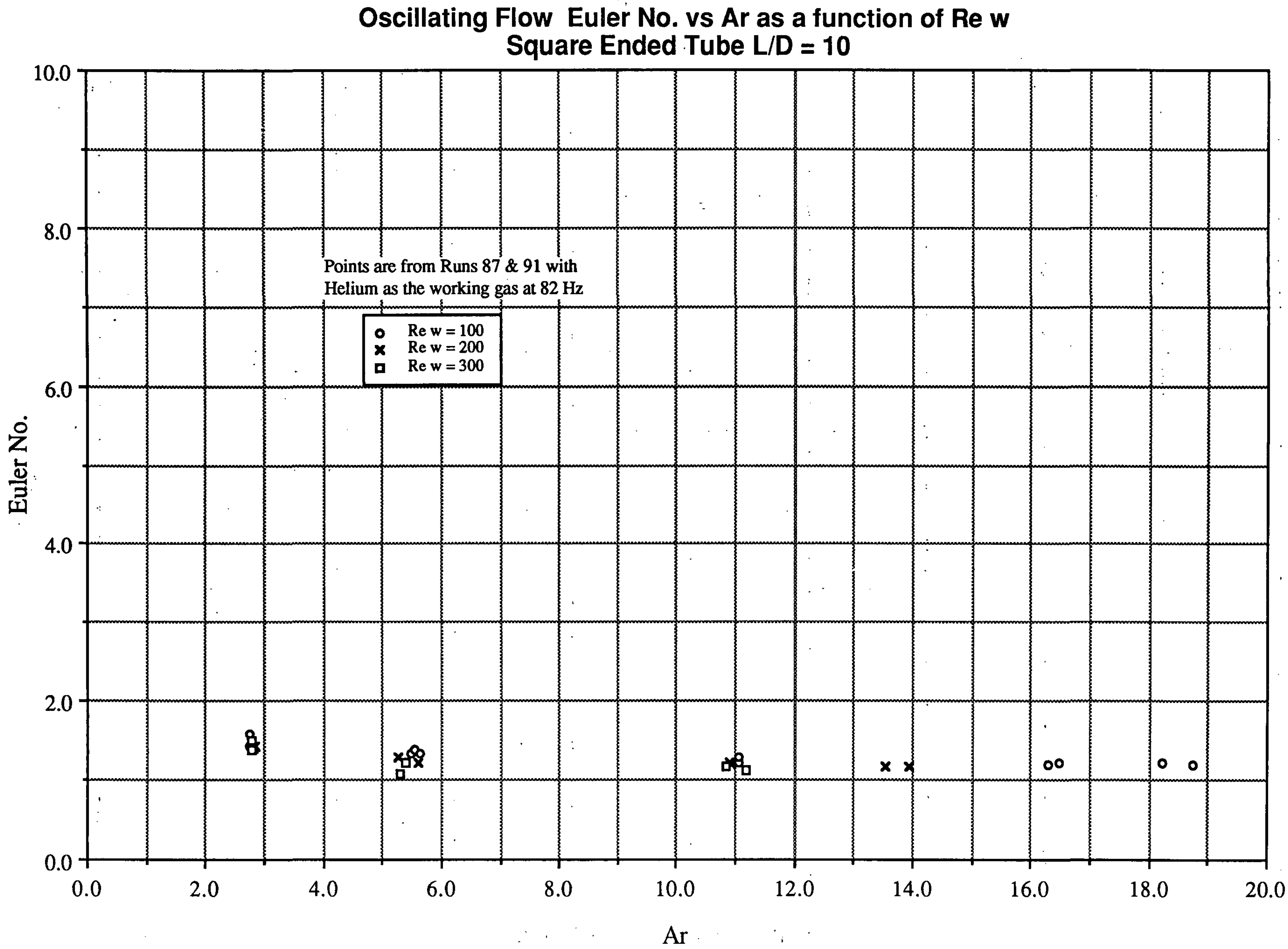

Oscillating Flow Euler No. vs Ar as a function of Re w
Square Ended Tube L/D = 10
Points are from Runs 87 & 91 with
Helium as the working gas at 82 Hz
Re w = 100
Re w = 200
Re w = 300
Euler No.
Ar
0.0
2.0
4.0
6.0
8.0
10.0
12.0
14.0
16.0
18.0
20.0

FIGURE 6.2-12

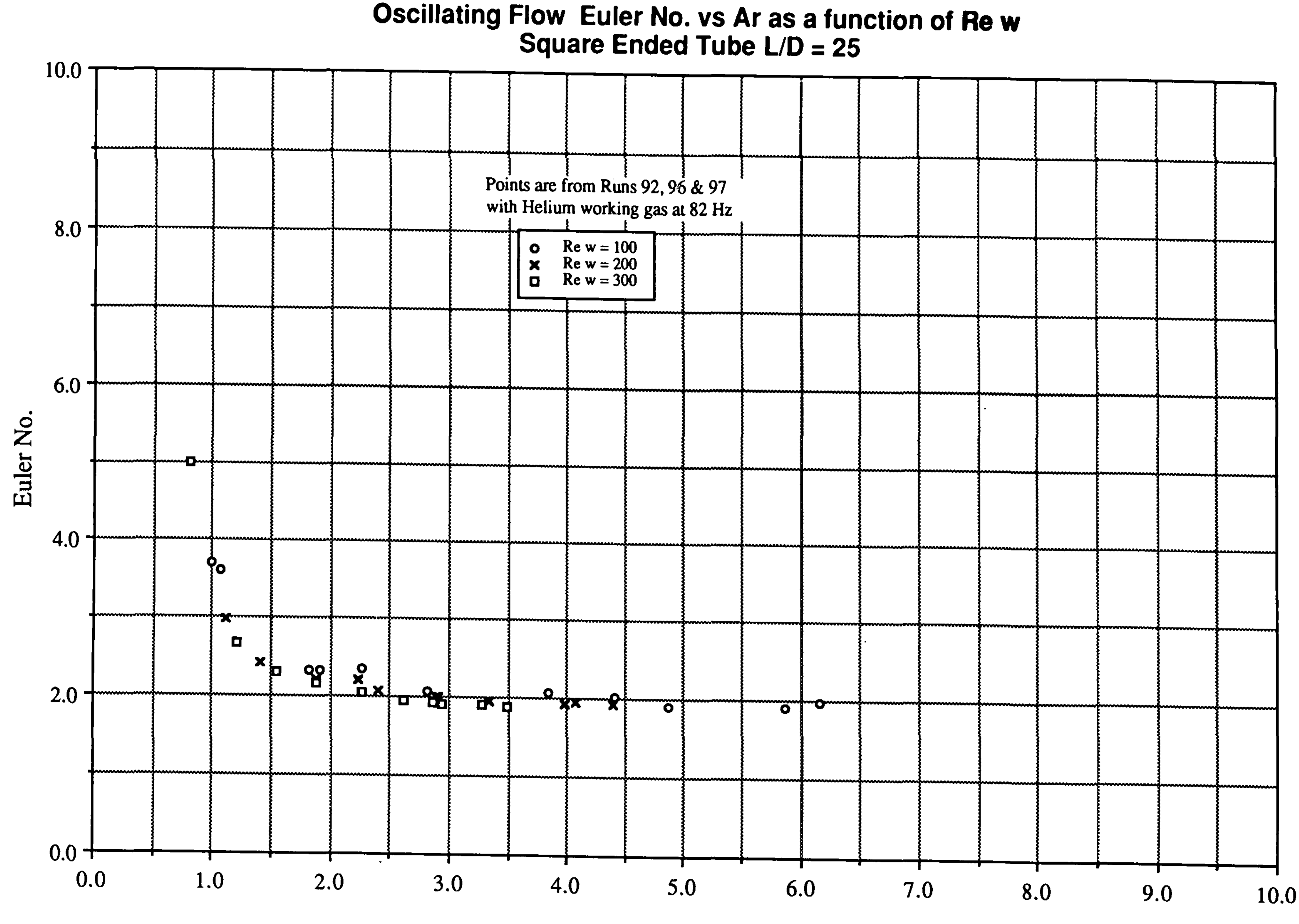
Oscillating Flow Euler No. vs Ar as a function of Re w
Square Ended Tube L/D = 25
Points are from Runs 92, 96 & 97
with Helium working gas at 82 Hz
Re w = 100
Re w = 200
Re w = 300
Euler No.
Ar
0.0
2.0
4.0
6.0
8.0
10.0
1.0
3.0
5.0
7.0
9.0

FIGURE 6.2-13

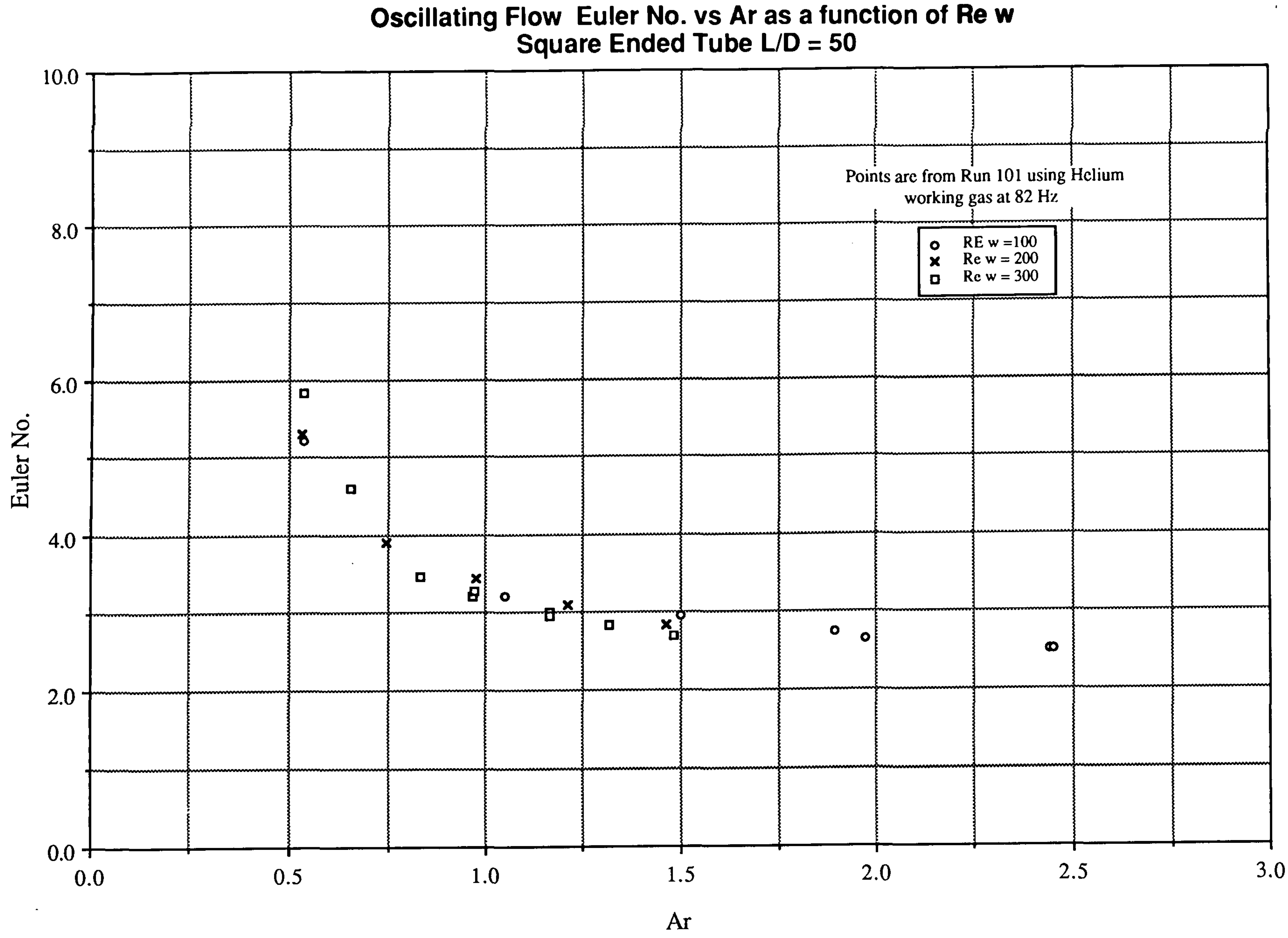

Oscillating Flow Euler No. vs Ar as a function of Re w
Square Ended Tube L/D = 50
Points are from Run 101 using Helium working gas at 82 Hz
RE w =100
Re w = 200
Re w = 300
Euler No.
Ar
10.0
8.0
6.0
4.0
2.0
0.0
0.0
0.5
1.0
1.5
2.0
2.5
3.0

FIGURE 6.2-14

Oscillating Flow Euler No. vs Ar as a function of Re w
Square Ended Tube L/D = 100

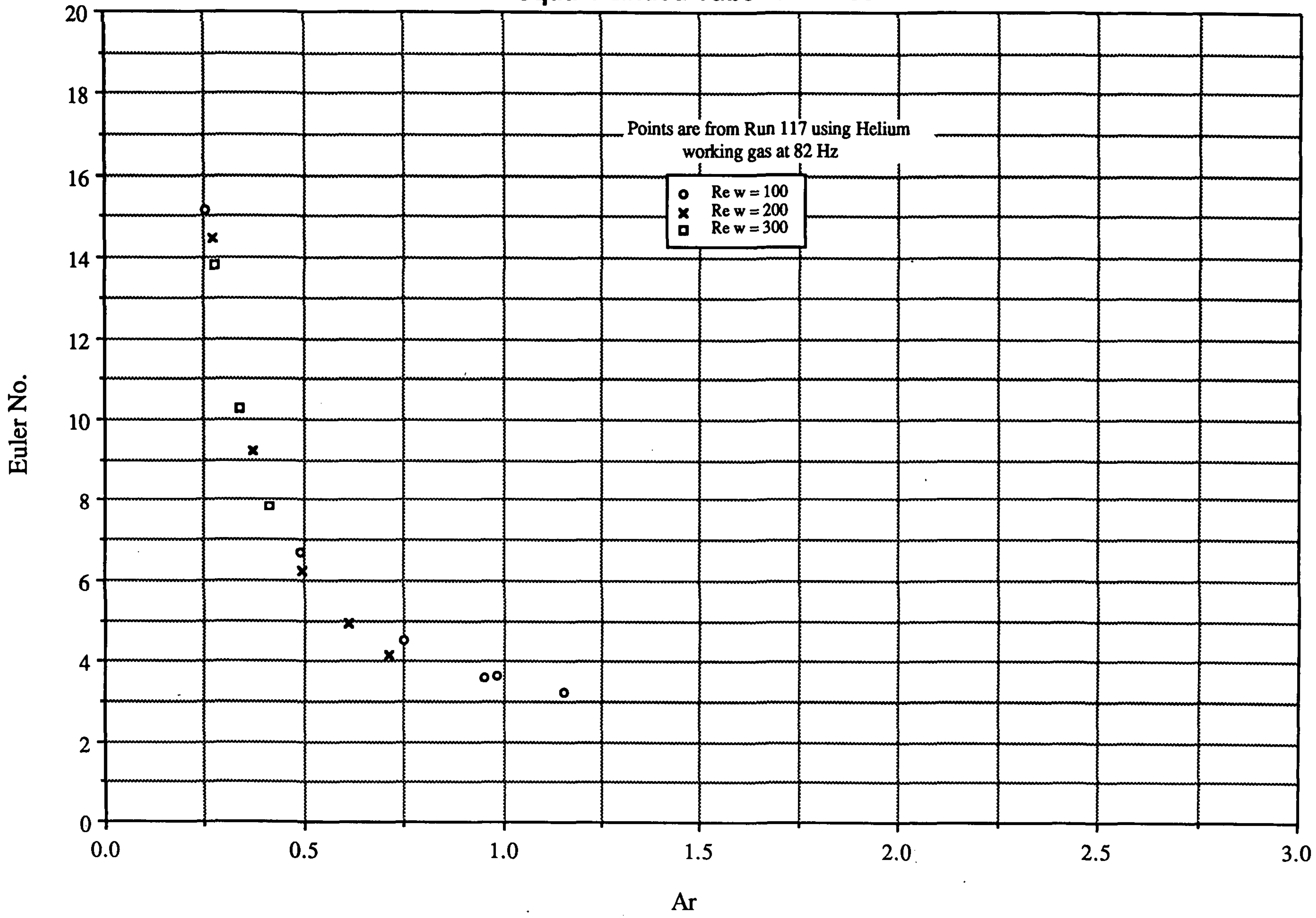

FIGURE 6.2-15

Oscillating Flow Euler No. vs. Ar as a function of Re w
Rounded Tube L/D = 5.35

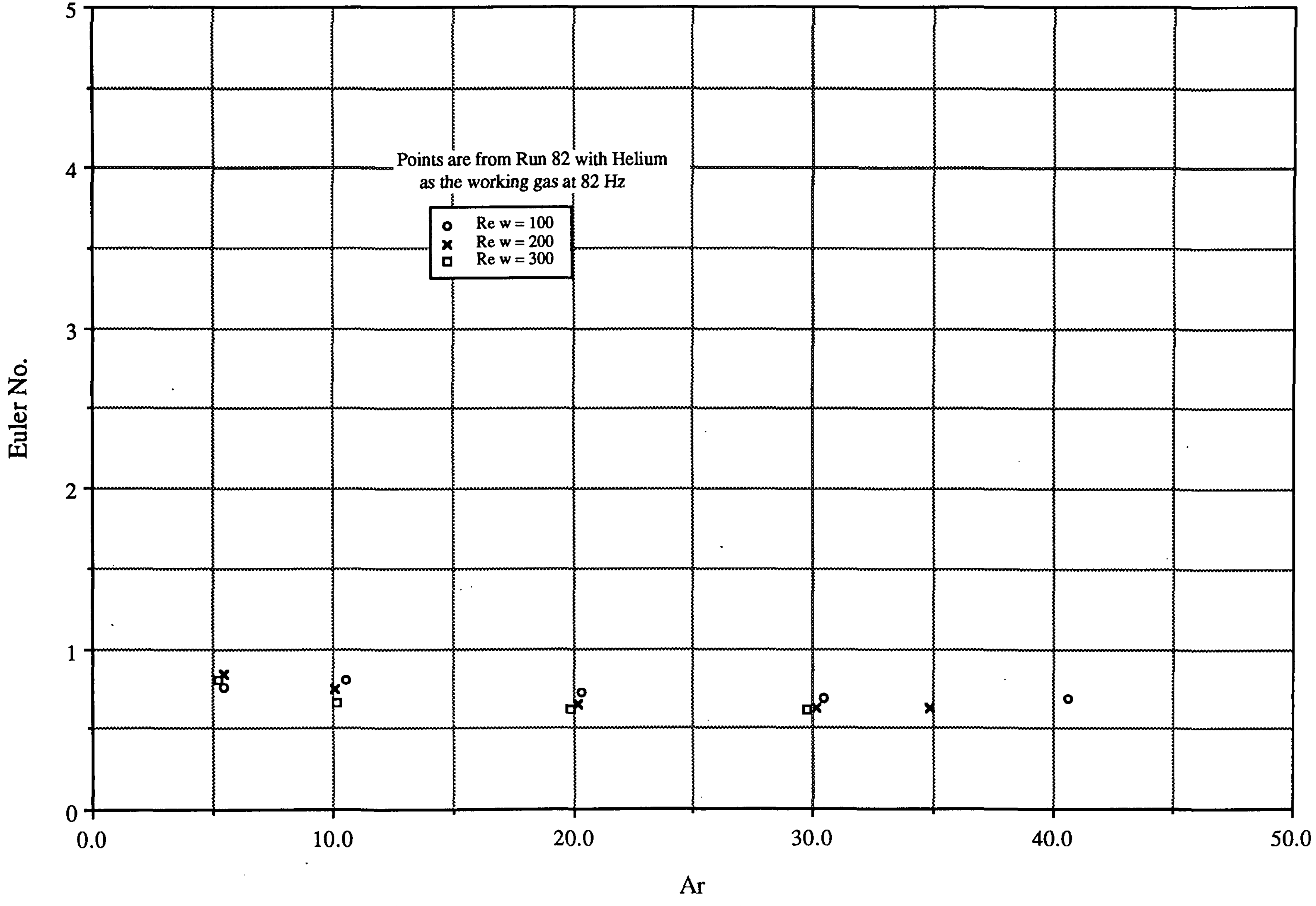

FIGURE 6.2-16

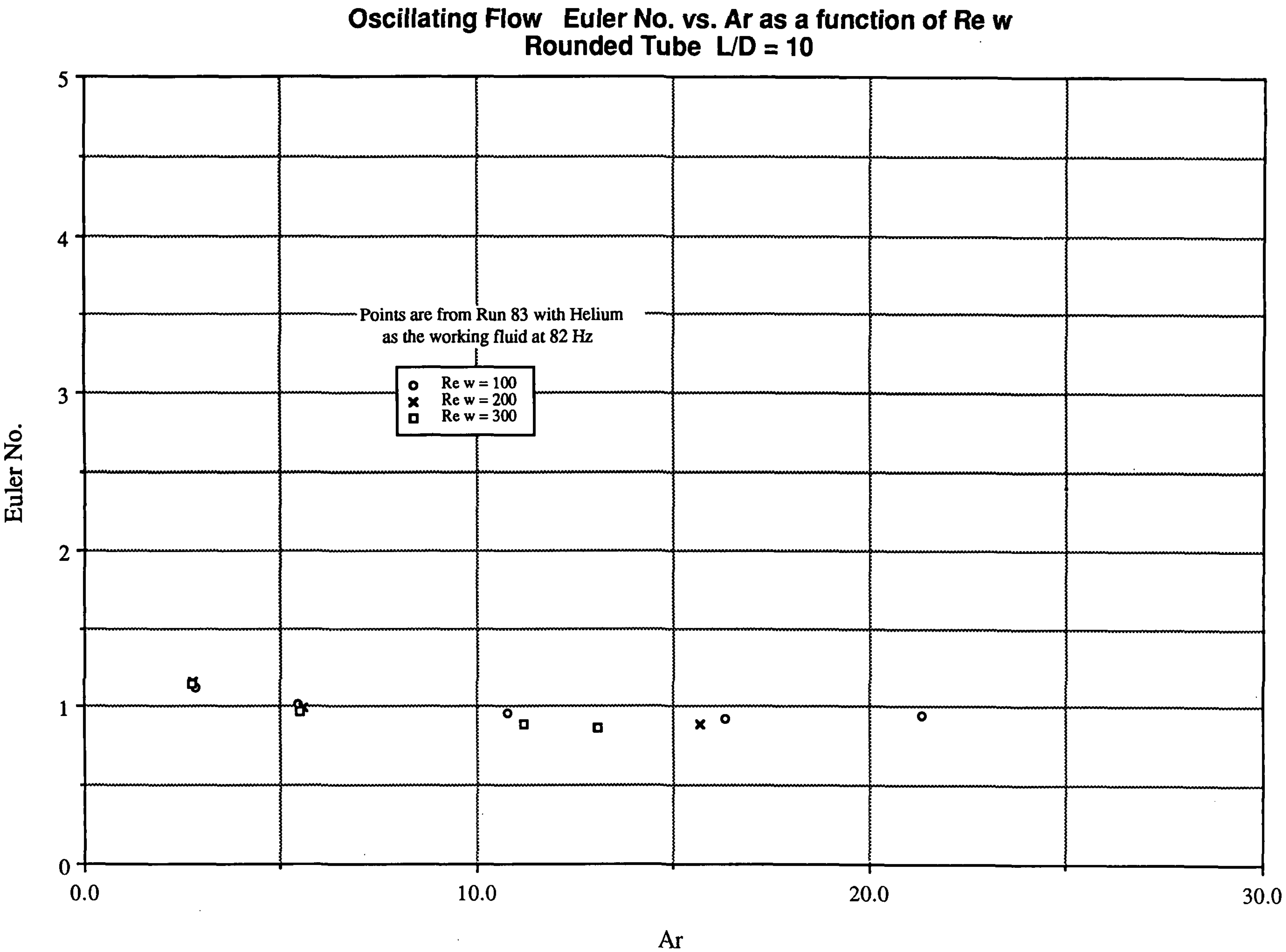

Oscillating Flow Euler No. vs. Ar as a function of Re w
Rounded Tube L/D = 10
Points are from Run 83 with Helium
as the working fluid at 82 Hz
Re w = 100
Re w = 200
Re w = 300
Euler No.
0
1
2
3
4
5
0.0
10.0
20.0
30.0
Ar

FIGURE 6.2-17

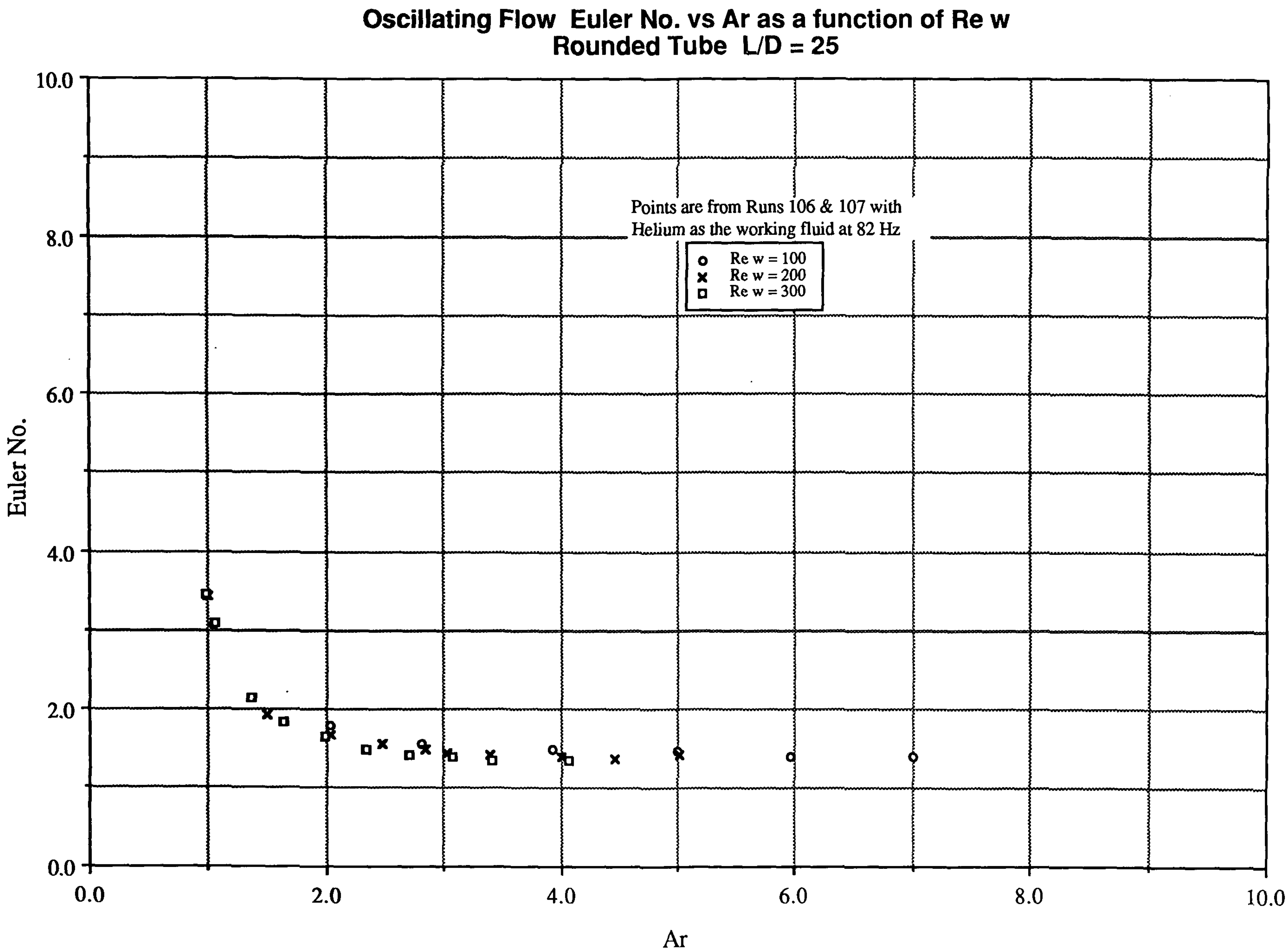

Oscillating Flow Euler No. vs Ar as a function of Re w
Rounded Tube L/D = 25
Points are from Runs 106 & 107 with
Helium as the working fluid at 82 Hz
Re w = 100
Re w = 200
Re w = 300
Euler No.
10.0
8.0
6.0
4.0
2.0
0.0
0.0
2.0
4.0
6.0
8.0
10.0
Ar

FIGURE 6.2-18

Oscillating Flow Euler No. vs. Ar as a function of Re w
Rounded Tube L/D = 50

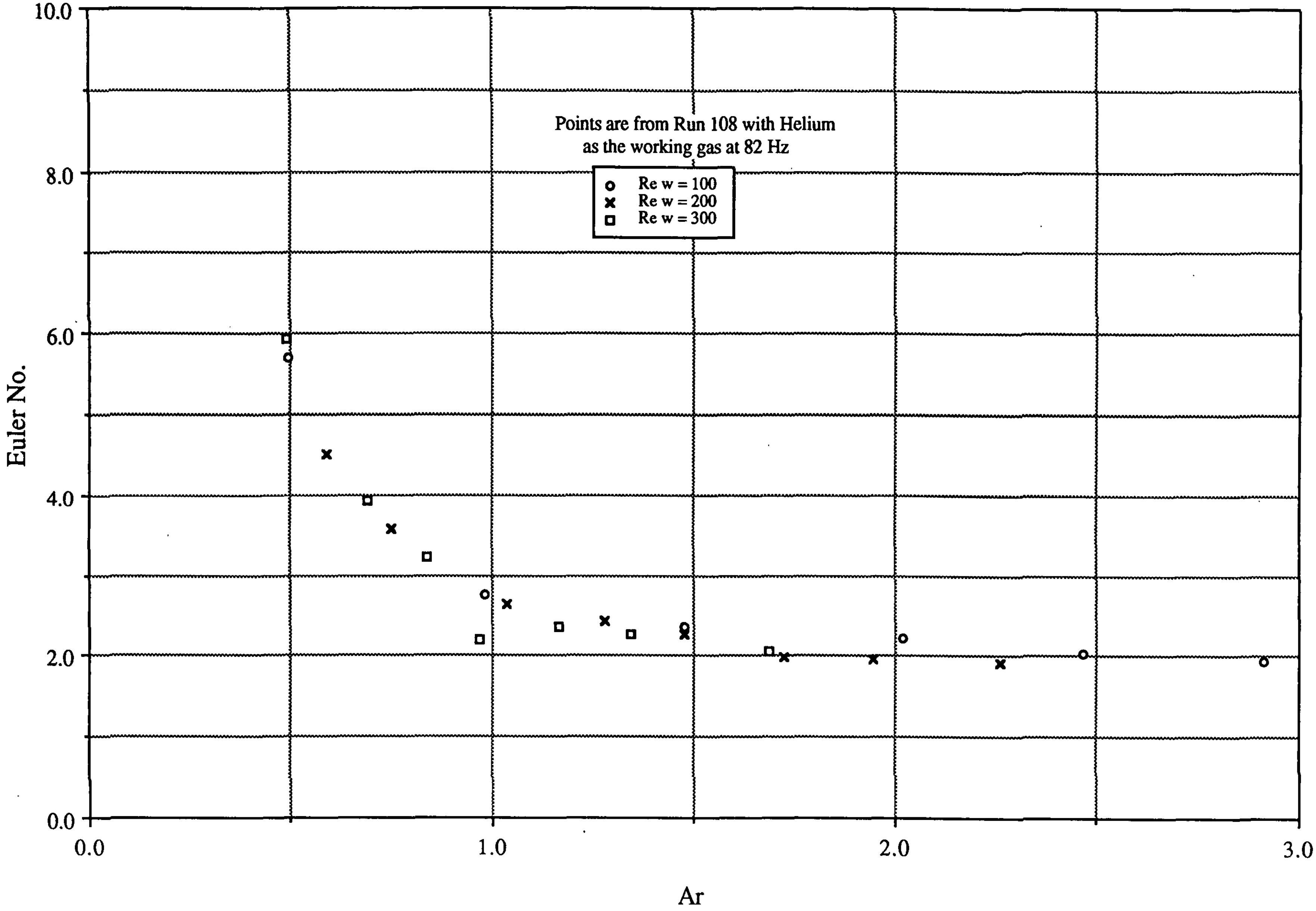

FIGURE 6.2-19

Oscillating Flow Euler No. vs Ar as a function of Re w
Rounded Tube L/D = 100

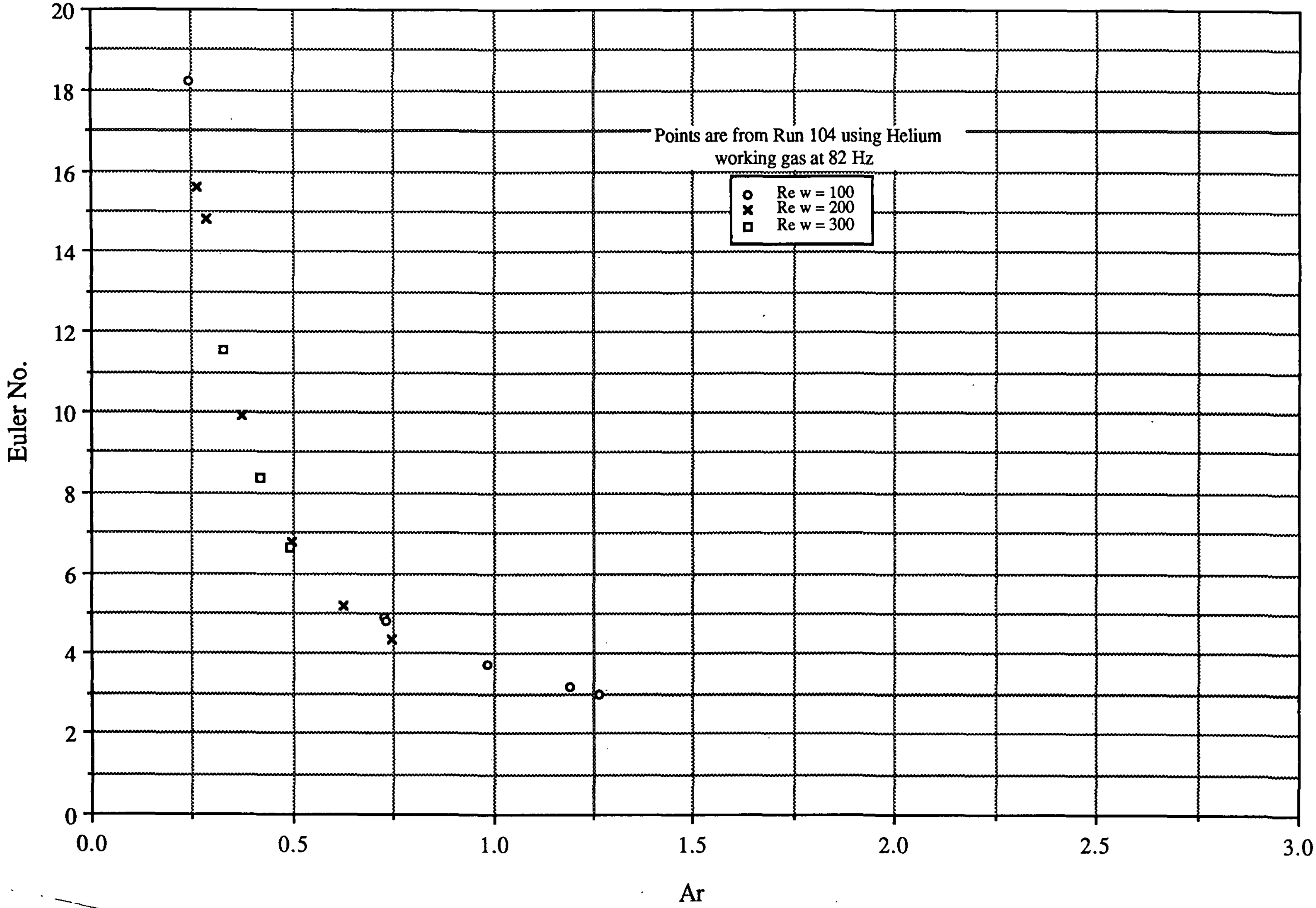

FIGURE 6.2-20

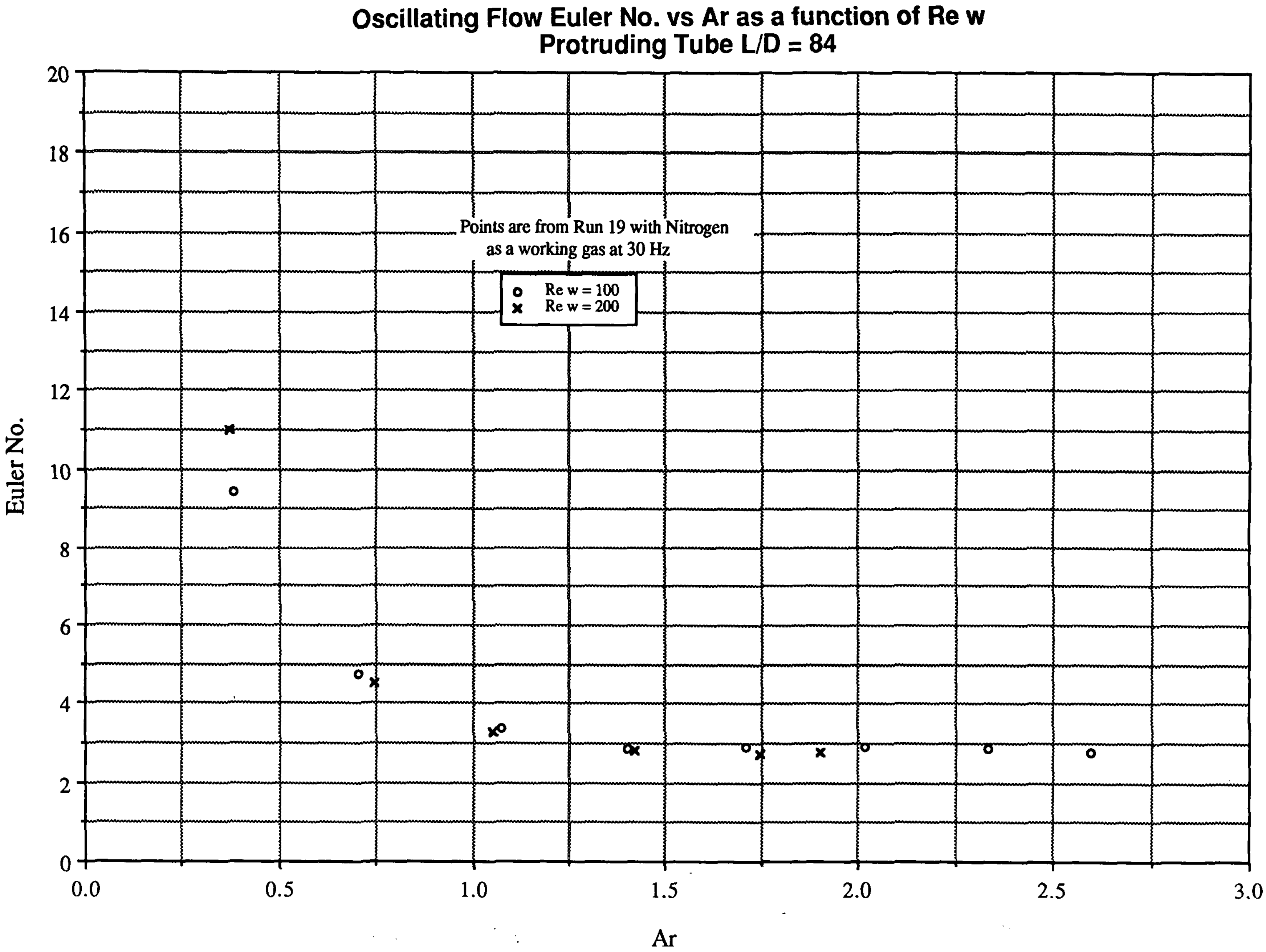
Oscillating Flow Euler No. vs Ar as a function of Re w
Protruding Tube L/D = 84
Points are from Run 19 with Nitrogen as a working gas at 30 Hz
Re w = 100
Re w = 200
Euler No.
Ar
0
2
4
6
8
10
12
14
16
18
20
0.0
0.5
1.0
1.5
2.0
2.5
3.0

FIGURE 6.2-21

Oscillating Flow Euler No. vs Re max as a function of Re w
Square Ended Tube L/D = 25

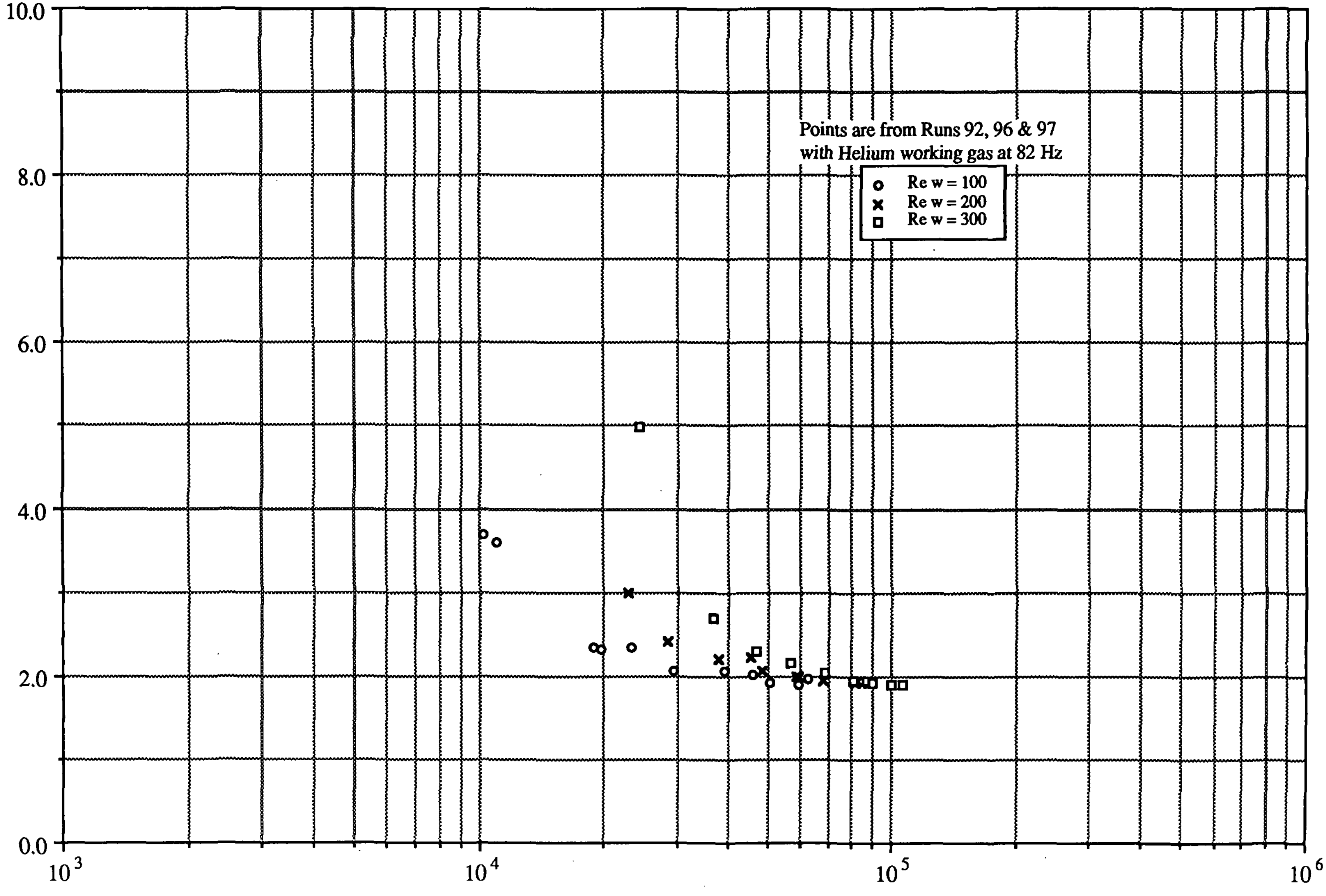

FIGURE 6.2-22

Oscillating Flow Euler No. vs Re max as a function of Re w
Square Ended Tube L/D = 50

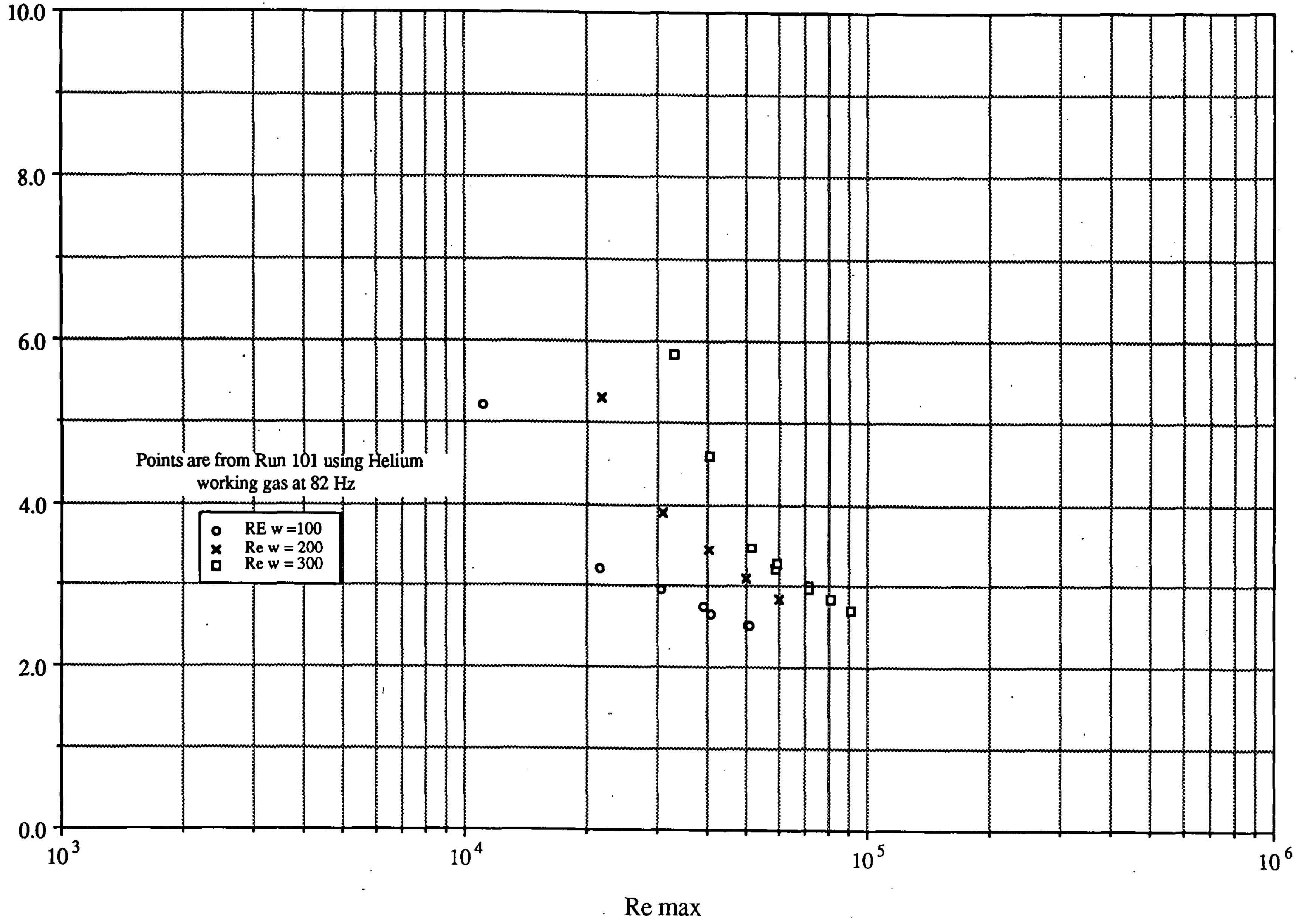

FIGURE 6.2-23

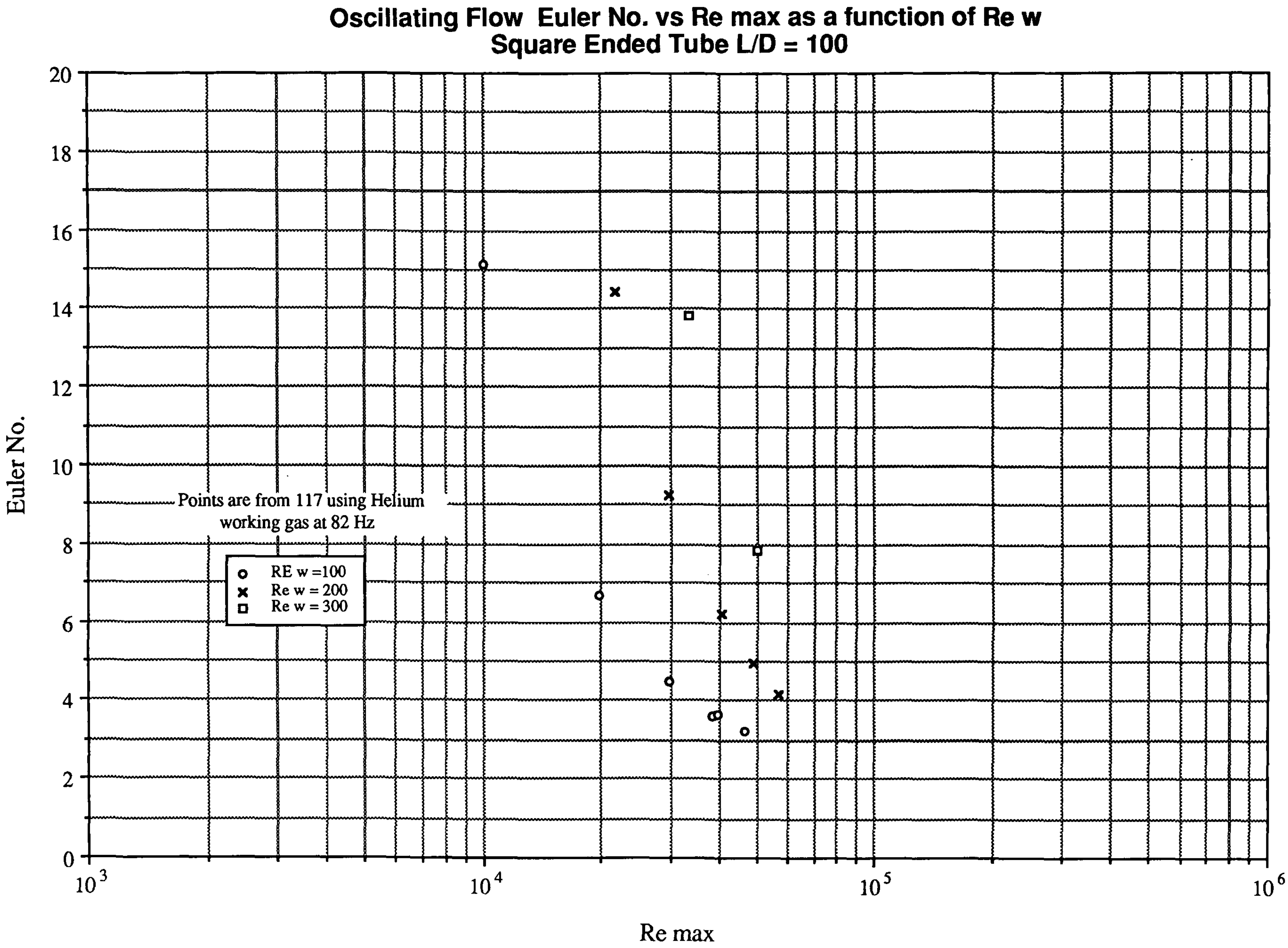

Oscillating Flow Euler No. vs Re max as a function of Re w
Square Ended Tube L/D = 100
Euler No.
Re max
Points are from 117 using Helium working gas at 82 Hz
RE w =100
Re w = 200
Re w = 300

FIGURE 6.2-24

Oscillating Flow Euler No. vs Re max as a function of Re w
Rounded Tube L/D = 25

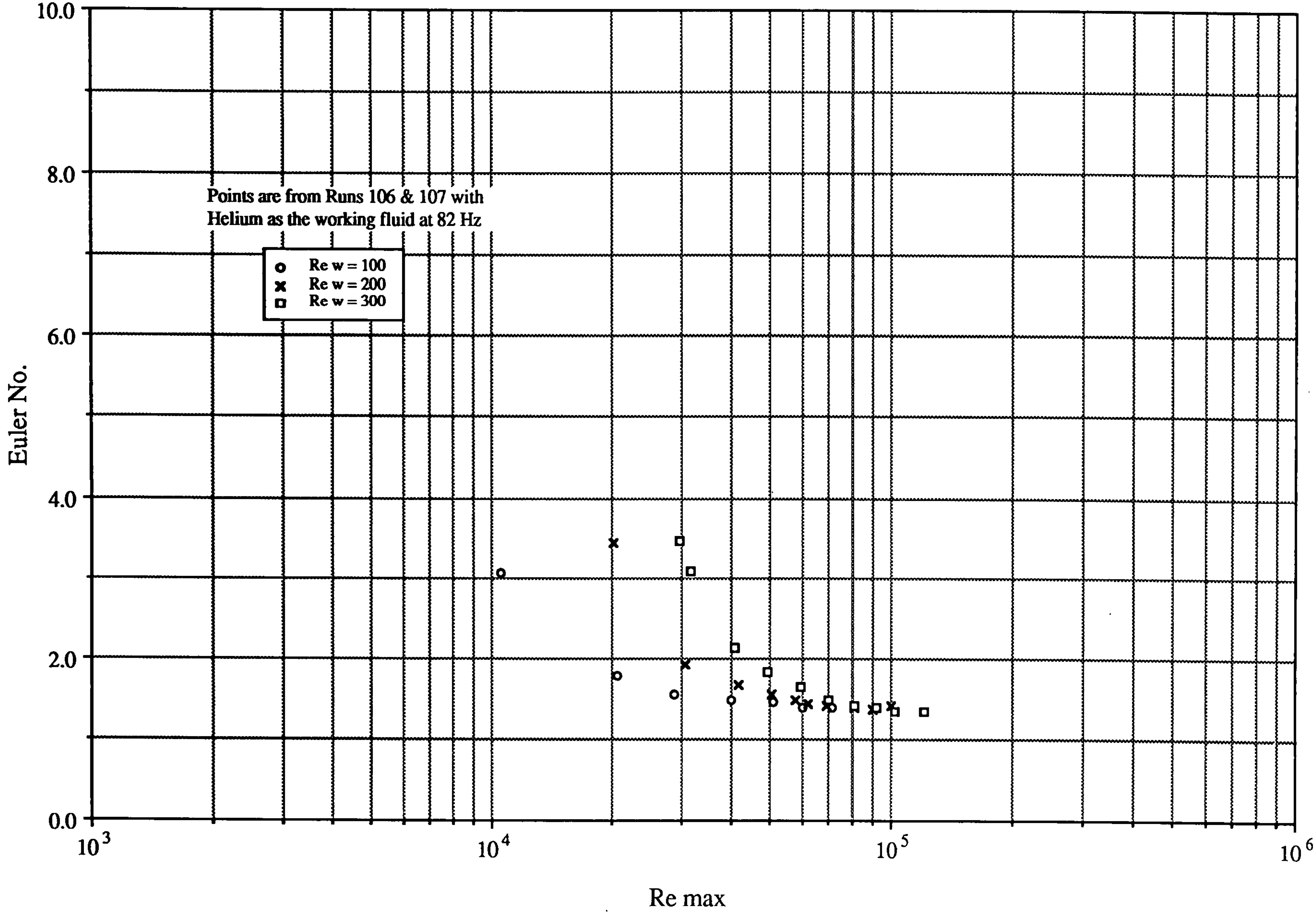

FIGURE 6.2-25

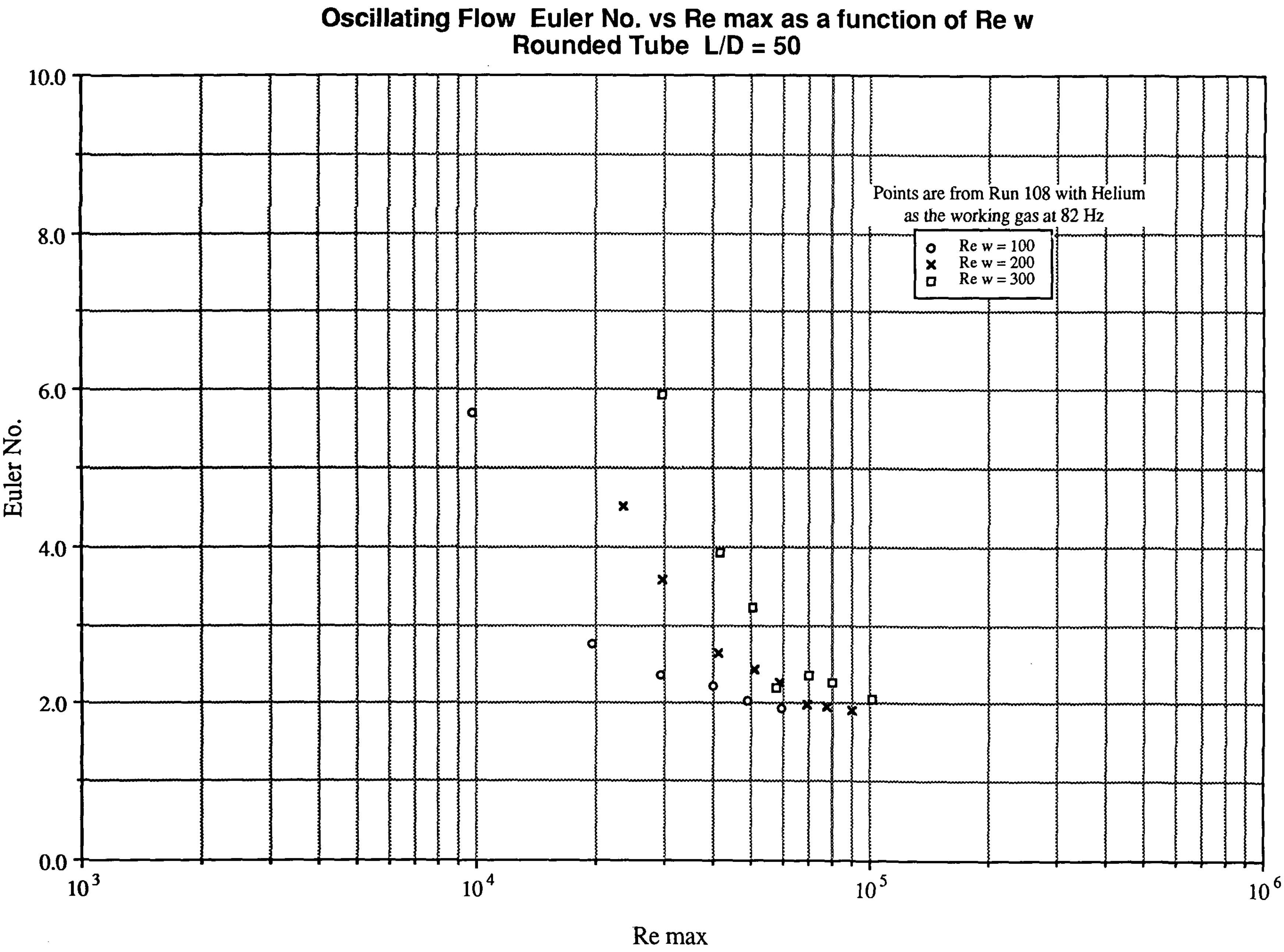
Oscillating Flow Euler No. vs Re max as a function of Re w
Rounded Tube L/D = 50
10.0
8.0
6.0
4.0
2.0
0.0
Euler No.
10^3
10^4
10^5
10^6
Re max
Points are from Run 108 with Helium as the working gas at 82 Hz
Re w = 100
Re w = 200
Re w = 300

FIGURE 6.2-26

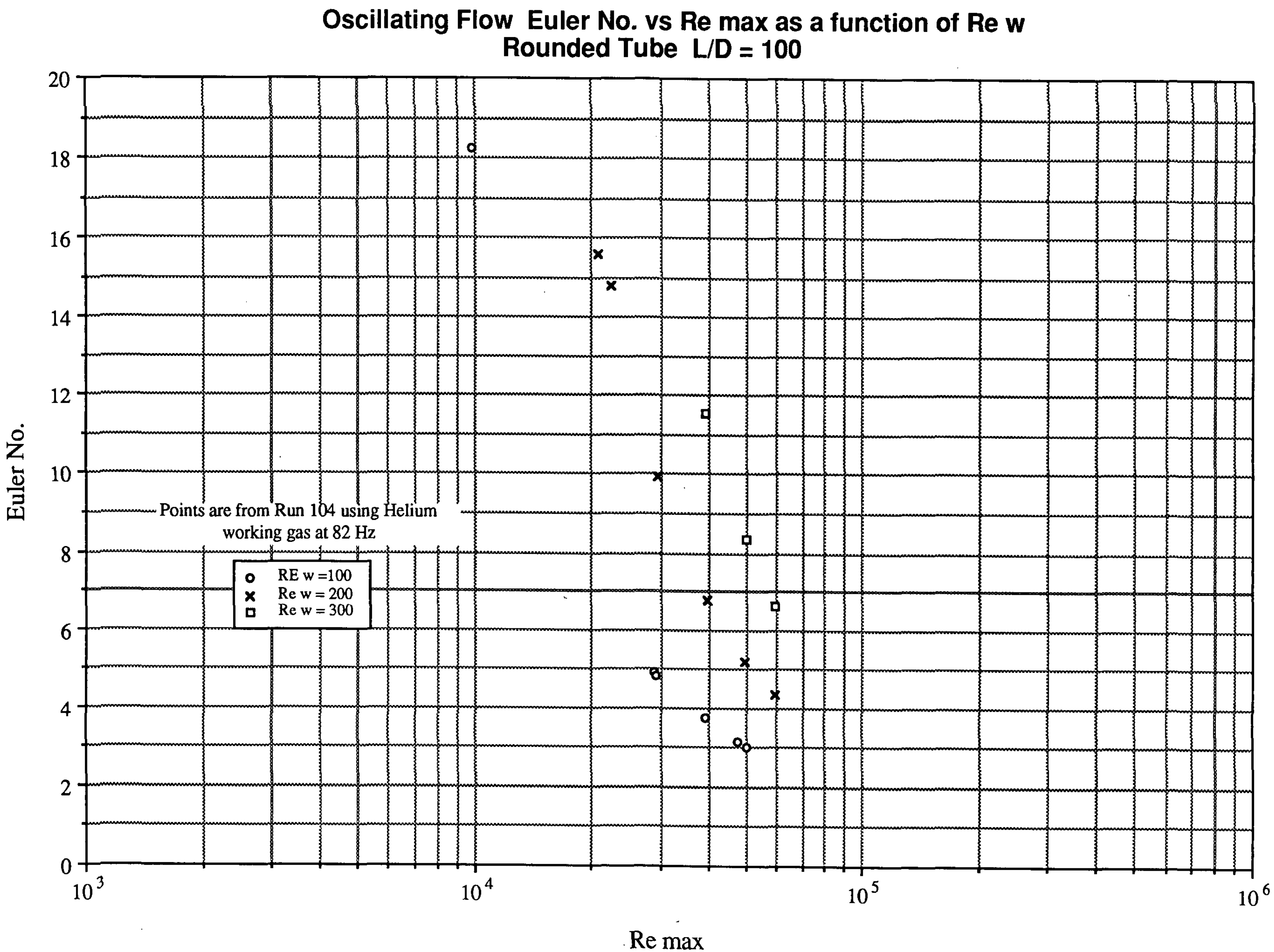
Oscillating Flow Euler No. vs Re max as a function of Re w
Rounded Tube L/D = 100
Euler No.
Re max
Points are from Run 104 using Helium working gas at 82 Hz
RE w =100
Re w = 200
Re w = 300
20
18
16
14
12
10
8
6
4
2
0
10^3
10^4
10^5
10^6

FIGURE 6.2-27

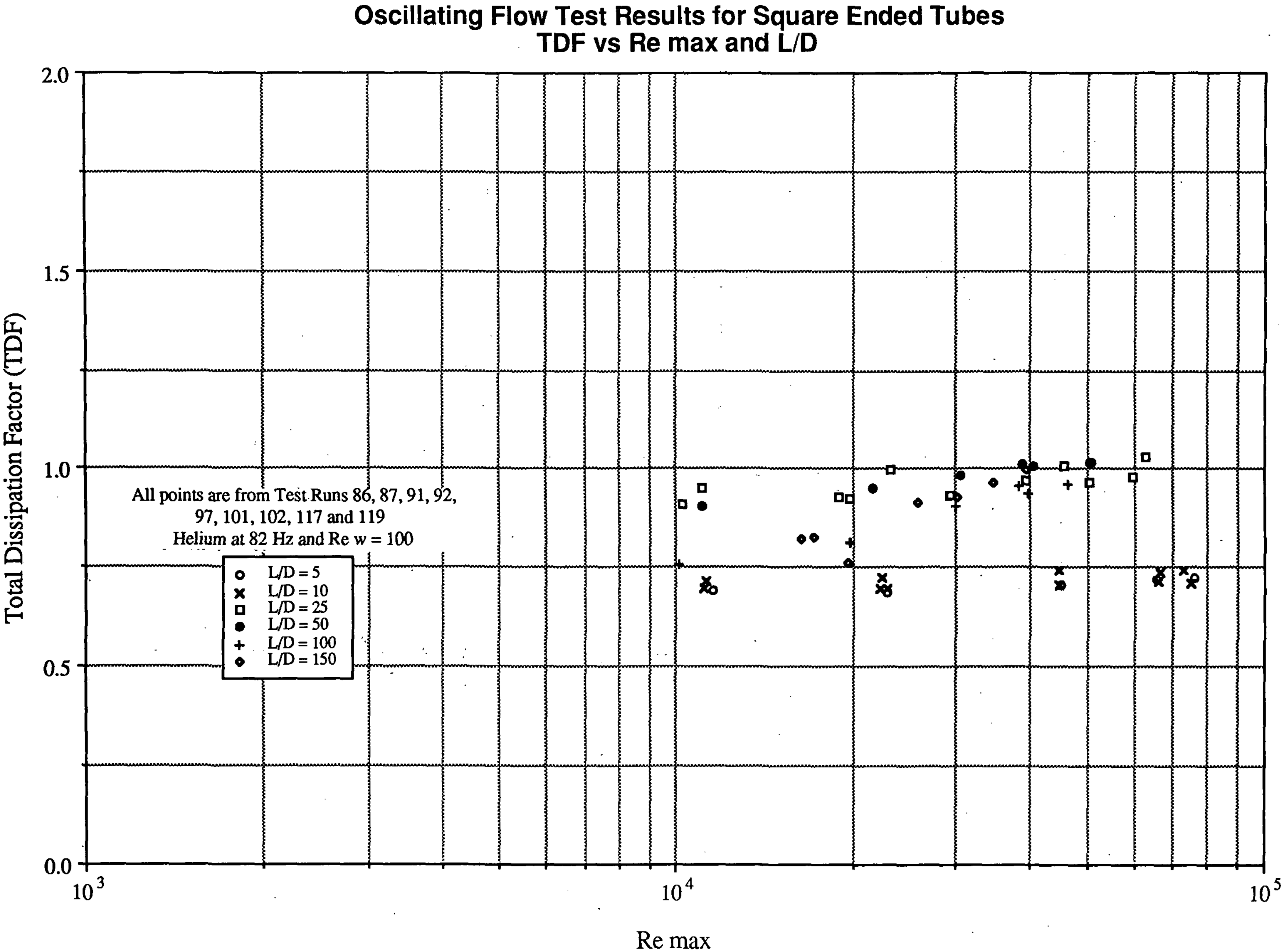
Oscillating Flow Test Results for Square Ended Tubes
TDF vs Re max and L/D
Total Dissipation Factor (TDF)
2.0
1.5
1.0
0.5
0.0
10^3
10^4
10^5
Re max
All points are from Test Runs 86, 87, 91, 92, 97, 101, 102, 117 and 119
Helium at 82 Hz and Re w = 100
L/D = 5
L/D = 10
L/D = 25
L/D = 50
L/D = 100
L/D = 150

FIGURE 6.2-28

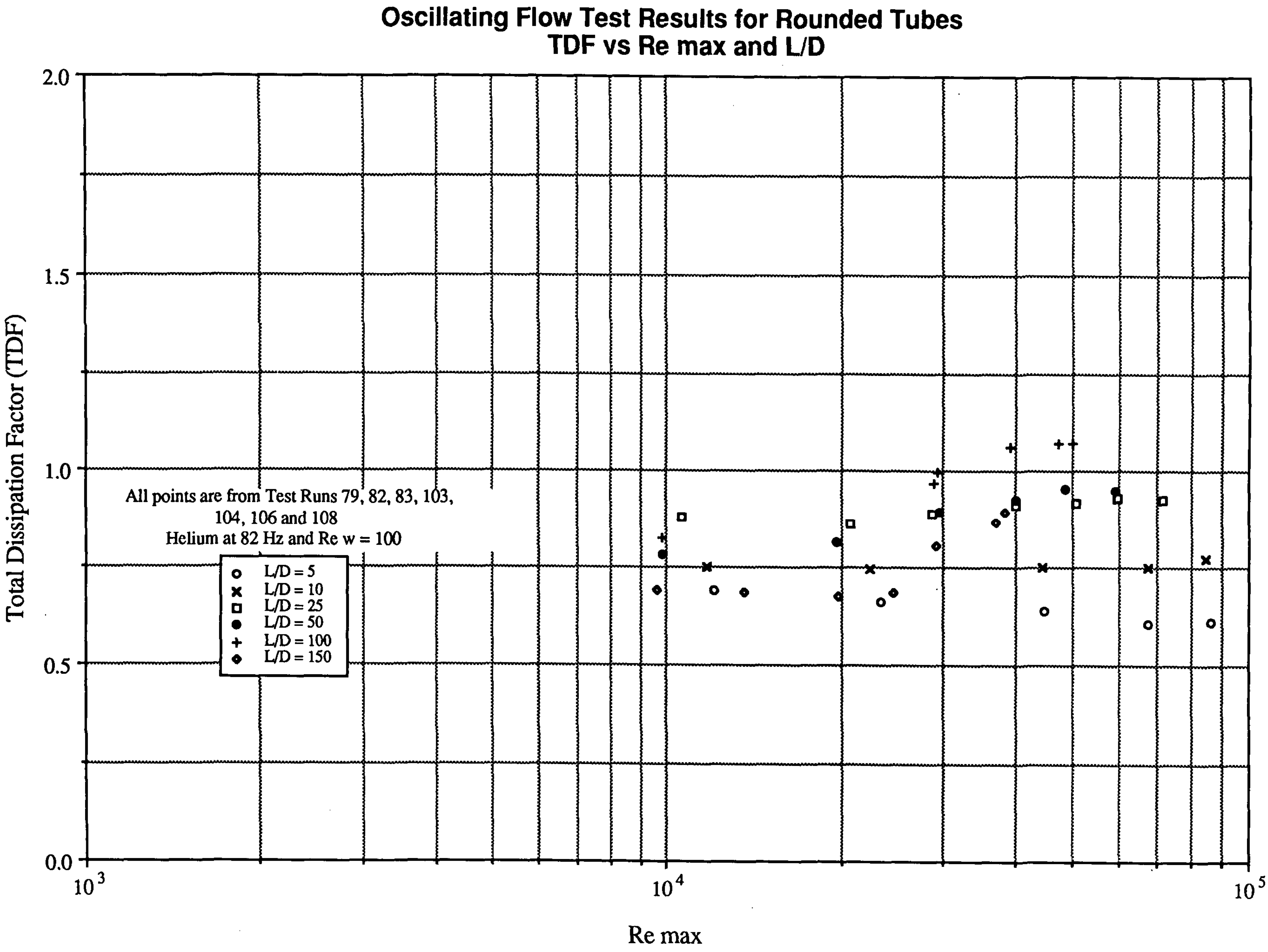
Oscillating Flow Test Results for Rounded Tubes
TDF vs Re max and L/D
Total Dissipation Factor (TDF)
2.0
1.5
1.0
0.5
0.0
10 3
10 4
10 5
Re max
All points are from Test Runs 79, 82, 83, 103, 104, 106 and 108
Helium at 82 Hz and Re w = 100
L/D = 5
L/D = 10
L/D = 25
L/D = 50
L/D = 100
L/D = 150

FIGURE 6.2-29

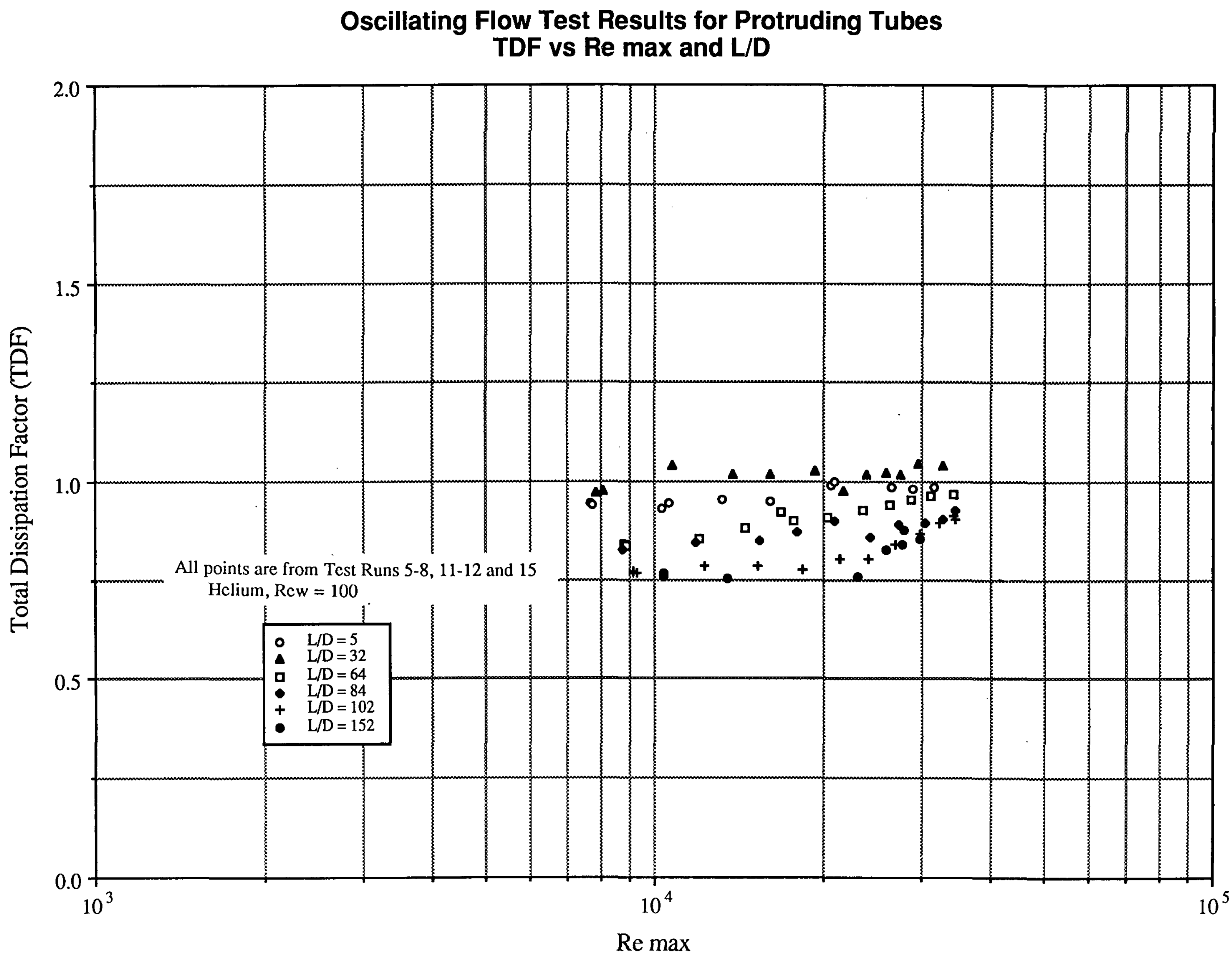
Oscillating Flow Test Results for Protruding Tubes
TDF vs Re max and L/D
Total Dissipation Factor (TDF)
2.0
1.5
1.0
0.5
0.0
All points are from Test Runs 5-8, 11-12 and 15
Helium, Rcw = 100
L/D = 5
L/D = 32
L/D = 64
L/D = 84
L/D = 102
L/D = 152
10^3
10^4
10^5
Re max

FIGURE 6.2-30

Oscillating Flow Test Results for Square Ended Tubes
TDF vs Ar and L/D

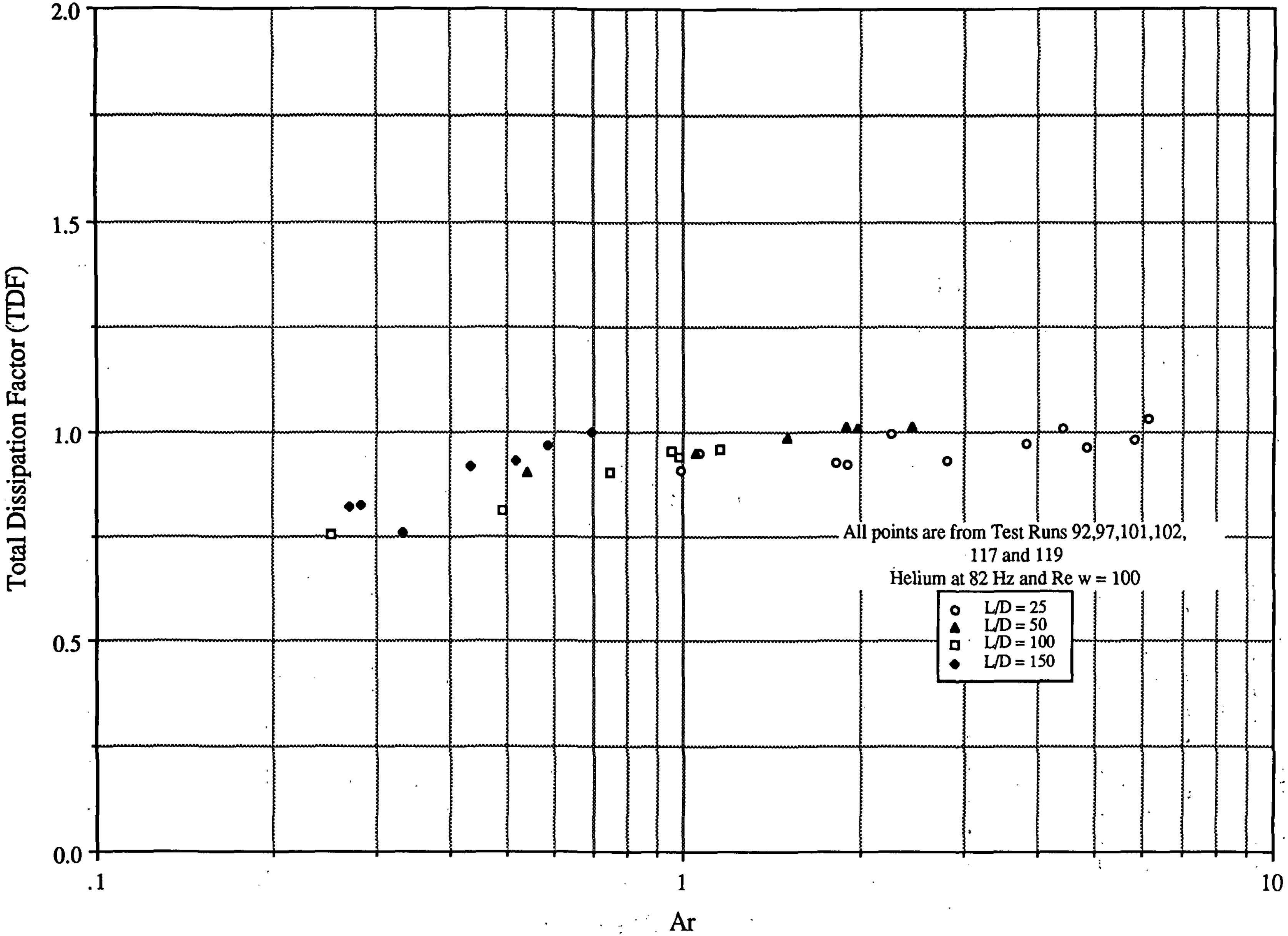

FIGURE 6.2-31

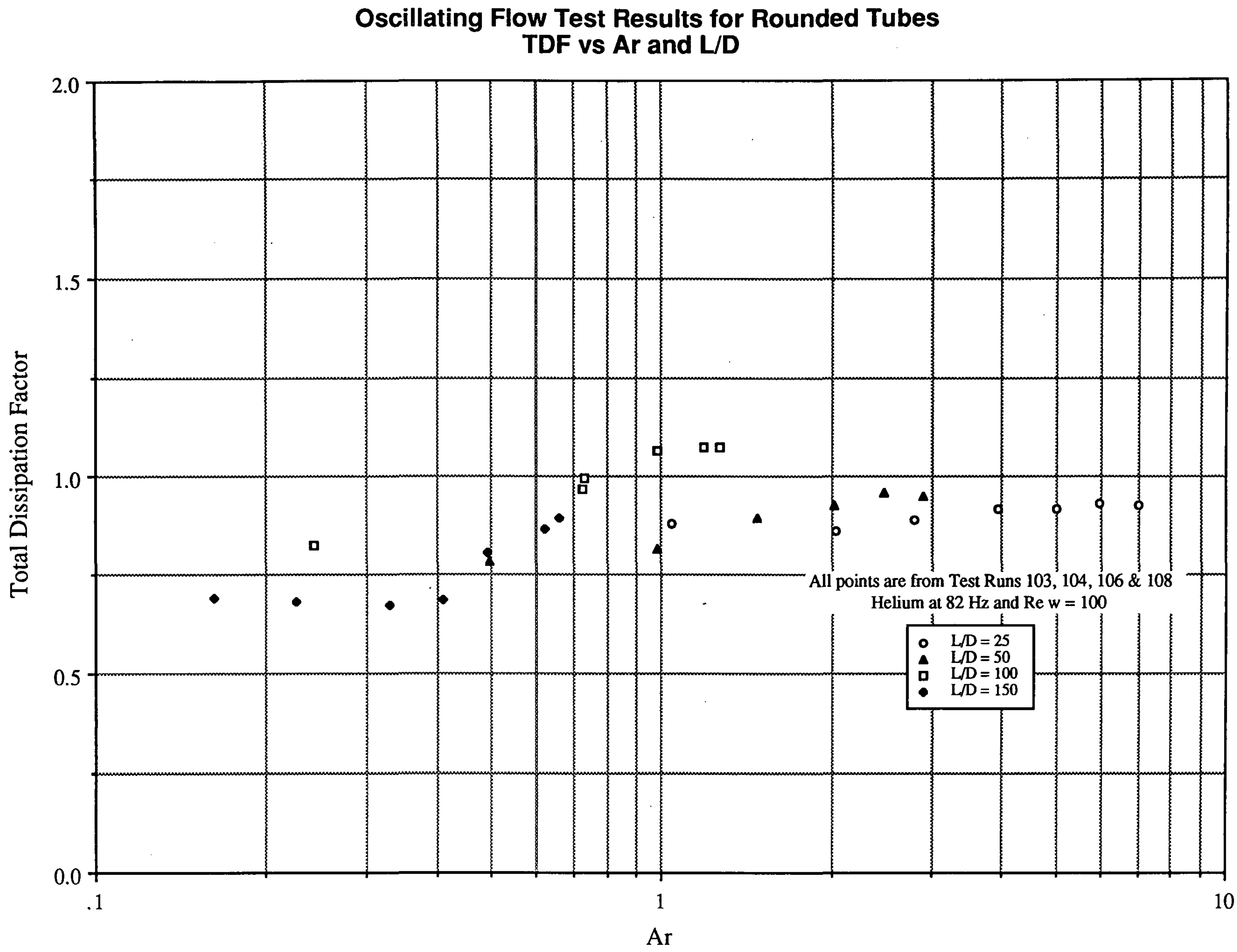
Oscillating Flow Test Results for Rounded Tubes
TDF vs Ar and L/D
Total Dissipation Factor
2.0
1.5
1.0
0.5
0.0
.1
1
10
Ar
All points are from Test Runs 103, 104, 106 & 108
Helium at 82 Hz and Re w = 100
L/D = 25
L/D = 50
L/D = 100
L/D = 150

FIGURE 6.2-32

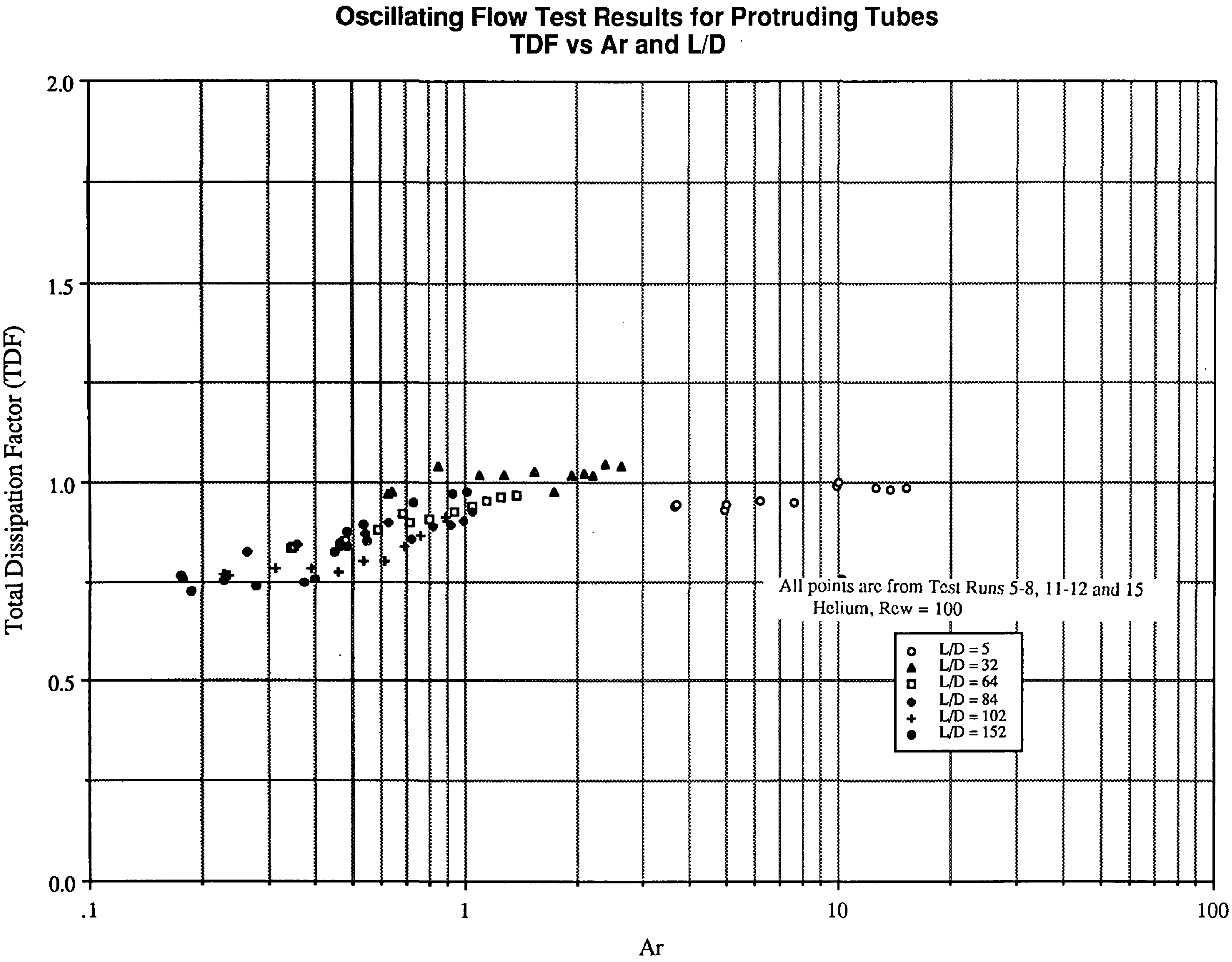
Oscillating Flow Test Results for Protruding Tubes
TDF vs Ar and L/D
2.0
1.5
1.0
0.5
0.0
Total Dissipation Factor (TDF)
.1
1
10
100
Ar
All points are from Test Runs 5-8, 11-12 and 15
Helium, Rew = 100
L/D = 5
L/D = 32
L/D = 64
L/D = 84
L/D = 102
L/D = 152

FIGURE 6.2-33

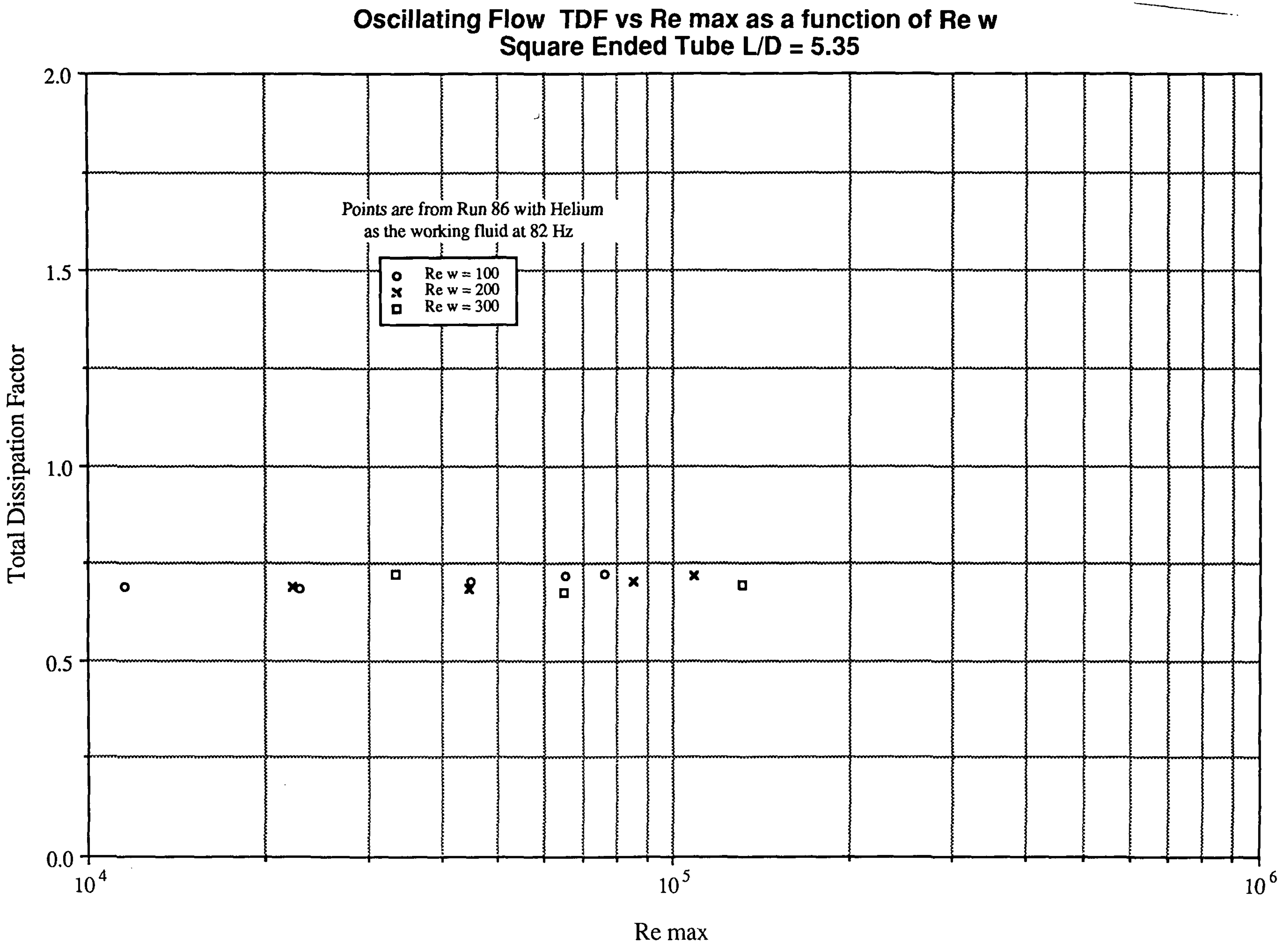

Oscillating Flow TDF vs Re max as a function of Re w
Square Ended Tube L/D = 5.35
Points are from Run 86 with Helium
as the working fluid at 82 Hz
Re w = 100
Re w = 200
Re w = 300
Total Dissipation Factor
Re max
2.0
1.5
1.0
0.5
0.0
10 4
10 5
10 6

FIGURE 6.2-34

Oscillating Flow TDF vs Re max as a function of Re w
Square Ended Tube L/D = 10

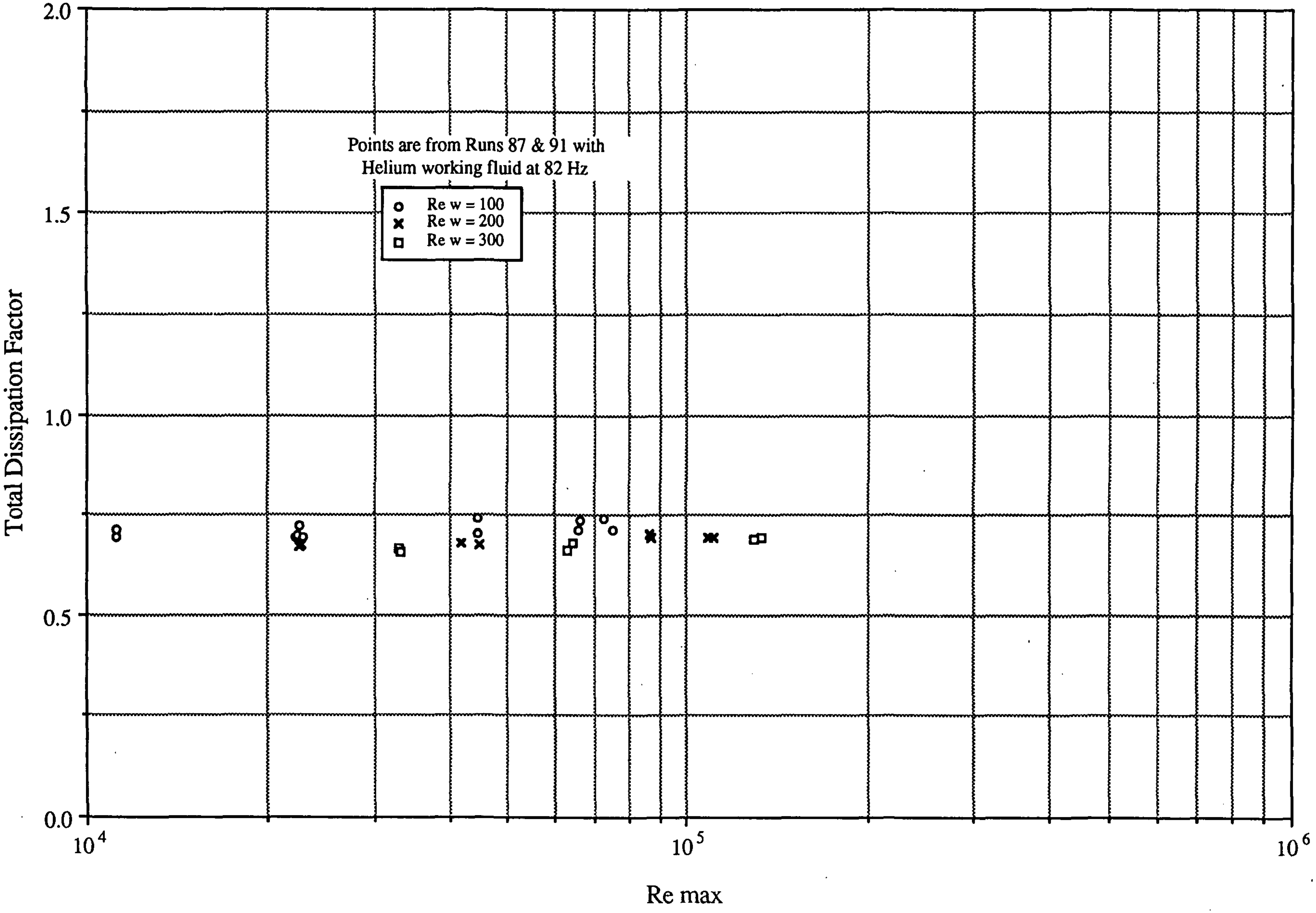

FIGURE 6.2-35

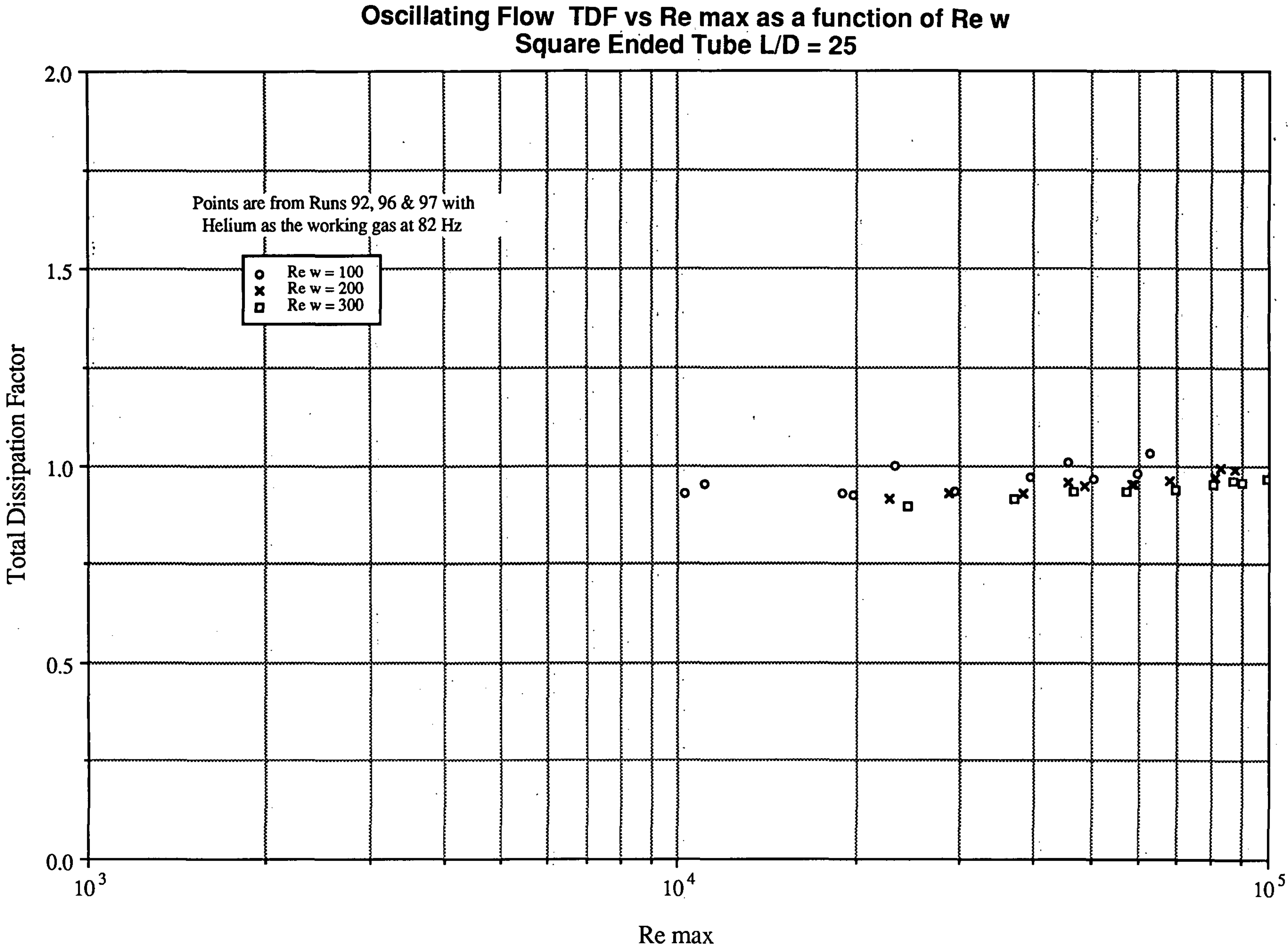

Oscillating Flow TDF vs Re max as a function of Re w
Square Ended Tube L/D = 25
Points are from Runs 92, 96 & 97 with
Helium as the working gas at 82 Hz
Re w = 100
Re w = 200
Re w = 300
Total Dissipation Factor
2.0
1.5
1.0
0.5
0.0
10^3
10^4
10^5
Re max

FIGURE 6.2-36

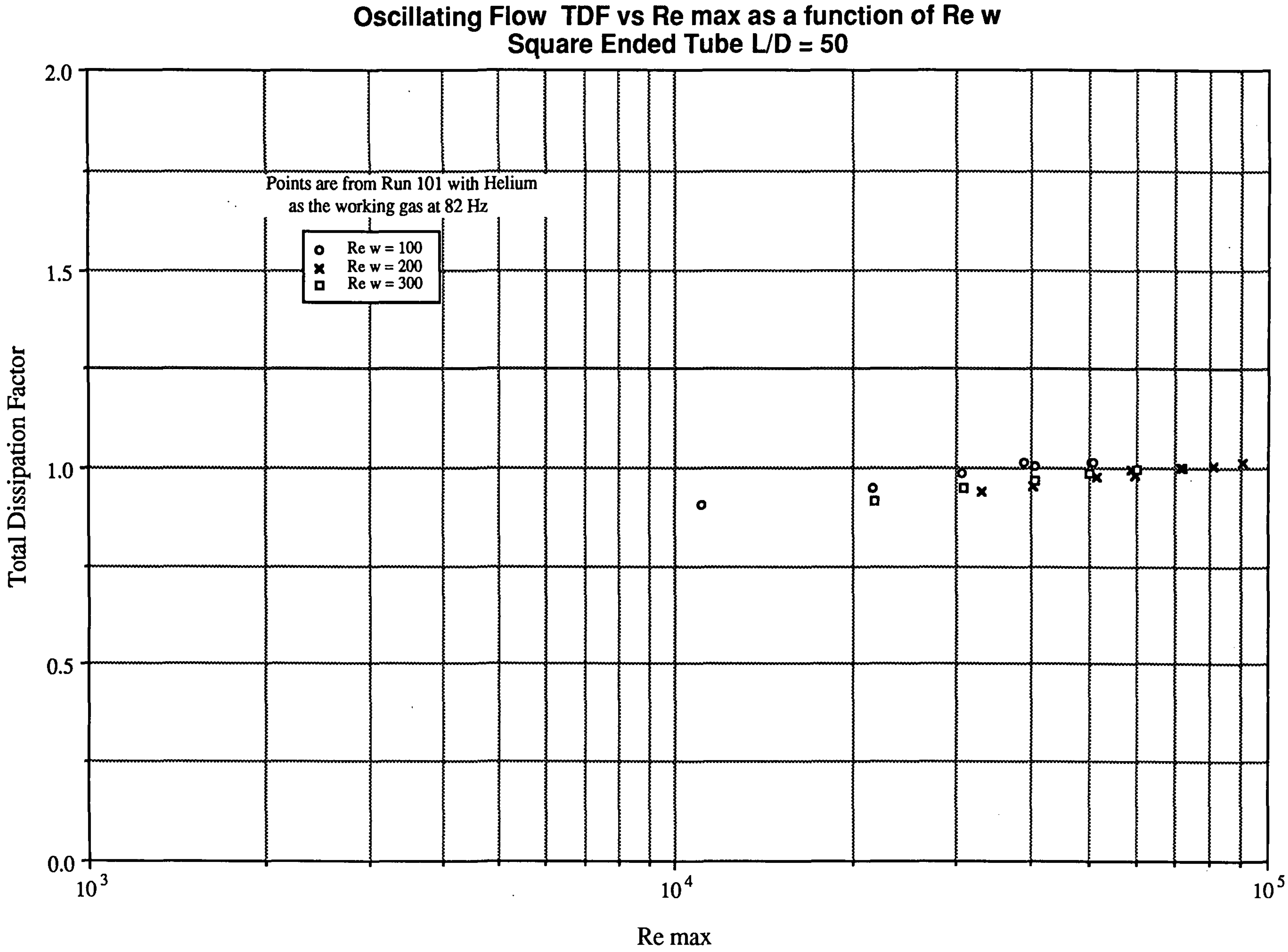

Oscillating Flow TDF vs Re max as a function of Re w
Square Ended Tube L/D = 50
Points are from Run 101 with Helium
as the working gas at 82 Hz
Re w = 100
Re w = 200
Re w = 300
Total Dissipation Factor
Re max
2.0
1.5
1.0
0.5
0.0
10 3
10 4
10 5

FIGURE 6.2-37

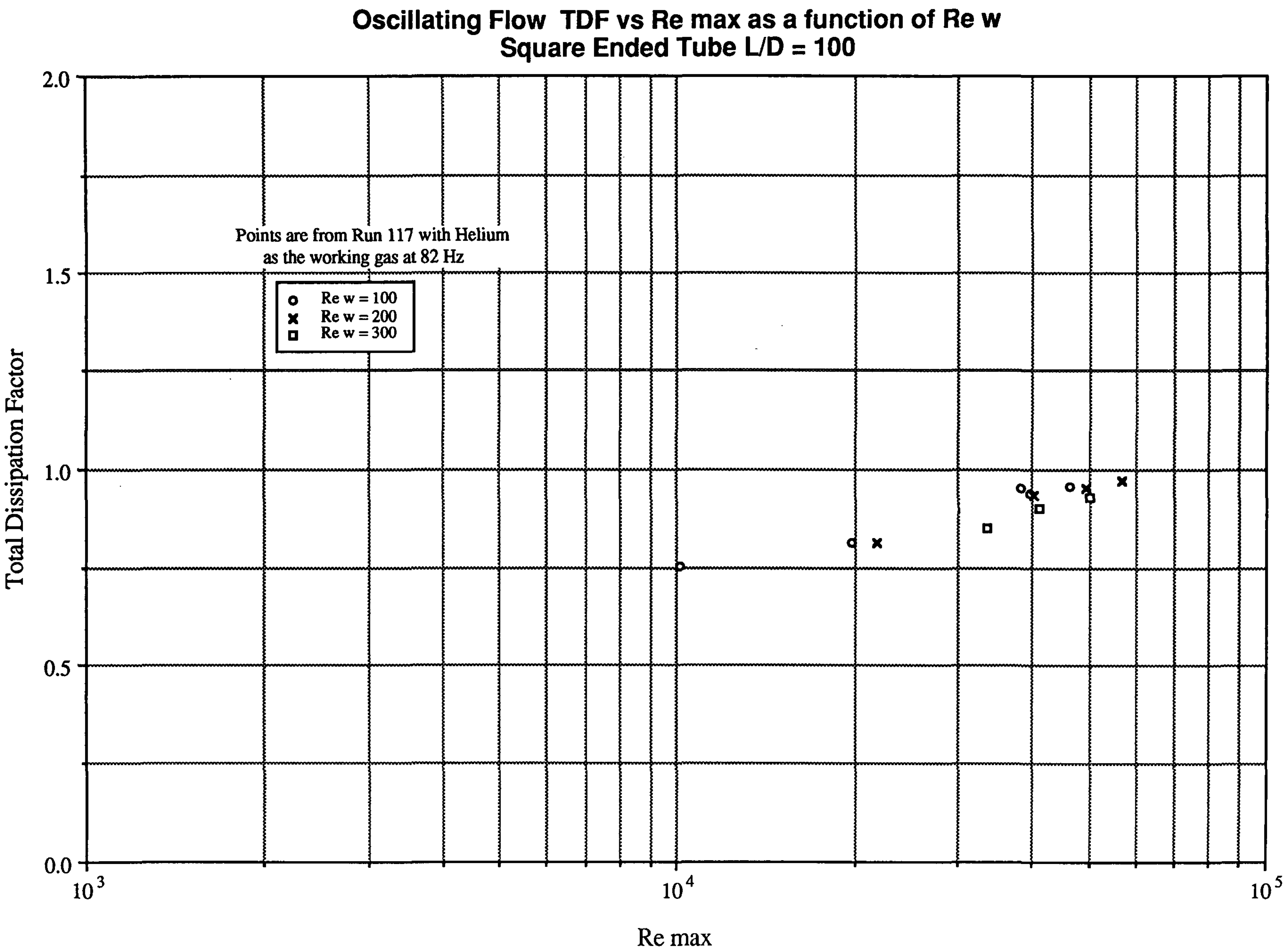
Oscillating Flow TDF vs Re max as a function of Re w
Square Ended Tube L/D = 100
Points are from Run 117 with Helium
as the working gas at 82 Hz
Re w = 100
Re w = 200
Re w = 300
Total Dissipation Factor
2.0
1.5
1.0
0.5
0.0
10^3
10^4
10^5
Re max

FIGURE 6.2-38

Oscillating Flow TDF vs Re max as a function of Re w
Square Ended Tube L/D = 150

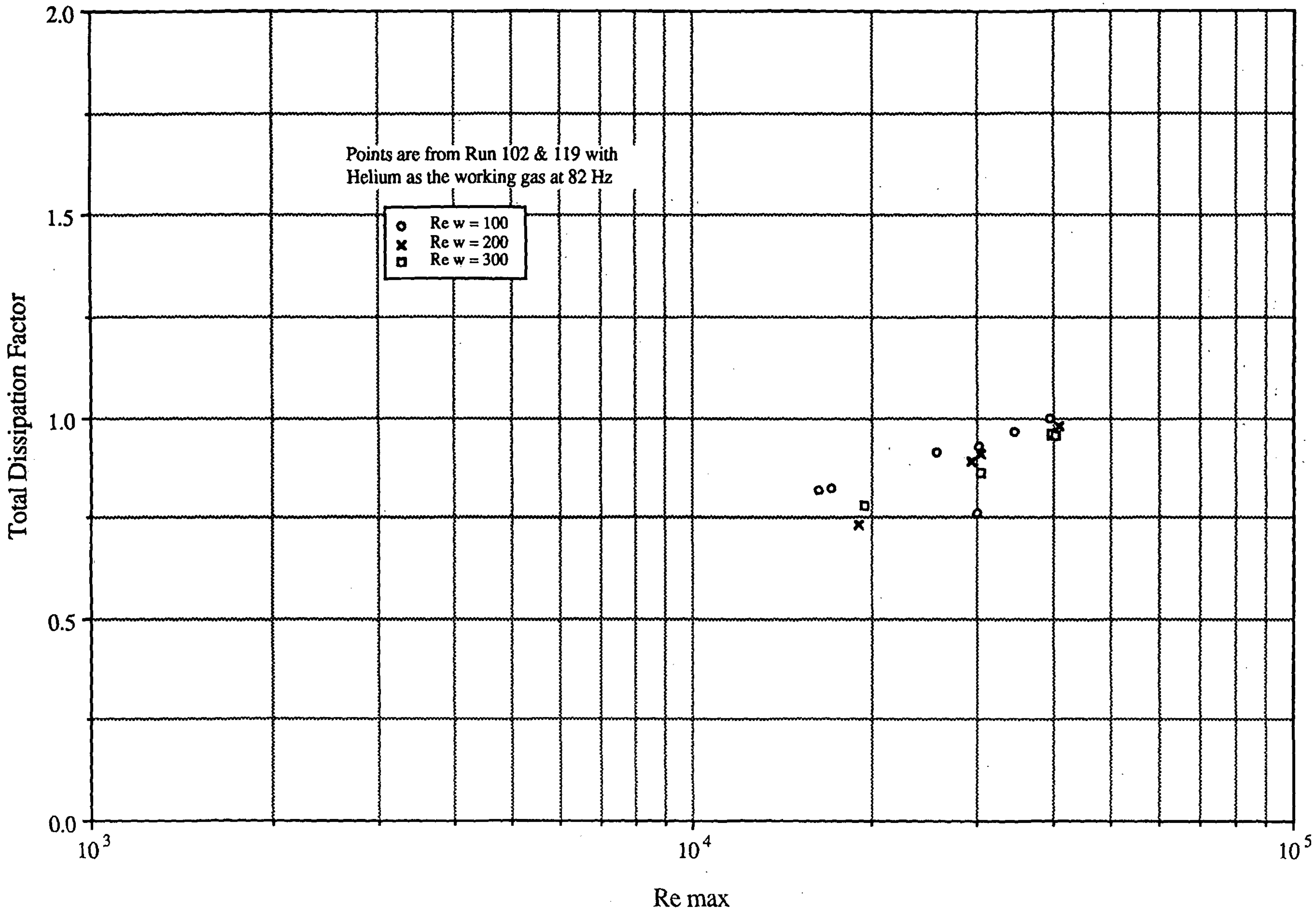

FIGURE 6.2-39

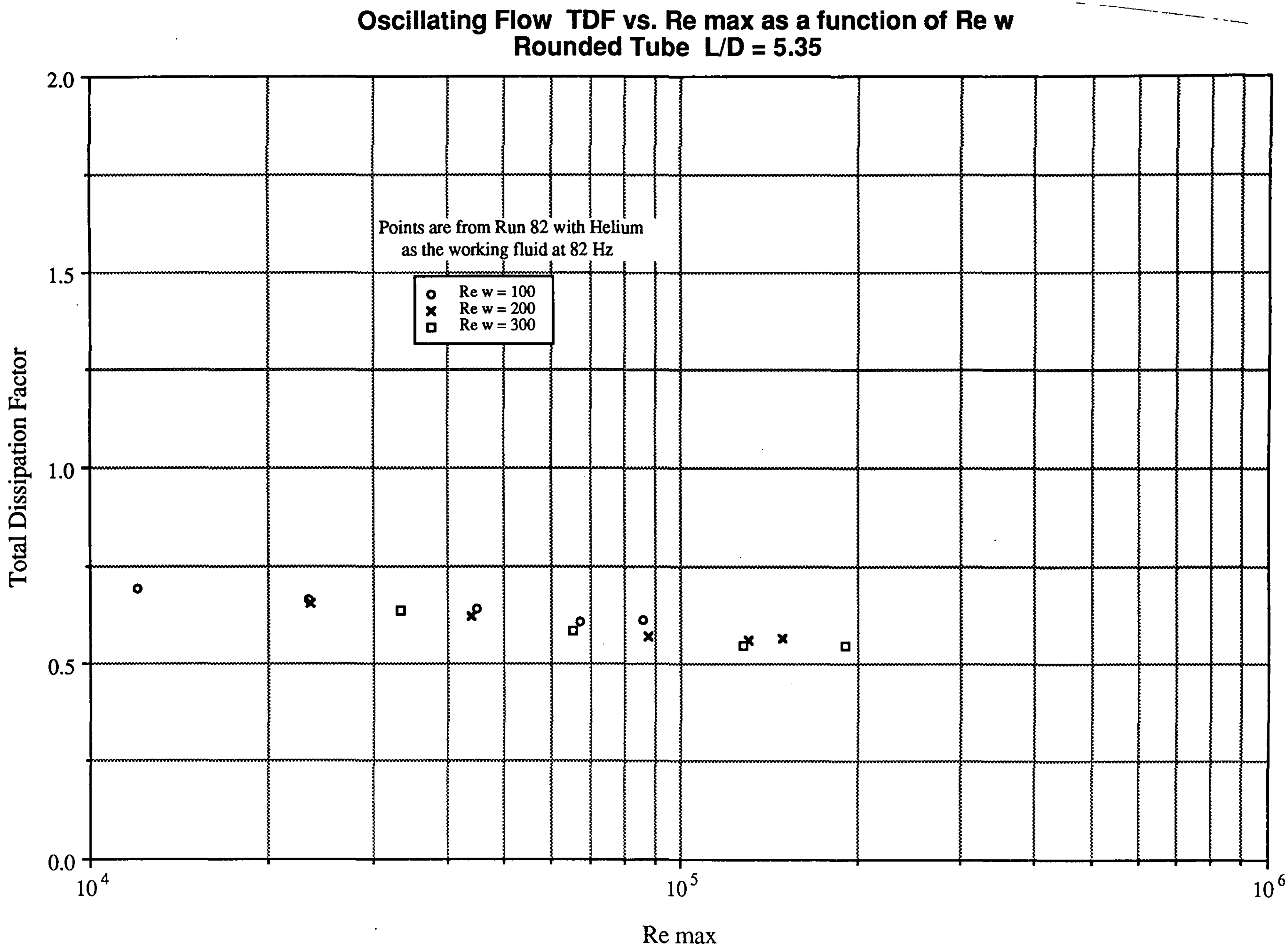

Oscillating Flow TDF vs. Re max as a function of Re w
Rounded Tube L/D = 5.35
Points are from Run 82 with Helium
as the working fluid at 82 Hz
Re w = 100
Re w = 200
Re w = 300
Total Dissipation Factor
2.0
1.5
1.0
0.5
0.0
10^4
10^5
10^6
Re max

FIGURE 6.2-40

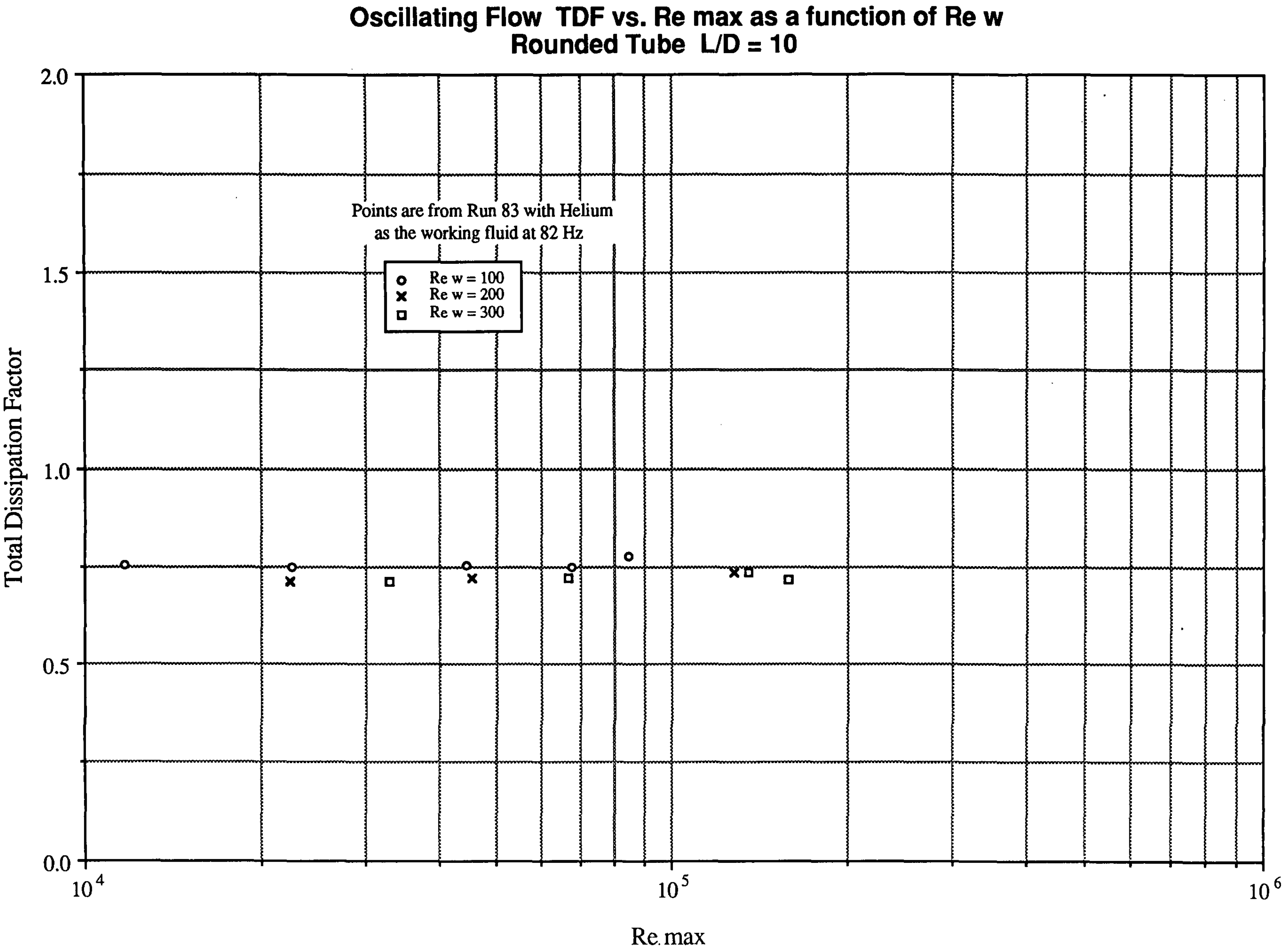

Oscillating Flow TDF vs. Re max as a function of Re w
Rounded Tube L/D = 10
Points are from Run 83 with Helium
as the working fluid at 82 Hz
Re w = 100
Re w = 200
Re w = 300
Total Dissipation Factor
2.0
1.5
1.0
0.5
0.0
10^4
10^5
10^6
Re max

FIGURE 6.2-41

Oscillating Flow TDF vs. Re max as a function of Re w
Rounded Tube L/D = 25

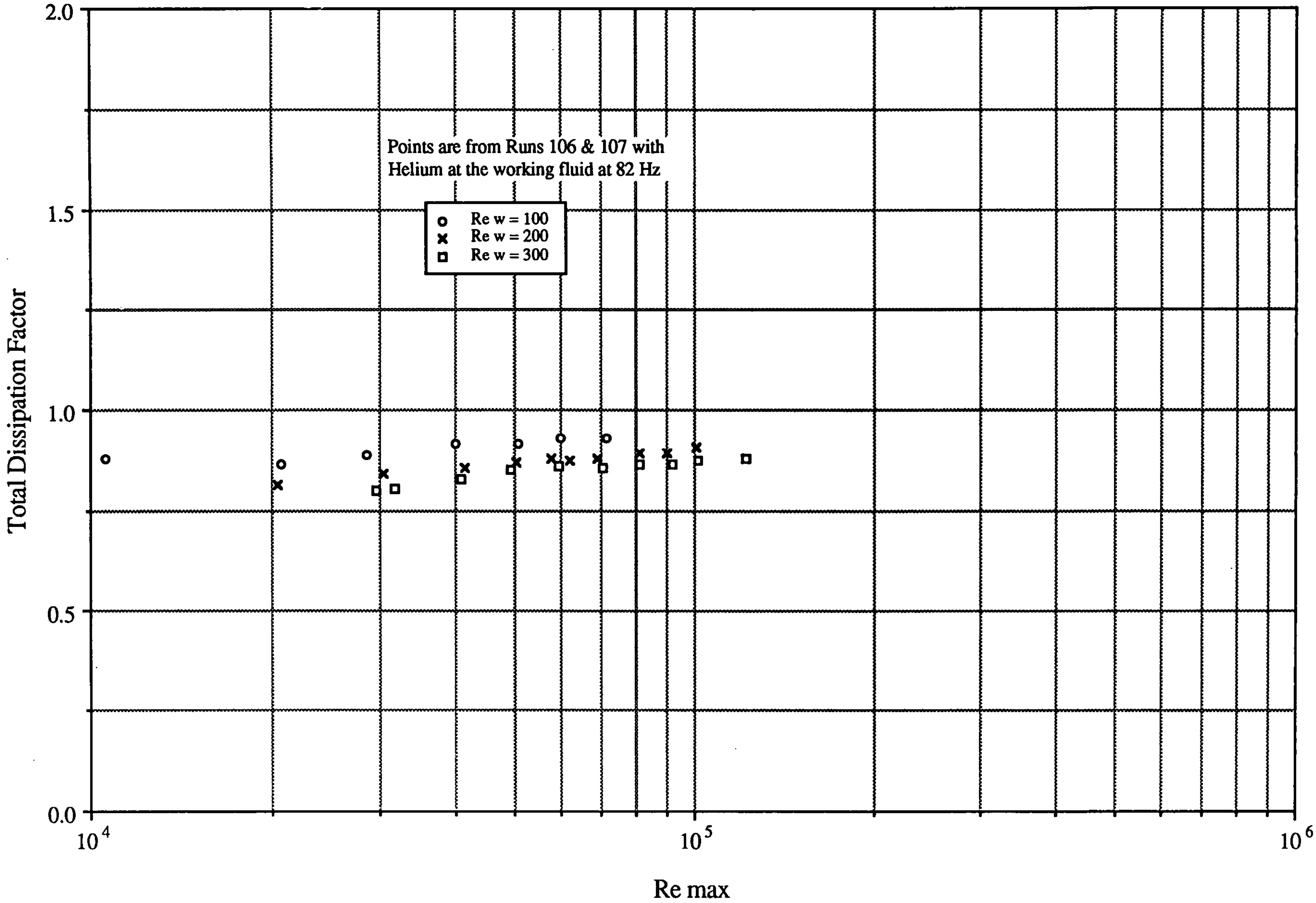

FIGURE 6.2-42

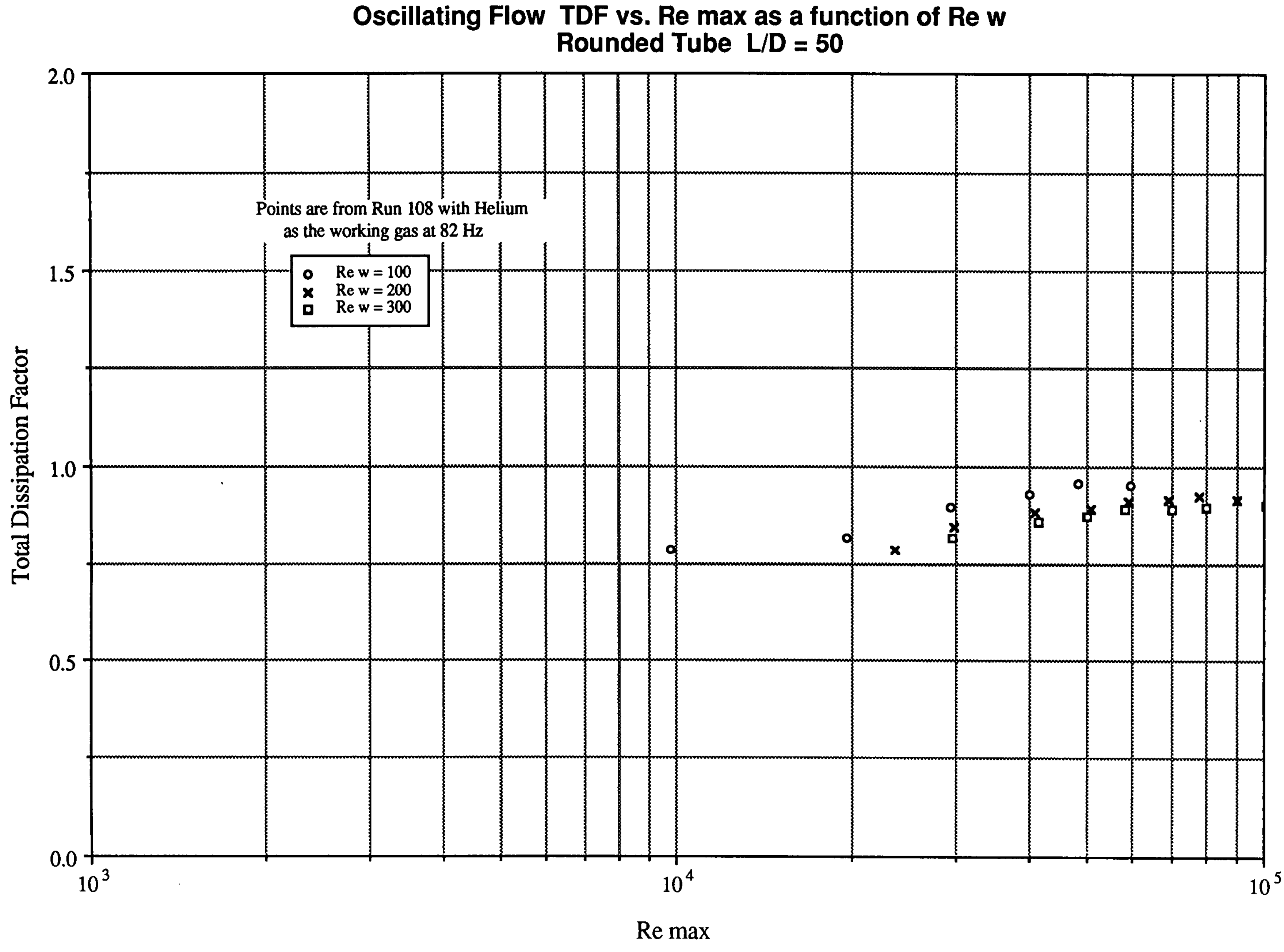
Oscillating Flow TDF vs. Re max as a function of Re w
Rounded Tube L/D = 50
Points are from Run 108 with Helium
as the working gas at 82 Hz
Re w = 100
Re w = 200
Re w = 300
Total Dissipation Factor
Re max
2.0
1.5
1.0
0.5
0.0
10 3
10 4
10 5

FIGURE 6.2-43

REGENERATOR OSCILLATING FLOW TEST RESULTS

Figures 6.2-44 through 6.2-68

Oscillating Flow Test Results for 41μm Stacked Screen
Maximum Pressure Drop Amplitude vs Re max and Re w

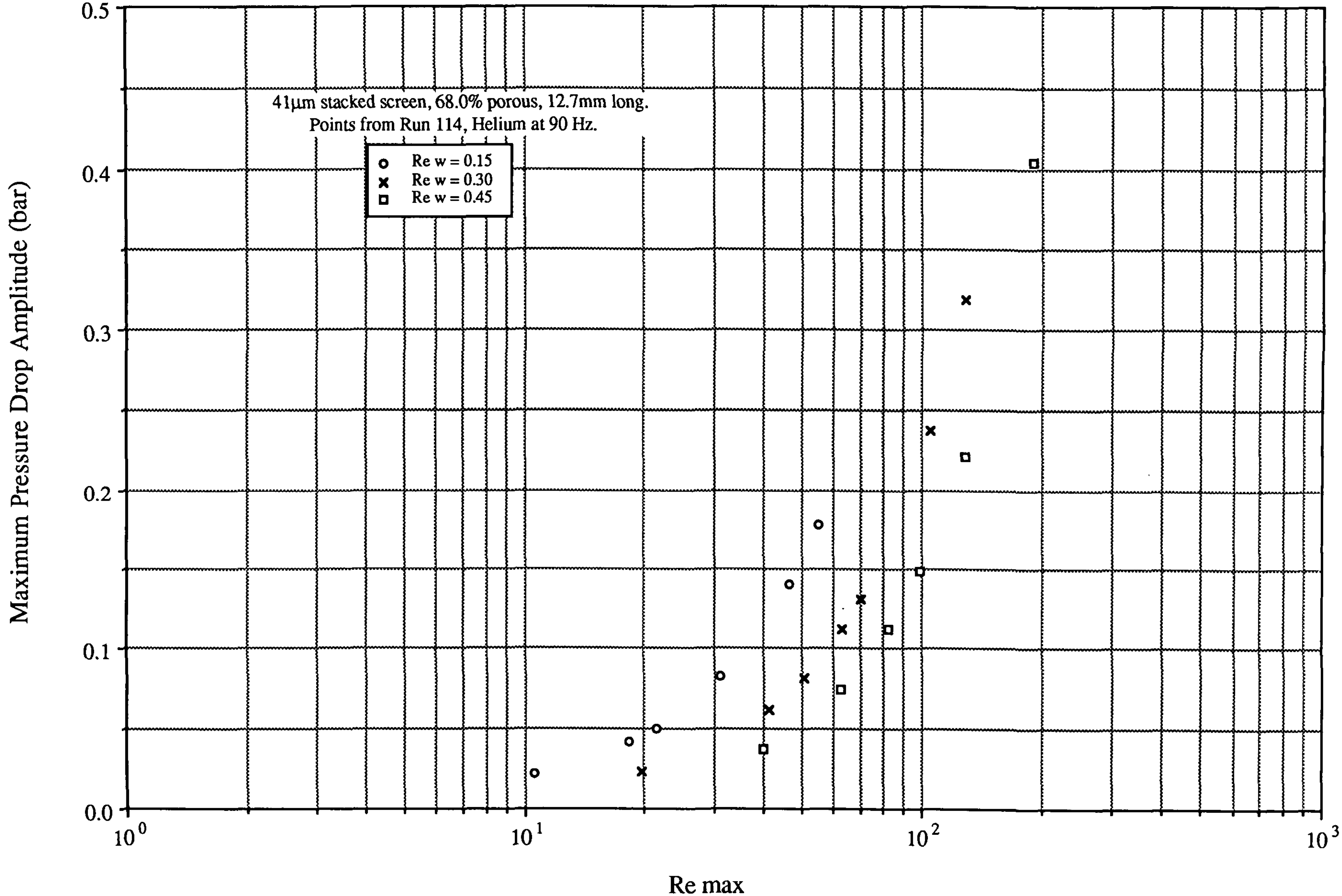

FIGURE 6.2-44

Oscillating Flow Test Results for 53μm Stacked Screen
Maximum Pressure Drop Amplitude vs Re max and Re w

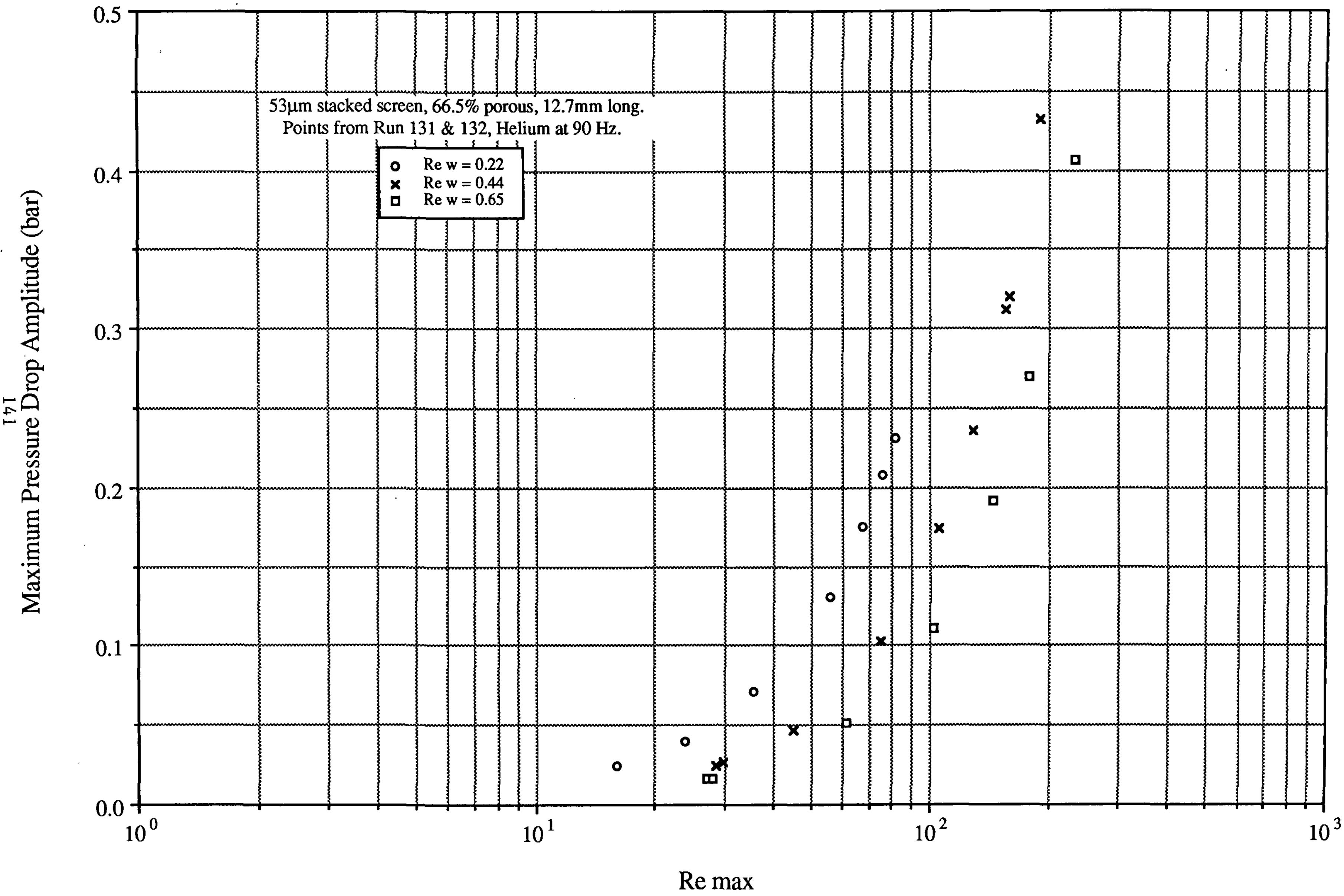

FIGURE 6.2-45

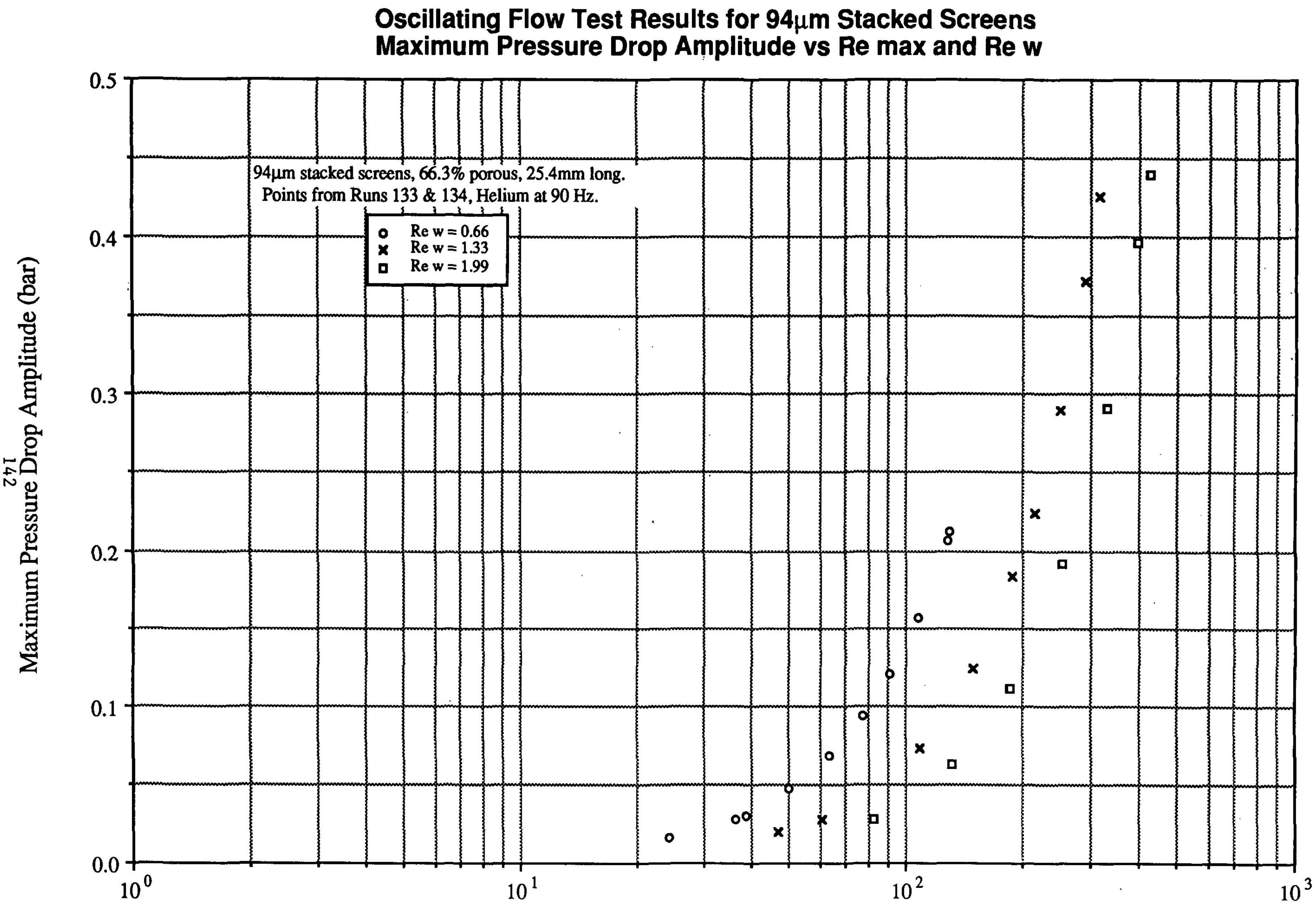

Oscillating Flow Test Results for 94µm Stacked Screens
Maximum Pressure Drop Amplitude vs Re max and Re w
94µm stacked screens, 66.3% porous, 25.4mm long.
Points from Runs 133 & 134, Helium at 90 Hz.
Re w = 0.66
Re w = 1.33
Re w = 1.99
Maximum Pressure Drop Amplitude (bar)
Re max
0.0
0.1
0.2
0.3
0.4
0.5
10^0
10^1
10^2
10^3

FIGURE 6.2-46

Oscillating Flow Test Results for 191μm Stacked Screens
Maximum Pressure Drop Amplitude vs Re max and Re w

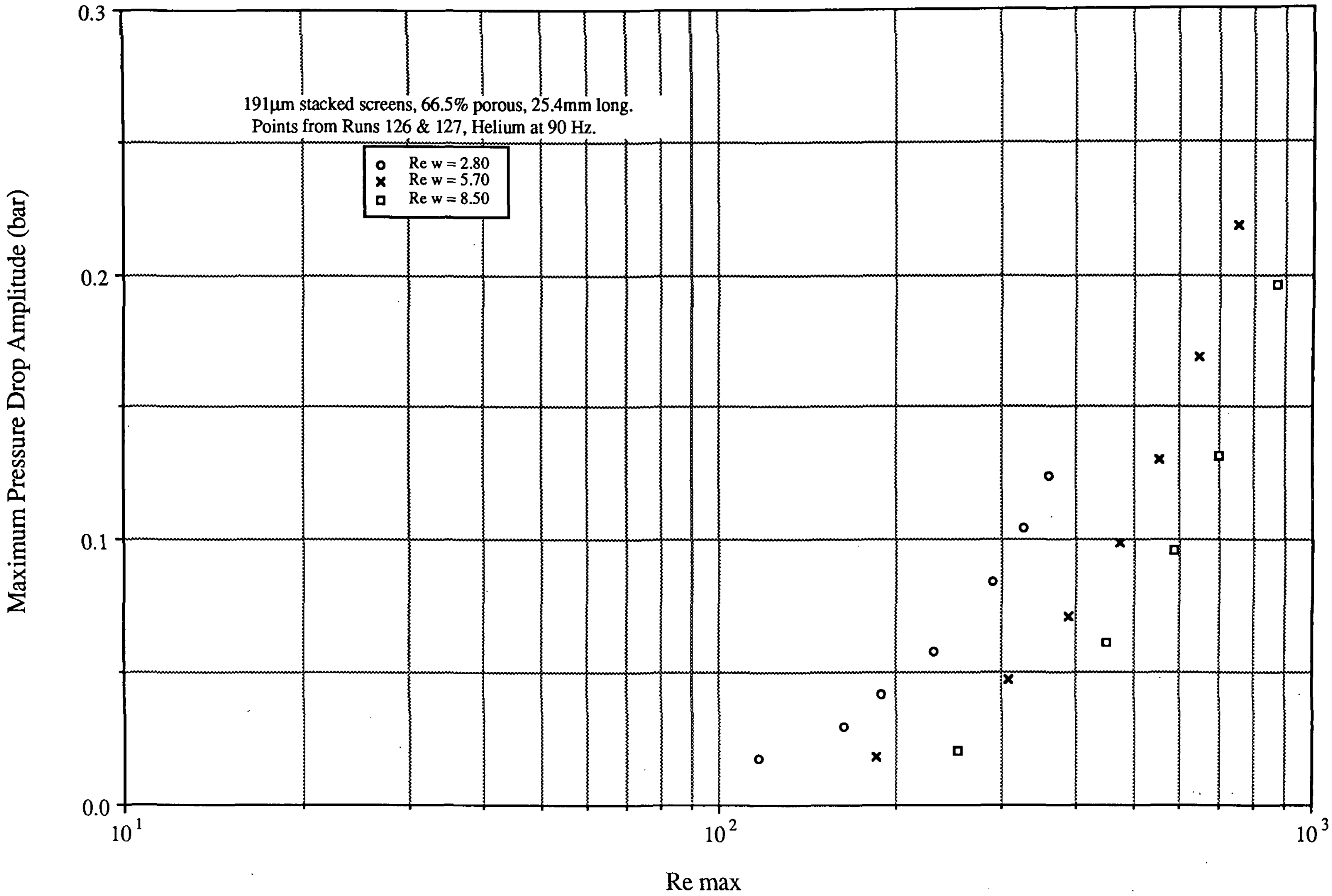

143

FIGURE 6.2-47

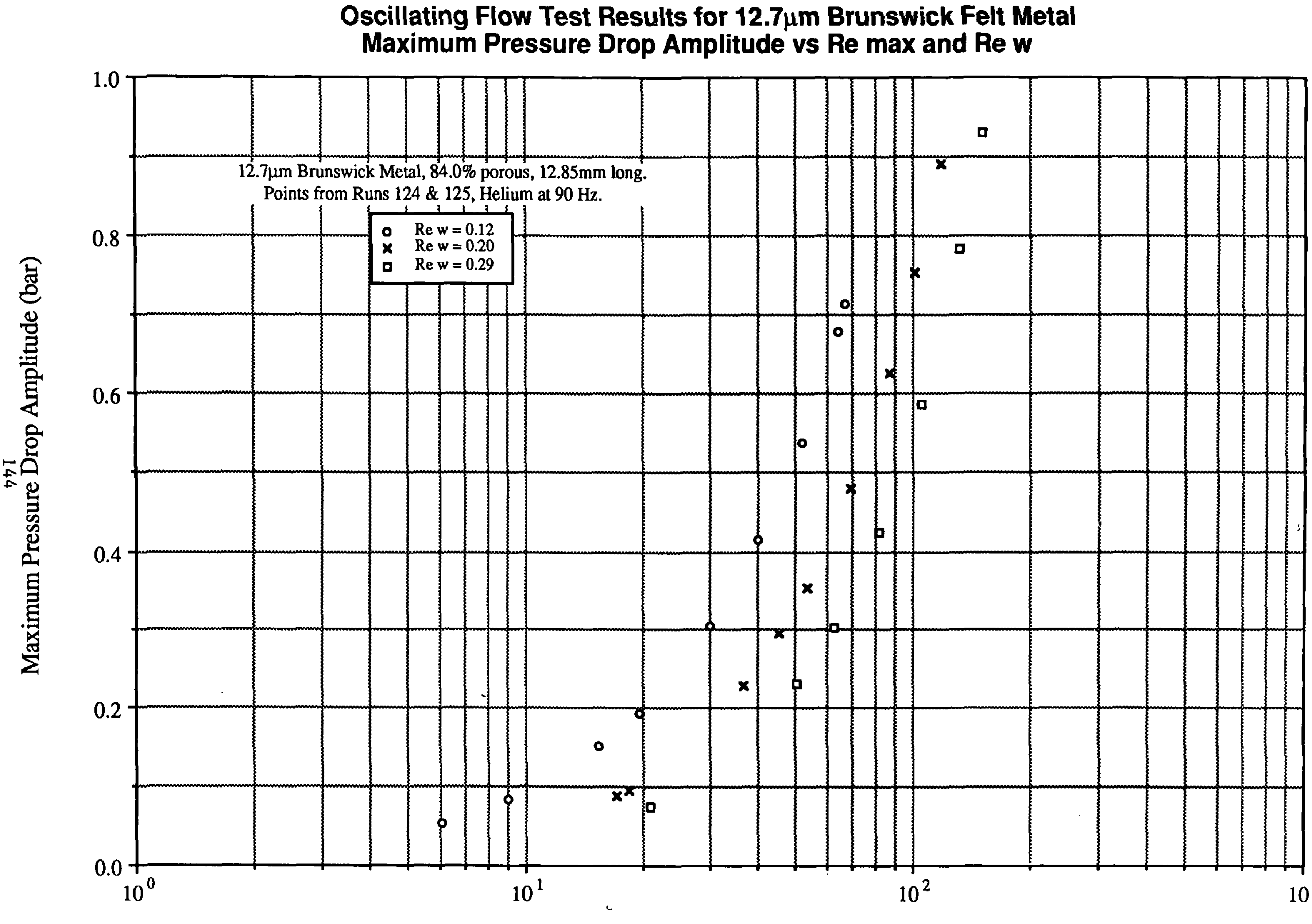

Oscillating Flow Test Results for 12.7μm Brunswick Felt Metal
Maximum Pressure Drop Amplitude vs Re max and Re w
12.7μm Brunswick Metal, 84.0% porous, 12.85mm long.
Points from Runs 124 & 125, Helium at 90 Hz.
Re w = 0.12
Re w = 0.20
Re w = 0.29
Maximum Pressure Drop Amplitude (bar)
Re max
1.0
0.8
0.6
0.4
0.2
0.0
10^0
10^1
10^2
10^3

FIGURE 6.2-48

Oscillating Flow Test Results for Metex Knit Wire
Maximum Pressure Drop Amplitude vs Re max and Re w

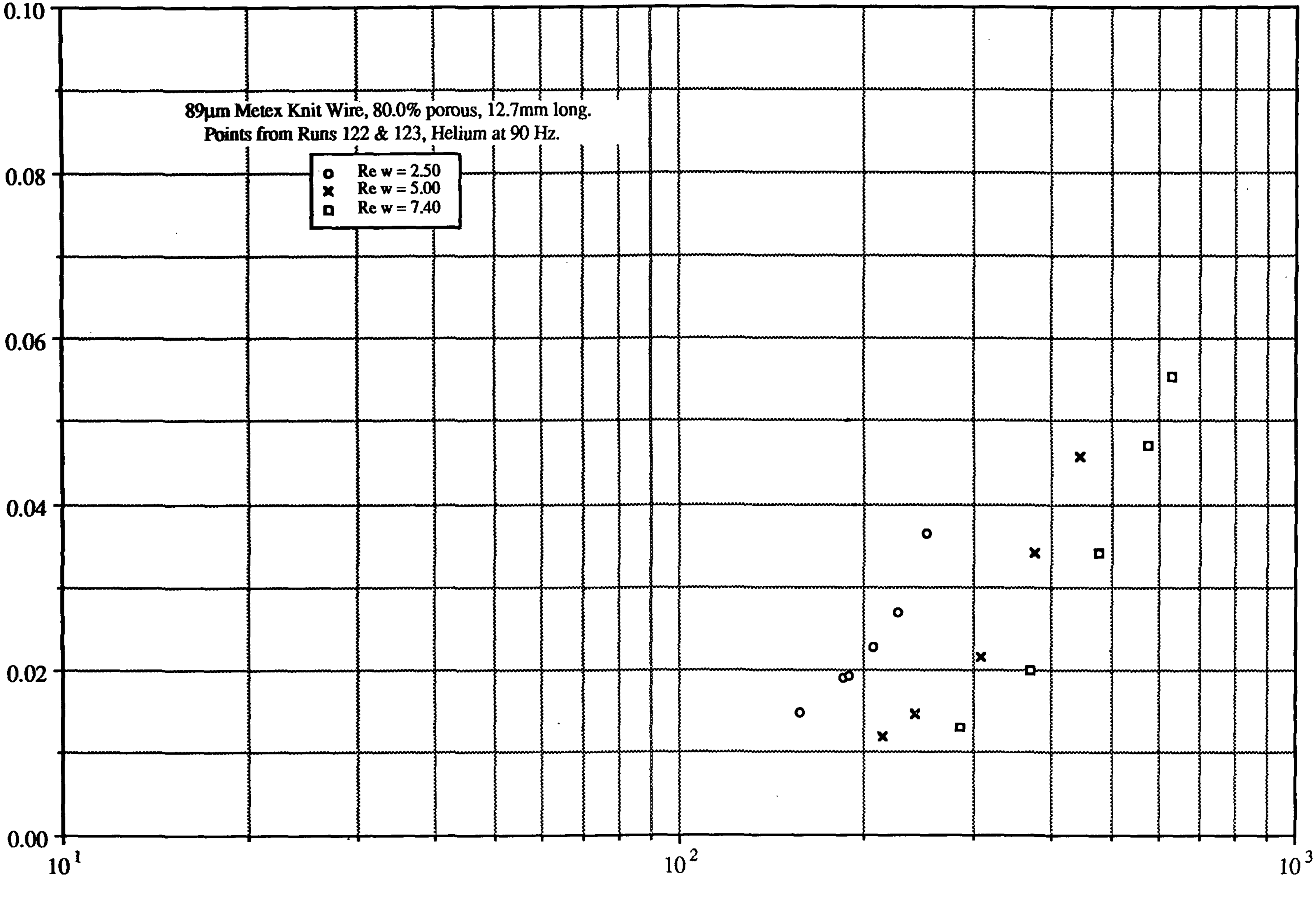

FIGURE 6.2-49

Oscillating Flow Test Results for 41μm Sintered Screens
Maximum Pressure Drop Amplitude vs Re max and Re w

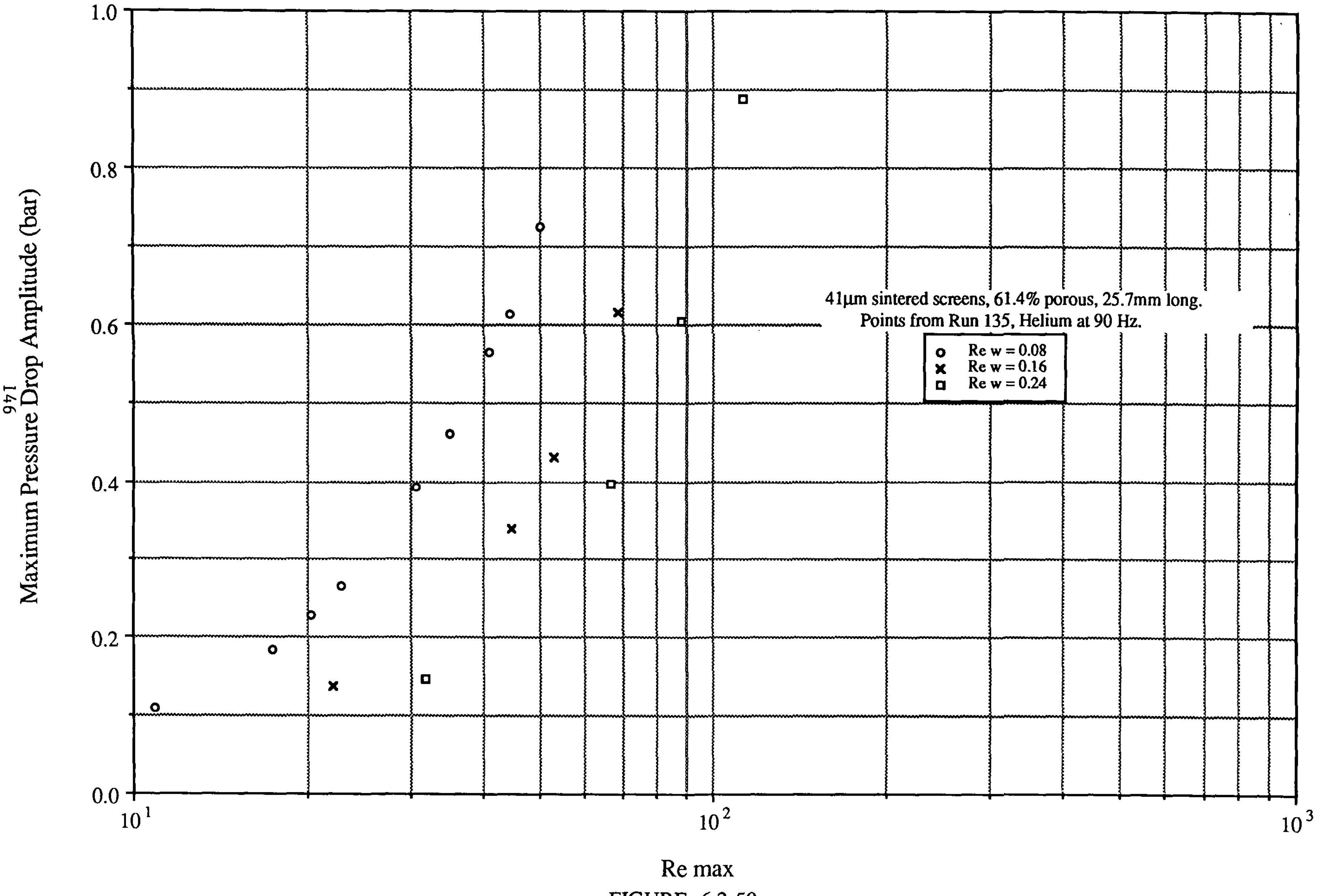

FIGURE 6.2-50

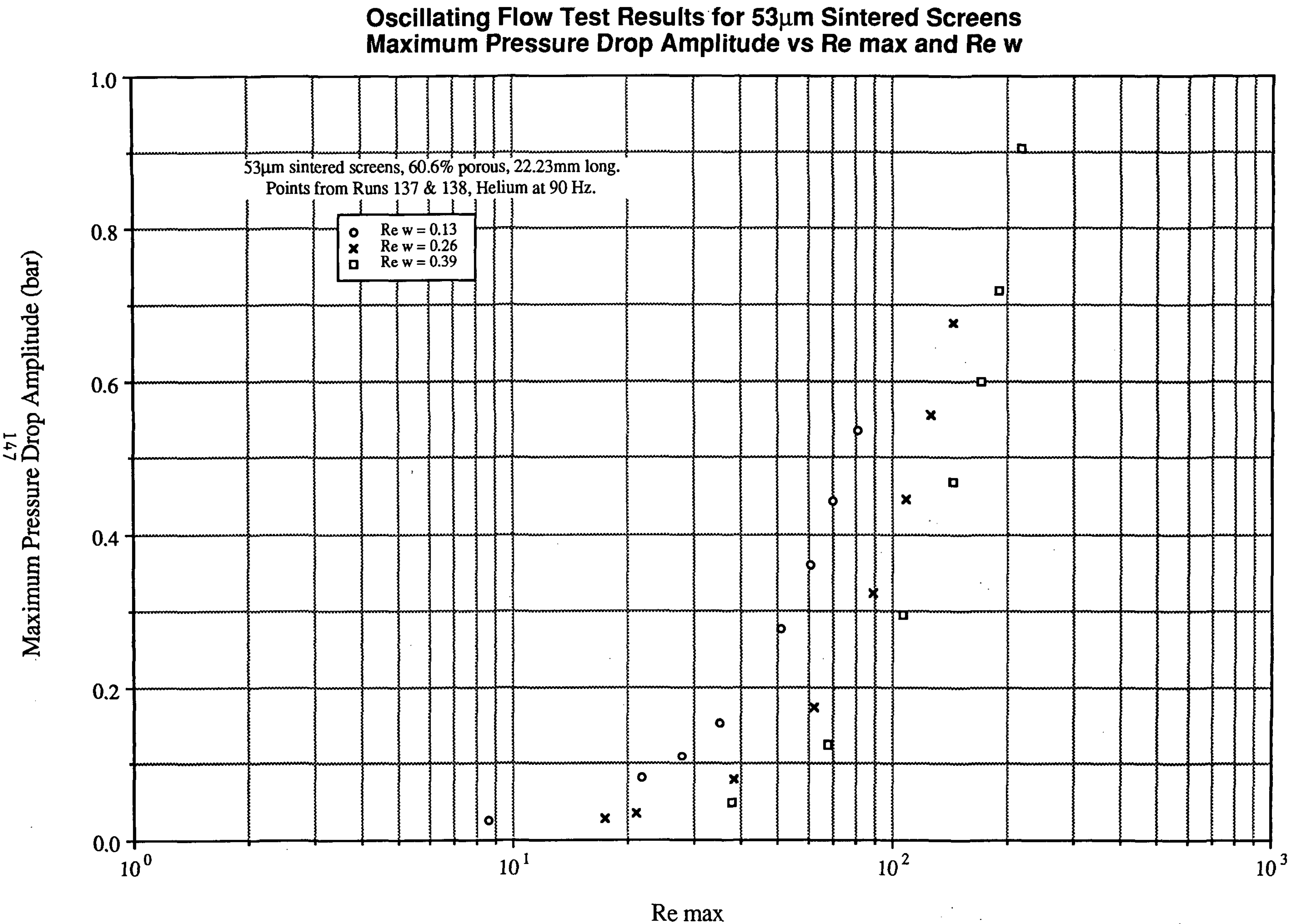

Oscillating Flow Test Results for 53µm Sintered Screens
Maximum Pressure Drop Amplitude vs Re max and Re w
53µm sintered screens, 60.6% porous, 22.23mm long.
Points from Runs 137 & 138, Helium at 90 Hz.
Re w = 0.13
Re w = 0.26
Re w = 0.39
Maximum Pressure Drop Amplitude (bar)
Re max
1.0
0.8
0.6
0.4
0.2
0.0
10^0
10^1
10^2
10^3

FIGURE 6.2-51

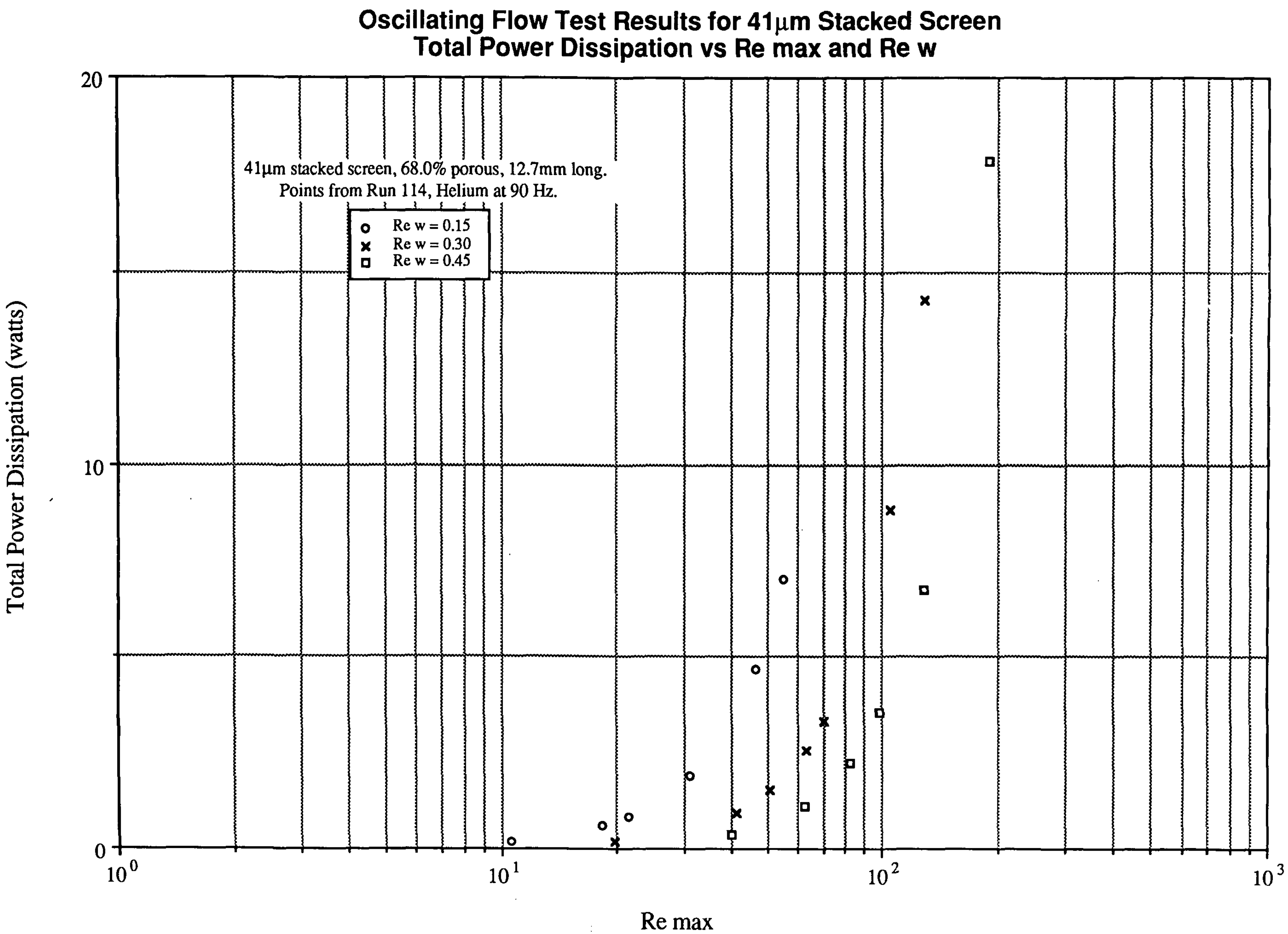

Oscillating Flow Test Results for 41μm Stacked Screen
Total Power Dissipation vs Re max and Re w
41μm stacked screen, 68.0% porous, 12.7mm long.
Points from Run 114, Helium at 90 Hz.
Re w = 0.15
Re w = 0.30
Re w = 0.45
Total Power Dissipation (watts)
20
10
0
10^0
10^1
10^2
10^3
Re max

FIGURE 6.2-52

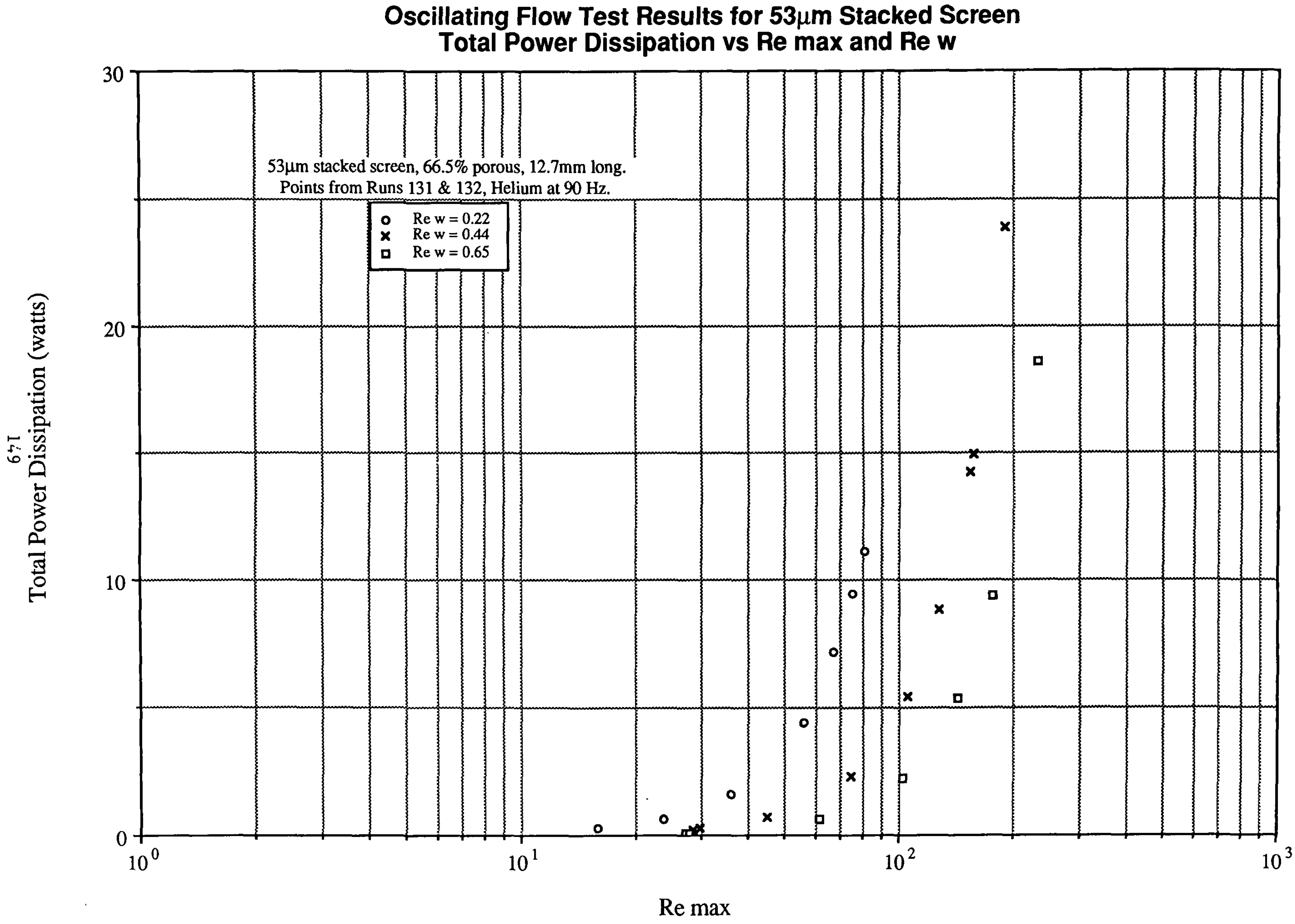

Oscillating Flow Test Results for 53µm Stacked Screen
Total Power Dissipation vs Re max and Re w
53µm stacked screen, 66.5% porous, 12.7mm long.
Points from Runs 131 & 132, Helium at 90 Hz.
Re w = 0.22
Re w = 0.44
Re w = 0.65
Total Power Dissipation (watts)
30
20
10
0
10^0
10^1
10^2
10^3
Re max
149

FIGURE 6.2-53

Oscillating Flow Test Results for 94µm Stacked Screens
Total Power Dissipation vs Re max and Re w

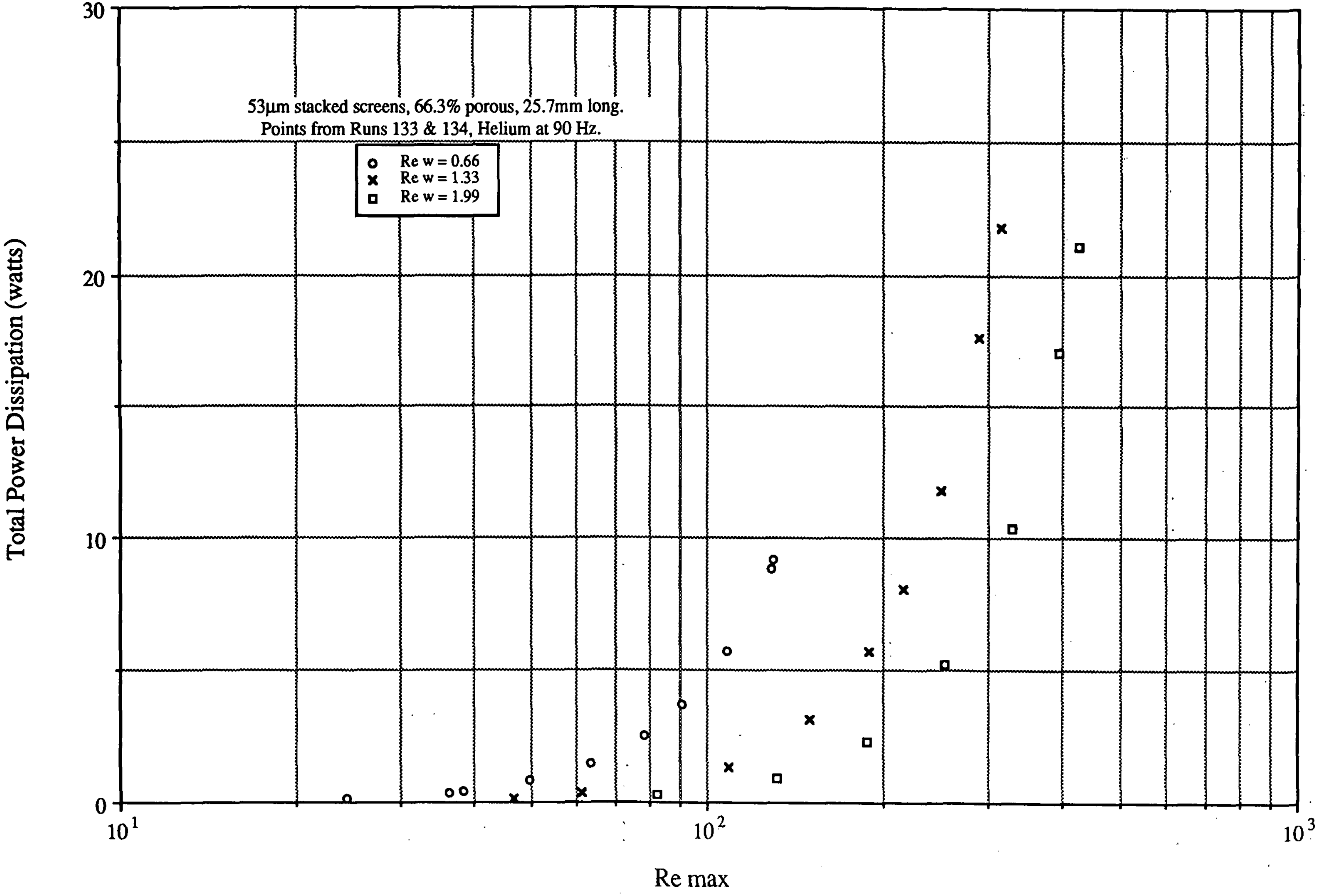

FIGURE 6.2-54

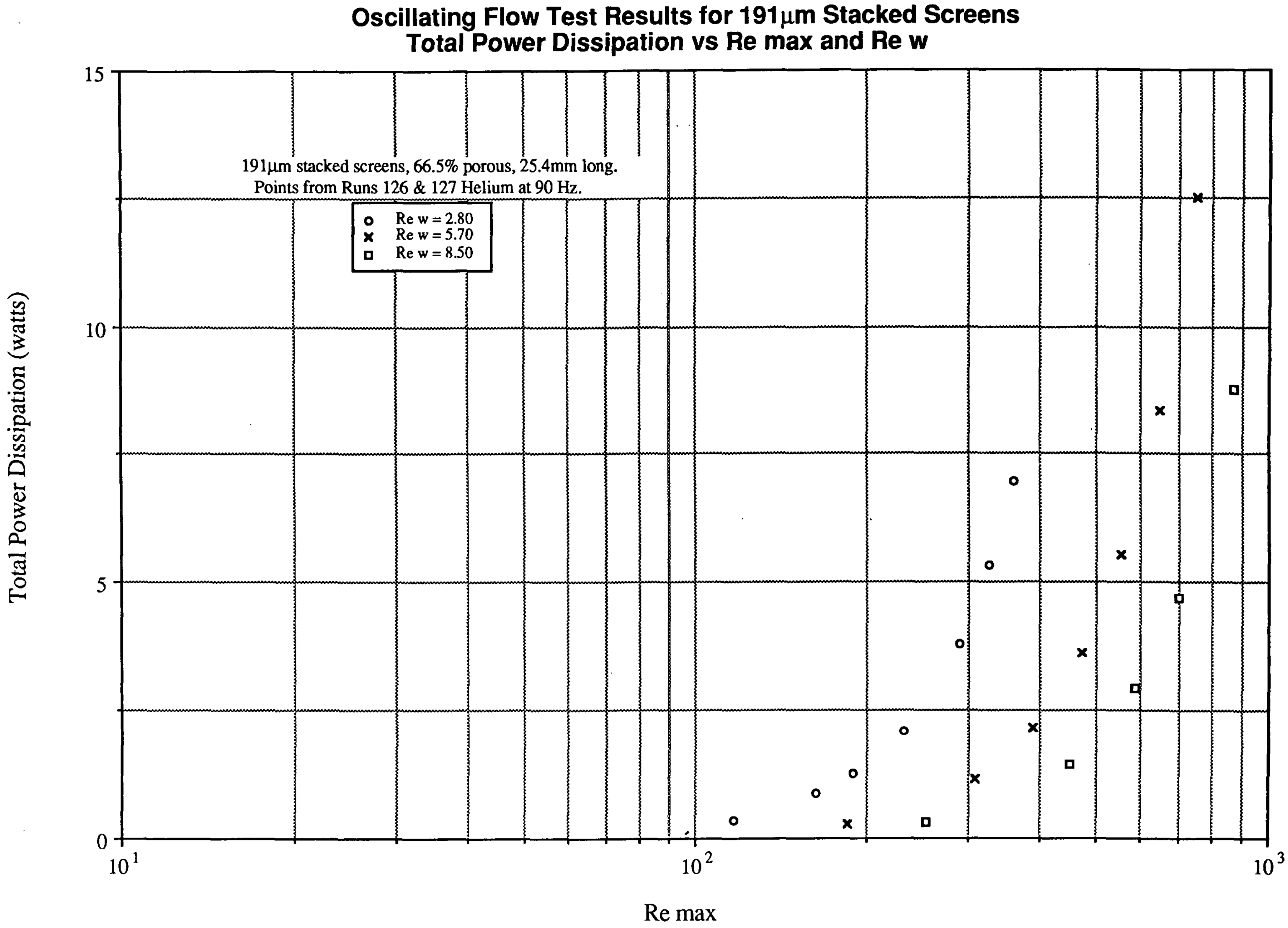
Oscillating Flow Test Results for 191μm Stacked Screens
Total Power Dissipation vs Re max and Re w
191μm stacked screens, 66.5% porous, 25.4mm long.
Points from Runs 126 & 127 Helium at 90 Hz.
Re w = 2.80
Re w = 5.70
Re w = 8.50
Total Power Dissipation (watts)
15
10
5
0
10^1
10^2
10^3
Re max

FIGURE 6.2-55

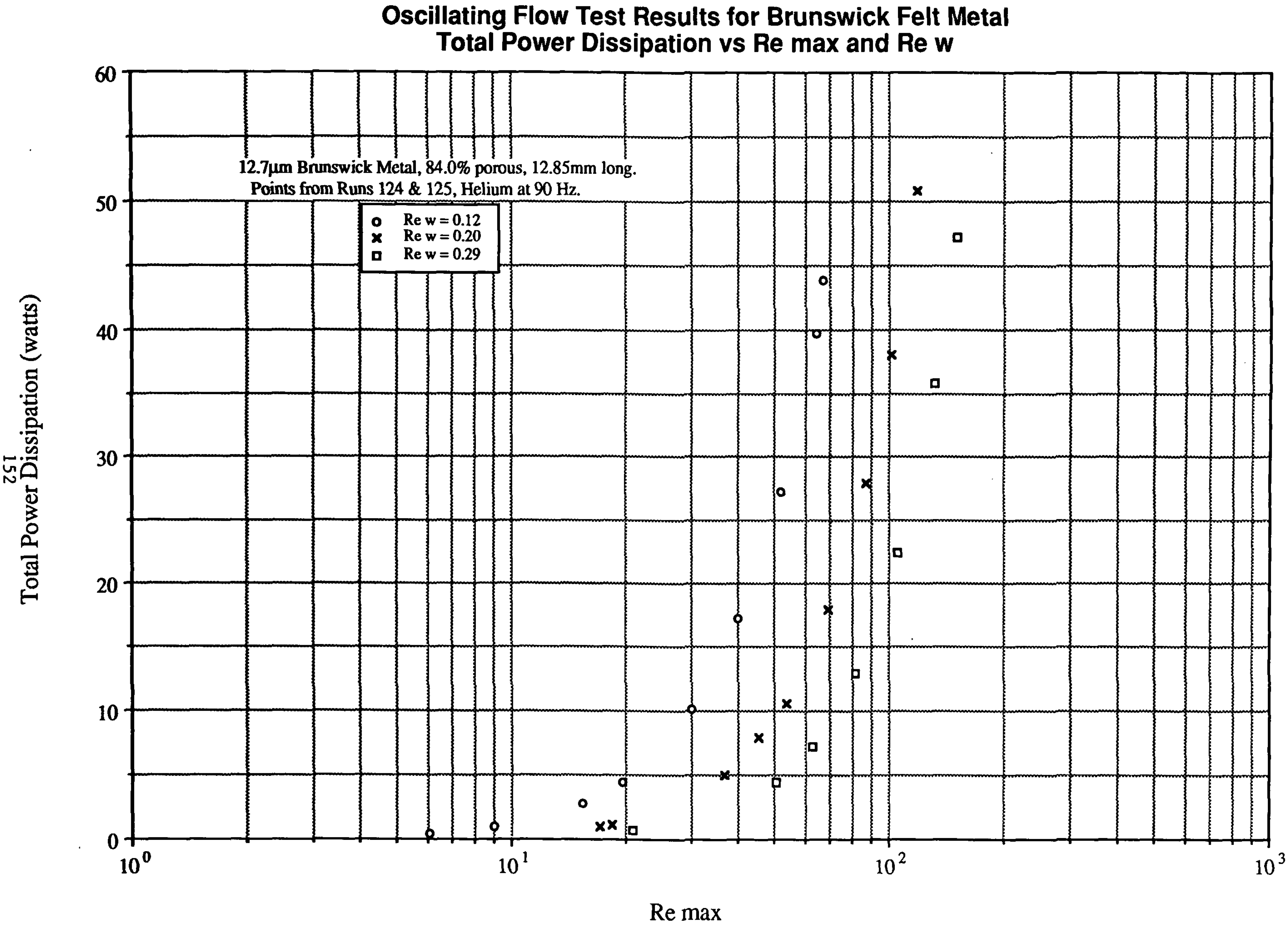

Oscillating Flow Test Results for Brunswick Felt Metal
Total Power Dissipation vs Re max and Re w
12.7μm Brunswick Metal, 84.0% porous, 12.85mm long.
Points from Runs 124 & 125, Helium at 90 Hz.
Re w = 0.12
Re w = 0.20
Re w = 0.29
Total Power Dissipation (watts)
0
10
20
30
40
50
60
10^0
10^1
10^2
10^3
Re max

FIGURE 6.2-56

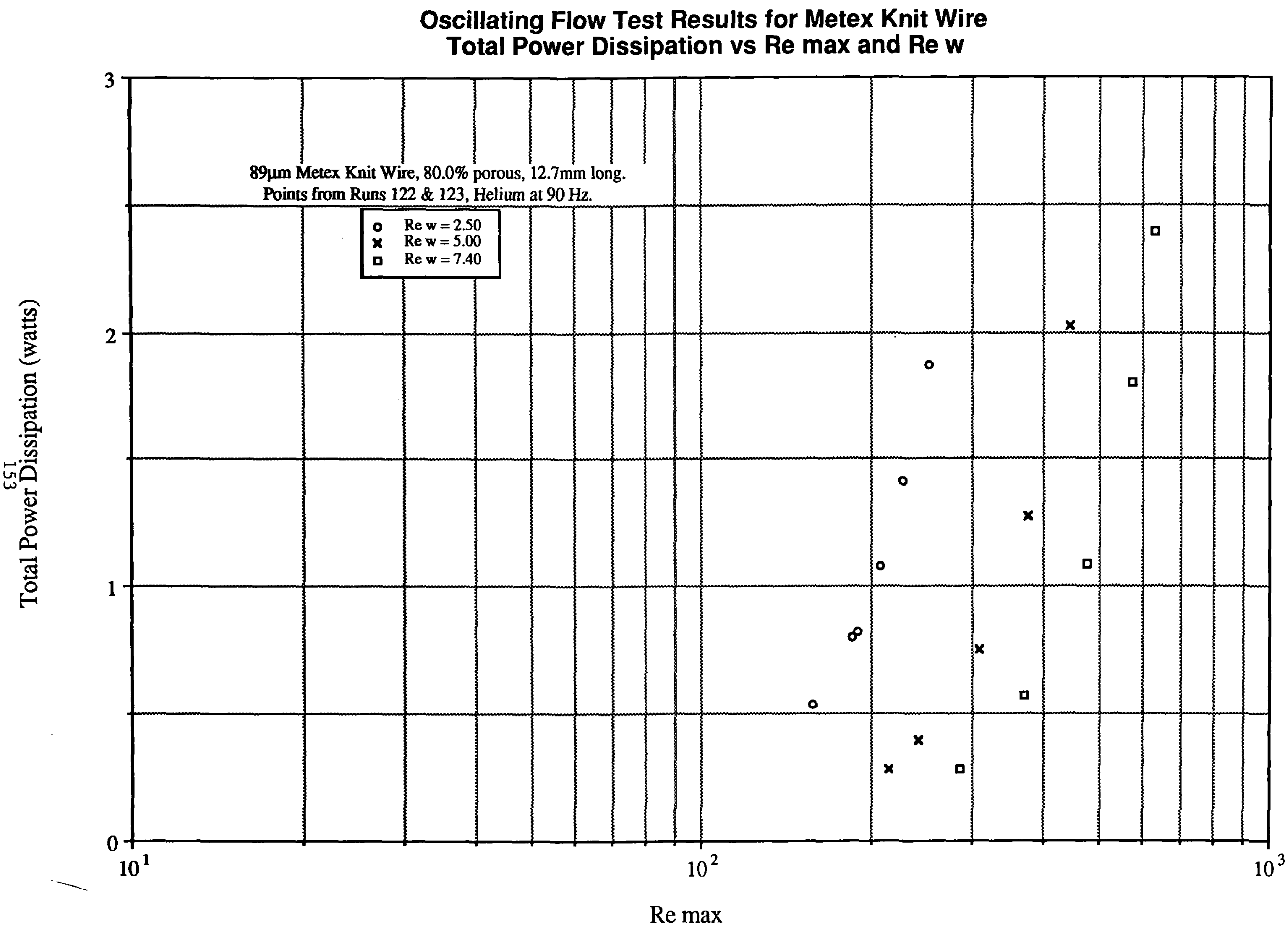

Oscillating Flow Test Results for Metex Knit Wire
Total Power Dissipation vs Re max and Re w
89µm Metex Knit Wire, 80.0% porous, 12.7mm long.
Points from Runs 122 & 123, Helium at 90 Hz.
Re w = 2.50
Re w = 5.00
Re w = 7.40
Total Power Dissipation (watts)
Re max
0
1
2
3
10 1
10 2
10 3

FIGURE 6.2-57

Oscillating Flow Test Results for 41μm Sintered Screens
Total Power Dissipation vs Re max and Re w

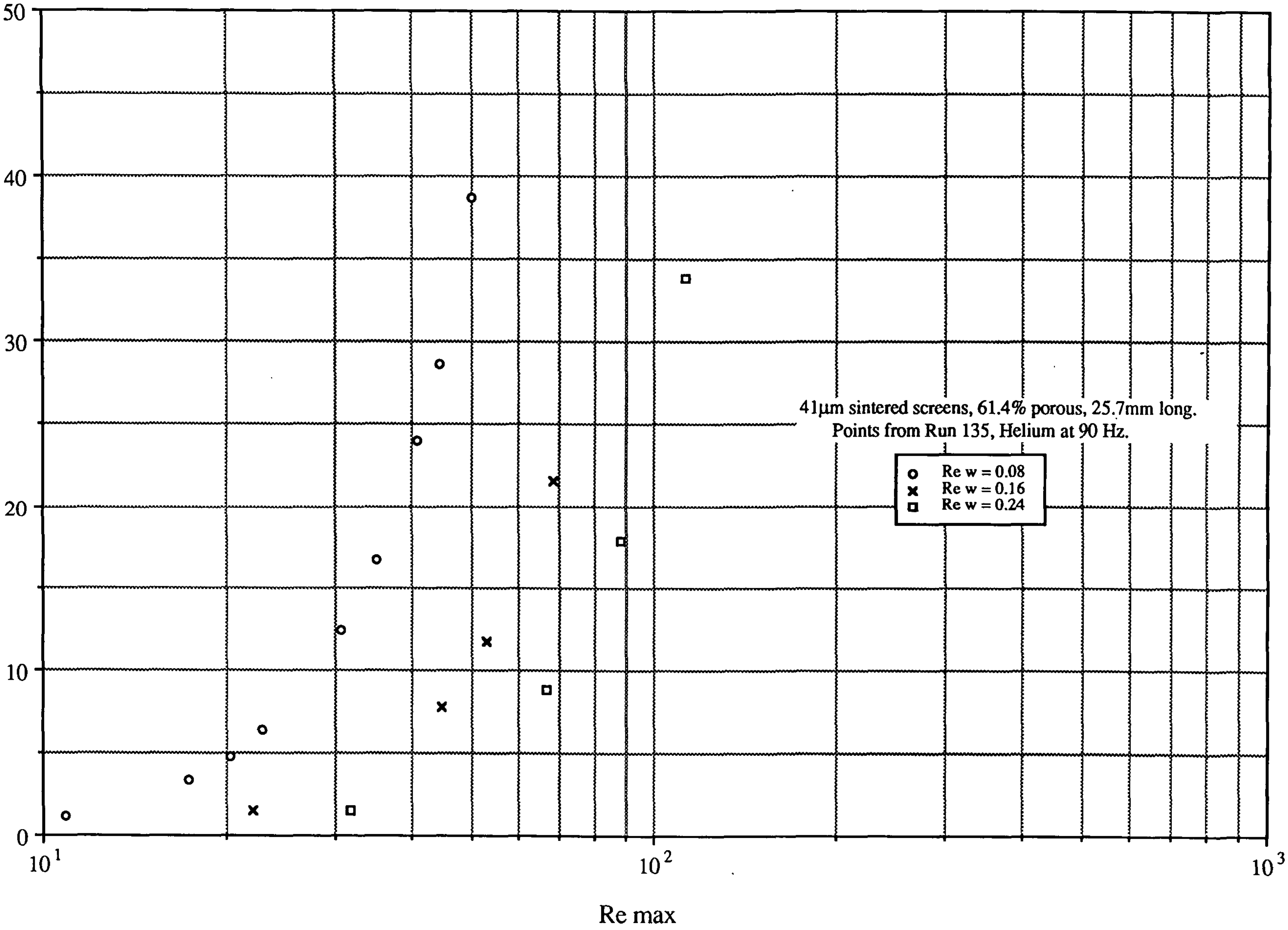

FIGURE 6.2-58

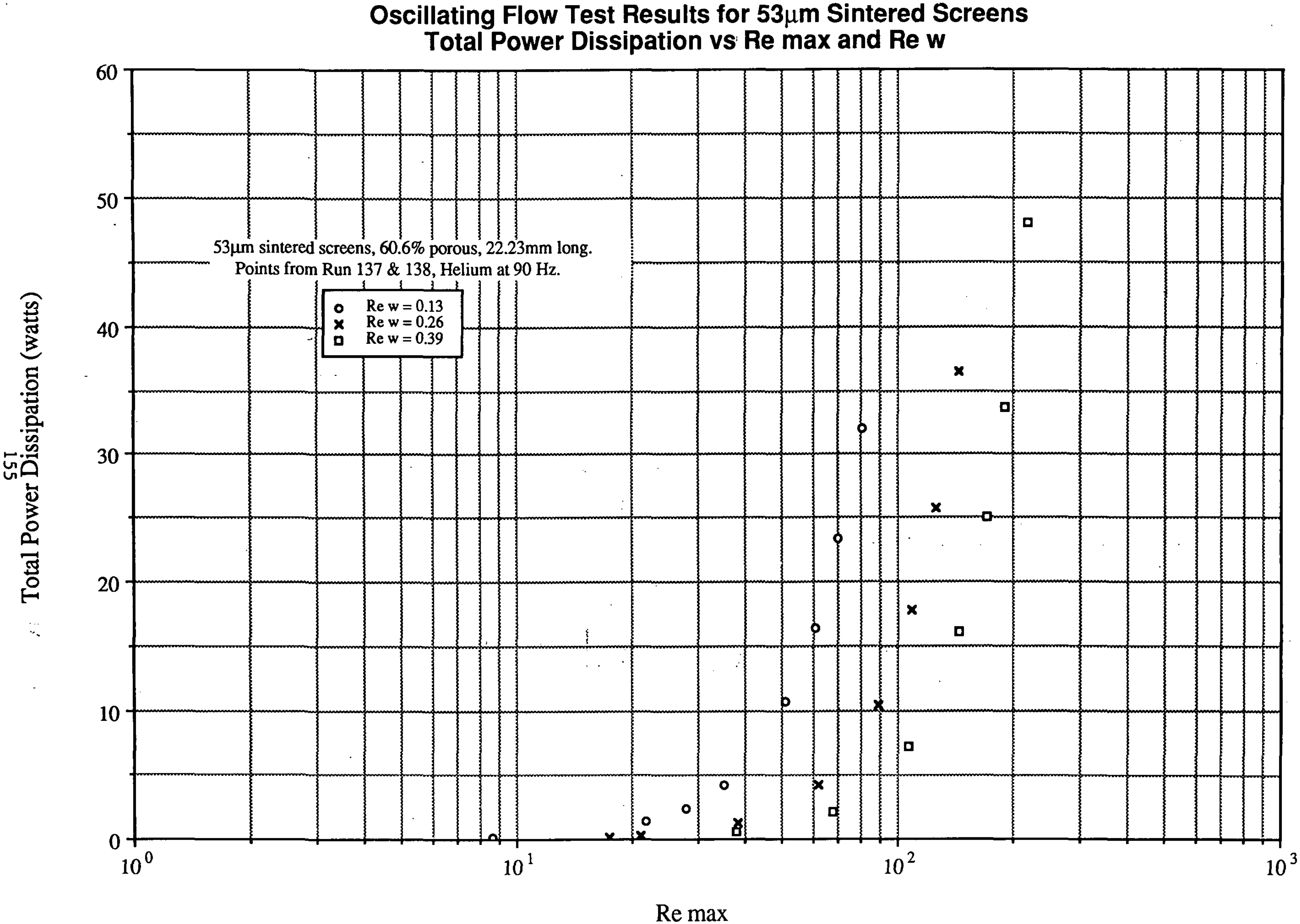

Oscillating Flow Test Results for 53µm Sintered Screens
Total Power Dissipation vs Re max and Re w
Total Power Dissipation (watts)
60
50
40
30
20
10
0
53µm sintered screens, 60.6% porous, 22.23mm long.
Points from Run 137 & 138, Helium at 90 Hz.
Re w = 0.13
Re w = 0.26
Re w = 0.39
10^0
10^1
10^2
10^3
Re max

FIGURE 6.2-59

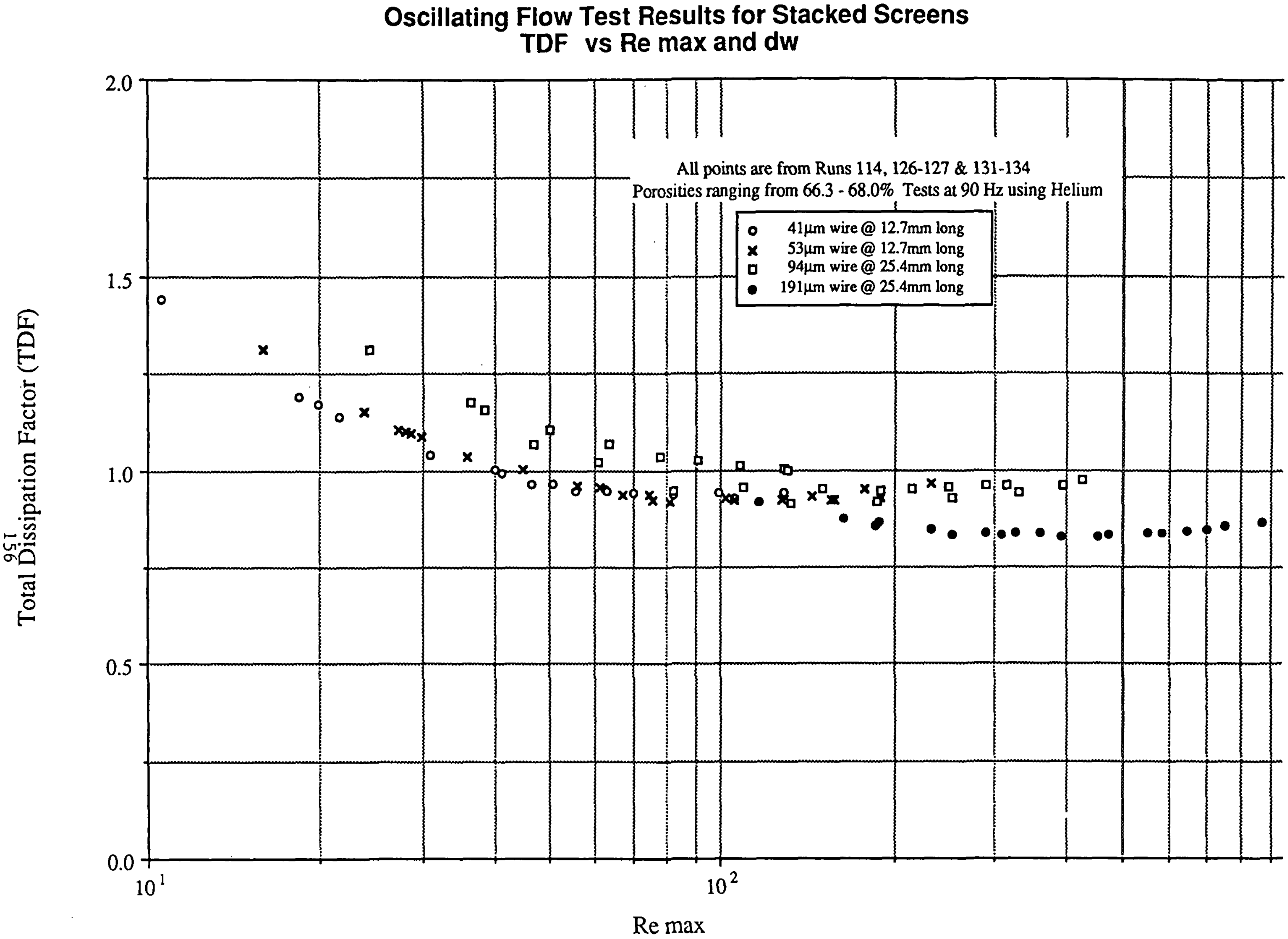

Oscillating Flow Test Results for Stacked Screens
TDF vs Re max and dw
All points are from Runs 114, 126-127 & 131-134
Porosities ranging from 66.3 - 68.0% Tests at 90 Hz using Helium
41µm wire @ 12.7mm long
53µm wire @ 12.7mm long
94µm wire @ 25.4mm long
191µm wire @ 25.4mm long
Total Dissipation Factor (TDF)
2.0
1.5
1.0
0.5
0.0
10^1
10^2
Re max

FIGURE 6.2-60

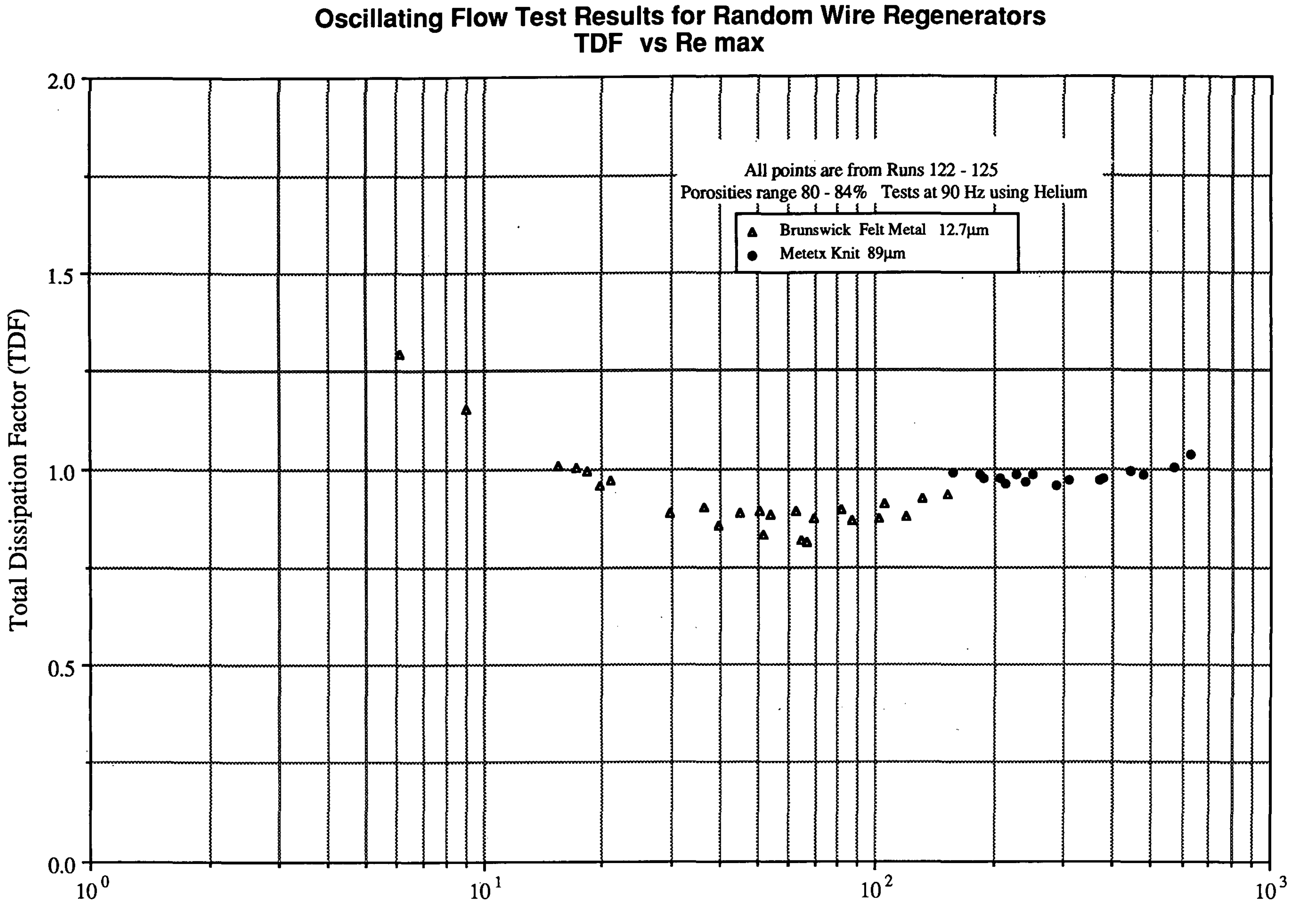

Oscillating Flow Test Results for Random Wire Regenerators
TDF vs Re max
All points are from Runs 122 - 125
Porosities range 80 - 84% Tests at 90 Hz using Helium
Brunswick Felt Metal 12.7µm
Metetx Knit 89µm
Total Dissipation Factor (TDF)
Re max
2.0
1.5
1.0
0.5
0.0
10^0
10^1
10^2
10^3

FIGURE 6.2-61

Oscillating Flow Test Results for Sintered Screens
TDF vs Re max and dw

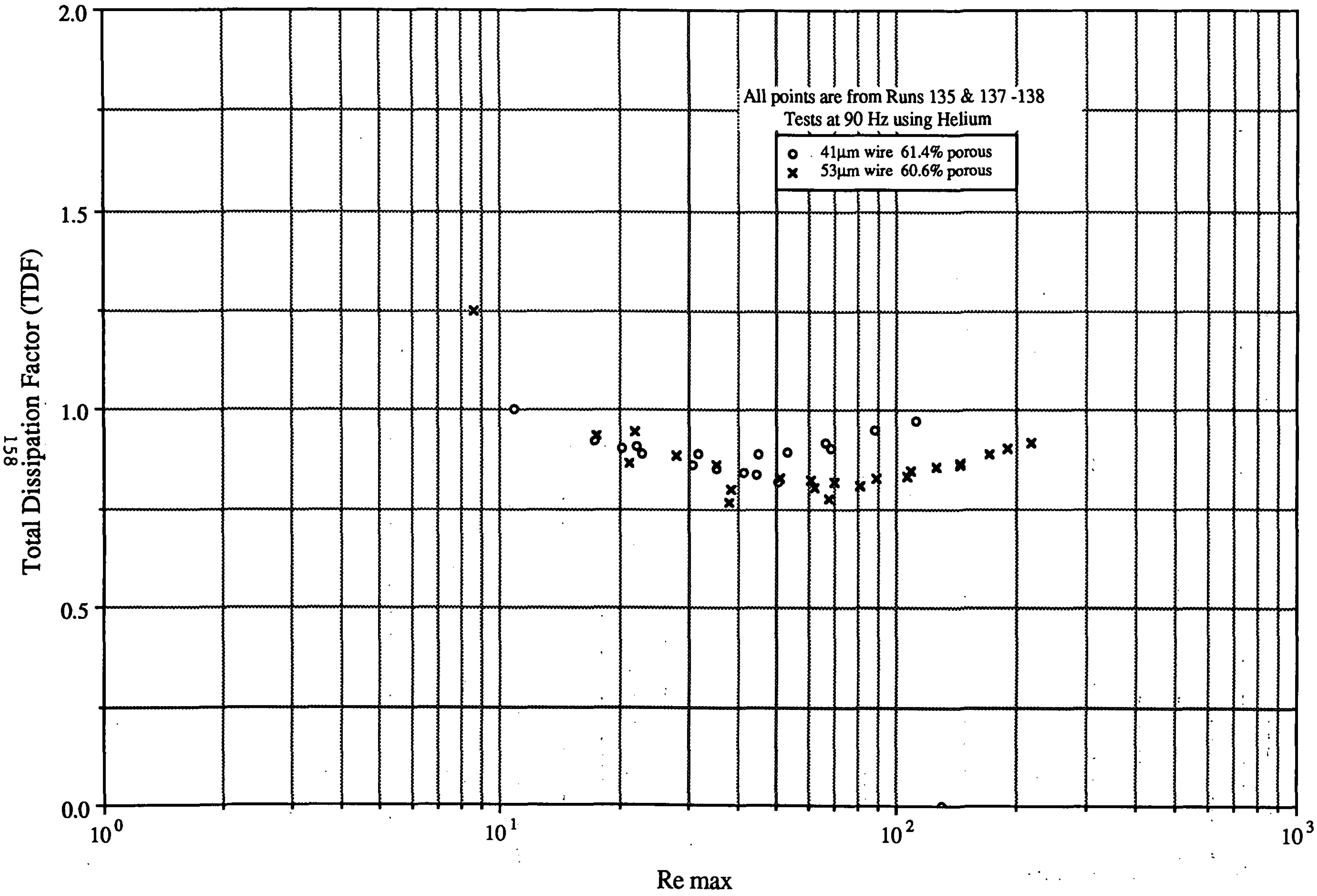

FIGURE 6.2-62

Oscillating Flow Test Results for 41μm Stacked Screens
TDF vs Re max and Re w

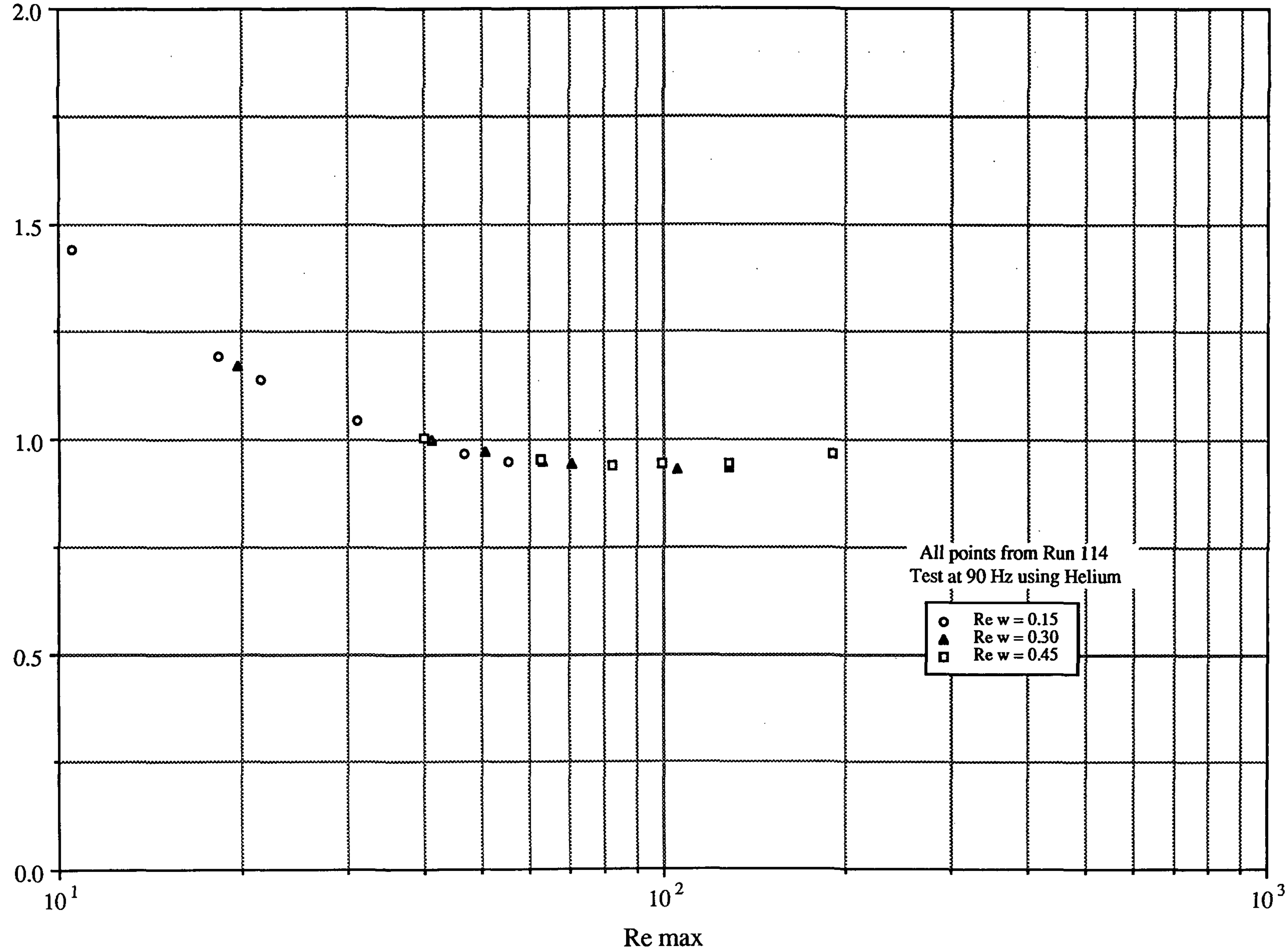

FIGURE 6.2-63

Oscillating Flow Test Results for 53μm Stacked Screen
TDF vs Re max and Re $_\omega$

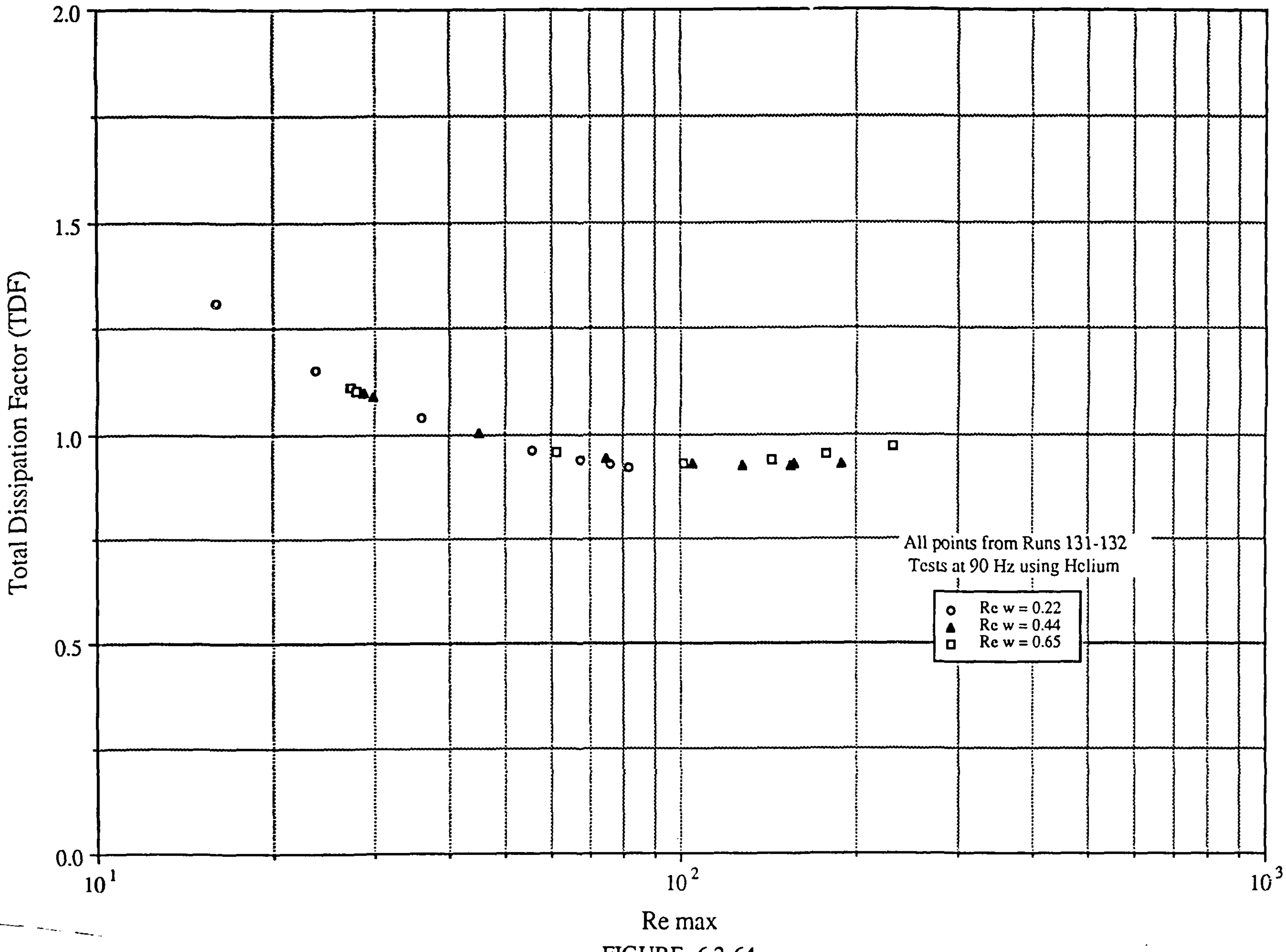

FIGURE 6.2-64

Oscillating Flow Test Results for 12.7μm Brunswick Felt Metal
TDF vs Re max and Re w

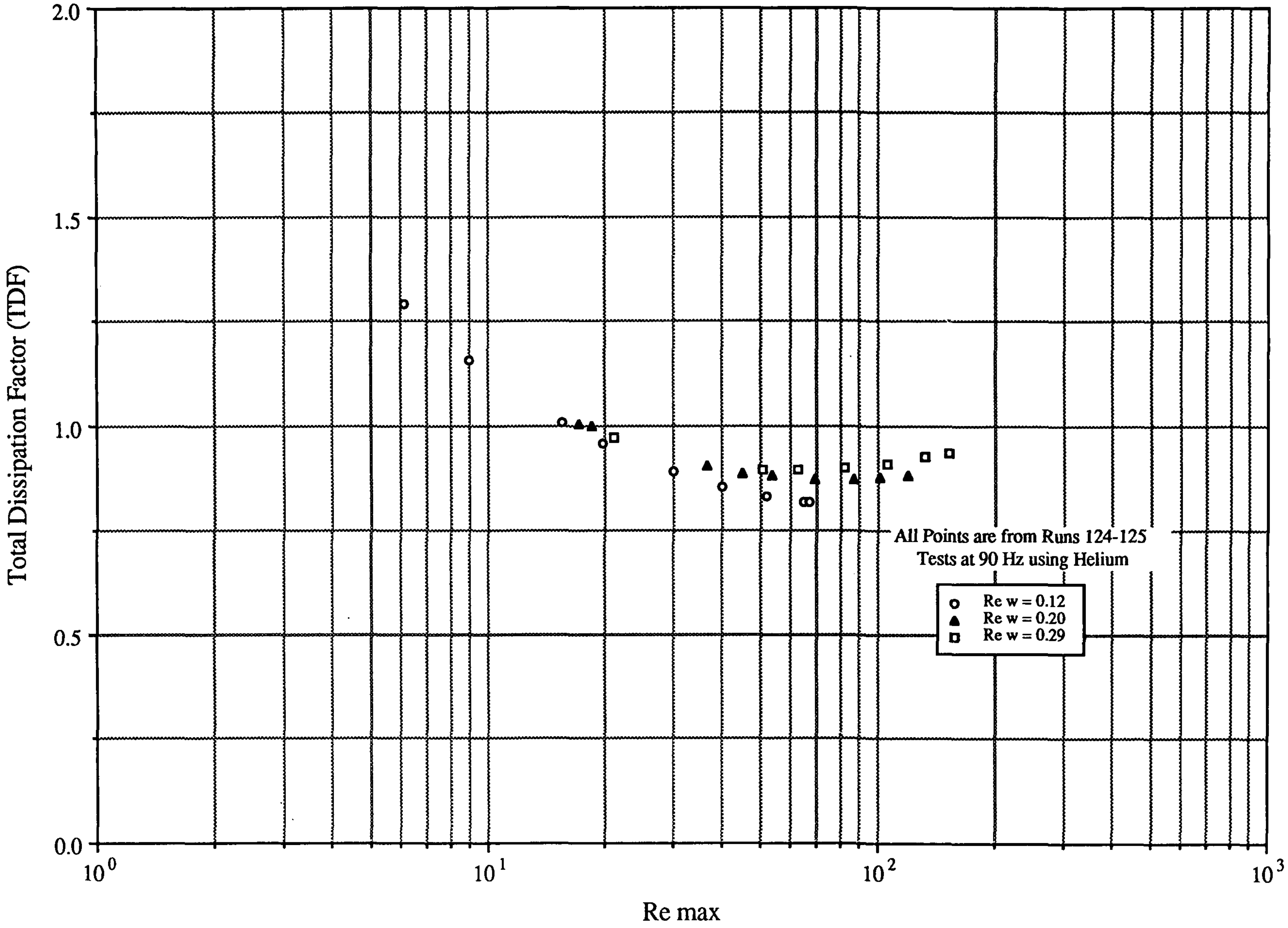

FIGURE 6.2-65

Oscillating Flow Test Results for 89 µm Metex Knit
TDF vs Re max and Re w

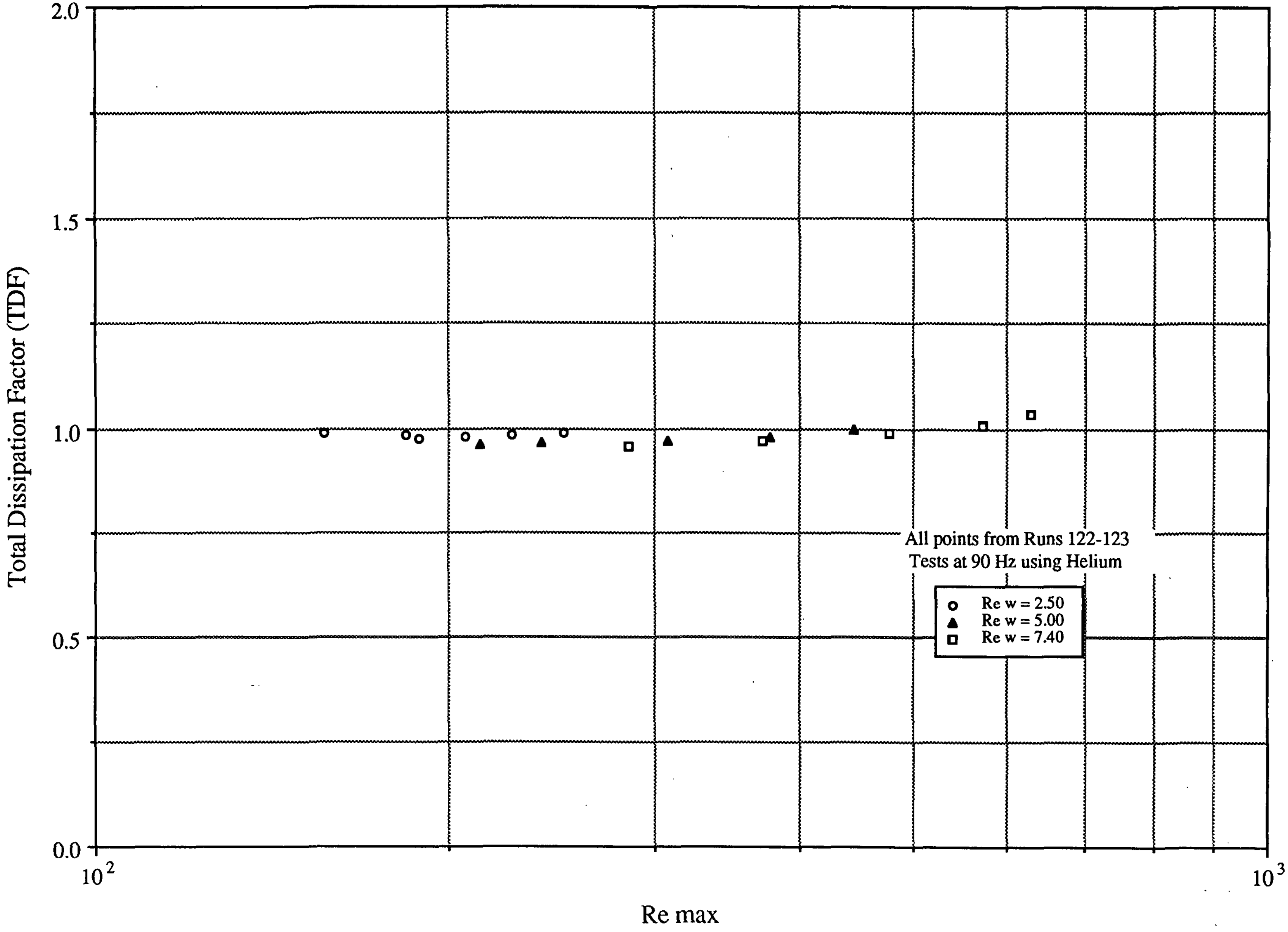

FIGURE 6.2-66

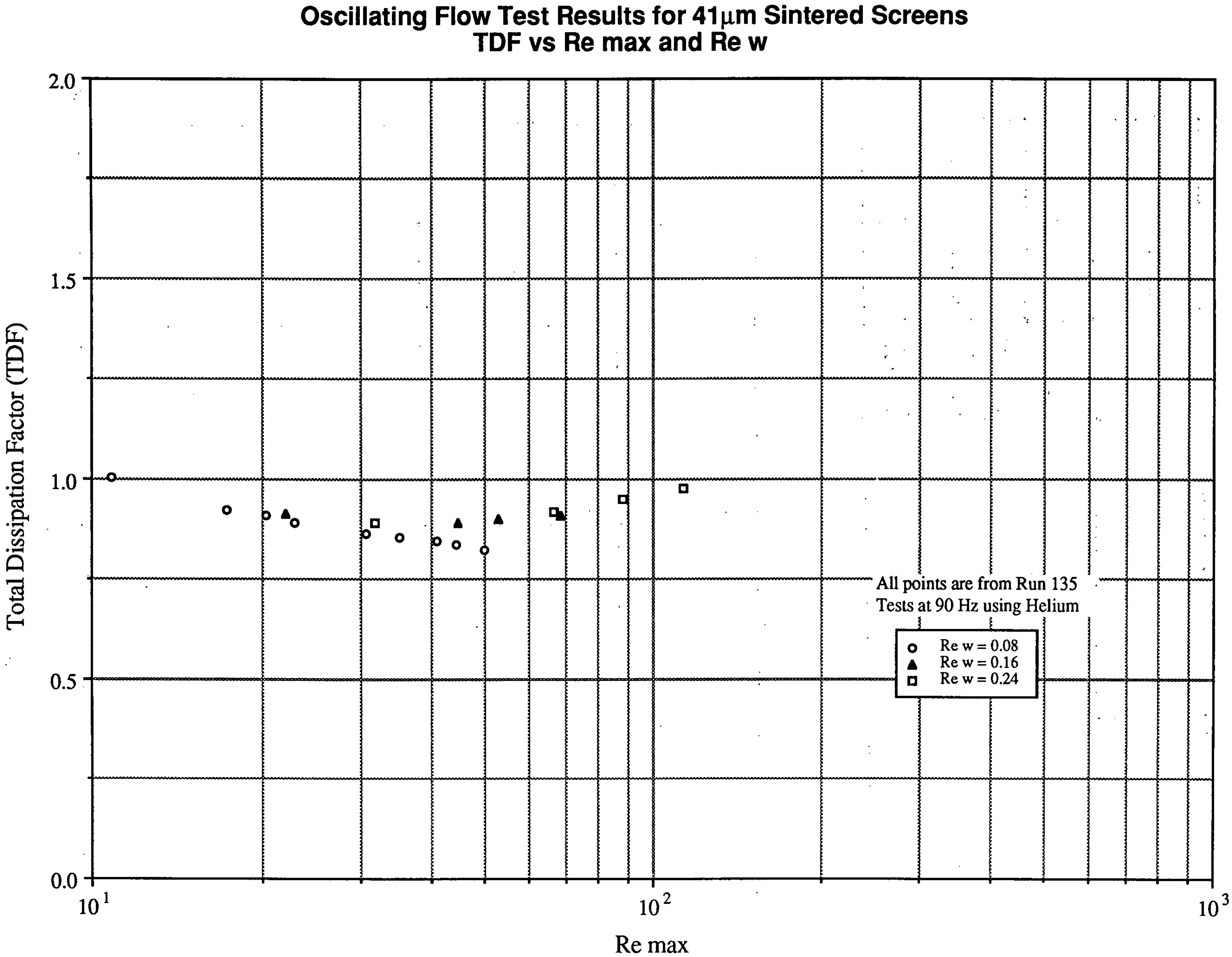
Oscillating Flow Test Results for 41μm Sintered Screens
TDF vs Re max and Re w
Total Dissipation Factor (TDF)
2.0
1.5
1.0
0.5
0.0
10^1
10^2
10^3
Re max
All points are from Run 135
Tests at 90 Hz using Helium
Re w = 0.08
Re w = 0.16
Re w = 0.24

FIGURE 6.2-67

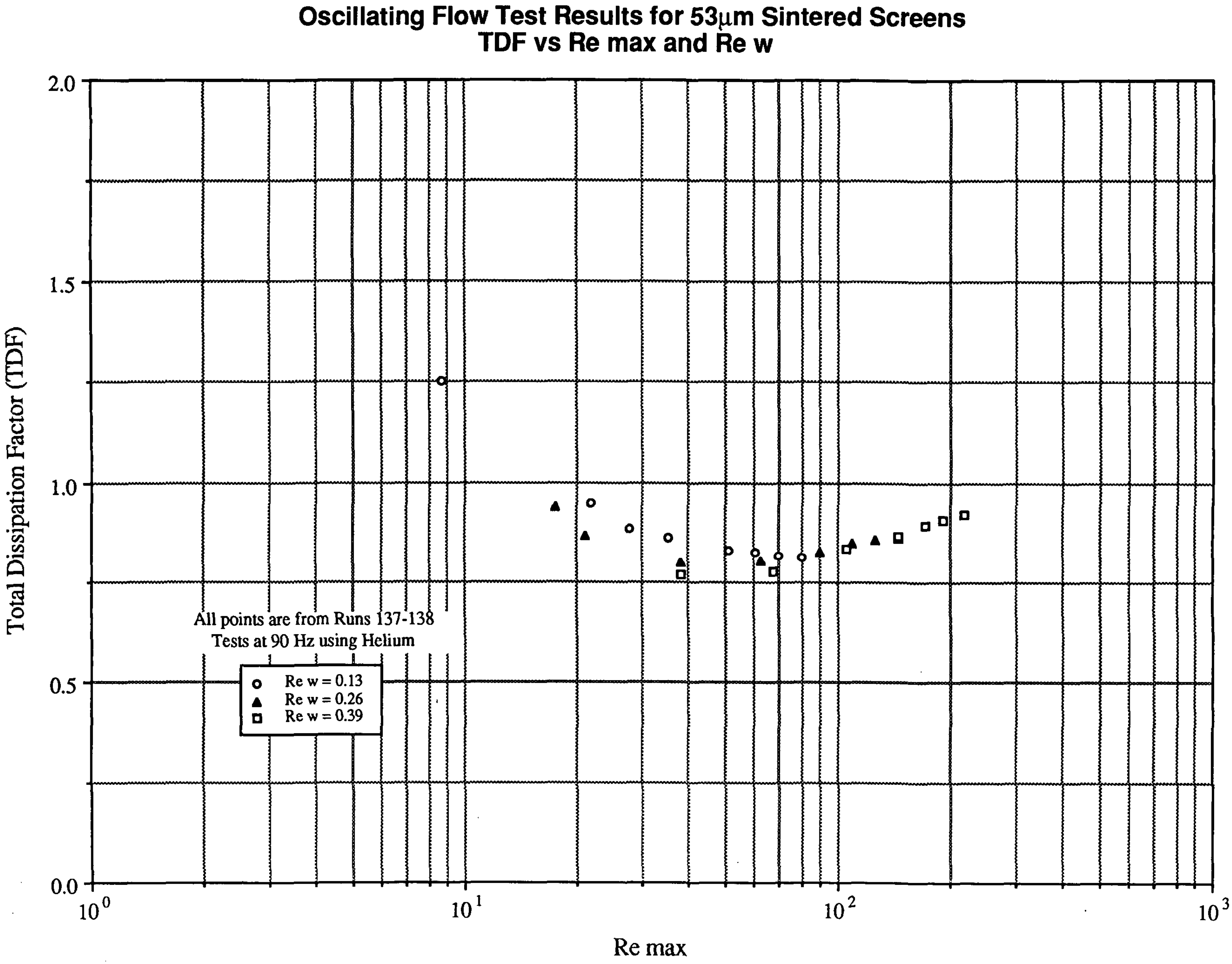
Oscillating Flow Test Results for 53μm Sintered Screens
TDF vs Re max and Re w
Total Dissipation Factor (TDF)
Re max
2.0
1.5
1.0
0.5
0.0
10^0
10^1
10^2
10^3
All points are from Runs 137-138
Tests at 90 Hz using Helium
Re w = 0.13
Re w = 0.26
Re w = 0.39

FIGURE 6.2-68

Section 7

7.0 DISCUSSION OF TEST RESULTS

The steady and oscillating flow loss test matrices are outlined in Section 5 and the test results are graphically presented in Section 6. Additional detailed documentation for the tube and regenerator heat exchangers tested in this study is found in Appendix B. In this section, these test results are discussed and some broad conclusions are drawn regarding the flow losses in an oscillating flow field as compared with a unidirectional steady flow field. The test results for the tube and regenerator heat exchangers are discussed in sections 7.1 and 7.2, respectively.

7.1 TUBE HEAT EXCHANGERS

7.1.1 Tube Steady Flow Loss Test Results

The tube steady flow loss test results are plotted in Section 6 (Figures 6.1-1 through 6.1-9) and tabulated in Appendix B for squared, rounded, and protruding entrance/exit configurations. The flow loss test results presented in these plots are discussed in this section.

ΔP vs. *Re*

The plots of ΔP vs. *Re* in Figures 6.1-1 through 6.1-3 show, as expected, that the steady flow pressure drop across the tube heat exchanger increases with increasing tube length (diameter was not varied) and increasing *Re*.

Euler number vs. *L/D*

The plots of Euler number vs. *L/D* are shown in Figures 6.1-4 through 6.1-6. The total steady flow entrance/exit flow loss coefficient (K_t) for the three entrance/exit configurations that were tested were determined by plotting the Euler number vs. *L/D*. A straight line was plotted through the data above L/D = 20; the value of K_t was taken as the Euler number at the intersection of this line and the y-axis. These are nominal measurements for K_t, representative and valid over the range of Reynolds numbers tested. They are summarized below in Table 7.1-1 for each of the three entrance/exit configurations. The nominal flow loss coefficients for these entrance/exit configurations as determined from the literature (8,9) were found to be similar to these test results.

Table 7.1-1

Comparison of K_t (Measured and Predicted)

Entrance/Exit Configuration	K_t *Measured*	K_t *Predicted*
Square ended	1.5	1.5
Round ended	1.0	1.05
Protruding ends	1.8	1.8

Pratio vs. Re

The predicted entrance/exit flow loss coefficients given in Table 7.1-1 were used in the steady flow pressure drop calculation of *P*ratio for these test results. The plots of *P*ratio vs. *Re* are shown in Figures 6.1-7 through 6.1-9 for the three different entrance/exit configurations. The *P*ratio for the square-ended tubes (K_t = 1.5) are shown in Figure 6.1-7. Note that for this configuration, *P*ratio is near 1.0. This means that there is good agreement between the measured and predicted pressure drops over the range of tube lengths and *Re* that were tested. That is, the predicted pressure drop based on the entrance/exit form loss coefficient (K_t = 1.5) and the friction factor correlation as discussed in Section 6 correlate well with these test results. There is a qualification to this generalization. Note that for test sample lengths with $L/D \leq 10$, *P*ratio is significantly less that 1.0. This reflects that at low L/D (i.e., $L/D \leq 10$) the flow velocity profile is not fully developed and, therefore, a K_t = 1.5 is inappropriate for square-ended tube lengths less than ten hydraulic diameters.

The *P*ratio results for the rounded tubes (K_t = 1.05) are shown in Figure 6.1-8. The values of *P*ratio for these tests are less than 1.0, generally ranging from 0.85 to 0.9, except for the L/D = 100 test sample. This suggests that K_t = 1.05 is a high value for this test configuration, assuming that the predicted friction factor is adequate. It is not clear why the L/D = 100 test results are seemingly inconsistent with the other test results.

The *P*ratio results for the protruding tubes (K_t = 1.8) are shown in Figure 6.1-9. The values of *P*ratio for these tests were generally between 0.9 and 1.0. Hence, there is fairly good agreement between the measured and the predicted pressure drop.

7.1.2 Tube Oscillating Flow Loss Test Results

The tube oscillating flow loss test results are plotted in Section 6 and tabulated in Appendix B for the squared, rounded, and protruding entrance/exit configurations as a function of Re_{max} and Re_{ω} and with varying L/D. The results presented in these plots are discussed in this section.

ΔP_{max} vs. Re_{max}

The plots of ΔP_{max} vs. Re_{max} at a constant value of $Re_{\omega} = 100$ for the three entrance/exit configurations are shown in Figures 6.2-1 through 6.2-3. In addition, the ones at a constant value of $Re_{\omega} = 200$ are shown in Figures 6.2-4 and 6.2-5, and the ones at a constant value of $Re_{\omega} = 300$ are shown in Figures 6.2-6 and 6.2-7. These plots show that, as expected, ΔP_{max} increases with increasing Re_{max} and increasing L/D. We also noted that ΔP_{max} decreases as the entrance/exit configuration goes from protruding, to squared, and then to rounded. This reflects the decrease in flow losses with increasing tube entrance streamlining. In addition, with all other parameters held constant (i.e., Re_{max}, entrance/exit configuration, L/D) we note that ΔP_{max} decreases with increasing Re_{ω}. This implies that ΔP_{max} decreases with increasing oscillating frequency at constant Re_{max}. In practice, it is difficult to keep Re_{max} constant with increasing oscillating frequency.

Total Dissipation Power vs. Re_{max}

The plots of Total Dissipation Power (pV work) vs. Re_{max} at constant $Re_{\omega} = 100$ are shown in Figures 6.2-8 through 6.2-10. These plots show similar trends to the ΔP_{max} vs. Re_{max} plots presented above. All of these results are also similar for plots at constant $Re_{\omega} = 200$ and at constant $Re_{\omega} = 300$. These results are included in Appendix B. These

results show that the total dissipated power increases with increasing Re_{max} and increasing L/D. The dissipated power also decreases as the entrance/exit configuration goes from protruding, to squared, and then to rounded. We also note that total dissipated power decreases with increasing Re_{ω} at constant Re_{max}.

Euler number vs. A_r

Plots of the oscillating flow Euler number as a function of the flow tidal amplitude and the kinetic Reynolds number at constant dimensionless tube length are presented in Figures 6.2-11 through 6.2-21 for all three entrance/exit tube configurations tested. Before these results are discussed, we will speak, first, to the significance of these oscillating flow parameters.The tidal amplitude ratio is defined as

$$A_r = \frac{2X_{max}}{L} = \frac{D_h Re_{max}}{2LRe_{\omega}} \tag{7.1-1}$$

The tidal amplitude is the peak-to-peak fluid displacement (moving as a plug) relative to the tube length. When $A_r << 1$, most of the fluid contacting the tube oscillates within the tube during the cycle. Another way to view this is that only a small percentage of the total fluid having contact with the tube over the cycle actually enters or exits the tube. However, when $A_r >> 1$, the fluid traverses completely through the tube, residing in the upstream and downstream spaces during most of the cycle. In fact, for $A_r = 1$ all fluid contacting the tube has seen a tube entrance/exit.

Now let us inspect the Euler number for an oscillating flow. This is defined as

$$\mathrm{Eu} = \frac{2\Delta P_{max}}{\rho\,(u_{max})^2} \tag{7.1-2}$$

The Euler number is the ratio of the static pressure force to the fluid momentum force. For the sinusoidal flow field, it is here defined at the maximum or peak values of these parameters. Note that the maximum pressure drop and the maximum velocity do not normally occur at the same point in the cycle. The Euler number characterizes irreversible momentum energy losses due to sudden geometric enlargements and contractions and highly turbulent frictional flow. For a constant geometric configuration, a relatively large Euler number (Eu >> 1) is indicative of a flow field that is dominated by skin shear stresses. A smaller Euler number, which is approaching unity, is indicative of a flow field that is dominated by irreversible momentum losses (form losses) due to enlargements and contractions of the flow path and/or highly turbulent frictional flow.

Now consider a fluid oscillating in and out of a square-ended tube. The Euler number vs. the tidal amplitude plots are shown in Figures 6.2-11 through 6.2-15 at different constant dimensionless tube lengths. These results show that the Euler number decreases rapidly as the tidal amplitude increases from 0 to 1. Then, at approximately $A_r \simeq 1$ to 2, the Euler number begins to level off at a constant value. These results suggest that at small values of the tidal amplitude (i.e., $A_r < 1$) the flow field is dominated by laminar flow shear stresses and that form losses due to entrance effects have little significance. This is explained as follows: As the tidal amplitude increases from $A_r = 0$ to $A_r = 1$, the Re_{max} is also increasing since the $A_r \, \alpha \, Re_{max}$. Hence, the maximum instantaneous friction factor is decreasing rapidly according to the relationship given in Equation (7.1-3), which shows that the friction factor for laminar flow has a strong inverse dependence with the instantaneous Reynolds number.

$$f_{lam} \, \alpha \text{ constant } Re^{-1} \qquad (7.1\text{-}3)$$

As the tidal amplitude increases to values greater than $A_r = 1$ to 2, the curve tends to level off at a constant Euler number, but still above the value of Eu = 1.0. This says that the friction factor is becoming a constant value with increasing Re_{max} and that the flow field is now dominated by form losses. This characteristic of turbulent flow is seen in Equation (7.1-4), where the turbulent friction factor is a relatively weak function of the instantaneous Reynolds number.

$$f_{turb} \; \alpha \; \text{constant} \; Re^{-0.25} \tag{7.1-4}$$

Hence, for $A_r > 1$, all the flow traverses through a tube entrance/exit, which generally trips the flow field into the turbulent regime. Whereas, at low A_r (i.e., $A_r < 1$), the flow is encouraged to be laminar by a dominant and stabilizing pressure field within a geometrically uniform tube where momentum forces are small.

Note further that since the results at $L/D = 5.35$ and $L/D = 10$ (presented in Figures 6.2-11 and 6.2-12) are similar in magnitude, this indicates that the pressure force is dominated by the momentum forces associated with the contraction and expansion of the fluid flow (the form losses). These figures show that the entrance/exit flow loss coefficient (K_t) is approximately equal to 1.0 to 1.1. Remember the value of K_t, as presented here, is correlated to peak valued parameters of a sinusoidal oscillating flow field as compared with averaged or cycle-integrated parameters.

Similar test results are observed for the tubes with rounded and protruding entrance/exits. The Euler number vs. the tidal amplitude plots for the rounded entrance/exit tubes are shown in Figures 6.2-16 through 6.2-20. Note that the curves level off at a constant Euler number that is less than the square-ended tubes. This reflects the lower entrance/exit flow losses due to the rounded entrance/exit configuration.

The Euler number vs. the tidal amplitude plots of the protruding entrance/exit tubes are shown in Figure 6.2-21. Again, these results are similar to the results presented above for the square-ended tubes. Note that with increasing tidal amplitude this curve approaches a constant Euler number greater than that for either the rounded or the squared configuration. Again, this reflects the increased entrance/exit flow losses due to the protruding entrance/exit configuration.

In summary, we have noted that as A_r increases, the overall character of the Euler number vs. A_r curve becomes evident, with $A_r \simeq 1$ to 2 being the point below which ($A_r < 1$) the flow field in the tube is dominated by laminar flow and above which ($A_r >> 1$) the flow field in the tube is dominated by turbulent flow. The difference between these regimes is the percentage of the mass flow in a cycle traversing the tube that sees the tube entrance. The entrance effect is a mechanism for triggering or maintaining turbulent flow.

Euler number vs. Re_{max} and Re_ω

Plots of the oscillating flow Euler number as a function of Re_{max} are presented in Figures 6.2-22 through 6.2-27 for square-ended and round-ended tubes. These plots, in fact, are similar to the Euler number vs. the tidal amplitude plots discussed in the previous section, since the tidal amplitude is proportional to Re_{max}, that is

$$A_r = \frac{D_h}{2L}\frac{Re_{max}}{Re_\omega} \tag{7.1-5}$$

and hence:

$$A_r \, \alpha \, Re_{max} \tag{7.1-6}$$

The significance of the plots in this section is that the effect of Re_ω is broken out. The results show that at constant Re_{max}, the Euler number increases with increasing Re_ω. This is consistent with Seume's experimental findings in which he noted that the onset of turbulent fluctuation is delayed with increasing Re_ω (11). However, with increasing Re_{max} and, hence, increasing tidal amplitude, flow becomes increasingly dominated by turbulent flow. Thus, the Euler number tends to level at a constant value as the tidal amplitude >>1.

Total Dissipation Factor vs. Re_{max} and L/D

The Total Dissipation Factor (TDF) is the ratio of the measured irreversible oscillating flow losses to the calculated flow losses based on the cycle integration of steady flow, unidirectional correlations. The plots of TDF vs. Re_{max} and L/D are shown in Figures 6.2-28 through 6.2-30 for the three entrance/exit configurations at a constant value of $Re_\omega = 100$. The results at a constant value of $Re_\omega = 200$ and $Re_\omega = 300$ show similar trends and these results are tabulated in Appendix B. The cycle-integrated steady flow calculations for the square-ended tube results presented in Figure 6.2-28 were based on $K_t = 1.5$ and the friction factor correlations given in Section 6. These results show that TDF varies from 0.75 to 1.0 as Re_{max} increases from 10^4 to 10^5. Also note that TDF is less than 0.75 for results where $L/D \leq 10$. This reflects the inadequacy of standard entrance/exit flow loss coefficients at $L/D \leq 10$. It is interesting that TDF approaches 1.0 as Re_{max} increases from 10^4 to 10^5. This will be explored later in this text.

For the rounded tubes shown in Figure 6.2-29, the cycle-integrated steady flow calculation was based on $K_t = 1.05$ and the appropriate friction factor discussed in Section 6. TDF ranges from 0.6 to 1.1 with increasing Re_{max}. Again we note that the correlation between the measured and predicted flow losses increases as Re_{max} increases. Also, the test samples of $L/D \leq 10$ tend to correlate poorly.

Similar trends are seen for the protruding tube results as shown in Figure 6.2-30. TDF ranges from 0.75 to 1.05 when $K_t = 1.8$ was used in the calculation of TDF with the appropriate friction factor discussed in Section 6. These results also show a strong effect of tube length on the correlation of TDF, with correlation improving with increasing Re_{max}.

Total Dissipation Factor vs. A_r and L/D

In this section, the results that were presented above in the form of TDF vs. Re_{max} plots, (Figures 6.2-28 through 6.2-30) are now recast into TDF vs. A_r plots. This will help us make sense of these results. We noted above that the correlation between measured and predicted flow losses (TDF) improved as Re_{max} increased from approximately 10^4 to 10^5. Also, it is observed that as the tube length increased, the greater the value of Re_{max} must be to achieve a good correlation of TDF.

If this data is recast into the form of TDF vs. A_r, these trends begin to make more sense. Remember that

$$A_r \propto Re_{max} \qquad (7.1\text{-}7)$$

and

$$A_r \propto 1/L \qquad (7.1\text{-}8)$$

Also remember from our discussions in the section in which Euler number vs. A_r was presented, it was noted that where the flow parameters were such that $A_r < 1$, the flow field in the tube is dominated by laminar flow. When $A_r >> 1$, the flow field is dominated by turbulent flow.

The plots of TDF vs. A_r and L/D are shown in Figures 6.2-31 through 6.2-33 at a constant value of $Re_\omega = 100$ for the three entrance/exit configurations. A review of these plots show that the correlation of TDF drops off as A_r decreases below unity ($A_r < 1$). This means that the correlation between the measured flow losses and the predicted flow losses is good as long as the flow field is predominantly turbulent, which occurs when $A_r > 1$; that is, when all of the flow in the tube sees the tube entrance over the cycle. As the fluid enters the tube, turbulent eddy currents are created due to the entrance which encourage the flow field inside the tube to maintain a turbulent character. In addition, the complementary result is that, for a flow field with $A_r < 1$, these calculations, based on steady flow correlations, overpredict the flow losses in the laminar oscillating flow by up to 35 percent (within the parametric bounds of these tests). This may be conservative by design standards, but it also implies that the analogous heat transfer calculations may be significantly overpredicting heat fluxes in tube heat exchangers when $A_r < 1$.

In summary, these results show that TDF ~ 1.0 when the flow field is highly turbulent and the tube is long enough that the proper value of K_t is employed. In situations where the flow should be turbulent according to steady flow theory but is suspected to be laminar based on oscillating flow results, the predicted flow losses are greater than the measured flow losses, that is (TDF < 1). In general, the cycle-integrated steady flow calculation does not underpredict the flow losses in an oscillating flow field. These results should be viewed with respect to the findings of a study performed by Seume (11) which speaks to flow transition in oscillating flow. He concluded, with constant geometric configuration, that

1. The onset of turbulent fluctuation is delayed with increasing Re_ω .
2. The onset of turbulence occurs earlier in the cycle with increasing Re_{max} .
3. Transition occurs at higher values of Re_{max} than one would predict based on steady flow experience (ie. Re = 10,000 to 15,000).

Total Dissipation Factor vs. Re_{max} and Re_{ω}

The plots of TDF as a function of Re_{max} and Re_{ω} are presented in Figures 6.2-34 through 6.2-39 for square-ended tubes at six different lengths. Similar results are presented in Figures 6.2-40 through 6.2-43 for rounded tubes at four different lengths. These results are similar to those seen in the Euler number vs. Re_{max} and Re_{ω} plots presented above.

7.2 REGENERATOR HEAT EXCHANGERS

7.2.1 Steady Flow Loss Test Results

The regenerator steady flow loss test matrix is outlined in Section 5 and test results are presented in Section 6. Additional detailed data for stacked and sintered screens, and Metex knit wire and Brunswick felt metal regenerators are tabulated in Appendix B.

ΔP vs. Re

The plots of ΔP vs. Re in Figures 6.1-10 through 6.1-12 show, as expected, that ΔP increases with increasing Re and with decreasing regenerator wire diameter (i.e., decreasing hydraulic diameter).

Regenerator Friction Factor vs. Re

The plots of measured regenerator friction factor vs. Re for stacked screens, random fiber, and sintered screen regenerators are shown in Figures 6.1-13 through 6.1-15. These results show that the data fit a different friction factor correlation for each regenerator. The correlations that fit these steady flow test results are given in Table 7.2-1.

Pratio vs. Re

The plot of *P*ratio vs. *Re* for stacked screens is presented in Figure 6.1-16. This plot shows that *P*ratio increases with increasing screen wire diameter. The predicted pressure drop used in the calculation *P*ratio was determined using the friction factor correlations from GLIMPS as presented in Section 6. In general, these *P*ratio results show that there is poor agreement between the ΔP test results and the predicted ΔP based on the GLIMPS correlations. Most noticeable in these results is that the value of *P*ratio increased from approximately 1.2 to 1.9 as the stacked wire screen diameter increased from 41 μm to 191 μm. The regenerator porosity is held fairly constant at 66 percent to 68 percent. Thus, these results show that for the stacked screen regenerators the agreement between test results and calculated predictions based on Equations (6.1-7) and (6.1-8) decreases as the regenerator wire diameter increases.

For the random fiber regenerators, Figure 6.1-17 shows that the agreement between measured pressure drop and predicted pressure drop is within 20 percent for the Metex knit wire regenerator, but that the *P*ratio increases to 1.9 for the Brunswick felt metal regenerator. These predicted pressure drops were based on Equation (6.1-9). The test results for the sintered screens correlate well with Equations (6.1-7) and (6.1-8), as shown in Figure 6.1-18.

7.2.2 Oscillating Flow Loss Test Results

The oscillating flow loss test results for all of the regenerator samples are plotted in Section 6 and tabulated in Appendix B.

ΔP_{max} vs. Re_{max}

The plots of ΔP_{max} vs. Re_{max} for the stacked screen, random fiber, and sintered screen regenerators are shown in Figures 6.2-44 through 6.2-51. These graphs show that ΔP_{max} increases with increasing Re_{max}, decreasing mesh wire diameter, and decreasing Re_{ω}.

Total Dissipation Power vs. Re_{max}

The plots of Total Dissipation Power vs. Re_{max} are shown in Figures 6.2-52 through 6.2-59. These results reflect the same trends noted above for the ΔP_{max} plots; that Total Dissipation Power is strongly dependent on Re_{max} and Re_{ω}.

Total Dissipation Factor vs. Re_{max} and d_w

The plots of Total Dissipation Factor vs. Re_{max} are shown in Figures 6.2-60 through 6.2-62. These results show that the oscillating flow losses are comparable to the integrated steady flow calculation; the largest differences are about 40 percent. The predicted flow losses used in the calculation of TDF were handled differently from those for the tube

calculations that were presented in section 7.1. The predicted flow losses for the tubes were based on the equations used in GLIMPS, Equations (6.1-5) and (6.1-6). As discussed in section 7.2.1, the GLIMPS correlations for the regenerators did not agree well with the steady flow tests. Thus, for the regenerator calculations of TDF, the predicted flow losses were based on the friction factor correlations derived from the measured steady flow test data. These are given in Table 7.2-1. Also, the data points plotted in Figures 6.2-60 through 6.2-62 were taken at various Re_ω. Figures 6.2-63 through 6.2-68 separate out the Re_ω effect.

Total Dissipation Factor vs. Re_{max} and Re_ω

The plots of TDF as a function of Re_{max} and Re_ω are presented in Figures 6.2-63 and 6.2-64 for stacked screen regenerators. Similar results are presented in Figures 6.2-65 and 6.2-66 for the Metex knit wire and Brunswick felt metal regenerators and in Figures 6.2-67 and 6.2-68 for the sintered screen regenerators. These results are similar to those seen in the TDF vs. Re_{max} and d_w plots presented above. These plots show that Re_ω does not have a significant effect on the value of TDF.

Table 7.2-1

Test Results
Regenerator Friction Factor Correlations

Regenerator	Wire Diameter (μm)	Porosity (%)	Friction Factor Correlation
Stacked Screens			
	41	68.0	$f \sim 35.8\, Re^{-0.51}$
	53	66.5	$f \sim 39.0\, Re^{-0.48}$
	94	66.3	$f \sim 29.0\, Re^{-0.41}$
	191	68.0	$f \sim 19.4\, Re^{-0.30}$
Sintered			
	41	61.4	$f \sim 66.5\, Re^{-0.68}$
	53	60.6	$f \sim 32.9\, Re^{-0.54}$
Random Fiber			
Metex knit wire	89	80.0	$f \sim 21.96\, Re^{-0.38}$
Brunswick felt metal	12.7	84.0	$f \sim 128.52\, Re^{-0.66}$

Section 8

8.0 CONCLUSIONS AND RECOMMENDATIONS

The total dissipation factor (TDF), as defined in Section 6, compares the flow loss in an actual oscillating flow field to the flow loss predicted by integrating over the cycle using steady flow friction factors, entrance/exit coefficients and the measured mass flows. Friction factors derived from steady flow measurements are currently used in most Stirling engine simulations. The majority of total dissipation factors measured in this test program indicate that oscillating flow yields flow losses that vary from equal to those of predicted values to about 40 percent less. The agreement between measured and predicted flow losses is near unity as long as the flow fields is dominated by the turbulent regime. This is generally the case when Re_{max} exceeds 20,000 and $A_r > 1$. For regenerators, some of the data show total dissipation factors greater than one. Most of this data are for low Re_{max} values with relatively high measurement errors; also, in this region, some extrapolated (from the steady flow test data) values of the steady flow friction factor had to be used to calculate the predicted part of the TDF.

The significance of these differences remains to be evaluated. In a kinematic engine where the motions of the pistons are defined, the effect on engine performance should not be large. A more significant effect would be expected for a free-piston engine where a difference in the actual pressure drop from that anticipated could lead to an operating stroke or phasing of the pistons that are not at the design values. This could lead to a larger effect on resulting engine performance. These oscillating flow results should be incorporated into existing Stirling computer simulations to analyze their importance.

These test results may also have implications for heat transfer. A reduced pressure drop may correspond to a reduced heat transfer in the heat exchangers. The computer simulations have shown that the designs currently being studied for space power applications are particularly sensitive to heat transfer at the low temperature ratios necessary for a space power system. In future designs, the cross-sectional flow areas of the heat

exchangers could possibly be reduced to improve the heat transfer (since the pressure drop may be lower than that predicted by currently used steady flow correlations).

The University of Minnesota (1,4,5,11) is also investigating oscillating flow in tubes as part of a NASA Lewis program to understand Stirling engine losses. Their approach is to use larger tubes with flow at lower oscillating frequencies (but at the proper values of dimensionless parameters) to allow detailed measurements to be made of the flow parameters inside the tube. Their work is meant as a complement to this Sunpower program which measured overall effects on actual-size engine hardware operating at actual engine oscillating frequencies. Simon and Seume have measured a delay in the transition from laminar to turbulent flow during acceleration of the fluid and a delay in the transition from turbulent to laminar flow during deceleration (11). The relationship of this effect to the results of this report should become clearer in the future.

One of the main objectives of this report is to present the data in a form to allow further evaluation. It is hoped that the data can be utilized in Stirling computer simulations, compared to test data of other researchers, and possibly analyzed by other methods.

Recommendations for future work include the following:

1. It is desirable to obtain values of the oscillating flow friction factors f_r and f_i as described in Section 2. To do this, further work must be done on methods to separate out the entrance and exit effects in oscillating flow and to handle the higher harmonics on the test data.

2. Extend the ranges of testing for the dimensionless parameters Re_{max} and Re_{ω} to cover the full ranges as indicated by Simon and Seume (1). Using water as the working fluid

would allow testing in the standard transition region. Water testing would also remove the uncertainties associated with compressibility effects. Also, it may be possible to test a geometry at laminar conditions for which the governing equations can be solved.

3. Check the existing regenerator test data against a variety of regenerator correlations to look for the best fit. In addition, the rig could be used to run a wider variety of regenerator geometries to establish a larger database.

4. For further tests, the instrumentation should be carefully reviewed for both the oscillating and steady flow rigs to minimize instrumentation errors. A parallel arrangement with several different range transducers may be ideal for the steady flow rig.

5. At some point, a second driver should be added to the rig to incorporate the effects of oscillating pressure level. The rig could also be used to test other related Stirling engine effects such as gas spring losses.

REFERENCES

1. Seume, J.R. and Simon, T.W.: A Survey of Oscillating Flow in Stirling Engine Heat Exchangers, NASA CR-182108, March 1988.

2. Tew, R.C, Jr.: Overview of Heat Transfer and Fluid Flow and Problem Areas Encountered in Stirling Engine Modeling, Technical Memorandum 100131, NASA Lewis Research Center, Cleveland, Ohio, February 1988.

3. Gedeon, D.: Mean-Parameter Modelling of Oscillating Flow: Journal of Heat Transfer, Vol. 108, pp. 513-518, August 1986.

4. Seume, J.R., Goldberg, L.F. and Simon, T.W.: Description of an Oscillating Flow Test Program, Proc. 22nd IECEC, pp. 1753-1758, 1987.

5. Seume, J.R. and Simon, T.W.: Oscillating Flow in Stirling Engine Heat Exchangers, Proc. 21st Intersociety Energy Conversion Engineering Conference, pp. 533-538, 1986.

6. Brown, Alec T.: Space Power Demonstrator Engine, Phase I Final Report, NASA CR-179555, MT187TR36; 1987.

7. Penswick, L. Barry: 1050 K Stirling Space Engine Design, NASA CR-182149, 1988.

8. Kays, W.M. and London, A.L.: Compact Heat Exchangers, 3rd ed., McGraw-Hill Book Company, 1984.

9. General Electric Company, Corporate Research and Development: Fluid Flow Data Book, Schenectady, NY.

10. Gedeon, D.: GLIMPS Stirling Cycle Simulation, Gedeon Associates, Athens, Ohio, 1987.

11. Seume, J.R.: An Experimental Investigation of Transition In Oscillating Pipe Flow, PhD Thesis, University of Minnesota, 1988.

12. Draper, N. and Smith, H.: Applied Regression Analysis, 2d ed., Wile-Interscience, 1981.

13. Lambert, J.D. : Computational Methods in Ordinary Differential Equations, Wiley, P., New York, N.Y., p. 106, 1973.

14. Lindgren, B.W.: Statistical Theory, 2d ed., MacMillan, N.Y., 1968.

Appendix A

Appendix A

Data Reduction

The pressure drop (wall shear stress) suffered by a fluid in a duct under oscillating-flow conditions differs fundamentally from that in the same duct under steady flow conditions. The fluid near the wall, moving slower, responds more quickly to a pressure gradient than does the central flow. The central velocity, therefore, lags the near-wall velocity to some extent, giving rise to a velocity profile that can actually be bi-directional at times — certainly different from that of steady flow. One expects then, that the relationship between pressure drop and instantaneous flow velocity will differ from the steady-flow case. The question is: How much?

This appendix documents the data reduction process for Sunpower's oscillating-flow pressure-drop test rig. The theory and software documented here were, for the most part, contrived and written by David Gedeon, acting as a consultant to Sunpower. This appendix was also written by him as a condensation of a number of his memos that he drafted over the course of the work. Any inconsistencies and errors reported then have — we hope — now been corrected, making this the definitive reference for data reduction.

This data reduction process was, for the most part, developed prior to the testing. As mentioned in the text, f_r, f_i and CDF were not finally used to reduce the data due to problems with separating the entrance and exit losses from the core friction and also with higher-order harmonics. The data were correlated primarily with the total dissipation factor, TDF. The program XREDUCE discussed in this appendix was written to attempt to resolve the problems mentioned above. However, funding limitations prevented full usage of this data reduction procedure in this SBIR project.

A.1 Nomenclature

A	Frontal area
d	Sample duct hydraulic diameter
f_i, f_r	General linearized friction factors
C_p, C_v	Gas specific heats
E	Fluid energy in piston cylinder
F	Force per unit volume due to wall shear stress
$g = \rho u$	Section-average mass flow rate per unit area
K	Entrance/exit loss coefficient
L	Length of test sample
M	Fluid mass in piston cylinder
P	Pressure
Q	Gas-wall heat flux in piston cylinder
R	Gas constant
$Re_{max} = \rho u_m d/\mu$	Peak Reynolds number
$Re_\omega = \rho\omega d^2/(4\mu)$	Kinetic Reynolds number
t	Time coordinate
T	Temperature
u	Section-average velocity
u_m	Velocity amplitude (of first harmonic if non-sinusoidal)
V	Piston cylinder volume
x	Axial coordinate

Greek

$\delta = u_m/\omega$	Tidal amplitude
μ	Viscosity
ω	Angular frequency
ρ	Fluid density
σ	Sample/Cylinder area ratio

Operators

Hm	Harmonic operator: Hm(f) = first harmonic in f Fourier series
RSS	Root sum squared
$\dot{}$	Time derivative: $\dot{f} = df/dt$
$<>$	Spatial-average: $< f >= 1/L \int f\, dx$
$\tilde{}$	Error component: $\tilde{f}$ = standard deviation of f considered as a random variable

A.2 An Exact Laminar Solution

For non-steady one-dimensional fluid flow, the momentum equation can be written

$$\frac{\partial P}{\partial x} = F - \frac{\partial g}{\partial t} - \frac{\partial}{\partial x}(gu) \tag{A.1}$$

where u is section-average velocity, $g = \rho u$ is the mass flux per unit area and F is the force per unit volume due to wall shear stress. The last two terms on the right are easy enough to deal with; it is F that concerns us.

An exact solution of the momentum equation in the case of incompressible laminar sinusoidal flow between parallel plates (see reference [3]) tells us that F can be expressed as

$$-F = f_i \left(\frac{u_m}{2\omega d}\right) \frac{\partial g}{\partial t} + f_r \left(\frac{u_m}{2d}\right) g \tag{A.2}$$

where f_r and f_i are the real and imaginary parts of a constant dimensionless complex friction factor, u_m is the velocity amplitude, d is hydraulic diameter and ω is angular frequency. Everything is constant on the right except g which is a sinusoidal function of time. f_r determines the component of wall stress in phase with the velocity while f_i determines the component 90 degrees out of phase. One can show that the second term on the right of (A.2) is responsible for energy dissipation while the first term is non-dissipative – merely tending to enhance the apparent density of the fluid.

In reference [3], both f_r and f_i are functions of the kinetic Reynolds number (or dimensionless frequency) Re_ω defined by

$$Re_\omega = \frac{\rho \omega d^2}{4\mu} \tag{A.3}$$

For low frequency oscillation, f_i approaches zero while f_r reduces to the ordinary Darcy friction factor for laminar flow evaluated at u_m. As Re_ω increase above about 10, both f_i and f_r begin to differ from the steady flow case. For large Re_ω (above about 100), f_i and f_r approach each other in magnitude and are both proportional to $Re_\omega^{0.5}$.

Equation (A.2) can serve as a model for the more general case of compressible, turbulent non-sinusoidal oscillating flow. In principle it would seem possible to find f_r and f_i in terms of which F could be expressed in the manner of equation (A.2) although higher harmonics in F and g might be expected to cause practical difficulties. For turbulent flow, even if g is nearly sinusoidal, F may be quite non-sinusoidal. So non-sinusoidal, it turns out, that forcing F to fit into the form of (A.2) seems quite silly at times. Nevertheless, we choose to keep the linearized expression (A.2) in mind anyway as a possible future correlation form. A significant virtue of (A.2) for computer modeling applications is that it can be applied even if the amplitude and phase of g are not precisely known in advance — even to non-sinusoidal flows.

A.3 Experimental Data Reduction

In broad strokes, the data reduction process is comprised of three steps, repeated for each oscillating-flow experiment:

1. Solve for the mass flux $g(t)$ within the sample duct.
2. By use of the fluid momentum equation, isolate F, the part of the total sample pressure drop due to fluid shear stress at the wall, and present this information in terms of standard engineering notions such as core friction factor and entrance loss coefficient.
3. Do an error analysis.

Step (1) is necessary because there is no direct mass flow rate instrumentation on the test rig — one must solve for the mass flow rate in the sample duct using pressure and piston displacement signals, together with a lumped-parameter energy equation for the fluid in the piston cylinder. Once g is determined, the only unknown in the fluid momentum equation is F, the pressure gradient induced by the shear stress at the wall-fluid boundary — the frictional pressure gradient for short. The problem is: Once you know what the frictional pressure gradient is, what do you do with it? There are several possibilities all of which attempt to more-or-less conform to the conventions established in the steady-flow literature. More details later. Step (3) is the hard part. Most of the difficult reading in this appendix concerns error analysis. For this reason I have put all the error analysis theory in a separate section where disinterested readers will find it easy to skip.

A.3.1 Representing Time-Varying Functions

By its very nature, oscillating-flow data reduction deals with periodic functions of time which are not necessarily sinusoidal — or even close. In the actual nitty-gritty of data reduction, all these functions are represented in terms of truncated Fourier series — currently up to the seventh harmonic. To be sure, the raw pressure and displacement signals are digitally sampled at discrete time intervals and stored in a large array. But before data reduction begins, they are converted to Fourier series form. Doing this has several advantages. Among these are:

- Functions can be differentiated, integrated, normalized, added, dot-product multiplied, etc. by use of simple algebraic formulas involving their Fourier coefficients.
- Certain types of *noise* in the data can be easily spotted. The dreaded Helmholtz oscillations, which show up as large coefficients for higher harmonics, come to mind. A Fourier series representation tends to isolate the noise from the other components of the signal.

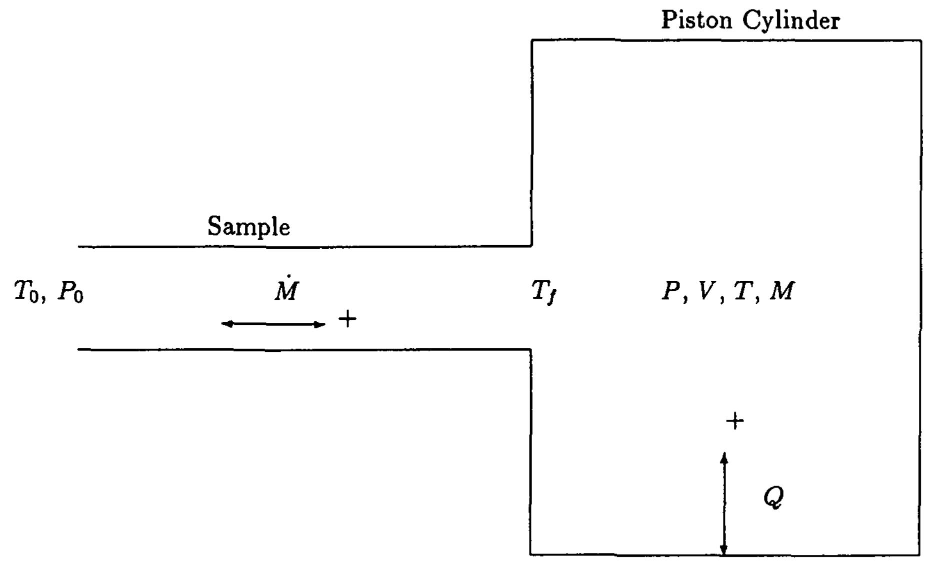

Figure A.1: The lumped-parameter rig model

- The data is easily linearized by ignoring all but the first harmonic coefficients. This makes approximate relationships like the linearized form for F of equation (A.2) easy to work with.

A disadvantage of Fourier series is that there are some subtle errors one can make when converting raw data from a tabulated function to a series. This appendix does not deal with this issue at all. It assumes, as a starting point, that any Fourier series that is input to the data reduction process is accompanied by an estimate of its overall error.

A.3.2 Solving for Sample Duct Mass Flux

The following analysis applies to the case where the test fluid is compressible — that is: a gas. The incompressible case is trivial since then density is constant and the volumetric flow rate in the sample duct is the same as that in the piston cylinder.

The lumped-parameter gas energy equation for the piston cylinder volume V in figure A.1 may be written

$$\dot{E} = -P\dot{V} + C_p T_f \dot{M} + Q \tag{A.4}$$

where P is pressure, C_p is the specific heat, T_f is the flow temperature at the cylinder entrance, M is the fluid mass, and Q is the gas-wall heat flux in the

piston cylinder. E is the internal energy of the assumed ideal gas given by

$$E = C_v MT = (C_v/R)PV \tag{A.5}$$

I assume heat flux Q is given by

$$Q = hA(T_0 - T) \tag{A.6}$$

where h is a film heat transfer coefficient and A is the cylinder surface area. T_0 is a sort of ambient temperature, representing the temperature of sample duct walls as well as that of the surrounding gas in the pressure vessel. The flow temperature T_f is not measured. Instead I assume it is given by

$$T_f = \begin{cases} T_0 & \text{for } \dot{M} \geq 0 \\ T & \text{for } \dot{M} < 0 \end{cases} \tag{A.7}$$

After differentiating equation (A.5), substituting into equation (A.4) for $\dot{E}$ and simplifying, the mass flow rate ($\dot{M} = dM/dt$) works out to

$$\dot{M} = \frac{PV}{RT_f}\left[\frac{\dot{V}}{V} + C_v/C_p\frac{\dot{P}}{P} - R/C_p\frac{Q}{PV}\right] \tag{A.8}$$

Unfortunately (A.8) cannot be used directly to find $\dot{M}$ since temperature T is not a measured variable and, therefore, Q and T_f are not known in advance. However, it is possible to solve (A.8) as a differential equation. $M(t)$ is then uniquely determined under the boundary conditions that the solution is periodic and outside temperature T_0 and pressure P_0 are known.

Here are the details: The input variables measured directly in experimental tests are

- T_0: the representative temperature of the sample duct wall (constant).
- $P(t)$: the time-varying absolute gas pressure in the piston cylinder.
- $V(t)$: the time-varying piston cylinder volume.

Cylinder gas mass as a function of time $M(t)$ is then solved as an initial-value problem — a differential equation in time where the initial value is specified. The initial value is taken as

$$M(0) = \frac{P(0)V(0)}{RT_0} \tag{A.9}$$

Actually, the initial value doesn't matter much. The solution runs for as many cycles as required for $M(t)$ to match up at the cycle-division times — that is: until it is periodic.

Numerically solving the above initial-value problem requires a procedure for calculating $\dot{M}$ as a function t, M and the input variables P, V etc. Once such a procedure is available, any standard differential equation solving routine can solve $M(t)$. Evaluating $\dot{M}$ at any given time is conveniently broken down into five steps.

1. Determine T from the equation of state $T = PV/RM$.

2. Determine gas-to-wall heat flux Q from (A.6). The trick is to find a good value for h. However, since Q is a relatively small term in the energy equation it turns out not to matter very much. The data reduction software takes h as an input constant (mean effective value). It is the user's responsibility to supply the correct value by use of an appropriate empirical engineering correlation.

3. Calculate the square bracket term in (A.8) from Q and the input variables.

4. Determine the inlet flow temperature T_f from (A.7), where the sign of $\dot{M}$ is determined from the sign of the square bracket term in (A.8). That is, assume flow into the cylinder occurs at temperature T_0 and flow out of the cylinder occurs at temperature T. Actually, there is some error introduced here because T_f cannot really change discontinuously. Fortunately, most experiments are run with very low temperature amplitudes so the errors tend to be small.

5. Finish calculating the right-hand side of (A.8)

More details can be found in section A.5 which documents the actual software.

A.3.3 Determining Frictional Pressure Drop

The next step is to determine the frictional pressure gradient from the total pressure drop across the sample duct.

For purposes of argument define four pressures P_0 through P_3 located as shown in figure A.2. P_3 is the one that is experimentally measured and varies roughly sinusoidally while P_0 is constant. P_1 and P_2 are the pressures just inside either end of the sample duct after correcting for entrance effects. That is, I assume P_1-P_0 and P_3-P_2 are determined by entrance effects while P_2-P_1 is determined by core friction and acceleration terms according to the momentum equation (A.1). In reality, entrance effects cannot be separated from core friction so neatly, but the present model makes the analysis tractable. I also use subscripts 0–3 on other variables such as u and g to denote values at the locations shown on figure A.2.

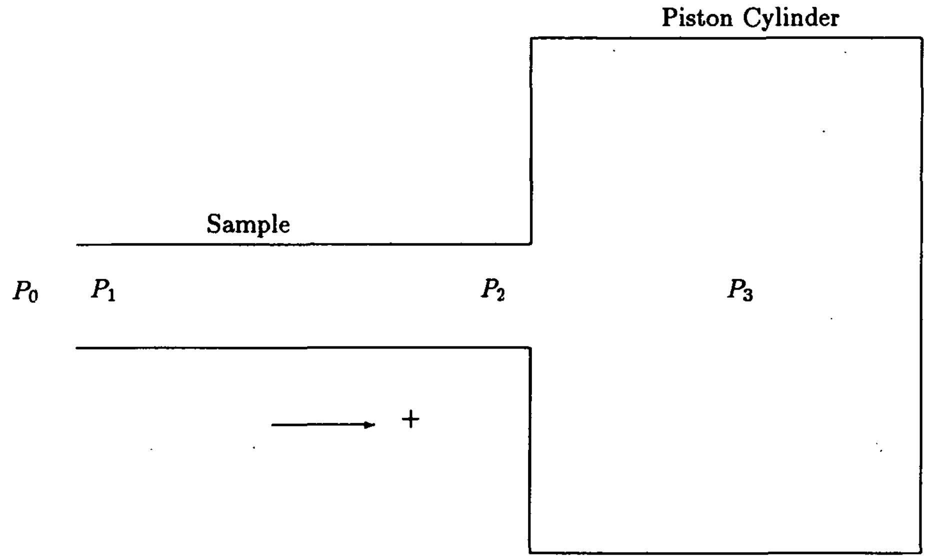

Figure A.2: Four key pressure points in the test rig.

An Expression for $P_3 - P_2$

Bernoulli's law applies to flow in regions such as tube entrances where there is an abrupt change in area — even for oscillating flow. Bernoulli's law is

$$\Delta(u^2/2) = -\int dP/\rho \tag{A.10}$$

Assuming density doesn't change much in the region 2–3, equation (A.10) integrates to

$$P_3 - P_2 \approx \frac{1}{2} g_2 u_2 (1 - \sigma^2) \tag{A.11}$$

where

$$\sigma = u_3/u_2 \approx A_2/A_3 \tag{A.12}$$

A_2 is the sample duct flow area and A_3 is the cylinder cross section area. Adding an assumed entrance loss coefficient K_2 gives

$$P_3 - P_2 \approx \frac{1}{2} g_2 u_2 (1 - \sigma^2) - \frac{1}{2} g_2 |u_2| K_2 \tag{A.13}$$

Note that even if g and u are sinusoidal $P_3 - P_2$ will not be. It will have a second harmonic due to the first term on the right of (A.13) and a third harmonic due to the second term.

An Expression for $P_1 - P_0$

Bernoulli's law applies in the region 0–1 as well. I assume the velocity in region 0 is zero and introduce a loss coefficient K_1 so that

$$P_1 - P_0 \approx -\frac{1}{2}g_1 u_1 - \frac{1}{2}g_1|u_1|K_1 \tag{A.14}$$

An Expression for $P_2 - P_1$

Momentum equation (A.1) can be integrated with respect to x in the region 1–2 to give

$$P_2 - P_1 = L < F > -L\frac{\partial}{\partial t} < g > +g_1 u_1 - g_2 u_2 \tag{A.15}$$

where L is the sample duct length and $<>$ denotes the sample duct spatial average.

Total Pressure Drop

Adding equations (A.13), (A.14) and (A.15) gives an expression for the instantaneous total pressure drop which is measured in the rig tests

$$\begin{aligned} P_3 - P_0 \;\approx\; & \frac{1}{2}g_2 u_2(-\sigma^2 - 1) + \frac{1}{2}g_1 u_1 - L\frac{\partial}{\partial t} < g > +L < F > \\ & -\frac{1}{2}g_2|u_2|K_2 - \frac{1}{2}g_1|u_1|K_1 \end{aligned} \tag{A.16}$$

Solving for F

We want to use (A.16) to correlate $< F >$ and $< g >$. This will make the most sense if F and g are relatively uniform along the sample duct, so I go ahead and make this assumption now. That is, I assume that the only valid experiment is one where g and u are fairly uniform within the entire sample and approximately equal to their values at the cylinder inlet. These values are, of course, readily obtained from the solution of the $M(t)$ differential equation discussed previously. More later on the errors caused by this assumption. Replacing g_1 and g_2 with g and u_1 and u_2 with u in (A.16) and then solving for F gives an equation which is useful for isolating the frictional pressure gradient in an experimental data point

$$F \approx \frac{1}{L}(P_3 - P_0) + \frac{\sigma^2}{2L}gu + \frac{K_t}{2L}g|u| + \frac{\partial g}{\partial t} \tag{A.17}$$

In (A.17) I have combined K_1 and K_2 into an overall entrance/exit loss coefficient K_t and dropped the $<>$ notation around F with the understanding that the value of F on the left is a mean effective value for the entire sample duct.

Solving for Both F and K_t

Equation (A.17) assumes that the loss coefficient K_t on the right side is known in advance so that F can be explicitly solved. For very long ducts, or porous materials, the K_t term is small so any error in F due to an error in K_t will also be relatively small. But what about short ducts where entrance losses are a major component of the total pressure drop?

In this case it is no longer a good idea to assume K_t is known in advance. Rather, it is a better idea to actually solve for K_t as part of the data reduction process. To do this requires testing a range of ducts of different lengths, instead of just a single sample.

The best way to understand the basic idea is to consider the steady flow case first. Say we were to hold everything constant except length L in a series of steady-flow pressure drop experiments. If all experiments were above some critical length L_0, then we would expect a plot of total pressure drop vs L to be pretty close to a straight line. The slope of this line would be due to core friction F and the y-intercept (offset when extrapolated to $L = 0$) would represent a constant entrance loss K_t. Both slope and y-intercept are easy to measure.

In oscillating flow we can do a similar sequence of experiments — varying L but keeping mass flow rate, etc. the same. Now the total pressure drop is represented as a Fourier series but we can still plot pressure drop vs length — this time for each component of the Fourier series. We will wind up with a slope and a y-intercept for each term, or in other words the components of two new Fourier series. By rearranging equation (A.17) slightly it can be put into a form that allows us to take advantage of this information

$$P_3 = \left(F - \frac{\partial g}{\partial t}\right) L + \left(P_0 - \frac{1}{2} g u \sigma^2 - \frac{1}{2} g|u|K_t\right) \tag{A.18}$$

Now (A.18) is in the form

$$P_3 = C(t)L + D(t) \tag{A.19}$$

where

$$C(t) = F - \frac{\partial g}{\partial t} \tag{A.20}$$

$$D(t) = P_0 - \frac{1}{2} g u \sigma^2 - \frac{1}{2} g|u|K_t \tag{A.21}$$

Both $C(t)$ and $D(t)$ depend on g and u but are independent of L (at least for $L > L_0$ and so long as g does not vary much with position). So if we run a series of experiments with fixed g and u — varying only L — then we are can solve for C and D. Equation (A.19) is understood to apply termwise to each component of the Fourier series for P_3, so we are really solving for the Fourier components of C and D. Once we know C and D we can easily back out F from C and the

irreversible entrance pressure-drop term $\frac{1}{2}g|u|K_t$ from D. I discuss the details of solving for C and D later in section A.5.

There are two catches. First, the critical length L_0 below which the theory breaks down is not known in advance. Non-linearity of data is a symptom of $L \leq L_0$. For laminar steady flow, Kays and London [8] give a table of friction factors in entry lengths (fig. 6-23 P. 138) suggesting that $L_0/d \approx R_e/20$ where d is hydraulic diameter and R_e is Reynolds number. They give no friction-factor data for turbulent steady flow but thermal entry length tables suggest that $L_0/d \approx 40$ — independently of Reynolds number. It is not clear to what extent these steady flow results might carry over to oscillating flow. Second, given identical piston strokes and frequencies, the sample duct pressure drop changes a little each time one varies length, in turn affecting the mass flux g due to the compressibility of the fluid. So it is difficult in practice to perform a sequence of tests varying L while keeping g fixed. This suggests one would get the best results with *nearly* incompressible flows, although the variability of g can be factored into the error analysis.

The criterion for *nearly incompressible* flow can be made more precise. Equation (A.8) gives the differential equation for the cylinder fluid mass time derivative $\dot{M}$ in the case of an ideal gas. Ignoring surface heat transfer

$$\dot{M} \approx \frac{PV}{RT_f}\left(\frac{\dot{V}}{V} + \frac{1}{\gamma}\frac{\dot{P}}{P}\right) \tag{A.22}$$

where V is cylinder volume, R is the gas constant, $\gamma = C_p/C_v$ and T_f is the flow temperature at the inlet. Mass flux g is just proportional to $\dot{M}$. The criterion for *nearly incompressible* flow is that

$$\left|\frac{\dot{P}}{P}\right| \ll \left|\frac{\dot{V}}{V}\right| \tag{A.23}$$

A.3.4 Representing the Data

Once one has found Fourier-coefficient representations for core friction F and, perhaps, the entrance-loss term $\frac{1}{2}g|u|K_t$, the question arises: How does one make this information useful to the engineer? There are several options.

Linearized Friction Factors

Equation (A.2) is an obvious place to start. Here F is expressed in terms of two Darcy friction factors f_i and f_r in a form that can be evaluated in terms of readily available variables. The idea is that f_i and f_r could be correlated as functions of various characteristic dimensionless groups (such as: Re_ω and Re_{max}), but would be constants in any given oscillating-flow situation. This representation works fine if F and g are sinusoidal, but not otherwise.

In the case when either F or g are non-sinusoidal there is no guarantee that constants f_i and f_r satisfying (A.2) exist. It is possible to find non-constant f_i and f_r (perhaps as functions of instantaneous velocity) that satisfy (A.2) for a particular experiment but there seems to be no way to uniquely determine them and no guarantee that they would be useful for other data points. One problem is that velocity profiles take some time to develop; and therefore, F depends on the entire periodic-flow interval, not just instantaneous velocity.

Even so, one may proceed by ignoring higher harmonics. In any rig experiment we obtain g and F as Fourier series. If we insert just the first harmonics (denoted by Hm(g) and Hm(F) into (A.2) and understand u_m to be the amplitude of the first harmonic of u, then we can uniquely determine f_r and f_i from

$$-\,\mathrm{Hm}(F) = f_i\left(\frac{u_m}{2\omega d}\right)\frac{\partial}{\partial t}(\mathrm{Hm}(g)) + f_r\left(\frac{u_m}{2d}\right)\mathrm{Hm}(g) \qquad \text{(A.24)}$$

The value of F predicted in this way can then be compared with the experimentally derived Fourier series for F in order to estimate the error of the approximation. The data reduction program, in fact, does all this. See section A.5 for more details.

Enhancement Factors CDF and TDF

Another way to proceed is to derive correction factors that multiply steady-flow pressure-drop correlations in order to get the right answer in the oscillating flow case. We are doomed to failure here, too, if we expect to get exact results in an instantaneous sense. There are just too many ways that F and g can be non-sinusoidal to have any hope of coming up with a manageable expression for these hypothetical multipliers. If, however, we ask only to get the right answer in the time-averaged sense, then our hopes are much better.

If one is to proceed this way, then the most obvious requirement that comes to mind is that the pumping dissipation should come out right. That is: even though our pressure drop correlation might give the wrong answer at any given instant; over the whole cycle, the predicted pumping dissipation will be correct. We define two factors in this way, CDF (Core Dissipation Factor) if we plan to correct just the Darcy friction factor f of steady flow or, TDF (Total Dissipation Factor) if we plan to multiply the entire steady-flow pressure drop formula including the entrance/exit loss term.

More precisely, the Core Dissipation Factor CDF is defined as the ratio of pumping dissipation produced by the experimental core-frictional pressure gradient F to that produced by a steady-flow friction factor

$$\mathrm{CDF} = \frac{\displaystyle\int Fu}{\displaystyle\int f\frac{g|u|}{2d}u} \qquad \text{(A.25)}$$

where u is gas velocity, g is mass flow rate per unit area, d is hydraulic diameter and f is a Darcy friction factor obtained from a steady-flow correlation applied at the instantaneous flow conditions. The idea is that if a computer simulation calculates frictional pressure gradients by multiplying the steady-flow friction factor by CDF, the pumping dissipation will come out right. That is

$$\mathsf{CDF} \int f \frac{g|u|}{2d} u = \int F u \tag{A.26}$$

Of course the instantaneous values of the corrected steady-flow pressure gradient cannot be expected to match F, nor can the phase angle with respect to g be expected to come out right. But since pumping dissipation is probably all that really matters in most engineering situations, the CDF correction factor is very useful. Section A.4 shows how to estimate the error in CDF.

Similarly, the Total Dissipation Factor (TDF) is defined as the ratio of pumping dissipation produced by the total measured pressure drop ΔP to that produced by the steady-flow predicted pressure drop

$$\mathsf{TDF} = \frac{\int \Delta P u}{\int \left((f \frac{l}{d} + K) \frac{g|u|}{2} \right) u} \tag{A.27}$$

There is at least one problem with the notions of CDF and TDF: In some cases, the steady-flow friction factor f and entrance/exit loss coefficient K may be unknown. The only hopes then are to:

1. Experimentally come up with steady-flow correlations for f and K, or

2. Make up correlations for f and K and apply them consistently.

Option (1) is clearly the best but even option (2) may make some sense if it is properly documented. For example, if one has a reliable pressure drop correlation for woven screen matrices he might go ahead and use it for random-fiber matrices assuming that any discrepancies will be automatically taken up by the CDF and TDF factors.

Once obtained over a range of experiments, CDF and TDF could, in principle, be correlated as functions of Re_ω, Re_{max}, etc. Then, either factor could be readily incorporated into a stirling computer simulation currently using steady-flow theory for pressure drop. Again, the instantaneous pressure drops so obtained would be in error but the overall pumping dissipation would come out right.

Effective Entrance Coefficient K_entrance

When using the CDF enhancment factor to correct the steady-flow friction factor one still needs to account for entrance losses. The effective loss coefficient

K_entrance allows us to do just that. The definition of K_entrance is

$$\text{K\_entrance} = \frac{\int \frac{1}{2} g|u|K_t u}{\int \frac{1}{2} g|u|u} \tag{A.28}$$

where the entrance loss factor $\frac{1}{2}g|u|K_t$ in the numerator is obtained in the manner explained in section A.3.3. K_entrance, of course, is a constant whereas K_t is a function of time. The idea is that if a computer simulation were to calculate entrance pressure drop by multiplying the instantaneous velocity head $\frac{1}{2}g|u|$ by K_entrance, then the overall entrance pumping loss would come out right. That is, it would wind up the same as that produced by the actual term $\frac{1}{2}g|u|K_t$. Again, the instantaneous value and phase angle of entrance pressure drop would be wrong but that would not matter in most engineering situations.

A.4 Hunting for Errors

They sought it with thimbles, they sought it with care:
They pursued it with forks and hope;
They threatened its life with a railway-share;
They charmed it with smiles and soap.
— Lewis Carroll

For some reason error analysis tends to be messier and more difficult than coming up with the answer in the first place. At every stage of the data reduction process errors tend to creep in so that by the time the final results are in, they are accompanied by a mind boggling list of cumulative errors. The data reduction program keeps track of all this but humans are apt to get confused.

There are really just three simple rules to keep in mind which are designed to make the job possible:

1. Assume all errors are random and independent.
2. Formulate all errors as representative values for the entire cycle — not instantaneous errors.
3. Work with dimensionless *relative* errors.

Rule (1) means that we can treat cumulative errors by root-sum-squaring the individual components. Many component errors are neither random nor independent of other errors. None the less, if we are to get anywhere at all we must assume they are. Rule (2) keeps us from getting bogged down in errors as functions of time which would offer little solace to practicing engineers at the expense of much obfuscation. Rule (3) means that absolute error estimates are normalized by some representative value for the random variable in question. This way a relative error of 0.01 means the same thing no matter what units are used.

The strategy adopted by the rest of this section is to present all the individual component error terms in logical order. Section A.5 documents the manner in which they are combined to give the various total errors output by the data reduction software.

A.4.1 Error Algebra

Before we get started, some brief and informal discussion of error algebra is in order. Here, I take the term *error* to be synonymous with the more precise notion of *standard deviation* of a random variable.

Sums of Errors

The question is: Given two or more component errors, what is the error of their sum? The answer turns out to be fairly simple. Let $\tilde{r}_1$ and $\tilde{r}_2$ represent

the standard deviations of two random independent variables r_1 and r_2. Then according to standard statistical theory for sums of random variables ([14], pp. 126–129) the standard deviation of their sum is given by

$$\text{error of } (r_1 + r_2) = \sqrt{\tilde{r_1}^2 + \tilde{r_2}^2} = \text{RSS}(\tilde{r_1}, \tilde{r_2}) \tag{A.29}$$

where RSS denotes the root-sum-squared operator. This notion generalizes to an arbitrary number n of error terms in the obvious way. We will make heavy use of the RSS operator.

Products of Errors

A little more difficult: Given two or more component errors, what is the error of their product. This works out quite like the product rule for differentiation. Let r_1 and r_2 be as before. Assume that for either subscript

$$r_i = \bar{r}_i + \tilde{r}_i \tag{A.30}$$

where $\bar{r}_i$ denotes the mean value of random variable r_i. Then, evidently, the product of r_1 and r_2 is given by

$$r_1 r_2 = \bar{r}_1 \bar{r}_2 + \bar{r}_1 \tilde{r_2} + \bar{r}_2 \tilde{r_1} + \tilde{r_2} \tilde{r_1} \tag{A.31}$$

neglecting the last term on the right and considering the middle two terms to be themselves random errors it follows from the previous result on sums that

$$\text{error of } (r_1 r_2) = \text{RSS}(\bar{r}_2 \tilde{r_1}, \bar{r}_1 \tilde{r_2}) \tag{A.32}$$

For relative errors, the product rule has a particularly simple form. Dividing the previous equation by $\bar{r}_1 \bar{r}_2$ gives

$$\text{relative error of } (r_1 r_2) = \text{RSS}\left(\frac{\tilde{r_1}}{\bar{r}_1}, \frac{\tilde{r_2}}{\bar{r}_2}\right) \tag{A.33}$$

Time-averaged Errors

The previous rules for sums and products of errors actually applied to instantaneous errors. What about representative errors over a full cycle? The sum rule is the same as before — just think of the $\tilde{r}_i$ as representative errors for the full cycle. The product rule is also the same as before except, in addition to thinking of the $\tilde{r}_i$ as representative values, you must think of $\bar{r}_i$ as normalized values according to

$$||\bar{r}_i|| = \sqrt{1/2\pi \int_0^{2\pi} \bar{r}_i^2 d\,\omega t} \tag{A.34}$$

In other words, you must think of $\bar{r}_i$ as a time-RMS value. This result assumes that the error terms $\tilde{r}_i$ are time independent.

A.4.2 Errors in Mass Flow Rate

Here's what can go wrong when calculating the sample duct mass flow rate by solving the differential equation for $M(t)$ as outlined in section A.3.2.

Model Error

Equation (A.8) is slightly in error because it ignores gas kinetic energy compared to thermal energy. This is justified because of the relatively low Mach number within the cylinder — about 0.02 for air based on a maximum piston velocity of 6m/s. The ratio of gas kinetic energy to thermal energy is on the order of the Mach number squared or at most about 10^{-4}. This error affects the solution of $M(t)$ only slightly and is neglected by the data reduction software on the grounds that it should be quite small compared to some other errors.

Numerical Error

Truncation and round-off error occur whenever a differential equation is numerically solved. The solution of (A.8) for $M(t)$ is no exception. Truncation error can be estimated by running a series of solutions of the same problems with decreasing time step. Comparing terms in the Fourier expansions of the resultant M(t) allows an estimate of error as a function of time step. Truncation error should approach zero as the time step approaches zero. In the presence of round-off error though, total error will increase dramatically below a threshold time step.

The data reduction program neglects both truncation and round-off error in its error estimates, assuming that suitable pains were taken during the code development to insure that these errors are quite small.

Errors in Input signals

The errors in $P(t)$ and $V(t)$ (actually piston position) may be significant in some cases. These are factored into the error analysis using the above rules for combining random errors. Details are in section A.5.

Errors in Heat Transfer Coefficient

The assumed value for heat transfer coefficient h used in determining the gas-to-wall heat flux Q is almost certainly in error. The data reduction program estimates the effect of an error in h by use of the above error combination formulas. Although the relative error in h is large, its overall effect is generally quite small because the heat transfer term Q is small compared to some of the other terms in the gas energy equation.

Errors in T_f

Equation (A.7), which estimates the inlet flow temperature T_f, is a rather simplified model of reality. It is clear from (A.8) that, since $1/T_f$ multiplies the entire expression, errors in $\dot{M}$ are strongly affected by errors in T_f. The principle error in T_f is probably the assumption that $T_f = T_0$ for flow into the cylinder. For ineffective heat exchanger samples and low flow amplitudes this will not be the case. To cover the worst possible situation, we estimate the error in T_f as equal to the amplitude of the cylinder gas temperature T(t). Since temperature amplitudes are usually small, this is not as extreme as it first sounds.

Variation in Mass Flow Rate Along the Sample Duct

In certain circumstances mass flow rate may vary significantly within the sample duct. Certainly, this is likely if the sample length is more than a small fraction of the sonic wavelength. Even without sonic phenomena this can happen for high-pressure-drop samples at low flow displacement amplitudes. An error bound for mass flow rate variation can be calculated without actually solving for mass flux as a function of position.

The gas continuity equation in the sample duct can be written

$$\frac{\partial g}{\partial x} = -\frac{\partial \rho}{\partial t} \tag{A.35}$$

where ρ is density and g is mass flow rate per unit area. Using the equation of state in the form $\rho = P/(RT)$, (A.35) can be written

$$\frac{\partial g}{\partial x} = -1/R\frac{\partial}{\partial t}(P/T) \tag{A.36}$$

We can make use of equation (A.36), provided that we can make some reasonable estimates of P and T in the sample.

P is easy. If the sample duct is not too long — say $L < \nu/4$ where ν is the sonic wavelength (sonic velocity / frequency) — then P must vary pretty close to linearly between the measured $P(t)$ at the cylinder end and the constant P_0 at the pressure-vessel end.

T is a bit trickier. It is a safe bet that the gas in the sample lies somewhere between isothermal and adiabatic and for either extreme (A.36) can be simplified. For the isothermal case $T = T_0$ and (A.36) becomes

$$\frac{\partial g}{\partial x} = -1/(RT_0)\frac{\partial P}{\partial t} \tag{A.37}$$

For the adiabatic case, recall that P and T are related by

$$\frac{P^{\frac{\gamma-1}{\gamma}}}{T} = \frac{P_0^{\frac{\gamma-1}{\gamma}}}{T_0} \tag{A.38}$$

where γ is the ratio of specific heats. Using (A.38) to eliminate T from (A.36) and simplifying gives

$$\frac{\partial g}{\partial x} = -1/(\gamma R T_0) \left(\frac{P_0}{P}\right)^{\frac{\gamma-1}{\gamma}} \frac{\partial P}{\partial t} \tag{A.39}$$

On the time-average, $(P_0/P) \approx 1$, so that for the purposes of error estimates it is adequate to simplify this to

$$\frac{\partial g}{\partial x} \approx -1/(\gamma R T_0) \frac{\partial P}{\partial t} \tag{A.40}$$

The true $\frac{\partial g}{\partial x}$ lies somewhere between the values computed by (A.37) and (A.40).

The assumption that at any given instant pressure varies linearly along the sample duct implies that $\frac{\partial P}{\partial t}$ also varies linearly along the sample and by (A.37) and (A.40) that $\frac{\partial g}{\partial x}$ does likewise. Therefore, a representative value for $\frac{\partial g}{\partial x}$ over the entire sample is $1/2\frac{\partial g}{\partial x}$ evaluated at the sample inlet. If the isothermal case (worst) is assumed, then an estimate of the total variation of g across the sample is

$$\Delta g = -L/(2 R T_0) \frac{\partial P}{\partial t} \tag{A.41}$$

where L is the sample duct length and P is the pressure at the inlet. Again, (A.41) only applies to sample ducts where $L < \nu/4$, ν being the sonic wavelength at the test frequency.

Seal Leakage Error

The leakage across the moving piston seal is another source of error — generally small. The leakage is estimated from a standard formula applying to laminar-flow clearance seals. The details are reported in section A.5.

A.4.3 Errors in F and K_t

More errors arise when equations (A.17) or (A.19) are used to extract core friction F and possibly entrance/exit loss term $1/2\, g|u|K_t$ as outlined in section A.3.3. The details depend somewhat on which equation is used, and are presented in section A.5. Generally, error analysis proceeds by application of the product and sum error combination formulae above. Two key errors are $\tilde{g}$, the error in g, and $\tilde{u}$, the error in u. $\tilde{g}$ is estimated as above. The error $\tilde{u}$ is estimated by applying the rule for the product of errors to the expression

$$u = g/\rho \tag{A.42}$$

which results in

$$\tilde{u} = \mathrm{RSS}(\tilde{g}/\rho, \tilde{\rho} u/\rho) \tag{A.43}$$

A somewhat anomalous term in equation (A.17) is $\frac{\partial g}{\partial t}$. How does one estimate its error? One way is to first introduce the additional assumption that g is nearly sinusoidal. More precisely, assume g is given by a Fourier expansion where the the first harmonic is dominant

$$g \approx A\sin(\omega t) + B\cos(\omega t) \tag{A.44}$$

Also assume that A and B are random variables and the error g is due mainly to errors in A and B. Differentiating (A.44) with respect to time gives

$$\frac{\partial g}{\partial t} = \omega A\cos(\omega t) - \omega B\sin(\omega t) \tag{A.45}$$

Then it makes sense to estimate the time-averaged error of $\frac{\partial g}{\partial t}$ as the time-average error of g multiplied by ω. It then follows that a reasonable bound for $\tilde{\frac{\partial g}{\partial t}}$ is

$$\widetilde{\frac{\partial g}{\partial t}} = \omega\tilde{g} \tag{A.46}$$

In the event one uses (A.19) to back out both F and K_t from a sequence of experiments, we have access to additional information: the scatter in the actual data for P as a function of length. The linear regression theory used to evaluate the slope and y-intercept coefficients C and D, can also estimate their errors directly from the data. These errors are also included in the error analysis as described in section A.5

A.4.4 Errors in f_r and f_i

The higher harmonics, as well as the previously mentioned errors in F, all contribute to the error in the linearized friction factors f_r and f_i. The *higher harmonics* in F refer to the part of F not accounted for by application of (A.2) — the so-called residual of F. This residual of F is itself represented as a Fourier series whose RMS norm divided by the RMS norm of the original F is taken as a relative error component of f_r and f_i. RMS norm is, of course, in the sense of equation (A.34) which is particularly easy to evaluate for Fourier-series representations.

A.4.5 Errors in CDF and TDF

CDF and TDF are defined in terms of integrals over a cycle so their error analysis is a bit different than anything yet.

Here is how to estimate the error in CDF. Equation (A.25), which defines CDF, can be made more manageable by using the intermediate value theorem of calculus which tells us that

$$\int_a^b Fu = (Fu)^*(b-a) \tag{A.47}$$

where $(Fu)^*$ is a representative value of Fu in the interval $[a,b]$. Likewise

$$\int_a^b f\frac{g|u|}{2d}u = (f\frac{g|u|}{2d}u)^*(b-a) \tag{A.48}$$

Plugging these results into (A.25) gives

$$\mathsf{CDF} = 2d\frac{(Fu)^*}{(fg|u|u)^*} \tag{A.49}$$

Now assuming the representative values for $(Fu)^*$ and $(fg|u|u)^*$ occur at about the same time, we may cancel u leaving

$$\mathsf{CDF} \approx 2d\left(\frac{F}{fg|u|}\right)^* \tag{A.50}$$

Assuming f and d in (A.50) are exact, and that the errors in F, g and u are independent (which they aren't), the rule for combining products of relative errors gives

$$\text{Relative error in } \mathsf{CDF} = \text{RSS}\left(\tilde{F}/\overline{F}, \tilde{g}/\overline{g}, \tilde{u}/\overline{u},\right) \tag{A.51}$$

The *barred* quantities in (A.51) are assumed to be the Fourier series norms (RMS values) calculated by the data reduction program.

The error in TDF, defined by equation (A.27), proceeds along similar lines. The first step is to eliminate the integrals in (A.27) using the intermediate value theorem and cancel the u's leaving.

$$\mathsf{TDF} \approx \left(\frac{\Delta P}{(f\frac{l}{d}+K)\frac{g|u|}{2}}\right)^* \tag{A.52}$$

where the * superscript indicates a representative value (at some unspecified time) for the quantity in parenthesis. Assuming the products and factors on the RHS are all statistically independent (which they aren't) and applying the error product rule

$$\text{Relative error in } \mathsf{TDF} = \text{RSS}\left(\tilde{\Delta P}/\overline{\Delta P}, \tilde{F}/\overline{F}, \tilde{g}/\overline{g}, \tilde{u}/\overline{u},\right) \tag{A.53}$$

where $F = f\frac{l}{d} + K$. The *barred* quantities are assumed to be the Fourier series norms (RMS values) calculated by the data reduction program.

If we assume we know f and K exactly then we can eliminate $\tilde{F}/\overline{F}$ from the RSS. Actually, it is only fair to assume we know $f(Re)$ exactly, which means that f will be in error at any given time because g is in error. However, f is not a strong function of g so that any error introduced thereby will be of the order $\tilde{g}/\overline{g}$, which is already accounted for in the formula. So, it follows that we might as well go ahead and eliminate $\tilde{F}/\overline{F}$ from the error expression. The final formula is

$$\text{Relative error in } \mathsf{TDF} = \text{RSS}\left(\tilde{\Delta P}/\overline{\Delta P}, \tilde{g}/\overline{g}, \tilde{u}/\overline{u},\right) \tag{A.54}$$

A.5 Data Reduction Software

This section documents the key procedures of the actual data reduction software. All software is written in the Microsoft dialect of Pascal using separately compiled units. Using units allows the code to be broken down into logical and self-contained parts for easy maintenance and comprehension.

We use standard ASCII text files for data storage, with fixed-length records and variables delimited by commas. Although not the most efficient format, ASCII format can be universally read and understood.

Most program files begin with the prefixes TR or X — TR stands for *Test Rig*, X stands for nothing in particular. The TR-series pertain to data reduction where the entrance loss coefficient is specified as input. Historically, the TR-series came first. The X-series pertains to data reduction where the entrance coefficient is solved from the information contained in several data points. The X-series of software was supposed to supersede the TR-series but it didn't quite work out that way. Both versions of the data reduction program remain in active use. The TR-series is easier to work with since it requires only a single data point, but users must be careful to keep in mind that the results can vary depending upon the value of the entrance loss coefficient specified as input. The X-series is more mathematically rigorous but it requires data input from several experiments to run.

This documentation focuses on the historical development of that part of the software which actually implements the data-reduction algorithm. First comes a careful documentation of the TR series software. Next comes a somewhat less-careful documentation of the X series software, covering mainly the changes made in the TR series necessary to get there. The parts of the software dealing with input, output and graphics are touched upon only briefly.

A.5.1 The TR-Series

Here is a summary of all the programs and units comprising the TR-series.

TRY_IT The controlling program.

TRGLOBAL A unit with global variable declarations and some public procedures.

TRREDUCE A unit containing the procedures which actually perform the data-reduction algorithm.

TRFFAC A unit containing steady-flow friction factor correlations for comparison purposes.

TRGETFIL A unit for reading input data which varies from run to run.

TRASCII A unit for reading input data which is more-or-less fixed.

TRCAL A unit for adjusting and filtering raw input data for use by TRREDUCE.

TRPLOT A unit which takes care of graphical and tabular output.

Although obscured by a lot of overhead, unit TRREDUCE is really the heart of the overall program. The following material documents TRREDUCE in considerable detail, closely paralleling the construction of the actual Pascal code. (A sans-serif typeface indicates actual Pascal names.) export_reduce is the name of the highest level procedure in the unit, itself a short block of code which calls a number of lower-level procedures. Each lower-level procedure may call still lower lower-level procedures until at last everything is done. In this report, as well as the actual program, distinct blocks of code are headed by a name preceded by the word procedure or function (e.g. procedure solve_M). The underscore character _ is used to separate individual words in long procedure names which are chosen to indicate their purpose. A description of the code block in English follows each heading with branches to other code blocks indicated by remarks such as: call procedure solve_M, etc. After flipping back and forth between procedures you can get a pretty good understanding of what's going on.

Procedure export_reduce

At this level, the data reduction process is viewed in its broadest outline form.

1. Call procedure initialize which does variable initializations.

2. If the working fluid is compressible then call procedure solve_M which solves the differential equation for dimensionless cylinder gas mass as a function of time $M(\tau)$.

3. Call procedure FC_calc to calculate M_series the Fourier series representation of $M(\tau)$. procedure FC_M actually calculates $M(\tau)$ and is passed as an argument to FC_calc.

4. Call procedures FC_differentiate and FC_scale to differentiate and scale M_series in order to obtain g_series the Fourier series representation of sample duct mass flow rate per unit area.

5. If the working fluid is compressible then call procedure FC_calc to calculate T_series the Fourier series representation of dimensionless fluid temperature $T(\tau)$. Procedure FC_T actually calculates $T(\tau)$ and is passed as an argument to FC_calc.

6. Calculate u_series the Fourier series representation of fluid velocity; the cases for compressible and incompressible fluids are different.

Compressible Case call procedure FC_calc to calculate u_series. Procedure FC_u actually calculates $u(\tau)$ from instantaneous mass flow rate and density and is passed as an argument to FC_calc.

Incompressible Case call procedures FC_copy and FC_scale to copy and scale g_series to u_series; this is possible since density is constant.

7. Call procedure FC_calc to calculate F_series the Fourier series representation of F, the force per unit volume due to fluid shear stress at the sample duct wall. Procedure FC_F actually calculates F and is passed as an argument to FC_calc.

8. Call procedure calc_g_err to calculate variable g_err, the representative error in g_series.

9. Call procedure calc_u_err to calculate variable, u_err the representative error in u_series.

10. Call procedure calc_F_err to calculate variable, F_err the representative error in F_series. F_err depends on g_err and u_err.

11. Call procedure calc_ffac to calculate linearized friction factors ffac_r and ffac_i.

12. Call procedure calc_F to calculate the Fourier series F_residual_series which is F_series after terms accounted for by ffac_r and ffac_i have been subtracted. Procedure FC_F_residual actually calculates the residual and is passed as an argument to calc_F. For sinusoidal mass flow rate, F_residual_series contains the higher harmonics of F_series — those ignored by the linearized friction factors ffac_r and ffac_i.

13. Call procedure calc_ffac_err to calculate variable ffac_rel_err the overall relative error produced by the linearized friction factor representation for F. Ffac_rel_err includes the effects of F_err as well as the terms in F_residual_series.

14. Call procedure FC_calc to calculate F_stdy_pred_series the Fourier series representation of frictional pressure gradient F_s as predicted by a steady-flow correlation. Procedure FC_Fstdy actually calculates F_s and is passed as an argument to FC_calc.

15. Call procedure calc_Cosc to calculate the core dissipation factor CDF, known in the program by the name C_osc.

16. Call procedure calc_Cosc_err to calculate C_osc_rel_err the relative error in C_osc.

17. Call procedure FC_calc to calculate DP_stdy_pred_series the Fourier series representation of total pressure drop ΔP_s as predicted by a steady-flow correlation. Procedure FC_DPstdy actually calculates ΔP_s and is passed as an argument to FC_calc.

18. Call procedure calc_dissipation_fac to calculate the total dissipation factor (TDF), known in the program by the name dissipation_fac.

19. Call procedure calc_dissipation_fac_err to calculate dissipation_fac_rel_err the relative error in dissipation_fac.

20. Call procedure calc_dimless_groups to calculate the variable Re_max, Re_omega, tidal_ampl_ratio and peak_Mach_number which will be useful in correlating data from several experiments.

21. Call function calc_PV_power to return the value of the variable PV_power the PV power dissipated in the piston cylinder.

Procedure initialize

This procedure gets things started as follows:

1. Calculate the properties of the working fluid. For gases, values for Cp and Cv are taken from tables at 300K, viscosity is calculated from the Sutherland formula applied at the average sample duct wall temperature; for water, density is taken from tables at 300K and is 1% accurate over a range of 273K to 328K (32F to 130F) and viscosity is calculated from three-point quadratic interpolation and is 0.5% accurate in the range 289K to 311K (60 to 100F).

2. Calculate some simple geometrical dependent variables and various normalization variables P0 (mean pressure), V0 (mean cylinder volume), T0 (mean sample wall temperature) and M0 (mean cylinder fluid mass).

3. Calculate the dimensionless heat transfer coefficient Nq and dimensionless wall temperature Ts to be used in solving the $M(\tau)$ differential equation for compressible fluids.

4. Allocate and define sine and cosine arrays CSN↑[i] and SN↑[i] for the discrete time points $\tau_i = 2\pi i/(\text{Imax} + 1)$; Imax+1 is the number of discrete sample points over one cycle period. Imax is a constant declared in TR-GLOBAL. CSN and SN are pointers to dynamically allocated arrays — hence CSN↑ and SN↑ are the actual arrays. In this way the bounds of the array need not be known ahead of time.

5. Allocate and initialize records G↑[i] which contain the variables M (dimensionless cylinder mass), P (dimensionless pressure), V (dimensionless

volume), Ptau ($\frac{\partial P}{\partial \tau}$) and Vtau ($\frac{\partial V}{\partial \tau}$) at the time τ_i. G is a pointer to a dynamically allocated array of records of type node defined in TRGLOBAL. G↑[i].M is the value $M(\tau_i)$ and so forth. P and V are initialized using function FC_eval which evaluates the input Fourier series for pressure and piston position at τ_i. Ptau and Vtau are initialized using function FC_deriv_eval which evaluates the tau derivatives of pressure and piston position. M is initialized based on P, V and Ts for a compressible fluid and just V for an incompressible fluid. P, V, Ptau and Vtau remain constant during program execution; for compressible fluids M is solved in procedure solve_M.

Procedure solve_M

Solves the differential equation for dimensionless cylinder mass $M(\tau)$ using the Adams-Bashforth-Moulton fourth-order linear multi-step predictor-corrector method [13]. FOR i:= 0 to Imax, solve_M solves $M(\tau_i)$ based on values for M and $dM/d\tau$ for the current and previous four indices. $dM/d\tau$ is provided by function Mderiv. Time stepping continues until the $M(\tau_i)$ values for two successive cycles are the same to within tolerance. The solution is stored in the M field of the array of records G↑ initialized in procedure initialize. Details of the Adams-Bashforth-Moulton implementation are contained in procedures ABM_step and ABM_shift of TRREDUCE.

Function Mderiv

Returns the dimensionless cylinder mass derivative $dM/d\tau$ as a function of i and M. Calculation of $dM/d\tau$ is based on the cylinder gas energy equation in the form of A.8. In dimensionless form that equation becomes

$$M_\tau = \frac{PV}{RT_f}\left[\frac{V_\tau}{V} + C_v/C_p\frac{P_\tau}{P} + N_q(T - T_s)\right] \qquad (A.55)$$

where

τ	=	ωt (angular frequency x time)
P	=	pressure / P0
V	=	cylinder volume / V0
T	=	gas temperature / T0
T_s	=	cylinder wall temperature / T0
T_f	=	T if $M_\tau < 0$ else
	=	sample duct wall temperature / T0 = 1
M	=	gas mass / M0
Cv, Cp	=	gas specific heats
N_q	=	hfilm x S0 /($C_p\omega$M0)
hfilm	=	mean cylinder heat transfer coefficient
S0	=	mean cylinder wetted surface

τ subscripts indicate τ-derivatives. The node record G↑[i] is accessed which contains values for P (dimensionless pressure), V (dimensionless volume), $dP/d\tau$ and $dV/d\tau$ at τ_i. N_q and T_s are fixed variables calculated in procedure initialize. T is calculated from the dimensionless equation of state

$$T = PV/M \tag{A.56}$$

Procedure FC_calc

Calculate the Fourier series representation for periodic functions tabulated at the discrete points $\tau_i = 2\pi i/(\text{Imax} + 1)$. FC_calc has the dummy procedure F(i,val) in its argument list. An actual procedure replaces F when FC_calc is called. Procedure F returns val as a function of i — that is returns val(τ_i). FC_calc uses trapezoid-rule numerical integration of val(τ_i) $\cos(n\tau_i)$ and val(τ_i) $\sin(n\tau_i)$ where n is the order of the harmonic. $\cos(n\tau_i)$ and $\sin(n\tau_i)$ are equal to CSN↑[(n*i) MOD (Imax+1)] and SN↑[(n*i) MOD (Imax+1)], respectively, where CSN↑ and SN↑ are the sine and cosine arrays defined in procedure initialize. FC_calc calculates Fourier coefficients up to order Hmax which is a constant declared in TRGLOBAL. If val(τ_i) contains no harmonics greater than Hmax, then the calculated Fourier series representation will be exact. The series is returned in dummy variable S which represents an actual Fourier series in the calling routine.

Function FC_eval

Evaluates the Fourier series S at time τ_i; S and i are arguments. FC_eval = A[0]/2 + summation from 1 to Hmax of [A[n] $\cos(n\tau_i)$ + B[n] $\sin(n\tau_i)$]. $cos(n\tau_i)$ and $\sin(n\tau_i)$ are computed from CSN↑ and SN↑ as in procedure FC_calc.

Function FC_deriv_eval

Similar to FC_eval except evaluates the τ-derivative of Fourier series S at time τ_i. Uses the fact that $d(\cos(n\tau))/d\tau = n\sin(n\tau)$ and $d(sin(n\tau))/d\tau = -n\cos(n\tau)$.

Procedure FC_differentiate

Differentiates term-wise the Fourier series S to produce the Fourier series dS; S and dS are arguments.

Function FC_dot

Returns the dot product of Fourier series arguments S1 and S2 defined by

$$\text{S1} \cdot \text{S2} = 1/2\pi \int_0^{2\pi} S_1 S_2 d\tau \tag{A.57}$$

where S_1 and S_2 denote the actual time-functions corresponding to series S1 and S2.

Function FC_norm

Returns the Euclidean norm of Fourier series argument S — that is: $\sqrt{S \cdot S}$.

Procedure FC_scale

Multiplies Fourier series S by a scalar factor fac; S and fac are arguments.

Procedure FC_copy

Copies Fourier series S1 to Fourier series S2; S1 and S2 are arguments.

Procedure FC_M

Returns val $= M(\tau_i)$, the dimensionless gas mass; val and i are arguments. Accesses the node record G↑[i] and sets val:= G↑[i].M.

Procedure FC_T

Returns val $= T(\tau_i)$, the dimensionless gas temperature; val and i are arguments. Accesses the node record G↑[i] and sets val:= P*V/M.

Procedure FC_u

Returns val $= u(\tau_i)$, the representative (dimensional) fluid velocity; val and i are arguments.

1. Accesses the node record G↑[i] and calculates density $\rho(\tau_i) = (M0/V0) * (M/V)$.
2. Calculate mass flow rate per unit area $g(\tau_i)$ using function FC_eval passing g_series as an argument.
3. Sets val:= $g(\tau_i)/\rho(\tau_i)$.

Procedure FC_F

Returns val $= F(\tau_i)$, the representative (dimensional) force per unit volume due to fluid shear stress at wall at τ_i; val and i are arguments. Based on equation A.17.

1. The first term in (A.17) is calculated by referencing the node record G↑[i] and using the P field therein.

2. g and u required for the second and third terms in (A.17) are obtained using function FC_eval with the Fourier series g_series and u_series (calculated earlier) passed as arguments.

3. $\frac{\partial g}{\partial t}$ required for the fourth term in (A.17) is obtained by using function FC_deriv_eval with the Fourier series g_series passed as an argument. The result $\frac{\partial g}{\partial \tau}$ is multiplied by the angular frequency ω to obtain $\frac{\partial g}{\partial t}$.

Procedure FC_Fstdy

Returns val $= F_s$ the frictional pressure gradient predicted by steady-flow correlation function F_Darcy. F_Darcy resides in unit TRFFAC. The instantaneous velocity u, which is passed as an argument, is evaluated from Fourier series u_series.

Procedure FC_DPstdy

Returns val $= \Delta P_s$ the total pressure drop predicted by steady-flow correlation function F_Darcy augmented by entrance loss coefficient total_entrance_loss. Similar to FC_Fstdy in its use of function F_Darcy.

procedure FC_F_residual

Returns val = the residual in F after subtracting terms accounted for by the linearized friction factors ffac_r and ffac_i; val and i are arguments.

$$\mathsf{val} = F + f_i \frac{u_m}{2d}\frac{\partial g}{\partial \tau} + f_r \frac{u_m}{2d} g \tag{A.58}$$

where f_i is ffac_i, f_r is ffac_r, u_m is fluid velocity amplitude and d is sample duct hydraulic diameter.

1. F required for the first term in (A.58) is obtained using function FC_eval with Fourier series F_series passed as an argument.

2. $\frac{\partial g}{\partial \tau}$ and g required for the remaining terms in (A.58) are obtained using functions FC_deriv_eval and FC_eval with Fourier series g_series passed as an argument.

Procedure calc_g_err

Returns g_err, the sample-wide error in g from all error sources. For an incompressible fluid, g_err is simply proportional to the transducer position error which is an input variable. For a compressible fluid g_err is much more complicated and, following along the lines established in section A.4, g_err depends on the errors from three sources: error in the $M(\tau)$ solution, variations of g across the sample and piston seal leakage.

1. First calc_g_err evaluates the variable Mt_solution_err which is the cycle-average error from all sources in the solution of the cylinder-fluid-mass differential equation. This results in an error in g (variable g_err_solution) of Mt_solution_err / flow_area.

   Mt_solution_err is obtained by first rewriting equation (A.8) in the following form

$$\dot{M} = \frac{P}{RT_f}\dot{V} + \frac{V}{\gamma RT_f}\dot{P} + \frac{hA}{C_pT_f}(T - T_0) \tag{A.59}$$

   the error in each term is further broken down using the product rule for combining errors discussed in section A.4. The variables that are considered to have random errors are P, $\dot{P}$, V, $\dot{V}$, T_f and h. After application of the product rule Mt_solution_err breaks down into the RSS of eight separate terms denoted by E1 through E8 in the actual program listing. Terms E1 through E8 require RMS mean values for quantities P, V, T and $\dot{P}$, $\dot{V}$ and $(T - T\_0)$. P0, V0 and T0 are used for the first three quantities. The second three quantities are more difficult since they oscillating about a zero (or very small) mean. The idea is first to represent them as Fourier series and then to calculate their RMS values using function FC_norm.

2. The variation in g along the sample duct length (variable g_variation) is estimated based on equation (A.41) The error is proportional to pressure derivative $\frac{\partial P}{\partial t}$. Again, rather than explicitly time-averaging the error over the cycle a RMS value for $\frac{\partial P}{\partial t}$ is used, obtained from the Fourier series representation of $\frac{\partial P}{\partial t}$ and function FC_norm.

3. The error in g due to seal leakage (variable g_err_seal) is estimated from the following approximate equation for leakage through annular clearance gaps.

$$\text{leak mass flow rate} \approx \frac{\pi DG^3}{12\mu RTL} P \Delta P \tag{A.60}$$

   where

D	=	Piston diameter
G	=	Clearance gap
L	=	Seal length
P	=	Gas pressure
R	=	Gas constant
T	=	Gas temperature
μ	=	Viscosity

   A representative value for ΔP (pressure difference across seal) is evaluated using FC_norm on the pressure Fourier series minus its mean-term coefficient.

4. The final g_err is the RSS of g_err_solution, g_variation and g_err_seal.

Procedure calc_u_err

Returns u_err, the sample-wide error in fluid velocity from all error sources. For an incompressible fluid u_err = g_err / density where g_err is the error in mass flow rate per unit area computed in calc_g_err. For a compressible fluid u_err is based on equation (A.43).

Procedure calc_F_err

Returns F_err, the representative error from all sources in F. Calc_F_err uses the product rule for errors applied to the various terms of equation (A.17). The methodology is analogous to that for procedure calc_g_err. F_err ultimately depends on the representative errors g_err and u_err calculated earlier, as well as the pressure-signal error and the estimated entrance-loss-coefficient error which are input variables.

Procedure calc_ffac

Returns the linearized friction factors ffac_r and ffac_i based on equation (A.24).

Procedure calc_ffac_err

Returns ffac_rel_err, the relative error in the linearized friction factor representation for F. Ffac_rel_err includes the effects of errors in F_series (F_err) as well as higher harmonics (F_residual_series) not represented by the linearized friction factors.

1. Calculate variable F_residual_norm using function FC_norm applied to Fourier series F_residual_series.

2. Calculate the relative friction factor error from

$$\text{ffac\_rel\_err} = \frac{1}{||F||}\,\mathrm{RSS}(\text{ F\_residual\_norm, F\_err }) \tag{A.61}$$

   where $||F||$ is the norm of Fourier series F_series obtained using function FC_norm and F_err was previously calculated in procedure calc_F_err.

Procedure calc_Cosc

Returns C_osc, the core dissipation factor (CDF) defined by equation (A.25). The factors $fg|u|/(2d)$ in (A.25) are just F_s which is embodied in series F_stdy_pred_series. Integrals of Fu and $F_s u$ are performed as simple algebraic operations by function FC_dot.

Procedure calc_Cosc_err

Returns C_osc_rel_err the relative error in C_osc using equation (A.51). Uses previously calculated component errors F_err, g_err and u_err; and uses function FC_norm to evaluate the norms of the various Fourier series.

Procedure calc_dissipation_fac

Returns dissipation_fac the total dissipation factor (TDF) defined by equation (A.27). The factor $(fl/d+K)g|u|/2$ in (A.27) is just ΔP_s which is embodied in series DP_stdy_pred_series. Integrals of $\Delta P\, u$ and $\Delta P_s\, u$ are performed as simple algebraic operations by function FC_dot.

Procedure calc_dissipation_fac_err

Returns dissipation_fac_rel_err the relative error in dissipation_fac using equation (A.54). Actual pressure drop series DP_series is obtained by subtracting the mean coefficient from input series pressure. Uses input error pressure_fast_err and previously calculated component errors g_err and u_err. Function FC_norm evaluates the norms of the various Fourier series.

Procedure calc_dimless_groups

Returns u_amp, Re_max, Re_omega, tidal_ampl_ratio and peak_Mach_no; the velocity amplitude, peak Reynolds number, dimensionless frequency, tidal amplitude ratio δ/L and Mach number. δ is the tidal amplitude (1/2 of total flow excursion) and L is the sample duct length. u_amp, Re_max and Re_omega are the same as u_m, Re_{max} and Re_ω.

A.5.2 The X-Series

The X-series data reduction software follows the theory presented in section A.3.3. That section showed how the fluid momentum equation could be put into the form of equation (A.19) which was linear in sample duct length and involved two unknown coefficients $C(t)$ and $D(t)$ — themselves expressed in terms of frictional pressure gradient F and entrance coefficient K_t — which were to be solved from the data.

The details of solving C and D from (A.19) are based on linear regression applied term-wise to the Fourier series representation of P. Assume that P, C and D are written as Fourier series

$$P = P_0 + P_{A1}\cos\tau + P_{B1}\sin\tau + P_{A2}\cos 2\tau + P_{B2}\sin 2\tau \ldots \quad (A.62)$$

$$C = C_0 + C_{A1}\cos\tau + C_{B1}\sin\tau + C_{A2}\cos 2\tau + C_{B2}\sin 2\tau \ldots \quad (A.63)$$

$$D = D_0 + D_{A1}\cos\tau + D_{B1}\sin\tau + D_{A2}\cos 2\tau + D_{B2}\sin 2\tau \ldots \quad (A.64)$$

where $\tau = \omega t$. Then (A.19) must hold termwise giving

$$P_0 = C_0 L + D_0 \tag{A.65}$$

$$P_{An} = C_{An} L + D_{An};\; n = 1 \ldots N \tag{A.66}$$

$$P_{Bn} = C_{Bn} L + D_{Bn};\; n = 1 \ldots N \tag{A.67}$$

Now, given a sequence of experiments with varying L, linear regression can be used to solve for the C and D coefficients in each of the above equations.

Linear Regression in the Abstract

Some standard results on linear regression theory — see Draper & Smith [12] — are quoted here. The faithful may skip over this section.

Let (X_i, Y_i) be a set of observation pairs for $i = 1 \ldots n$. Assume the Y_i are *the random variables (corresponding to pressure in our case) and the* X_i are exact (corresponding to length). Then the least-squares best fit line to the plotted data is

$$Y = b_0 + b_1 X \tag{A.68}$$

where

$$b_1 = \frac{\sum X_i Y_i - \sum X_i \sum Y_i / n}{\sum X_i^2 - (\sum X_i)^2 / n} \tag{A.69}$$

$$b_0 = \overline{Y} - b_1 \overline{X} \tag{A.70}$$

Here, $\overline{Y}$ and $\overline{X}$ denote the average values for Y_i and X_i and all sums are from 1 to n.

When it comes time to calculating error in the reduced data, the following error estimates will be useful. The standard deviation of the Y_i from the mean is

$$\mathrm{sd}(Y_i - \overline{Y}) = \sqrt{\frac{\sum (Y_i - \overline{Y})^2}{n-1}} \tag{A.71}$$

And letting $\hat{Y}_i$ denote the value of the regression line at Y_i, the standard deviation of the Y_i from the regression line is

$$\mathrm{sd}(Y_i - \hat{Y}_i) = \sqrt{\frac{\sum (Y_i - \hat{Y}_i)^2}{n-2}} \tag{A.72}$$

The following results assume that the data points really do fall on a straight line except for a random error in each Y_i having standard deviation s. This assumption fits our theory — at least above critical length L_0. The standard deviation of the regression-line slope is then

$$\mathrm{sd}(b_1) = \frac{s}{\sqrt{\sum (X_i - \overline{X})^2}} \tag{A.73}$$

And the standard deviation of the regression-line y-intercept is

$$\mathrm{sd}(b_0) = s\sqrt{\frac{\sum X_i^2}{n\sum(X_i - \overline{X})^2}} \tag{A.74}$$

For practical applications, s is assumed to equal the standard deviation of the Y_i from the regression line given by (A.72).

Software Changes

The new data reduction process required several changes in the previous software. In order to document these changes, I've invented a new word — L-group — to refer to a group of experiments where everything (stroke, frequency, P_0 ...) is the same except sample duct length. The new data reduction procedure is based on L-groups instead of individual experiments. Within an L-group we hope that $g(t)$ is uniform from experiment to experiment.

Programs and Units Here is a list of all the programs and units in the X-series. The key units XGROUP and XREDUCE are described in more detail later on.

XGLOBAL A unit containing global variable declarations (in XGLOBAL.INT) and some general purpose routines (in XGLOBAL.PAS).

XGROUP A unit whose main purpose is to do the linear regression analysis on pressure vs length data for an L-group of experiments.

XREDUCE A unit derived from the former program TRREDUCE except data is now reduced an L-group at a time instead of for each data point. Essentially, XREDUCE backs out core friction and entrance pressure drop. To do its job, it requires the output variables of unit XGROUP.

XFFAC A unit containing steady flow friction-factor correlations for the various allowed sample types (currently: tubes, parallel plates, fins, and screens). Used by XREDUCE for generating steady-flow core friction comparisons.

XGRUCE The driver program for the data reduction process, whose name, of course, is a combination of XGROUP and XREDUCE. The user types XGRUCE at the console to start the data reduction process. Then XGRUCE does the following things

- Prompts for the ID numbers for an L-group of data points and reads the data.
- Calls XGROUP.
- Calls XREDUCE.

- Writes the reduced data to the end of the database file XREDUCE.PRN.
- Writes the reduced data a second time to the temporary file XPLOT.PRN

XVARIN A unit, used by XGRUCE, that reads input data from the experiment-level parameter and data files.

XPLOT The driver program for obtaining hard-copy data and various plots from the reduced data. The user types XPLOT at the console to start the program. Program XPLOT always reads from the temporary file XPLOT.PRN.

PICTURE A unit containing some procedures that help in creating graphic screen-images. Used by XPLOT and XGROUP.

GRAPHICS An assembly language module containing primitive graphics-screen oriented routines. For example, the elemental routine that draws a straight line between two points is located here.

Disk Files Here is a summary of the files read and written by the various programs in the X-series scheme of things. Except, the files containing the experiment-level parameters and data are not included here.

XREDUCE.PRN A cumulative data-base file in ASCII format containing the ultimate reduced data. Each record corresponds to an L-group of data points in TRDATA.PRN. Procedure reduced_data_IO in XGLOBAL.PAS is used to read and write to/from this file. A close look at this procedure will tell you exactly what is written and where.

XPLOT.PRN A temporary file usually containing the most recently reduced record of XREDUCE.PRN, but in general, may contain any number of records selected from XREDUCE.PRN with a text editor. Program XPLOT reads all the records in XPLOT.PRN and for each one produces tabular and graphical representations of the reduced data.

XTRUNC.PRN This file doesn't exist yet but the idea is that it could contain truncated records from XREDUCE.PRN. For example, if we left off the Fourier Series variables in XREDUCE.PRN we would reduce storage requirements from about 1400 bytes per record to less than 400. This file would be easier to manipulate with a data-base program in the event we ever get around to serious correlation analysis. A simple driver program (not yet written) could convert XREDUCE.PRN to XTRUNC.PRN.

Unit XGROUP Unit XGROUP does the following to an L-group of data points:

1. Makes sure that the variables that are supposed to remain constant within an L-group actually are (within a small tolerance). Otherwise a warning is printed and execution stops. The variables checked are: hfilm, temp_cyl_wall, temp_samp_wall and omega. See procedure process_0 for details.
2. Averages all the length data to obtain length_mean, the mean length.
3. Performs a linear regression analysis of pressure-vs-length to obtain the Fourier series pressure_offset and pressure_slope.
4. Averages all the piston position data to obtain the Fourier series position_mean.
5. Calculate position_deviation the standard deviation from the mean of the position samples.
6. Calculates DP_offset_deviation the standard deviation of the pressure regression line y-intercepts (mean pressure coefficient not included).
7. Calculates DP_slope_deviation the standard deviation of the pressure regression line slopes (mean pressure coefficient not included).
8. Calculates DP_mean_deviation the standard deviation from the mean of pressure samples (mean-pressure coefficient not included).
9. Calculates P0_mean_deviation the standard deviation from the average of the mean-pressure coefficients for the samples.
10. Displays pressure-vs-length data for the first harmonic coefficients (pressure.A[1] pressure.B[1]) together with the corresponding regression lines.

The idea behind the pressure display is to let the user visually check the validity of the regression line. The individual errors between the first Fourier pressure coefficients (pressure.A[1] and pressure.B[1]) and the regression line are plotted as vertical line segments off the main regression lines. If the errors are random and small ... good. If there is a non-random deviation from the regression line at short lengths, then the conclusion is that at least some of the experiments had lengths below the critical value L_0. These experiments should be discarded from the input file and XGROUP rerun. Nonlinearity at long lengths means that compressibility effects are beginning to perturb g. In other words, $\dot{P}/P$ is no longer small compared to $\dot{V}/V$ in (A.8). These experiments should also be discarded. As long as there is a significant linear region somewhere in the middle we should be able to reduce data reliably. If not — we have trouble. Take heart though, we can always use an incompressible fluid like water in the rig.

Warning: The remainder of this section is intended only for serious devotees of data reduction and may be skipped by the casual reader.

The Fourier-series variables are calculated in procedure process_1. They are the basis for the core-friction and entrance pressure-drop Fourier series calculated in XREDUCE. The standard-deviation variables are calculated in procedure process_2 and are the basis for the error analysis performed by XREDUCE.

Here's how the standard deviation variables for Fourier series are calculated. In general, when a standard deviation applies to a Fourier series as a whole, the individual error terms in the series are squared and summed. For example, say E represents an error series defined by the difference of the two series position and position_mean. Then it is not too hard to show that if one defines $E \cdot E$ to be

$$E \cdot E \equiv E_0^2 + \frac{1}{2}\sum(E_{An}^2 + E_{Bn}^2) \tag{A.75}$$

Then $E \cdot E$ measures the average value of E^2 over one cycle. Therefore $\sqrt{E \cdot E}$ is a good overall measure of the difference between position and position_mean. Now let E_i represent the sequence of error series (position$_i$ - position_mean). Then according to (A.71) we can obtain position_deviation as

$$\mathrm{sd}(Ei) = \sqrt{\frac{\sum(Ei \cdot Ei)}{n-1}} \tag{A.76}$$

The same same formula works for obtaining DP_mean_deviation if we take E_i to represent (pressure$_i$ - pressure_mean) with the mean coefficient set to zero. Variables pressure_offset_deviation and pressure_slope_deviation are calculated from (A.74) and (A.73) where s is taken as the standard deviation from the regression line of the actual pressure data. If we take E_i to represent (pressure$_i$ - regression line) with the mean coefficient set to zero, then according to (A.72)

$$s = \sqrt{\frac{\sum(Ei \cdot Ei)}{n-2}} \tag{A.77}$$

So far, it has been assumed that there are at least three data points in an L-group. This is enough data to do statistical analysis without running into zero denominators in some of the preceding formulae. However, there may be situations where XGROUP is asked to work with L-groups containing only two members — or even one. These somewhat pathological cases are now discussed.

Case of One Data Point In this case, the series pressure_offset is assumed zero — equivalent to assuming zero entrance pressure drop. The series pressure_slope is calculated assuming P is linear with L with $P = P_0$ at $L = 0$. Also, since there is no way to measure random error from the data itself, the standard deviation errors are either set to zero or based on the input error terms position_error, pressure_fast_err and pressure_mean_err. That is: position_deviation = position_error, DP_slope_deviation = (pressure_fast_err / length) and P0_mean_deviation = pressure_mean_err.

Case of Two Data Points In this case, pressure_offset and pressure_slope are both solved but, since two points define a line exactly, there is still no way to evaluate DP_offset_deviation and DP_slope_deviation from the data. Instead, the variable s in (A.73) and (A.74) is replaced with the input error pressure_fast_err. However, position_deviation, DP_mean_deviation and P0_mean_deviation can be evaluated from from the data in the same way as for three or more data points.

Unit XREDUCE Unit XREDUCE is much like the previous program TRREDUCE except it works from a slightly different set of input data. The new program uses length_mean instead of individual sample duct length, position_mean instead of individual piston position series and pressure_offset and pressure_slope instead of individual pressure series. Also the error analysis is based on the error terms position_deviation, DP_offset_deviation, DP_slope_deviation, DP_mean_deviation and P0_mean_deviation instead of the original position_err, pressure_mean_err and pressure_fast_err.

As before, the first step is to solve the initial value problem (Ordinary differential equation with initial-value boundary condition) for the cylinder gas mass as a function of time $M(t)$. This time $M(t)$ is solved for the piston position given by the position_mean series and pressure equal to the series pressure_slope times length_mean plus pressure_offset. That is, $M(t)$ is solved for a mean representative sample of the L-group. Otherwise the method is identical to that used in TRREDUCE. The representative mass flux per unit area g in the sample is obtained directly from $M(t)$.

The error in g is calculated as in TRREDUCE except that some of the individual error terms have been revised. The representative error in volume $\tilde{V}$ is now the product of position_deviation and piston_area, the representative error in pressure $\tilde{P}$ is now the RSS (root sum squared) of P0_mean_deviation and DP_mean_deviation and the representative error in $\frac{\partial P}{\partial t}$ is now the product of omega and DP_mean_deviation. One important implication is that the range of pressure drops across the various samples of the L-group is accounted for in the total error for g.

XREDUCE calculates both the sample-mean frictional pressure gradient F and the entrance pressure drop term $\frac{1}{2}g|u|K_t$. Here $\frac{1}{2}g|u|K_t$ is looked upon as a single quantity. The calculation for F is much simpler than before. Basically, F is calculated from (A.20) by adding $\frac{\partial g}{\partial t}$ to pressure_slope. The calculation for $\frac{1}{2}g|u|K_t$ is new but again, fairly straightforward. Essentially, $\frac{1}{2}g|u|K_t$ is calculated from (A.21) by subtracting pressure_offset and $\frac{1}{2}gu\sigma^2$ from P_0. Actually there is a slight reformulation that avoids erroneous mean values in F and $\frac{1}{2}gu\sigma^2$. Equation (A.1) is re-written as

$$\Delta P = \left(F - \frac{\partial g}{\partial t}\right) L - \left(\frac{1}{2}gu\sigma^2 + \frac{1}{2}g|u|K_t\right) \qquad \text{(A.78)}$$

Now, assuming $\Delta P = P - P_0$ averages out to zero we can write (A.78) in the

form

$$\Delta P = C^*(t)L + D^*(t) \tag{A.79}$$

where C^* and D^* are the previous C and D functions (pressure_slope and pressure_offset) except the time-mean values (which are present largely due to noise) are zeroed. F and $\frac{1}{2}g|u|K_t$ may now be solved from the two equations

$$C^*(t) = F - \frac{\partial g}{\partial t} \tag{A.80}$$

$$D^*(t) = -\frac{1}{2}gu\sigma^2 - \frac{1}{2}g|u|K_t \tag{A.81}$$

The error analysis for solved variables F and $\frac{1}{2}g|u|K_t$ is as follows. The total error of F is calculated as the RSS of the component errors in pressure_slope and $\frac{\partial g}{\partial t}$. The error in $\frac{\partial g}{\partial t}$ is taken as omega times $\tilde{g}$, as before. The error in pressure_slope is just DP_slope_deviation from unit XGROUP. Similarly, the total error of $\frac{1}{2}g|u|K_t$ is calculated as the RSS of the component errors in $\frac{1}{2}gu\sigma^2$ and D^* . The error in $\frac{1}{2}gu\sigma^2$ is calculated from the sub-component errors $\tilde{g}$ and $\tilde{u}$ as before. The error in D^* is just DP_offset_error from unit XGROUP.

As before XREDUCE calculates a steady-flow friction factor multiplier C_osc which is the same thing as CDF defined by equation (A.25).

A brand new thing done by XREDUCE is to solve for an effective entrance coefficient K_entrance defined by equation (A.28).

A.5.3 Glossary of Variables

The public input/output variables read/written by the data reduction programs are listed here. Table A.1 presents the input variables and table A.2 the output variables. The variables from both programs are combined in the tables.

run_date: wrd_string;	Date of run in format: mm/dd/yy
run_time: wrd_string;	Time of run in 24 hr format: hh:mm
run_number: INTEGER;	Run ID number
pt_number: INTEGER;	Data point number within a run
fluid: fluid_type;	Type of fluid
position_err: REAL;	Resolution of position transducer (m)
pressure_mean_err: REAL;	Resolution of mean pressure transducer; (N/m^2)
pressure_fast_err: REAL;	Resolution of fast pressure transducer; (N/m^2)
entrance_loss_err: REAL;	Likely error in total_entrance_loss coefficient
hfilm_err: REAL;	Absolute error in hfilm; ($W/(m^2K)$)
hfilm_pct_err: REAL;	Relative error in hfilm, in percent, from Pfiles
piston_diam: REAL;	Piston diameter (m)
volume_mean: REAL;	Volume between piston face and sample duct inlet at zero piston position (m^3)
seal_gap: REAL;	Radial gap for piston seal (m)
seal_length: REAL;	Piston seal length (m)
hfilm: REAL;	Average cylinder film heat transfer coefficient; (W/(m2K))
cyl_mean_surface: REAL;	Average cylinder wetted surface; (m2)
sample: sample_type;	Type of sample duct
length: REAL;	Sample duct length (m)
flow_area: REAL;	Sample duct mean flow area (m2); void volume / length
hyd_diam: REAL;	Sample duct hydraulic diameter (m); 4 × void volume / wetted surface
porosity: REAL;	Void volume / canister volume; 1.0 for tubes, etc.
total_entrance_loss: REAL;	Sum of sample duct entrance and exit velocity-head loss coefficients.
temp_cyl_wall: REAL;	Cylinder wall temperature (K)
temp_samp_wall: REAL;	Sample duct wall temperature (K); normalization temp.
omega: REAL;	Angular frequency (rad/s)
pressure: Fourier_series;	Fast pressure signal; (N/m^2)
position: Fourier_series;	Fast piston position signal; (m); positive for increasing volume

Table A.1: Data reduction input variables with actual Pascal type declarations. See TRGLOBAL listing for exact definition of types wrd_string, fluid_type, sample_type and Fourier_series.

mean_density: REAL;	Mean fluid density
velocity_ampl: REAL;	Flow velocity first-harmonic amplitude
Re_max: REAL;	Peak Reynolds number Re_{max} based on velocity_ampl
Re_omega: REAL;	Kinetic Reynolds number Re_ω
tidal_ampl_ratio: REAL;	Tidal amplitude to length ratio
peak_Mach_no: REAL;	Mach number based on velocity_ampl
PV_power: REAL;	Power exerted by piston on gas in cylinder
g_series: Fourier_series;	Sample duct mass flow rate per unit area ($kg/(m^2s)$)
g_err: REAL;	RSS of all errors in g_series
F_series: REAL;	Frictional pressure gradient F (N/m3)
F_err: REAL;	RSS of all errors in F_series
ffac_r,ffac_i: REAL;	Linearized friction factors f_r and f_i
ffac_rel_err: REAL;	Relative RSS error in ffac_r and ffac_i
F_residual_series: Fourier_series	Residual of F_series after subtracting linearized friction factor terms
F_stdy_pred_series: Fourier_series;	Predicted F from steady-flow correlation
C_osc: REAL;	Correction factor for steady-flow friction factor required to produce correct dissipation
C_osc_rel_err: REAL;	Relative error in C_osc (CDF)
dissipation_fac: REAL;	Correction factor for steady-flow total pressure drop $(fl/d+K)$ required to produce correct pumping dissipation
dissipation_fac_rel_err: REAL;	Relative error in dissipation_fac (TDF)
DP_entrance_series: Fourier_series;	Sample duct entrance pressure drop (N/m^2)
head_series: Fourier_series;	Velocity head in sample duct; $g\|u\|/2$ (N/m^2)
DP_entrance_err: REAL;	RSS of all errors in DP_entrance_series
K_entrance: REAL;	Effective entrance+exit coefficient that gives the same pumping dissipation as measured entrance ΔP

Table A.2: Data reduction output variables not previously listed. See TR-GLOBAL listing for exact definition of types wrd_string, fluid_type, sample_type and Fourier_series.

Appendix B

Appendix B

The following should be noted with regard to the data contained in Appendix B:

1. The reader should see Tables 5.1-2, 5.1-3, 5.2-2 and 5.2-3 for further details on these tabulated data. These tables cross-reference the run numbers with specific test samples and tests.

2. In the steady flow test results, Re_power is defined as the numerical value of the exponent of the Reynolds number in the applicable friction factor correlation. For the oscillating flow test results:

X_p = piston amplitude, mm
ΔP = maximum pressure amplitude, Pa
pV = rate of work done on the working gas, watts

For the regenerator oscillating flow test results, "correlation used" refers to the steady flow friction factor correlation used to calculate TDF.

3. Errors listed in these tables are given as a percent of reading.

4. Representative data from these tables were plotted in the figures of Section 6. However, not all of the data in this Appendix was plotted.

Steady Flow Test Results

Run# 7 L/D = 152 Fluid : nitrogen Pressure : 18.26 bar

Tubes 360 mm long diameter = 2.375 mm Entrance loss = 1.8

Pressure drop error (Pa) 1720 Constant mass flow error (kg/s) 1.2E-4

Point#	Re	Mass flow (kg/s)	Pressure drop (Pa)	Re power	P ratio
2	29460	9.65E-4 ± 12 %	4513 ± 38 %	-0.250	0.72 ± 44 %
3	39730	1.30E-3 ± 9 %	8409 ± 20 %	-0.250	0.79 ± 26 %
4	52290	1.71E-3 ± 7 %	14290 ± 12 %	-0.250	0.81 ± 17 %
5	71180	2.33E-3 ± 5 %	26000 ± 7 %	-0.250	0.83 ± 11 %
6	89450	2.93E-3 ± 4 %	40080 ± 4 %	-0.250	0.84 ± 8 %
7	116600	3.82E-3 ± 3 %	65640 ± 3 %	-0.250	0.84 ± 6 %
8	137700	4.52E-3 ± 3 %	89530 ± 2 %	-0.250	0.86 ± 5 %
9	144700	4.75E-3 ± 3 %	98890 ± 2 %	-0.250	0.87 ± 5 %
10	97740	3.20E-3 ± 4 %	47360 ± 4 %	-0.250	0.85 ± 7 %
11	81470	2.67E-3 ± 4 %	33410 ± 5 %	-0.250	0.84 ± 9 %
12	58310	1.91E-3 ± 6 %	17790 ± 10 %	-0.250	0.82 ± 15 %
13	38740	1.27E-3 ± 9 %	7991 ± 22 %	-0.250	0.78 ± 27 %
14	30310	9.92E-4 ± 12 %	4024 ± 43 %	-0.250	0.62 ± 48 %
15	95480	3.13E-3 ± 4 %	45310 ± 4 %	-0.250	0.84 ± 8 %

Run# 9 L/D = 152 Fluid : air Pressure : 3.36 bar

Tubes 360 mm long diameter = 2.375 mm Entrance loss = 1.8

Pressure drop error (Pa) 1720 Constant mass flow error (kg/s) 1.5E-4

Point#	Re	Mass flow (kg/s)	Pressure drop (Pa)	Re power	P ratio
6	19960	6.48E-4 ± 23 %	14860 ± 12 %	-0.250	0.97 ± 42 %
7	25900	8.40E-4 ± 18 %	23920 ± 7 %	-0.250	0.98 ± 32 %
13	33000	1.07E-3 ± 14 %	35170 ± 5 %	-0.250	0.97 ± 25 %

Run# 10 L/D = 152 Fluid : air Pressure : 3.36 bar

Tubes 360 mm long diameter = 2.375 mm Entrance loss = 1.8

Pressure drop error (Pa) 1720 Constant mass flow error (kg/s) 1.5E-4

Point#	Re	Mass flow (kg/s)	Pressure drop (Pa)	Re power	P ratio
3	21710	7.04E-4 ± 21 %	16880 ± 10 %	-0.250	0.98 ± 39 %

Run# 11 L/D = 152 Fluid : air Pressure : 7.00 bar

Tubes 360 mm long diameter = 2.375 mm Entrance loss = 1.8

Pressure drop error (Pa) 1720 Constant mass flow error (kg/s) 1.6E-4

Point#	Re	Mass flow (kg/s)	Pressure drop (Pa)	Re power	P ratio
3	19980	6.48E-4 ± 25 %	7173 ± 24 %	-0.250	0.97 ± 49 %
4	26160	8.48E-4 ± 19 %	11290 ± 15 %	-0.250	0.93 ± 36 %
5	32330	1.05E-3 ± 15 %	17090 ± 10 %	-0.250	0.96 ± 29 %
6	40000	1.30E-3 ± 12 %	25010 ± 7 %	-0.250	0.95 ± 23 %
7	50400	1.63E-3 ± 10 %	38840 ± 4 %	-0.250	0.97 ± 18 %
8	62150	2.02E-3 ± 8 %	56000 ± 3 %	-0.250	0.97 ± 14 %
9	69700	2.26E-3 ± 7 %	69700 ± 2 %	-0.250	0.98 ± 13 %
11	64480	2.09E-3 ± 8 %	59700 ± 3 %	-0.250	0.98 ± 14 %
12	56210	1.82E-3 ± 9 %	46560 ± 4 %	-0.250	0.97 ± 16 %
13	43280	1.40E-3 ± 11 %	28590 ± 6 %	-0.250	0.96 ± 21 %

Run# 15 L/D = 48 Fluid : air Pressure : 7.00 bar

Tubes 115.1 mm long diameter = 2.375 mm Entrance loss = 1.8

Pressure drop error (Pa) 1720 Constant mass flow error (kg/s) 1.6E-4

Point#	Re	Mass flow (kg/s)	Pressure drop (Pa)	Re power	P ratio
5	27980	9.09E-4 ± 18 %	6703 ± 26 %	-0.250	0.94 ± 40 %
6	34430	1.12E-3 ± 14 %	10150 ± 17 %	-0.250	0.96 ± 30 %
7	41190	1.34E-3 ± 12 %	14240 ± 12 %	-0.250	0.96 ± 24 %
8	50800	1.65E-3 ± 10 %	21500 ± 8 %	-0.250	0.97 ± 19 %
9	60300	1.96E-3 ± 8 %	30060 ± 6 %	-0.250	0.99 ± 15 %
10	70720	2.30E-3 ± 7 %	40690 ± 4 %	-0.250	0.99 ± 13 %
11	82170	2.67E-3 ± 6 %	53990 ± 3 %	-0.250	0.99 ± 11 %
12	97470	3.17E-3 ± 5 %	75160 ± 2 %	-0.250	1.00 ± 9 %
14	92660	3.01E-3 ± 5 %	67790 ± 3 %	-0.250	0.99 ± 10 %
15	60990	1.98E-3 ± 8 %	30550 ± 6 %	-0.250	0.98 ± 15 %

Run# 16 L/D = 48 Fluid : air Pressure : 3.36 bar

Tubes 115.1 mm long diameter = 2.375 mm Entrance loss = 1.8

Pressure drop error (Pa) 1720 Constant mass flow error (kg/s) 1.5E-4

Point#	Re	Mass flow (kg/s)	Pressure drop (Pa)	Re power	P ratio
5	19690	6.40E-4 ± 23 %	7823 ± 22 %	-0.250	0.97 ± 47 %
6	22680	7.38E-4 ± 20 %	9951 ± 17 %	-0.250	0.95 ± 40 %
7	24490	7.97E-4 ± 19 %	11850 ± 15 %	-0.250	0.97 ± 36 %
8	26520	8.62E-4 ± 17 %	13760 ± 13 %	-0.250	0.98 ± 33 %
9	28440	9.24E-4 ± 16 %	15760 ± 11 %	-0.250	0.98 ± 30 %
10	31560	1.03E-3 ± 15 %	19430 ± 9 %	-0.250	0.99 ± 27 %
11	33640	1.09E-3 ± 14 %	21610 ± 8 %	-0.250	0.98 ± 25 %
12	36160	1.18E-3 ± 13 %	24410 ± 7 %	-0.250	0.99 ± 23 %
13	38900	1.27E-3 ± 12 %	28010 ± 6 %	-0.250	0.99 ± 22 %
14	41710	1.36E-3 ± 11 %	32000 ± 5 %	-0.250	0.99 ± 20 %
15	31910	1.04E-3 ± 14 %	19340 ± 9 %	-0.250	0.99 ± 27 %
16	22540	7.33E-4 ± 20 %	9972 ± 17 %	-0.250	0.97 ± 40 %

Run# 17 L/D = 48 Fluid : nitrogen Pressure : 18.26 bar

Tubes 115.1 mm long diameter = 2.375 mm Entrance loss = 1.8

Pressure drop error (Pa) 1720 Constant mass flow error (kg/s) 1.2E-4

Point#	Re	Mass flow (kg/s)	Pressure drop (Pa)	Re power	P ratio
2	45580	1.50E-3 ± 8 %	7384 ± 23 %	-0.250	0.95 ± 27 %
3	53790	1.76E-3 ± 7 %	9978 ± 17 %	-0.250	0.93 ± 21 %
4	62280	2.04E-3 ± 6 %	13430 ± 13 %	-0.250	0.95 ± 16 %
5	70070	2.30E-3 ± 5 %	16590 ± 10 %	-0.250	0.94 ± 14 %
6	80770	2.65E-3 ± 5 %	22070 ± 8 %	-0.250	0.95 ± 11 %
7	91490	3.00E-3 ± 4 %	27550 ± 6 %	-0.250	0.94 ± 9 %
8	107000	3.52E-3 ± 3 %	37290 ± 5 %	-0.250	0.94 ± 8 %
9	128800	4.23E-3 ± 3 %	52530 ± 3 %	-0.250	0.93 ± 6 %
10	146000	4.80E-3 ± 2 %	66770 ± 3 %	-0.250	0.92 ± 5 %
11	156300	5.14E-3 ± 2 %	76250 ± 2 %	-0.250	0.93 ± 5 %
12	165500	5.44E-3 ± 2 %	85160 ± 2 %	-0.250	0.93 ± 4 %
13	177200	5.83E-3 ± 2 %	96260 ± 2 %	-0.250	0.93 ± 4 %
14	154300	5.07E-3 ± 2 %	74350 ± 2 %	-0.250	0.94 ± 5 %
15	139400	4.58E-3 ± 3 %	61030 ± 3 %	-0.250	0.93 ± 5 %
16	114500	3.77E-3 ± 3 %	42000 ± 4 %	-0.250	0.93 ± 7 %
17	74710	2.45E-3 ± 5 %	18630 ± 9 %	-0.250	0.93 ± 13 %

Run# 18 L/D = 32 Fluid : air Pressure : 7.00 bar

Tubes 76.2 mm long diameter = 2.375 mm Entrance loss = 1.8

Pressure drop error (Pa) 1720 Constant mass flow error (kg/s) 1.6E-4

Point#	Re	Mass flow (kg/s)	Pressure drop (Pa)	Re power	P ratio
4	27120	8.78E-4 ± 18 %	5961 ± 29 %	-0.250	0.98 ± 43 %
5	34030	1.10E-3 ± 15 %	8953 ± 19 %	-0.250	0.96 ± 32 %
6	41650	1.35E-3 ± 12 %	13260 ± 13 %	-0.250	0.96 ± 24 %
7	52320	1.69E-3 ± 9 %	20400 ± 8 %	-0.250	0.95 ± 19 %
8	60320	1.95E-3 ± 8 %	26810 ± 6 %	-0.250	0.95 ± 16 %
9	70420	2.28E-3 ± 7 %	36100 ± 5 %	-0.250	0.96 ± 13 %
10	79860	2.59E-3 ± 6 %	45640 ± 4 %	-0.250	0.96 ± 11 %
11	89910	2.92E-3 ± 5 %	57230 ± 3 %	-0.250	0.95 ± 10 %
12	97710	3.17E-3 ± 5 %	67610 ± 3 %	-0.250	0.96 ± 9 %
13	82370	2.67E-3 ± 6 %	47920 ± 4 %	-0.250	0.94 ± 11 %
14	58430	1.89E-3 ± 8 %	25060 ± 7 %	-0.250	0.95 ± 16 %
15	36400	1.18E-3 ± 14 %	10050 ± 17 %	-0.250	0.94 ± 29 %

Run# 19 L/D = 32 Fluid : air Pressure : 3.36 bar

Tubes 76.2 mm long diameter = 2.375 mm Entrance loss = 1.8

Pressure drop error (Pa) 1720 Constant mass flow error (kg/s) 1.5E-4

Point#	Re	Mass flow (kg/s)	Pressure drop (Pa)	Re power	P ratio
6	19840	6.43E-4 ± 23 %	6718 ± 26 %	-0.250	0.97 ± 48 %
7	24960	8.08E-4 ± 19 %	10280 ± 17 %	-0.250	0.96 ± 37 %
8	30340	9.83E-4 ± 15 %	14740 ± 12 %	-0.250	0.94 ± 29 %
9	35180	1.14E-3 ± 13 %	19480 ± 9 %	-0.250	0.95 ± 25 %
10	39940	1.29E-3 ± 12 %	25150 ± 7 %	-0.250	0.97 ± 21 %
11	40370	1.31E-3 ± 11 %	25110 ± 7 %	-0.250	0.95 ± 21 %
12	45800	1.48E-3 ± 10 %	32670 ± 5 %	-0.250	0.97 ± 18 %
13	30150	9.76E-4 ± 15 %	14350 ± 12 %	-0.250	0.94 ± 29 %

Run# 20 L/D = 32 Fluid : nitrogen Pressure : 18.26 bar

Tubes 76.2 mm long diameter = 2.375 mm Entrance loss = 1.8

Pressure drop error (Pa) 1720 Constant mass flow error (kg/s) 1.2E-4

Point#	Re	Mass flow (kg/s)			Pressure drop (Pa)			Re power	P ratio		
2	42290	1.38E-3	±	9 %	4158	±	41 %	-0.250	0.72	±	44 %
3	42420	1.38E-3	±	9 %	4125	±	42 %	-0.250	0.71	±	44 %
4	49030	1.60E-3	±	7 %	5184	±	33 %	-0.250	0.68	±	36 %
5	58920	1.92E-3	±	6 %	7574	±	23 %	-0.250	0.69	±	25 %
6	69820	2.28E-3	±	5 %	10640	±	16 %	-0.250	0.69	±	19 %
8	40520	1.32E-3	±	9 %	4800	±	36 %	-0.250	0.90	±	39 %
9	49760	1.63E-3	±	7 %	7225	±	24 %	-0.250	0.91	±	27 %
10	60850	1.99E-3	±	6 %	10610	±	16 %	-0.250	0.90	±	19 %
11	69420	2.27E-3	±	5 %	13720	±	13 %	-0.250	0.91	±	16 %
12	82040	2.68E-3	±	4 %	19110	±	9 %	-0.250	0.91	±	12 %
13	91610	2.99E-3	±	4 %	23690	±	7 %	-0.250	0.92	±	10 %
14	100700	3.29E-3	±	4 %	28570	±	6 %	-0.250	0.91	±	9 %
15	112200	3.67E-3	±	3 %	35240	±	5 %	-0.250	0.91	±	8 %
16	121300	3.97E-3	±	3 %	41100	±	4 %	-0.250	0.91	±	7 %
17	133900	4.38E-3	±	3 %	49520	±	3 %	-0.250	0.91	±	6 %
18	143200	4.68E-3	±	3 %	56170	±	3 %	-0.250	0.91	±	5 %
19	152700	4.99E-3	±	2 %	63560	±	3 %	-0.250	0.91	±	5 %
20	159800	5.22E-3	±	2 %	69700	±	2 %	-0.250	0.91	±	5 %
21	169700	5.55E-3	±	2 %	78150	±	2 %	-0.250	0.91	±	4 %
22	179400	5.87E-3	±	2 %	87220	±	2 %	-0.250	0.90	±	4 %
23	191700	6.26E-3	±	2 %	98690	±	2 %	-0.250	0.90	±	4 %
24	149900	4.90E-3	±	2 %	62050	±	3 %	-0.250	0.90	±	5 %
25	91420	2.99E-3	±	4 %	24220	±	7 %	-0.250	0.91	±	10 %

Run# 21 L/D = 5 Fluid : air Pressure : 7.00 bar

Tubes 12.7 mm long diameter = 2.375 mm Entrance loss = 1.8

Pressure drop error (Pa) 1720 Constant mass flow error (kg/s) 1.6E-4

Point#	Re	Mass flow (kg/s)	Pressure drop (Pa)	Re power	P ratio
4	31280	1.02E-3 ± 16 %	5681 ± 30 %	-0.250	0.93 ± 41 %
5	40410	1.31E-3 ± 12 %	9634 ± 18 %	-0.250	0.95 ± 28 %
6	51010	1.66E-3 ± 10 %	15190 ± 11 %	-0.250	0.94 ± 20 %
7	60380	1.96E-3 ± 8 %	21200 ± 8 %	-0.250	0.94 ± 16 %
8	70400	2.29E-3 ± 7 %	29200 ± 6 %	-0.250	0.96 ± 14 %
9	80830	2.62E-3 ± 6 %	38510 ± 4 %	-0.250	0.97 ± 12 %
10	91020	2.95E-3 ± 5 %	48130 ± 4 %	-0.250	0.96 ± 10 %
11	100400	3.26E-3 ± 5 %	55860 ± 3 %	-0.250	0.95 ± 9 %
12	109700	3.57E-3 ± 4 %	67540 ± 3 %	-0.250	0.96 ± 8 %
15	89830	2.92E-3 ± 5 %	45110 ± 4 %	-0.250	0.94 ± 10 %
16	71180	2.32E-3 ± 7 %	28560 ± 6 %	-0.250	0.93 ± 14 %
17	50140	1.63E-3 ± 10 %	14070 ± 12 %	-0.250	0.91 ± 21 %
18	30380	9.88E-4 ± 16 %	5278 ± 33 %	-0.250	0.92 ± 43 %

Run# 22 L/D = 5 Fluid : air Pressure : 3.36 bar

Tubes 12.7 mm long diameter = 2.375 mm Entrance loss = 1.8

Pressure drop error (Pa) 1720 Constant mass flow error (kg/s) 1.5E-4

Point#	Re	Mass flow (kg/s)	Pressure drop (Pa)	Re power	P ratio
7	26530	8.63E-4 ± 17 %	8183 ± 21 %	-0.250	0.90 ± 37 %
8	30790	1.00E-3 ± 15 %	11240 ± 15 %	-0.250	0.93 ± 30 %
9	35460	1.15E-3 ± 13 %	15050 ± 11 %	-0.250	0.94 ± 25 %
10	40800	1.33E-3 ± 11 %	19950 ± 9 %	-0.250	0.95 ± 22 %
11	45000	1.46E-3 ± 10 %	23770 ± 7 %	-0.250	0.94 ± 19 %
12	49380	1.61E-3 ± 9 %	29080 ± 6 %	-0.250	0.96 ± 17 %
13	31090	1.01E-3 ± 15 %	11430 ± 15 %	-0.250	0.93 ± 30 %

Run# 23 L/D = 5 Fluid : nitrogen Pressure : 18.26 bar

Tubes 12.7 mm long diameter = 2.375 mm Entrance loss = 1.8

Pressure drop error (Pa) 1720 Constant mass flow error (kg/s) 1.2E-4

Point#	Re	Mass flow (kg/s)			Pressure drop (Pa)			Re power	P ratio		
2	40660	1.34E-3	±	9 %	3888	±	44 %	-0.250	0.93	±	47 %
3	40780	1.34E-3	±	9 %	3876	±	44 %	-0.250	0.92	±	47 %
4	46350	1.52E-3	±	8 %	4886	±	35 %	-0.250	0.90	±	38 %
5	60270	1.98E-3	±	6 %	8360	±	21 %	-0.250	0.91	±	23 %
6	70280	2.31E-3	±	5 %	11220	±	15 %	-0.250	0.90	±	18 %
7	81310	2.67E-3	±	4 %	15120	±	11 %	-0.250	0.91	±	14 %
8	93550	3.07E-3	±	4 %	20060	±	9 %	-0.250	0.91	±	11 %
9	100200	3.29E-3	±	4 %	23120	±	7 %	-0.250	0.91	±	10 %
10	101900	3.35E-3	±	4 %	23430	±	7 %	-0.250	0.91	±	10 %
11	111200	3.66E-3	±	3 %	27720	±	6 %	-0.250	0.90	±	8 %
12	122500	4.03E-3	±	3 %	33960	±	5 %	-0.250	0.90	±	7 %
13	121900	4.01E-3	±	3 %	33120	±	5 %	-0.250	0.90	±	7 %
14	131100	4.31E-3	±	3 %	38550	±	4 %	-0.250	0.91	±	7 %
15	139800	4.60E-3	±	3 %	43390	±	4 %	-0.250	0.90	±	6 %
16	151500	4.98E-3	±	2 %	50590	±	3 %	-0.250	0.89	±	5 %
17	161200	5.30E-3	±	2 %	57240	±	3 %	-0.250	0.90	±	5 %
18	171500	5.64E-3	±	2 %	64420	±	3 %	-0.250	0.89	±	5 %
19	179300	5.90E-3	±	2 %	70290	±	2 %	-0.250	0.88	±	4 %
20	191500	6.30E-3	±	2 %	80050	±	2 %	-0.250	0.89	±	4 %
21	199900	6.58E-3	±	2 %	87200	±	2 %	-0.250	0.88	±	4 %
22	211300	6.96E-3	±	2 %	95420	±	2 %	-0.250	0.87	±	4 %
23	101000	3.32E-3	±	4 %	22850	±	8 %	-0.250	0.89	±	10 %

Run# 36 L/D = 150 Fluid : air Pressure : 7.00 bar

Tubes 356.3 mm long diameter = 2.375 mm Entrance loss = 1.5

Pressure drop error (Pa) 1720 Constant mass flow error (kg/s) 1.6E-4

Point#	Re	Mass flow (kg/s)			Pressure drop (Pa)			Re power	P ratio		
2	20790	6.82E-4	±	23 %	7849	±	22 %	-0.250	1.01	±	47 %
3	30860	1.01E-3	±	16 %	16020	±	11 %	-0.250	1.00	±	30 %
4	49570	1.63E-3	±	10 %	38600	±	4 %	-0.250	1.03	±	18 %
5	62360	2.04E-3	±	8 %	57050	±	3 %	-0.250	1.02	±	14 %
6	70710	2.32E-3	±	7 %	71490	±	2 %	-0.250	1.03	±	12 %

Run# 37 L/D = 150 Fluid : air Pressure : 3.36 bar

Tubes 356.3 mm long diameter = 2.375 mm Entrance loss = 1.5

Pressure drop error (Pa) 1720 Constant mass flow error (kg/s) 1.5E-4

Point#	Re	Mass flow (kg/s)	Pressure drop (Pa)	Re power	P ratio
1	21730	7.12E-4 ± 21 %	17970 ± 10 %	-0.250	1.04 ± 38 %
3	29210	9.63E-4 ± 16 %	30660 ± 6 %	-0.250	1.03 ± 28 %

Run# 38 L/D = 100 Fluid : air Pressure : 7.00 bar

Tubes 237.5 mm long diameter = 2.375 mm Entrance loss = 1.5

Pressure drop error (Pa) 1720 Constant mass flow error (kg/s) 1.6E-4

Point#	Re	Mass flow (kg/s)	Pressure drop (Pa)	Re power	P ratio
3	30520	1.00E-3 ± 16 %	12140 ± 14 %	-0.250	1.00 ± 31 %
4	40400	1.33E-3 ± 12 %	20100 ± 9 %	-0.250	1.00 ± 23 %
5	50120	1.66E-3 ± 10 %	30120 ± 6 %	-0.250	0.98 ± 18 %
6	59270	1.95E-3 ± 8 %	41300 ± 4 %	-0.250	1.01 ± 15 %
7	70090	2.31E-3 ± 7 %	56090 ± 3 %	-0.250	1.01 ± 13 %
8	69970	2.30E-3 ± 7 %	54960 ± 3 %	-0.250	1.02 ± 13 %
9	80240	2.63E-3 ± 6 %	70860 ± 2 %	-0.250	1.03 ± 11 %

Run# 39 L/D = 100 Fluid : air Pressure : 3.36 bar

Tubes 237.5 mm long diameter = 2.375 mm Entrance loss = 1.5

Pressure drop error (Pa) 1720 Constant mass flow error (kg/s) 1.5E-4

Point#	Re	Mass flow (kg/s)	Pressure drop (Pa)	Re power	P ratio
3	20300	6.69E-4 ± 22 %	11140 ± 15 %	-0.250	0.95 ± 42 %
4	31220	1.02E-3 ± 15 %	24810 ± 7 %	-0.250	0.98 ± 27 %

Run# 40 L/D = 75 Fluid : air Pressure : 7.00 bar

Tubes 178.1 mm long diameter = 2.375 mm Entrance loss = 1.5

Pressure drop error (Pa) 1720 Constant mass flow error (kg/s) 1.6E-4

Point#	Re	Mass flow (kg/s)	Pressure drop (Pa)	Re power	P ratio
3	30670	1.01E-3 ± 16 %	9918 ± 17 %	-0.250	0.96 ± 33 %
4	41170	1.35E-3 ± 12 %	17030 ± 10 %	-0.250	0.96 ± 23 %
5	49370	1.62E-3 ± 10 %	23950 ± 7 %	-0.250	0.97 ± 19 %
6	59750	1.96E-3 ± 8 %	33780 ± 5 %	-0.250	0.98 ± 15 %
7	69200	2.27E-3 ± 7 %	44490 ± 4 %	-0.250	0.98 ± 13 %
8	80060	2.63E-3 ± 6 %	58550 ± 3 %	-0.250	0.99 ± 11 %
9	89440	2.93E-3 ± 5 %	71450 ± 2 %	-0.250	0.99 ± 10 %

Run# 41 L/D = 75 Fluid : air Pressure : 3.36 bar

Tubes 178.1 mm long diameter = 2.375 mm Entrance loss = 1.5

Pressure drop error (Pa) 1720 Constant mass flow error (kg/s) 1.5E-4

Point#	Re	Mass flow (kg/s)	Pressure drop (Pa)	Re power	P ratio
2	20670	6.80E-4 ± 22 %	9634 ± 18 %	-0.250	0.94 ± 43 %
3	40220	1.32E-3 ± 11 %	33050 ± 5 %	-0.250	0.98 ± 21 %

Run# 42 L/D = 50 Fluid : air Pressure : 7.00 bar

Tubes 118.2 mm long diameter = 2.375 mm Entrance loss = 1.5

Pressure drop error (Pa) 1720 Constant mass flow error (kg/s) 1.6E-4

Point#	Re	Mass flow (kg/s)	Pressure drop (Pa)	Re power	P ratio
3	30030	9.81E-4 ± 16 %	8012 ± 21 %	-0.250	1.01 ± 36 %
4	39290	1.29E-3 ± 12 %	13350 ± 13 %	-0.250	0.99 ± 25 %
5	59270	1.95E-3 ± 8 %	29650 ± 6 %	-0.250	1.03 ± 16 %
6	49730	1.63E-3 ± 10 %	20910 ± 8 %	-0.250	1.01 ± 19 %
7	70520	2.31E-3 ± 7 %	40350 ± 4 %	-0.250	1.03 ± 13 %
8	80280	2.64E-3 ± 6 %	52140 ± 3 %	-0.250	1.03 ± 11 %
9	89370	2.96E-3 ± 5 %	64620 ± 3 %	-0.250	1.03 ± 10 %

Run# 43 L/D = 50 Fluid : air Pressure : 3.36 bar

Tubes 118.2 mm long diameter = 2.375 mm Entrance loss = 1.5

Pressure drop error (Pa) 1720 Constant mass flow error (kg/s) 1.5E-4

Point#	Re	Mass flow (kg/s)	Pressure drop (Pa)	Re power	P ratio
2	20000	6.55E-4 ± 23 %	7316 ± 24 %	-0.250	0.96 ± 46 %
3	30780	1.01E-3 ± 15 %	17030 ± 10 %	-0.250	0.99 ± 28 %
4	40850	1.34E-3 ± 11 %	29610 ± 6 %	-0.250	1.02 ± 20 %

Run# 44 L/D = 25 Fluid : air Pressure : 7.00 bar

Tubes 59.38 mm long diameter = 2.375 mm Entrance loss = 1.5

Pressure drop error (Pa) 1720 Constant mass flow error (kg/s) 1.6E-4

Point#	Re	Mass flow (kg/s)	Pressure drop (Pa)	Re power	P ratio
13	29800	9.78E-4 ± 16 %	6156 ± 28 %	-0.250	1.00 ± 40 %
14	41040	1.35E-3 ± 12 %	11300 ± 15 %	-0.250	0.99 ± 26 %
15	50860	1.67E-3 ± 10 %	16790 ± 10 %	-0.250	0.97 ± 20 %
16	59800	1.96E-3 ± 8 %	22650 ± 8 %	-0.250	0.96 ± 16 %
17	70490	2.32E-3 ± 7 %	31280 ± 5 %	-0.250	0.97 ± 13 %
18	79990	2.64E-3 ± 6 %	39830 ± 4 %	-0.250	0.96 ± 11 %
19	91620	3.01E-3 ± 5 %	51400 ± 3 %	-0.250	0.97 ± 10 %
20	103700	3.41E-3 ± 5 %	65820 ± 3 %	-0.250	0.99 ± 9 %

Run# 45 L/D = 25 Fluid : air Pressure : 3.36 bar

Tubes 59.38 mm long diameter = 2.375 mm Entrance loss = 1.5

Pressure drop error (Pa) 1720 Constant mass flow error (kg/s) 1.5E-4

Point#	Re	Mass flow (kg/s)	Pressure drop (Pa)	Re power	P ratio
2	20860	6.84E-4 ± 22 %	6041 ± 28 %	-0.250	0.94 ± 48 %
3	30960	1.02E-3 ± 15 %	13280 ± 13 %	-0.250	0.96 ± 29 %
4	40120	1.32E-3 ± 11 %	21810 ± 8 %	-0.250	0.97 ± 21 %
5	50510	1.66E-3 ± 9 %	34520 ± 5 %	-0.250	0.99 ± 17 %

Run# 47 L/D = 5 Fluid : air Pressure : 7.00 bar

Tubes 11.87 mm long diameter = 2.375 mm Entrance loss = 1.5

Pressure drop error (Pa) 1720 Constant mass flow error (kg/s) 1.6E-4

Point#	Re	Mass flow (kg/s)	Pressure drop (Pa)	Re power	P ratio
4	40400	1.31E-3 ± 12 %	5996 ± 29 %	-0.250	0.72 ± 36 %
5	49860	1.62E-3 ± 10 %	9102 ± 19 %	-0.250	0.72 ± 26 %
6	60640	1.96E-3 ± 8 %	13490 ± 13 %	-0.250	0.72 ± 19 %
7	70240	2.28E-3 ± 7 %	18280 ± 9 %	-0.250	0.73 ± 15 %
8	80590	2.61E-3 ± 6 %	23700 ± 7 %	-0.250	0.72 ± 13 %
9	91110	2.95E-3 ± 5 %	30300 ± 6 %	-0.250	0.73 ± 11 %
10	102300	3.32E-3 ± 5 %	38150 ± 5 %	-0.250	0.73 ± 10 %

Run# 48 L/D = 5 Fluid : air Pressure : 3.36 bar

Tubes 11.87 mm long diameter = 2.375 mm Entrance loss = 1.5

Pressure drop error (Pa) 1720 Constant mass flow error (kg/s) 1.5E-4

Point#	Re	Mass flow (kg/s)	Pressure drop (Pa)	Re power	P ratio
3	30350	9.85E-4 ± 15 %	7021 ± 24 %	-0.250	0.71 ± 36 %
4	40720	1.32E-3 ± 11 %	12980 ± 13 %	-0.250	0.73 ± 24 %
5	49860	1.62E-3 ± 9 %	19510 ± 9 %	-0.250	0.74 ± 18 %
6	60620	1.97E-3 ± 8 %	28730 ± 6 %	-0.250	0.75 ± 15 %

Run# 49 L/D = 10 Fluid : air Pressure : 7.00 bar

Tubes 23.7 mm long diameter = 2.375 mm Entrance loss = 1.5

Pressure drop error (Pa) 1720 Constant mass flow error (kg/s) 1.6E-4

Point#	Re	Mass flow (kg/s)	Pressure drop (Pa)	Re power	P ratio
4	39620	1.29E-3 ± 12 %	6434 ± 27 %	-0.250	0.74 ± 34 %
5	50160	1.63E-3 ± 10 %	10340 ± 17 %	-0.250	0.75 ± 24 %
6	59390	1.93E-3 ± 8 %	14490 ± 12 %	-0.250	0.75 ± 19 %
7	69820	2.28E-3 ± 7 %	19930 ± 9 %	-0.250	0.75 ± 15 %
8	79500	2.58E-3 ± 6 %	25510 ± 7 %	-0.250	0.75 ± 13 %
9	90180	2.93E-3 ± 5 %	32680 ± 5 %	-0.250	0.75 ± 11 %
10	102500	3.33E-3 ± 5 %	41230 ± 4 %	-0.250	0.75 ± 9 %
11	111900	3.65E-3 ± 4 %	49650 ± 3 %	-0.250	0.76 ± 8 %
12	122000	3.96E-3 ± 4 %	57460 ± 3 %	-0.250	0.75 ± 8 %
13	132400	4.32E-3 ± 4 %	68580 ± 3 %	-0.250	0.75 ± 7 %

Run # 50 L/D= 25 Fluid: air Pressure: 7.00 bar

Tubes 59.4 mm long diameter (mm) = 2.375 Entrance loss = 1.05

Pressure drop error (Pa) 1720 Constant mass flow error (kg/s) 1.6E-4

Point #	Re	Mass flow (kg/s)	Pressure drop (Pa)	Re power	P ratio	
5	40770	1.32E-3± 12%	7395± 23%	-0.250	.87±	31%
6	49120	1.59E-3± 10%	10730± 16%	-0.250	.89±	24%
7	60280	1.96E-3± 8%	15850± 11%	-0.250	.88±	18%
8	70190	2.27E-3± 7%	21260± 8%	-0.250	.89±	15%
9	80550	2.61E-3± 6%	27870± 6%	-0.250	.89±	12%
10	90070	2.92E-3± 5%	34630± 5%	-0.250	.90±	11%
11	101700	3.30E-3± 5%	43940± 4%	-0.250	.91±	9%
12	121800	3.96E-3± 4%	62440± 3%	-0.250	.92±	8%

Run # 51 L/D= 25 Fluid: nitrogen Pressure: 18.26 bar

Tubes 59.4 mm long diameter (mm) = 2.375 Entrance loss = 1.05

Pressure drop error (Pa) 1720 Constant mass flow error (kg/s) 1.2E-4

Point #	Re	Mass flow (kg/s)	Pressure drop (Pa)	Re power	P ratio	
2	49490	1.62E-3± 7%	4556± 38%	-0.250	.90±	40%
3	70100	2.30E-3± 5%	8886± 19%	-0.250	.89±	21%
4	90210	2.96E-3± 4%	14330± 12%	-0.250	.90±	14%
5	109600	3.60E-3± 3%	20750± 8%	-0.250	.87±	10%
6	148900	4.89E-3± 2%	37200± 5%	-0.250	.88±	6%
7	168400	5.52E-3± 2%	46750± 4%	-0.250	.87±	5%
8	190500	6.25E-3± 2%	59020± 3%	-0.250	.87±	4%
9	209500	6.87E-3± 2%	70860± 2%	-0.250	.88±	4%
10	230600	7.56E-3± 2%	85890± 2%	-0.250	.88±	3%

Run# 52 L/D = 50 Fluid : air Pressure : 7.00 bar

Tubes 118.7 mm long diameter = 2.375 mm Entrance loss = 1.05

Pressure drop error (Pa) 1720 Constant mass flow error (kg/s) 1.6E-4

Point#	Re	Mass flow (kg/s)	Pressure drop (Pa)	Re power	P ratio
3	29850	9.70E-4 ± 16 %	5667 ± 30 %	-0.250	0.88 ± 42 %
4	40090	1.30E-3 ± 12 %	10040 ± 17 %	-0.250	0.90 ± 27 %
5	49800	1.62E-3 ± 10 %	14740 ± 12 %	-0.250	0.88 ± 21 %
6	60470	1.96E-3 ± 8 %	21400 ± 8 %	-0.250	0.90 ± 16 %
7	70020	2.28E-3 ± 7 %	27730 ± 6 %	-0.250	0.88 ± 14 %
8	79620	2.59E-3 ± 6 %	35510 ± 5 %	-0.250	0.89 ± 12 %
9	90720	2.95E-3 ± 5 %	45390 ± 4 %	-0.250	0.90 ± 10 %
10	97670	3.27E-3 ± 5 %	54920 ± 3 %	-0.250	0.87 ± 9 %
11	109800	3.62E-3 ± 4 %	66860 ± 3 %	-0.250	0.89 ± 8 %

Run# 53 L/D = 50 Fluid : nitrogen Pressure : 18.26 bar

Tubes 118.7 mm long diameter = 2.375 mm Entrance loss = 1.05

Pressure drop error (Pa) 1720 Constant mass flow error (kg/s) 1.2E-4

Point#	Re	Mass flow (kg/s)	Pressure drop (Pa)	Re power	P ratio
1	220400	7.24E-3 ± 2 %	95400 ± 2 %	-0.250	0.86 ± 3 %
2	199700	6.56E-3 ± 2 %	94700 ± 2 %	-0.250	0.89 ± 4 %
3	182000	5.97E-3 ± 2 %	79380 ± 2 %	-0.250	0.88 ± 4 %
4	159700	5.24E-3 ± 2 %	62460 ± 3 %	-0.250	0.88 ± 5 %
5	141000	4.63E-3 ± 3 %	49780 ± 3 %	-0.250	0.89 ± 6 %
6	119700	3.93E-3 ± 3 %	36860 ± 5 %	-0.250	0.89 ± 7 %
7	98880	3.24E-3 ± 4 %	25960 ± 7 %	-0.250	0.90 ± 9 %
8	79670	2.61E-3 ± 5 %	17360 ± 10 %	-0.250	0.89 ± 13 %
9	60530	1.99E-3 ± 6 %	10780 ± 16 %	-0.250	0.93 ± 19 %
10	39040	1.28E-3 ± 9 %	4746 ± 36 %	-0.250	0.93 ± 40 %

Run# 56 L/D = 100 Fluid : air Pressure : 7.00 bar

Tubes 237.5 mm long diameter = 2.375 mm Entrance loss = 1.05

Pressure drop error (Pa) 1720 Constant mass flow error (kg/s) 1.6E-4

Point#	Re	Mass flow (kg/s)		Pressure drop (Pa)		Re power	P ratio	
3	30090	9.81E-4 ±	16 %	10010 ±	17 %	-0.250	0.99 ±	33 %
4	40900	1.33E-3 ±	12 %	17430 ±	10 %	-0.250	0.99 ±	23 %
5	50230	1.64E-3 ±	10 %	25740 ±	7 %	-0.250	1.00 ±	18 %
6	60020	1.96E-3 ±	8 %	35750 ±	5 %	-0.250	1.00 ±	15 %
7	69620	2.28E-3 ±	7 %	45650 ±	4 %	-0.250	0.99 ±	13 %
8	80900	2.65E-3 ±	6 %	61080 ±	3 %	-0.250	1.01 ±	11 %

Run# 58 L/D = 100 Fluid : nitrogen Pressure : 18.26 bar

Tubes 237.5 mm long diameter = 2.375 mm Entrance loss = 1.05

Pressure drop error (Pa) 1720 Constant mass flow error (kg/s) 1.2E-4

Point#	Re	Mass flow (kg/s)		Pressure drop (Pa)		Re power	P ratio	
1	168300	5.58E-3 ±	2 %	96450 ±	2 %	-0.250	0.97 ±	4 %
2	169300	5.60E-3 ±	2 %	98000 ±	2 %	-0.250	0.99 ±	4 %
3	150300	4.95E-3 ±	2 %	78160 ±	2 %	-0.250	0.99 ±	5 %
4	129900	4.28E-3 ±	3 %	59750 ±	3 %	-0.250	0.98 ±	6 %
5	110700	3.64E-3 ±	3 %	44750 ±	4 %	-0.250	0.99 ±	7 %
6	89530	2.94E-3 ±	4 %	30200 ±	6 %	-0.250	0.99 ±	9 %
7	70180	2.30E-3 ±	5 %	19950 ±	9 %	-0.250	1.01 ±	13 %
8	58970	1.94E-3 ±	6 %	14190 ±	12 %	-0.250	0.99 ±	16 %
9	50540	1.66E-3 ±	7 %	10790 ±	16 %	-0.250	1.00 ±	20 %
10	39840	1.31E-3 ±	9 %	7123 ±	24 %	-0.250	1.02 ±	29 %

Run# 60 L/D = 150 Fluid : air Pressure : 7.00 bar

Tubes 356.3 mm long diameter = 2.375 mm Entrance loss = 1.05

Pressure drop error (Pa) 1720 Constant mass flow error (kg/s) 1.6E-4

Point#	Re	Mass flow (kg/s)			Pressure drop (Pa)			Re power	P ratio		
3	31350	1.02E-3	±	16 %	10270	±	17 %	-0.250	0.71	±	32 %
4	42150	1.37E-3	±	12 %	21120	±	8 %	-0.250	0.85	±	22 %
5	49600	1.62E-3	±	10 %	28910	±	6 %	-0.250	0.87	±	18 %
6	60990	1.99E-3	±	8 %	42630	±	4 %	-0.250	0.89	±	15 %
7	69400	2.26E-3	±	7 %	54530	±	3 %	-0.250	0.90	±	13 %
8	78300	2.55E-3	±	6 %	67330	±	3 %	-0.250	0.91	±	11 %

Run# 61 L/D = 150 Fluid : nitrogen Pressure : 18.26 bar

Tubes 356.3 mm long diameter = 2.375 mm Entrance loss = 1.05

Pressure drop error (Pa) 1720 Constant mass flow error (kg/s) 1.2E-4

Point#	Re	Mass flow (kg/s)			Pressure drop (Pa)			Re power	P ratio		
1	150800	4.96E-3	±	2 %	96990	±	2 %	-0.250	0.94	±	5 %
2	130000	4.27E-3	±	3 %	73300	±	2 %	-0.250	0.93	±	5 %
3	130100	4.27E-3	±	3 %	73300	±	2 %	-0.250	0.94	±	5 %
4	112900	3.71E-3	±	3 %	56400	±	3 %	-0.250	0.92	±	6 %
5	102500	3.37E-3	±	4 %	46870	±	4 %	-0.250	0.91	±	7 %
6	92450	3.04E-3	±	4 %	38530	±	4 %	-0.250	0.90	±	8 %
7	78310	2.57E-3	±	5 %	28600	±	6 %	-0.250	0.90	±	10 %
8	55410	1.82E-3	±	7 %	14800	±	12 %	-0.250	0.87	±	16 %
9	42830	1.41E-3	±	9 %	9217	±	19 %	-0.250	0.86	±	24 %

Run # 85 Fluid: air Pressure: 7.00 bar

Screens 12.7 mm long porosity = 0.663 Wire diameter = 94µm

Pressure drop error (Pa) 586 Constant mass flow error (kg/s) 1.6E-4

Point #	Re	Mass flow (kg/s)	Pressure drop (Pa)	Re power	P ratio
5	115.4	2.09E-3± 8%	1847± 32%	-0.33	1.39± 35%
6	115.8	2.10E-3± 8%	1850± 32%	-0.33	1.38± 35%
7	146.5	2.65E-3± 6%	2686± 22%	-0.33	1.40± 24%
8	146	2.64E-3± 6%	2683± 22%	-0.33	1.40± 24%
9	180.5	3.27E-3± 5%	3762± 16%	-0.33	1.40± 18%
10	180.8	3.27E-3± 5%	3767± 16%	-0.33	1.41± 18%
11	211.9	3.83E-3± 4%	4865± 12%	-0.33	1.41± 14%
12	211.8	3.83E-3± 4%	4860± 12%	-0.33	1.40± 14%
13	236.5	4.28E-3± 4%	5819± 10%	-0.33	1.41± 12%
14	237.1	4.29E-3± 4%	5830± 10%	-0.33	1.41± 12%
15	269.9	4.88E-3± 3%	7203± 8%	-0.33	1.41± 9%
16	269.9	4.87E-3± 3%	7196± 8%	-0.33	1.41± 9%

Run # 86 Fluid: nitrogen Pressure: 18.26 bar

Screens 12.7 mm long porosity = 0.663 Wire diameter = 94µm

Pressure drop error (Pa) 586 Constant mass flow error (kg/s) 1.2E-4

Point #	Re	Mass flow (kg/s)	Pressure drop (Pa)	Re power	P ratic
3	216.9	3.91E-3± 3%	1974± 30%	-0.33	1.39± 30%
4	216.6	3.91E-3± 3%	1977± 30%	-0.33	1.40± 30%
5	291.2	5.26E-3± 2%	3164± 19%	-0.33	1.39± 19%
6	290.7	5.24E-3± 2%	3164± 19%	-0.33	1.40± 19%
7	349.3	6.31E-3± 2%	4307± 14%	-0.33	1.41± 14%
8	349.2	6.31E-3± 2%	4309± 14%	-0.33	1.40± 14%
9	423.5	7.64E-3± 2%	5906± 10%	-0.33	1.39± 11%
10	422.7	7.63E-3± 2%	5918± 10%	-0.33	1.41± 11%
11	505.1	9.12E-3± 1%	7897± 7%	-0.33	1.38± 7%
12	505	9.12E-3± 1%	7881± 7%	-0.33	1.37± 7%
13	564.1	1.02E-2± 1%	9494± 6%	-0.33	1.37± 6%
14	562.3	1.02E-2± 1%	9492± 6%	-0.33	1.35± 6%
15	618.3	1.12E-2± 1%	11040± 5%	-0.33	1.33± 5%
16	619.6	1.12E-2± 1%	11040± 5%	-0.33	1.35± 5%
17	679.3	1.23E-2± 1%	12960± 5%	-0.33	1.34± 5%
18	680.5	1.23E-2± 1%	12950± 5%	-0.33	1.34± 5%
19	718	1.30E-2± 1%	14200± 4%	-0.33	1.34± 4%
20	718.7	1.30E-2± 1%	14200± 4%	-0.33	1.33± 4%

Run # 87 Fluid: nitrogen Pressure 18.26 bar

Screens 25.4 mm long porosity = 0.663 Wire diameter = 94μm

Pressure drop error (Pa) 586 Constant mass flow error (kg/s) 1.2E-4

Point #	Re	Mass flow (kg/s)		Pressure drop (Pa)	Re power	P ratio	
1	147.2	2.67E-3±	5%	2458± 24%	-0.33	1.61±	25%
2	147.5	2.67E-3±	4%	2475± 24%	-0.33	1.61±	25%
3	147.1	2.66E-3±	5%	2446± 24%	-0.33	1.60±	25%
4	216.8	3.93E-3±	3%	4532± 13%	-0.33	1.59±	14%
5	217.1	3.93E-3±	3%	4551± 13%	-0.33	1.60±	14%
6	299.2	5.42E-3±	2%	7576± 8%	-0.33	1.58±	9%
7	298.9	5.41E-3±	2%	7580± 8%	-0.33	1.59±	9%
8	378.9	6.86E-3±	2%	11250± 5%	-0.33	1.58±	6%
9	378.9	6.87E-3±	2%	11230± 5%	-0.33	1.57±	6%
10	452.7	8.19E-3±	1%	15090± 4%	-0.33	1.57±	4%
11	453.1	8.20E-3±	1%	15080± 4%	-0.33	1.56±	4%
12	530.2	9.60E-3±	1%	19650± 3%	-0.33	1.55±	3%
13	530.8	9.61E-3±	1%	19640± 3%	-0.33	1.55±	3%
14	586	1.06E-2±	1%	23290± 3%	-0.33	1.53±	3%
15	586.9	1.06E-2±	1%	23250± 3%	-0.33	1.52±	3%
16	629.7	1.14E-2±	1%	25800± 2%	-0.33	1.51±	3%
17	631.8	1.14E-2±	1%	25790± 2%	-0.33	1.51±	3%
18	691.3	1.25E-2±	1%	30150± 2%	-0.33	1.52±	3%
19	691.2	1.25E-2±	1%	30130± 2%	-0.33	1.51±	3%

Run # 88 Fluid: air Pressure: 7.00 bar

Screens 25.4 mm long porosity = 0.663 Wire diameter = 94μm

Pressure drop error (Pa) 586 Constant mass flow error (kg/s) 1.6E-4

Point #	Re	Mass flow (kg/s)		Pressure drop (Pa)	Re power	P ratio	
3	79.77	1.43E-3±	11%	2301± 25%	-0.33	1.54±	31%
4	79.32	1.42E-3±	11%	2307± 25%	-0.33	1.56±	31%
5	105.5	1.90E-3±	8%	3522± 17%	-0.33	1.55±	22%
6	105.1	1.89E-3±	8%	3514± 17%	-0.33	1.56±	22%
7	144.4	2.59E-3±	6%	5747± 10%	-0.33	1.57±	14%
8	144.4	2.59E-3±	6%	5748± 10%	-0.33	1.57±	14%
9	173.1	3.11E-3±	5%	7718± 8%	-0.33	1.58±	12%
10	173.3	3.11E-3±	5%	7711± 8%	-0.33	1.58±	12%
11	200.1	3.59E-3±	4%	9679± 6%	-0.33	1.58±	9%
12	199.4	3.59E-3±	4%	9685± 6%	-0.33	1.58±	9%
13	227.3	4.08E-3±	4%	11980± 5%	-0.33	1.59±	8%
14	228.1	4.09E-3±	4%	11980± 5%	-0.33	1.59±	8%
15	247.1	4.43E-3±	4%	13650± 4%	-0.33	1.59±	8%
16	246.5	4.43E-3±	4%	13630± 4%	-0.33	1.58±	8%
17	275.2	4.95E-3±	3%	16250± 4%	-0.33	1.59±	6%
18	275.6	4.95E-3±	3%	16260± 4%	-0.33	1.59±	6%
19	276.2	4.96E-3±	3%	16270± 4%	-0.33	1.59±	6%

Run # 89 Fluid: air Pressure: 7.00 bar

Screens 25.4 mm long porosity = 0.665 Wire diameter = 191μm

Pressure drop error (Pa) 586 Constant mass flow error (kg/s) 1.6E-4

Point #	Re	Mass flow (kg/s)	Pressure drop (Pa)	Re power	P ratio
5	233.5	2.08E-3± 8%	1808± 32%	-0.33	1.88± 35%
6	233.6	2.08E-3± 8%	1812± 32%	-0.33	1.88± 35%
7	286.4	2.55E-3± 6%	2551± 23%	-0.33	1.90± 25%
8	286.5	2.55E-3± 6%	2567± 23%	-0.33	1.91± 25%

Run # 90 Fluid: air Pressure: 7.00 bar

Screens 25.4 mm long porosity = 0.665 Wire diameter = 191μm

Pressure drop error (Pa) 586 Constant mass flow error (kg/s) 1.6E-4

Point #	Re	Mass flow (kg/s)	Pressure drop (Pa)	Re power	P ratio
5	225.4	2.01E-3± 8%	1714± 34%	-0.33	1.87± 37%
6	226	2.02E-3± 8%	1714± 34%	-0.33	1.87± 37%
7	278.8	2.49E-3± 6%	2450± 24%	-0.33	1.89± 26%
8	279.3	2.50E-3+ 6%	2458± 24%	-0.33	1.88± 26%
9	317.7	2.84E-3± 6%	3047± 19%	-0.33	1.90± 21%
10	318.9	2.85E-3± 6%	3040± 19%	-0.33	1.89± 21%
11	366.7	3.27E-3± 5%	3854± 15%	-0.33	1.90± 17%
12	365.2	3.26E-3± 5%	3856± 15%	-0.33	1.90± 17%
13	411.7	3.68E-3± 4%	4717± 12%	-0.33	1.91± 14%
14	411.7	3.68E-3± 4%	4720± 12%	-0.33	1.91± 14%
15	447.1	4.00E-3± 4%	5445± 11%	-0.33	1.91± 13%
16	447.4	4.00E-3± 4%	5439± 11%	-0.33	1.91± 13%
17	477.7	4.27E-3± 4%	6114± 10%	-0.33	1.91± 12%
18	478.6	4.28E-3± 4%	6105± 10%	-0.33	1.91± 12%
19	512.4	4.58E-3± 3%	6861± 9%	-0.33	1.91± 10%
20	510.6	4.58E-3± 3%	6871± 9%	-0.33	1.91± 10%
21	551.7	4.94E-3± 3%	7834± 7%	-0.33	1.92± 9%
22	551.4	4.94E-3± 3%	7846± 7%	-0.33	1.91± 9%

Run # 91 Fluid: nitrogen Pressure: 18.26 bar

Screens 25.4 mm long porosity = 0.665 Wire diameter = 191µm

Pressure drop error (Pa) 586 Constant mass flow error (kg/s) 1.2E-4

Point #	Re	Mass flow (kg/s)		Pressure drop (Pa)	Re power	P ratio	
3	397.7	3.56E-3±	3%	1805± 32%	-0.33	1.92±	32%
4	397.8	3.56E-3±	3%	1814± 32%	-0.33	1.93±	32%
5	517.3	4.63E-3±	3%	2849± 21%	-0.33	1.93±	22%
6	517	4.63E-3±	3%	2844± 21%	-0.33	1.93±	22%
7	649.4	5.83E-3±	2%	4182± 14%	-0.33	1.92±	14%
8	649.9	5.82E-3±	2%	4201± 14%	-0.33	1.94±	14%
9	779.8	6.98E-3±	2%	5884± 10%	-0.33	1.99±	11%
10	785.5	7.03E-3±	2%	5888± 10%	-0.33	1.96±	11%
11	901.3	8.08E-3±	1%	7350± 8%	-0.33	1.91±	8%
12	899.7	8.07E-3±	1%	7369± 8%	-0.33	1.92±	8%
13	1052	9.46E-3±	1%	9661± 6%	-0.33	1.90±	6%
14	1057	9.45E-3±	1%	9671± 6%	-0.33	1.91±	6%
15	1148	1.03E-2±	1%	11160± 5%	-0.33	1.89±	5%
16	1148	1.03E-2±	1%	11180± 5%	-0.33	1.90±	5%
17	1222	1.10E-2±	1%	12420± 5%	-0.33	1.88±	5%
18	1226	1.10E-2±	1%	12430± 5%	-0.33	1.89±	5%
19	1302	1.17E-2±	1%	13790± 4%	-0.33	1.87±	4%
20	1301	1.17E-2±	1%	13770± 4%	-0.33	1.86±	4%
21	1376	1.23E-2±	1%	15150± 4%	-0.33	1.86±	4%
22	1375	1.24E-2±	1%	15140± 4%	-0.33	1.86±	4%

Run# 92 Fluid : air Pressure : 7.00 bar

Fibers 12.85 mm long porosity = 0.84 Wire diameter = 13 µm

Pressure drop error (Pa) 586 Constant mass flow error (kg/s) 1.6E-4

Point#	Re	Mass flow (kg/s)		Pressure drop (Pa)		Re power	Pratio	
1	14.73	9.42E-4 ±	17 %	4390 ±	13 %	-1.000	1.82 ±	22 %
2	14.64	9.36E-4 ±	17 %	4391 ±	13 %	-1.000	1.83 ±	22 %
3	22.08	1.41E-3 ±	11 %	7016 ±	8 %	-1.000	1.83 ±	14 %
4	22.11	1.41E-3 ±	11 %	7021 ±	8 %	-1.000	1.83 ±	14 %
5	28.88	1.85E-3 ±	9 %	9832 ±	6 %	-1.000	1.86 ±	11 %
6	28.97	1.85E-3 ±	9 %	9848 ±	6 %	-1.000	1.85 ±	10 %
7	34.54	2.21E-3 ±	7 %	12300 ±	5 %	-1.000	1.88 ±	9 %
8	34.51	2.21E-3 ±	7 %	12270 ±	5 %	-1.000	1.87 ±	9 %
9	40.75	2.61E-3 ±	6 %	15280 ±	4 %	-1.000	1.88 ±	7 %
10	40.71	2.60E-3 ±	6 %	15250 ±	4 %	-1.000	1.88 ±	7 %
11	48.26	3.09E-3 ±	5 %	19000 ±	3 %	-1.000	1.88 ±	6 %
12	48.15	3.08E-3 ±	5 %	19000 ±	3 %	-1.000	1.89 ±	6 %
13	55.18	3.54E-3 ±	5 %	22820 ±	3 %	-1.000	1.89 ±	5 %
14	55.28	3.54E-3 ±	5 %	22820 ±	3 %	-1.000	1.89 ±	5 %
15	60.39	3.87E-3 ±	4 %	25730 ±	2 %	-1.000	1.88 ±	5 %
16	60.38	3.86E-3 ±	4 %	25760 ±	2 %	-1.000	1.90 ±	5 %
17	66.43	4.25E-3 ±	4 %	29170 ±	2 %	-1.000	1.90 ±	4 %
18	66.29	4.25E-3 ±	4 %	29160 ±	2 %	-1.000	1.88 ±	4 %

Run# 93

Fluid : nitrogen — Pressure : 18.26 bar

Fibers 12.85 mm long porosity = 0.84 — Wire diameter = 13 µm

Pressure drop error (Pa) 586 — Constant mass flow error (kg/s) 1.2E-4

Point#	Re	Mass flow (kg/s)			Pressure drop (Pa)			Re power	Pratio		
1	44.99	2.89E-3	±	4 %	7170	±	8 %	-1.000	1.89	±	9 %
2	44.78	2.88E-3	±	4 %	7178	±	8 %	-1.000	1.92	±	9 %
3	62.08	3.99E-3	±	3 %	10960	±	5 %	-1.000	1.89	±	6 %
4	62.08	3.99E-3	±	3 %	10940	±	5 %	-1.000	1.89	±	6 %
5	77.97	5.00E-3	±	2 %	14970	±	4 %	-1.000	1.89	±	5 %
6	77.85	5.00E-3	±	2 %	14920	±	4 %	-1.000	1.88	±	5 %
7	102.5	6.59E-3	±	2 %	22040	±	3 %	-1.000	1.87	±	3 %
8	102.5	6.59E-3	±	2 %	22030	±	3 %	-1.000	1.86	±	3 %
9	117.6	7.56E-3	±	2 %	27000	±	2 %	-1.000	1.86	±	3 %
10	118	7.59E-3	±	2 %	27000	±	2 %	-1.000	1.84	±	3 %
11	131.2	8.44E-3	±	1 %	31280	±	2 %	-1.000	1.81	±	2 %
12	130.8	8.43E-3	±	1 %	31260	±	2 %	-1.000	1.80	±	2 %
13	127.5	8.21E-3	±	1 %	29920	±	2 %	-1.000	1.81	±	2 %
14	127.5	8.21E-3	±	1 %	29950	±	2 %	-1.000	1.82	±	2 %

Run# 94

Fluid : nitrogen — Pressure : 18.26 bar

Fibers 12.85 mm long porosity = 0.84 — Wire diameter = 13 µm

Pressure drop error (Pa) 586 — Constant mass flow error (kg/s) 1.2E-4

Point#	Re	Mass flow (kg/s)			Pressure drop (Pa)			Re power	Pratio		
1	40.5	2.60E-3	±	5 %	6309	±	9 %	-1.000	1.94	±	10 %
2	40.65	2.61E-3	±	5 %	6297	±	9 %	-1.000	1.93	±	10 %
3	57.99	3.72E-3	±	3 %	10090	±	6 %	-1.000	1.93	±	7 %
4	58.06	3.72E-3	±	3 %	10090	±	6 %	-1.000	1.92	±	7 %
5	77.22	4.95E-3	±	2 %	15010	±	4 %	-1.000	1.91	±	5 %
6	77.24	4.96E-3	±	2 %	15020	±	4 %	-1.000	1.92	±	5 %
7	97.92	6.28E-3	±	2 %	20780	±	3 %	-1.000	1.89	±	3 %
8	97.53	6.26E-3	±	2 %	20620	±	3 %	-1.000	1.89	±	3 %
9	116.2	7.47E-3	±	2 %	26650	±	2 %	-1.000	1.87	±	3 %
10	116.4	7.47E-3	±	2 %	26670	±	2 %	-1.000	1.87	±	3 %
11	131.3	8.43E-3	±	1 %	31760	±	2 %	-1.000	1.84	±	2 %
12	131.2	8.42E-3	±	1 %	31730	±	2 %	-1.000	1.84	±	2 %

Run # 95 Fluid: air Pressure: 7.00 bar

Screens 12.7 mm long porosity = 0.665 Wire diameter = 53µm

Pressure drop error (Pa) 586 Constant mass flow error (kg/s) 1.6E-4

Point #	Re	Mass flow (kg/s)	Pressure drop (Pa)	Re power	P ratio
1	29.64	9.49E-4± 17%	1557± 38%	-0.33	1.42± 47%
2	29.42	9.42E-4± 17%	1560± 38%	-0.33	1.44± 47%
3	42.97	1.38E-3± 12%	2595± 23%	-0.33	1.46± 31%
4	42.91	1.37E-3± 12%	2600± 23%	-0.33	1.47± 31%
5	60.19	1.93E-3± 8%	4163± 14%	-0.33	1.48± 19%
6	60.07	1.92E-3± 8%	4174± 14%	-0.33	1.49± 19%
7	74.44	2.38E-3± 7%	5676± 10%	-0.33	1.49± 15%
8	74.51	2.39E-3± 7%	5687± 10%	-0.33	1.49± 15%
9	74.51	2.39E-3± 7%	5687± 10%	-0.33	1.49± 15%
10	85.85	2.75E-3± 6%	7008± 8%	-0.33	1.49± 13%
11	85.77	2.75E-3± 6%	7011± 8%	-0.33	1.49± 13%
12	101.1	3.24E-3± 5%	8977± 7%	-0.33	1.49± 11%
13	101	3.24E-3± 5%	8973± 7%	-0.33	1.50± 11%
14	114.4	3.67E-3± 4%	10830± 5%	-0.33	1.50± 8%
15	114.2	3.67E-3± 4%	10850± 5%	-0.33	1.50± 8%
16	125.5	4.02E-3± 4%	12420± 5%	-0.33	1.50± 8%
17	125.4	4.02E-3± 4%	12460± 5%	-0.33	1.50± 8%
18	138.5	4.43E-3± 4%	14490± 4%	-0.33	1.50± 8%
19	138.3	4.44E-3± 4%	14500± 4%	-0.33	1.50± 8%
20	154	4.94E-3± 3%	17120± 3%	-0.33	1.50± 6%
21	153.7	4.93E-3± 3%	17120± 3%	-0.33	1.50± 6%

Run # 96 Fluid: nitrogen Pressure: 18.26 bar

Screens 12.7 mm long porosity = 0.665 Wire diameter = 53µm

Pressure drop error (Pa) 586 Constant mass flow error (kg/s) 1.2E-4

Point #	Re	Mass flow (kg/s)	Pressure drop (Pa)	Re power	P ratio
1	79.27	2.55E-3± 5%	2521± 23%	-0.33	1.49± 24%
2	79.13	2.54E-3± 5%	2517± 23%	-0.33	1.51± 24%
3	115.1	3.70E-3± 3%	4438± 13%	-0.33	1.50± 14%
4	115.2	3.70E-3± 3%	4444± 13%	-0.33	1.51± 14%
5	162.2	5.21E-3± 2%	7499± 8%	-0.33	1.51± 9%
6	162.6	5.22E-3± 2%	7512± 8%	-0.33	1.51± 9%
7	201.3	6.47E-3± 2%	10500± 6%	-0.33	1.50± 7%
8	201.1	6.46E-3± 2%	10520± 6%	-0.33	1.50± 7%
9	243.3	7.83E-3± 2%	14290± 4%	-0.33	1.48± 5%
10	243.5	7.83E-3± 2%	14300± 4%	-0.33	1.49± 5%
11	243.6	7.84E-3± 2%	14300± 4%	-0.33	1.50± 5%
12	243.3	7.83E-3± 2%	14300± 4%	-0.33	1.47± 5%
13	243.8	7.84E-3± 2%	14270± 4%	-0.33	1.49± 5%
14	243.9	7.84E-3± 2%	14330± 4%	-0.33	1.47± 5%
15	244.2	7.84E-3± 2%	14320± 4%	-0.33	1.49± 5%
16	286.2	9.21E-3± 1%	18420± 3%	-0.33	1.46± 3%
17	286	9.21E-3± 1%	18440± 3%	-0.33	1.47± 3%
18	308.9	9.95E-3± 1%	20840± 3%	-0.33	1.46± 3%
19	309.5	9.96E-3± 1%	20850± 3%	-0.33	1.46± 3%
20	330.5	1.06E-2± 1%	23170± 3%	-0.33	1.45± 3%
21	330.4	1.06E-2± 1%	23130± 3%	-0.33	1.45± 3%
22	352.9	1.14E-2± 1%	25970± 2%	-0.33	1.46± 3%
23	354.2	1.14E-2± 1%	25970± 2%	-0.33	1.46± 3%
24	382	1.23E-2± 1%	29310± 2%	-0.33	1.44± 3%
25	381.2	1.23E-2± 1%	29280± 2%	-0.33	1.43± 3%

Run# 97 Fluid : air Pressure : 7.00 bar

Fibers 25.4 mm long porosity = 0.8 Wire diameter = 89 µm

Pressure drop error (Pa) 586 Constant mass flow error (kg/s) 1.6E-4

Point#	Re	Mass flow (kg/s)	Pressure drop (Pa)	Re power	Pratio
7	229.3	2.62E-3 ± 6 %	1624 ± 36 %	-1.000	1.13 ± 37 %
8	228.8	2.62E-3 ± 6 %	1622 ± 36 %	-1.000	1.13 ± 37 %
9	273.2	3.12E-3 ± 5 %	2160 ± 27 %	-1.000	1.11 ± 28 %
10	273.9	3.13E-3 ± 5 %	2157 ± 27 %	-1.000	1.11 ± 28 %
11	317.1	3.64E-3 ± 4 %	2779 ± 21 %	-1.000	1.10 ± 22 %
12	318.2	3.64E-3 ± 4 %	2775 ± 21 %	-1.000	1.10 ± 22 %
13	348.8	3.99E-3 ± 4 %	3236 ± 18 %	-1.000	1.09 ± 19 %
14	348.8	3.99E-3 ± 4 %	3230 ± 18 %	-1.000	1.08 ± 19 %
15	374.5	4.28E-3 ± 4 %	3653 ± 16 %	-1.000	1.08 ± 16 %
16	375.9	4.30E-3 ± 4 %	3662 ± 16 %	-1.000	1.08 ± 16 %
17	409.5	4.68E-3 ± 3 %	4216 ± 14 %	-1.000	1.07 ± 14 %
18	409.3	4.68E-3 ± 3 %	4219 ± 14 %	-1.000	1.07 ± 14 %
19	437.5	5.00E-3 ± 3 %	4712 ± 12 %	-1.000	1.06 ± 13 %
20	436	5.00E-3 ± 3 %	4710 ± 12 %	-1.000	1.05 ± 13 %

Run # 98 Fluid: nitrogen Pressure 18.26 bar

Fibers 25.4 mm long porosity = 0.8 Wire diameter = 89µm

Pressure drop error (Pa) 586 Constant mass flow error (kg/s) 1.2E-4

Point #	Re	Mass flow (kg/s)	Pressure drop (Pa)	Re power	P ratio
1	356.9	4.09E-3± 3%	1208± 49%	-1.00	0.97± 49%
2	357.6	4.10E-3± 3%	1218± 48%	-1.00	0.98± 48%
3	450.8	5.17E-3± 2%	1857± 32%	-1.00	0.98± 32%
4	450.9	5.17E-3± 2%	1868± 31%	-1.00	0.99± 31%
5	539.8	6.19E-3± 2%	2537± 23%	-1.00	0.97± 23%
6	538.2	6.18E-3± 2%	2547± 23%	-1.00	0.97± 23%
7	610.4	7.01E-3± 2%	3176± 18%	-1.00	0.96± 19%
8	612.1	7.02E-3± 2%	3179± 18%	-1.00	0.96± 19%
9	711.7	8.17E-3± 1%	4116± 14%	-1.00	0.94± 14%
10	711.1	8.17E-3± 1%	4125± 14%	-1.00	0.94± 14%
11	711.9	8.17E-3± 1%	4136± 14%	-1.00	0.94± 14%
12	810.4	9.32E-3± 1%	5194± 11%	-1.00	0.92± 11%
13	810.6	9.32E-3± 1%	5190± 11%	-1.00	0.92± 11%
14	876.7	1.01E-2± 1%	5918± 10%	-1.00	0.91± 10%
15	875.5	1.01E-2± 1%	5927± 10%	-1.00	0.90± 10%
16	951.3	1.09E-2± 1%	6819± 9%	-1.00	0.89± 9%
17	951.2	1.09E-2± 1%	6821± 9%	-1.00	0.90± 9%
18	1047	1.21E-2± 1%	8012± 7%	-1.00	0.87± 7%
19	1110	1.28E-2± 1%	8837± 7%	-1.00	0.86± 7%
20	1108	1.28E-2± 1%	8774± 7%	-1.00	0.85± 7%

Run # 99 Fluid: air Pressure: 7.00 bar

Screens 12.7 mm long porosity = 0.68 Wire diameter = 41μm

Pressure drop error (Pa) 586 Constant mass flow error (kg/s) 1.6E-4

Point #	Re	Mass flow (kg/s)	Pressure drop (Pa)	Re power	P ratio
1	28.29	1.13E-3± 14%	2136± 27%	-0.33	1.14± 36%
2	28.24	1.13E-3± 14%	2142± 27%	-0.33	1.14± 36%
3	39	1.56E-3± 10%	3368± 17%	-0.33	1.18± 24%
4	39.32	1.57E-3± 10%	3364± 17%	-0.33	1.17± 24%
5	49.3	1.97E-3± 8%	4629± 13%	-0.33	1.19± 19%
6	49.26	1.97E-3± 8%	4635± 13%	-0.33	1.19± 19%
7	60.02	2.40E-3± 7%	6157± 10%	-0.33	1.20± 15%
8	59.83	2.39E-3± 7%	6155± 10%	-0.33	1.20± 15%
9	71.41	2.85E-3± 6%	7880± 7%	-0.33	1.20± 12%
10	71.31	2.85E-3± 6%	7878± 7%	-0.33	1.20± 12%
11	80.9	3.23E-3± 5%	9451± 6%	-0.33	1.20± 10%
12	80.74	3.22E-3± 5%	9449± 6%	-0.33	1.20± 10%
13	89.38	3.58E-3± 4%	11070± 5%	-0.33	1.20± 8%
14	90.03	3.59E-3± 4%	11080± 5%	-0.33	1.20± 8%
15	98.59	3.94E-3± 4%	12750± 5%	-0.33	1.21± 8%
16	98.63	3.94E-3± 4%	12740± 5%	-0.33	1.21± 8%
17	106.3	4.26E-3± 4%	14320± 4%	-0.33	1.21± 8%
18	106.7	4.26E-3± 4%	14310± 4%	-0.33	1.21± 8%
19	115	4.59E-3± 3%	16060± 4%	-0.33	1.21± 6%
20	115.1	4.59E-3± 3%	16050± 4%	-0.33	1.21± 6%
21	124.5	4.98E-3± 3%	18130± 3%	-0.33	1.20± 6%
22	124.2	4.98E-3± 3%	18120± 3%	-0.33	1.20± 6%

Run # 100 Fluid: nitrogen Pressure: 18.26 bar

Screens 12.7 mm long porosity = 0.68 Wire diameter = 41μm

Pressure drop error (Pa) 586 Constant mass flow error (kg/s) 1.2E-4

Point #	Re	Mass flow (kg/s)	Pressure drop (Pa)	Re power	P ratio
1	62.46	2.50E-3± 5%	2607± 22%	-0.33	1.20± 24%
2	62.26	2.49E-3± 5%	2636± 22%	-0.33	1.22± 24%
3	93.28	3.74E-3± 3%	4754± 12%	-0.33	1.21± 13%
4	93.23	3.74E-3± 3%	4740± 12%	-0.33	1.21± 13%
5	135.4	5.43E-3± 2%	8332± 7%	-0.33	1.21± 8%
6	135.2	5.43E-3± 2%	8324± 7%	-0.33	1.20± 8%
7	169	6.78E-3± 2%	11650± 5%	-0.33	1.20± 6%
8	168.7	6.77E-3± 2%	11650± 5%	-0.33	1.20± 6%
9	198.7	7.97E-3± 2%	15000± 4%	-0.33	1.18± 5%
10	198.4	7.96E-3± 2%	14980± 4%	-0.33	1.19± 5%
11	230.9	9.27E-3± 1%	18960± 3%	-0.33	1.17± 3%
12	231.2	9.27E-3± 1%	18990± 3%	-0.33	1.17± 3%
13	249.8	1.00E-2± 1%	21330± 3%	-0.33	1.16± 3%
14	250	1.00E-2± 1%	21320± 3%	-0.33	1.16± 3%
15	268.4	1.08E-2± 1%	23850± 2%	-0.33	1.15± 3%
16	268.5	1.08E-2± 1%	23820± 2%	-0.33	1.15± 3%
17	293	1.18E-2± 1%	26960± 2%	-0.33	1.12± 3%
18	292.7	1.18E-2± 1%	27010± 2%	-0.33	1.14± 3%
19	313	1.26E-2± 1%	29950± 2%	-0.33	1.13± 3%
20	313.4	1.26E-2± 1%	29960± 2%	-0.33	1.13± 3%

Run # 108 Fluid: air Pressure: 7.00 bar

Screens 22.23 mm long porosity = 0.606 Wire diameter = 53µm

Pressure drop error (Pa) 586 Constant mass flow error (kg/s) 1.6E-4

Point #	Re	Mass flow (kg/s)		Pressure drop (Pa)	Re power	P ratio	
1	19.98	8.23E-4±	19%	2292± 26%	-0.33	0.87±	41%
2	20.07	8.27E-4±	19%	2293± 26%	-0.33	0.86±	41%
3	34.09	1.41E-3±	11%	4580± 13%	-0.33	0.92±	23%
4	34.12	1.41E-3±	11%	4594± 13%	-0.33	0.92±	23%
5	46.92	1.93E-3±	8%	7056± 8%	-0.33	0.94±	16%
6	47.02	1.94E-3±	8%	7054± 8%	-0.33	0.94±	16%
7	56.77	2.34E-3±	7%	9239± 6%	-0.33	0.95±	13%
8	56.64	2.33E-3±	7%	9244± 6%	-0.33	0.96±	13%
9	65.91	2.72E-3±	6%	11470± 5%	-0.33	0.96±	11%
10	66.05	2.72E-3±	6%	11480± 5%	-0.33	0.96±	11%
11	78.71	3.25E-3±	5%	14860± 4%	-0.33	0.96±	9%
12	78.92	3.25E-3±	5%	14840± 4%	-0.33	0.97±	9%
13	90.57	3.73E-3±	4%	18280± 3%	-0.33	0.97±	7%
14	89.95	3.73E-3±	4%	18300± 3%	-0.33	0.96±	7%
15	100.1	4.14E-3±	4%	21380± 3%	-0.33	0.98±	7%
16	100.1	4.13E-3±	4%	21390± 3%	-0.33	0.98±	7%
17	109.2	4.51E-3±	4%	24360± 2%	-0.33	0.98±	7%
18	109.3	4.52E-3±	4%	24360± 2%	-0.33	0.98±	7%
19	118.2	4.86E-3±	3%	27250± 2%	-0.33	0.99±	5%
20	117.6	4.87E-3±	3%	27280± 2%	-0.33	0.98±	5%

Run # 109 Fluid: nitrogen Pressure: 18.26 bar

Screens 22.23 mm long porosity = 0.606 Wire diameter = 53µm

Pressure drop error (Pa) 586 Constant mass flow error (kg/s) 1.2E-4

Point #	Re	Mass flow (kg/s)		Pressure drop (Pa)	Re power	P ratio	
1	40.41	1.67E-3±	7%	2284± 26%	-0.33	0.92±	29%
2	40.52	1.67E-3±	7%	2345± 25%	-0.33	0.94±	28%
3	72.03	2.98E-3±	4%	5232± 11%	-0.33	0.96±	13%
4	72.12	2.98E-3±	4%	5242± 11%	-0.33	0.96±	13%
5	98.34	4.07E-3±	3%	8394± 7%	-0.33	0.97±	9%
6	98.53	4.07E-3±	3%	8399± 7%	-0.33	0.98±	9%
7	125.9	5.21E-3±	2%	12200± 5%	-0.33	0.98±	6%
8	126.2	5.22E-3±	2%	12190± 5%	-0.33	0.98±	6%
9	156.1	6.47E-3±	2%	17070± 3%	-0.33	0.98±	4%
10	156	6.46E-3±	2%	17040± 3%	-0.33	0.98±	4%
11	186.7	7.73E-3±	2%	22520± 3%	-0.33	0.97±	4%
12	186.5	7.72E-3±	2%	22560± 3%	-0.33	0.98±	4%
13	219.3	9.09E-3±	1%	28850± 2%	-0.33	0.97±	3%
14	219	9.09E-3±	1%	28900± 2%	-0.33	0.99±	3%
15	237.8	9.85E-3±	1%	32790± 2%	-0.33	0.97±	3%
16	237.9	9.86E-3±	1%	32830± 2%	-0.33	0.98±	3%

Run # 110 Fluid: air Pressure: 7.00 bar

Screens 25.4 mm long porosity = 0.614 Wire diameter = 41µm

Pressure drop error (Pa) 586 Constant mass flow error (kg/s) 1.6E-4

Point #	Re	Mass flow (kg/s)	Pressure drop (Pa)	Re power	P ratio
1	13.34	7.16E-4± 22%	3728± 16%	-0.33	0.93± 40%
2	13.47	7.23E-4± 22%	3735± 16%	-0.33	0.92± 40%
3	21.92	1.18E-3± 14%	6852± 9%	-0.33	1.00± 25%
4	22.02	1.18E-3± 14%	6858± 9%	-0.33	1.00± 25%
5	29.15	1.56E-3± 10%	9939± 6%	-0.33	1.04± 18%
6	29.16	1.56E-3± 10%	9940± 6%	-0.33	1.04± 18%
7	37.65	2.02E-3± 8%	13880± 4%	-0.33	1.06± 14%
8	37.53	2.01E-3± 8%	13890± 4%	-0.33	1.06± 14%
9	48.05	2.58E-3± 6%	19500± 3%	-0.33	1.08± 10%
10	48	2.58E-3± 6%	19510± 3%	-0.33	1.08± 10%
11	56.77	3.05E-3± 5%	24580± 2%	-0.33	1.08± 9%
12	56.79	3.04E-3± 5%	24590± 2%	-0.33	1.09± 9%
13	63.4	3.41E-3± 5%	28800± 2%	-0.33	1.09± 9%
14	63.38	3.40E-3± 5%	28790± 2%	-0.33	1.09± 9%
15	68.65	3.68E-3± 4%	32150± 2%	-0.33	1.10± 7%
16	68.44	3.67E-3± 4%	32150± 2%	-0.33	1.10± 7%

Run # 112 Fluid: air Pressure: 7.00 bar

Screens 25.4 mm long porosity = 0.614 Wire diameter = 41µm

Pressure drop error (Pa) 586 Constant mass flow error (kg/s) 1.6E-4

Point #	Re	Mass flow (kg/s)	Pressure drop (Pa)	Re power	P ratio
3	16.04	8.62E-4± 19%	4912± 12%	-0.33	1.01± 34%
4	15.95	8.57E-4± 19%	4923± 12%	-0.33	1.02± 34%

Run # 113 Fluid: air Pressure: 7.00 bar

Screens 25.4 mm long porosity = 0.614 Wire diameter = 41μm

Pressure drop error (Pa) 586 Constant mass flow error (kg/s) 1.6E-4

Point #	Re	Mass flow (kg/s)	Pressure drop (Pa)	Re power	P ratio
3	13.82	7.43E-4± 22%	4096± 14%	-0.33	0.98± 39%
4	13.88	7.45E-4± 21%	4091± 14%	-0.33	0.98± 38%
5	20.52	1.10E-3± 15%	6559± 9%	-0.33	1.03± 27%
6	20.51	1.10E-3± 15%	6561± 9%	-0.33	1.03± 27%
7	29.01	1.56E-3± 10%	10130± 6%	-0.33	1.07± 18%
8	28.93	1.55E-3± 10%	10150± 6%	-0.33	1.07± 18%
9	38.32	2.06E-3± 8%	14680± 4%	-0.33	1.09± 14%
10	38.4	2.06E-3± 8%	14680± 4%	-0.33	1.08± 14%
11	47.75	2.56E-3± 6%	19900± 3%	-0.33	1.11± 10%
12	47.76	2.57E-3± 6%	19890± 3%	-0.33	1.10± 10%
13	56.42	3.04E-3± 5%	24960± 2%	-0.33	1.11± 9%
14	56.62	3.04E-3± 5%	24960± 2%	-0.33	1.11± 9%
15	63.48	3.40E-3± 5%	29360± 2%	-0.33	1.12± 9%
16	63.31	3.40E-3± 5%	29370± 2%	-0.33	1.12± 9%
17	67.6	3.64E-3± 4%	32250± 2%	-0.33	1.12± 7%
18	67.74	3.64E-3± 4%	32220± 2%	-0.33	1.12± 7%

Run # 115 Fluid: nitrogen Pressure: 18.26 bar

Screens 25.4 mm long porosity = 0.614 Wire diameter = 41μm

Pressure drop error (Pa) 586 Constant mass flow error (kg/s) 1.2E-4

Point #	Re	Mass flow (kg/s)	Pressure drop (Pa)	Re power	P ratio
1	25.02	1.34E-3± 9%	3326± 18%	-0.33	1.06± 23%
2	24.92	1.33E-3± 9%	3302± 18%	-0.33	1.05± 23%
3	40.64	2.17E-3± 6%	6258± 9%	-0.33	1.08± 13%
4	40.74	2.18E-3± 6%	6265± 9%	-0.33	1.09± 13%
5	65.74	3.51E-3± 3%	12390± 5%	-0.33	1.11± 7%
6	65.63	3.51E-3± 3%	12400± 5%	-0.33	1.12± 7%
7	88.93	4.75E-3± 3%	19010± 3%	-0.33	1.12± 6%
8	88.87	4.75E-3± 3%	19010± 3%	-0.33	1.12± 6%
9	105.2	5.63E-3± 2%	24460± 2%	-0.33	1.12± 4%
10	105.1	5.62E-3± 2%	24460± 2%	-0.33	1.12± 4%
11	125.4	6.71E-3± 2%	31560± 2%	-0.33	1.11± 4%
12	125.2	6.70E-3± 2%	31520± 2%	-0.33	1.11± 4%
13	127.4	6.82E-3± 2%	32300± 2%	-0.33	1.11± 4%
14	127.3	6.81E-3± 2%	32240± 2%	-0.33	1.11± 4%

Oscillating Flow Test Results

Run number 5 Sample type: tubes L/D = 5

12.7 mm long 2.375 mm diameter Entrance loss = 1.8 helium 80 Hz

Point	Xp (mm)	P (bar)	Re max	Re w	Ar	Mach#	ΔP (Pa)	pV (W)	Euler#	TDF
6	0.72	14.47	7,717	98.4	3.67	0.03	1.52E3	0.09	1.72	0.94 ±40%
7	0.72	14.38	7,690	97.8	3.68	0.03	1.53E3	0.09	1.72	0.95 ±40%
8	0.97	14.54	10,580	99.2	4.99	0.04	3.17E3	0.22	1.91	0.94 ±23%
9	1.21	14.70	13,210	100.0	6.18	0.05	4.80E3	0.42	1.88	0.96 ±16%
10	1.49	14.61	16,100	98.8	7.62	0.06	6.87E3	0.76	1.78	0.95 ±12%
11	1.97	14.45	21,010	97.7	10.05	0.07	1.24E4	1.82	1.86	1.00 ±8%
12	2.48	14.55	26,430	98.1	12.60	0.09	1.88E4	3.52	1.80	0.99 ±6%
13	2.70	14.71	28,970	98.7	13.72	0.10	2.24E4	4.57	1.78	0.98 ±6%
14	2.98	14.57	31,600	97.7	15.12	0.11	2.73E4	6.07	1.81	0.99 ±5%
15	0.97	17.07	10,320	97.4	4.96	0.03	2.55E3	0.15	1.85	0.93 ±27%
16	1.94	17.05	20,640	97.5	9.90	0.06	1.07E4	1.25	1.94	0.99 ±9%
17	0.98	28.92	20,750	194.0	5.00	0.04	6.10E3	0.42	1.86	0.93 ±15%
18	1.48	28.78	31,370	193.6	7.58	0.06	1.36E4	1.50	1.82	0.98 ±9%
19	2.00	28.90	42,230	193.3	10.22	0.08	2.37E4	3.47	1.74	0.93 ±6%

Run number 6 Sample type: tubes L/D = 152

360 mm long 2.375 mm diameter Entrance loss = 1.8 helium 94 Hz

Point	Xp (mm)	P (bar)	Re max	Re w	Ar	Mach#	ΔP (Pa)	pV (W)	Euler#	TDF
1	0.73	14.43	10,360	97.2	0.18	0.04	2.26E4	0.59	13.89	0.76 ±13%
2	0.73	14.49	10,380	97.5	0.18	0.04	2.25E4	0.59	13.79	0.76 ±13%
3	0.95	14.65	13,490	98.1	0.23	0.05	3.06E4	1.25	11.16	0.77 ±11%
4	1.20	14.57	16,630	97.2	0.28	0.06	3.76E4	2.25	8.92	0.76 ±10%
6	1.74	14.52	23,060	95.8	0.40	0.08	5.63E4	5.64	6.82	0.72 ±9%
7	1.99	14.59	25,970	95.6	0.45	0.09	6.72E4	8.41	6.39	0.76 ±9%
8	2.20	14.54	27,760	94.0	0.49	0.10	7.62E4	11.40	6.19	0.83 ±10%
9	2.20	14.65	27,880	94.4	0.49	0.10	7.67E4	11.64	6.20	0.84 ±10%
10	2.47	14.06	29,720	89.9	0.55	0.11	8.91E4	16.06	6.02	0.88 ±10%
11	2.51	14.65	30,920	92.9	0.55	0.11	9.21E4	16.56	5.92	0.85 ±10%
12	0.99	28.99	25,810	185.7	0.23	0.05	5.50E4	2.27	10.19	0.78 ±10%
13	1.46	28.64	37,340	184.0	0.33	0.07	9.32E4	7.54	8.18	0.91 ±9%

Run number 7 Sample type: tubes L/D = 102

241.3 mm long 2.375 mm diameter Entrance loss = 1.8 helium 94 Hz

Point	Xp (mm)	P (bar)	Re max	Re w	Ar	Mach#	ΔP (Pa)	pV (W)	Euler#	TDF
1	0.71	14.70	9,165	98.7	0.23	0.03	1.38E4	0.31	10.97	0.77 ±14%
2	0.71	14.59	9,153	97.8	0.23	0.03	1.38E4	0.31	10.91	0.77 ±14%
3	0.72	14.55	9,315	97.7	0.23	0.03	1.41E4	0.33	10.77	0.77 ±14%
4	0.97	14.45	12,270	96.9	0.31	0.04	1.96E4	0.76	8.55	0.79 ±11%
5	1.22	14.47	15,350	97.0	0.39	0.05	2.55E4	1.43	7.10	0.79 ±9%
6	1.46	14.60	18,350	97.9	0.46	0.06	3.16E4	2.31	6.22	0.78 ±8%
7	1.71	14.69	21,480	98.4	0.54	0.08	3.94E4	3.71	5.69	0.80 ±7%
8	1.95	14.52	24,130	97.0	0.61	0.09	4.73E4	5.32	5.33	0.80 ±7%
9	2.22	14.51	26,990	96.3	0.69	0.10	5.53E4	7.75	4.93	0.84 ±7%
10	2.47	14.55	29,770	95.9	0.76	0.11	6.33E4	10.64	4.61	0.87 ±7%
11	2.68	14.63	32,270	96.5	0.82	0.11	6.80E4	13.52	4.24	0.89 ±7%
12	2.89	14.55	34,170	95.2	0.88	0.12	7.57E4	16.71	4.14	0.91 ±7%
13	2.92	14.73	34,650	95.6	0.89	0.12	7.74E4	17.22	4.11	0.90 ±7%
14	0.95	28.85	23,420	190.6	0.30	0.04	3.58E4	1.19	8.37	0.74 ±10%
15	1.45	28.81	35,620	191.1	0.46	0.06	6.48E4	4.52	6.58	0.87 ±7%
16	1.92	28.75	46,450	189.7	0.60	0.08	8.94E4	10.21	5.28	0.92 ±7%

Run number 8 Sample type: tubes L/D = 64

152.4 mm long 2.375 mm diameter Entrance loss = 1.8 helium 94 Hz

Point	Xp (mm)	P (bar)	Re max	Re w	Ar	Mach#	ΔP (Pa)	pV (W)	Euler#	TDF
1	0.72	14.85	8,909	100.7	0.34	0.03	1.09E4	0.22	9.41	0.83 ±15%
2	0.73	14.46	8,824	98.1	0.35	0.03	1.08E4	0.23	9.24	0.84 ±15%
3	1.01	14.48	12,040	98.3	0.48	0.04	1.52E4	0.56	7.01	0.85 ±11%
4	1.23	14.32	14,520	97.1	0.58	0.05	1.91E4	1.01	5.98	0.88 ±9%
5	1.44	14.23	16,840	96.6	0.68	0.06	2.17E4	1.63	5.03	0.92 ±8%
6	1.51	14.36	17,770	97.3	0.71	0.06	2.40E4	1.84	5.03	0.90 ±8%
7	1.72	14.60	20,330	98.4	0.80	0.07	2.84E4	2.67	4.59	0.91 ±7%
8	2.00	14.57	23,560	98.1	0.94	0.08	3.34E4	4.18	4.01	0.93 ±6%
9	2.24	14.63	26,280	98.3	1.04	0.09	3.78E4	5.81	3.65	0.94 ±6%
10	2.46	14.67	28,750	98.3	1.14	0.10	4.18E4	7.62	3.36	0.95 ±6%
11	2.70	14.54	31,110	97.1	1.25	0.11	4.64E4	9.90	3.15	0.97 ±6%
12	2.96	14.61	34,190	97.5	1.37	0.12	5.23E4	12.96	2.95	0.97 ±6%
13	0.96	28.98	22,310	192.8	0.45	0.04	2.85E4	0.86	7.45	0.85 ±11%
14	1.46	28.82	34,090	193.6	0.69	0.06	3.97E4	3.14	4.48	0.94 ±7%
15	1.94	28.83	44,920	192.6	0.91	0.08	5.73E4	7.23	3.70	0.96 ±6%

Run number 9 Sample type: tubes L/D = 126

300 mm long 2.375 mm diameter Entrance loss = 1.8 helium 94 Hz

Point	Xp (mm)	P (bar)	Re max	Re w	Ar	Mach#	ΔP (Pa)	pV (W)	Euler#	TDF
1	0.71	14.67	9,770	99.4	0.19	0.03	1.74E4	0.40	12.33	0.73 ±13%
2	0.96	14.53	12,980	98.3	0.26	0.05	2.50E4	0.96	9.91	0.75 ±11%
3	1.21	14.56	16,200	98.1	0.33	0.06	3.19E4	1.76	8.10	0.74 ±9%
4	1.50	15.18	20,430	102.1	0.40	0.07	4.01E4	3.10	6.64	0.73 ±8%
5	1.47	14.61	19,370	98.0	0.39	0.07	3.90E4	2.91	6.90	0.73 ±8%
6	1.72	14.69	22,500	98.2	0.45	0.08	4.77E4	4.59	6.27	0.75 ±8%
7	1.95	14.52	25,030	97.2	0.51	0.09	5.65E4	6.70	5.93	0.79 ±8%
8	2.23	14.64	28,250	97.1	0.58	0.10	6.73E4	9.94	5.52	0.84 ±8%
9	2.49	14.65	31,230	96.7	0.64	0.11	7.83E4	13.79	5.22	0.87 ±8%

Run number 10 Sample type: tubes L/D = 126

300 mm long 2.375 mm diameter Entrance loss = 1.8 helium 94 Hz

Point	Xp (mm)	P (bar)	Re max	Re w	Ar	Mach#	ΔP (Pa)	pV (W)	Euler#	TDF
1	0.98	28.67	25,280	190.7	0.26	0.05	4.49E4	1.66	9.04	0.73 ±10%
2	1.47	28.07	36,760	187.2	0.39	0.07	7.64E4	5.73	7.14	0.85 ±8%
3	1.44	28.59	36,650	190.3	0.38	0.07	7.61E4	5.52	7.28	0.85 ±8%
4	1.71	28.16	42,840	187.7	0.45	0.08	9.32E4	9.05	6.44	0.88 ±8%

Run number 11 Sample type: tubes L/D = 32

76.2 mm long 2.375 mm diameter Entrance loss = 1.8 helium 94 Hz

Point	Xp (mm)	P (bar)	Re max	Re w	Ar	Mach#	ΔP (Pa)	pV (W)	Euler#	TDF
1	0.70	14.54	7,861	98.2	0.62	0.03	4.00E3	0.14	4.32	0.97 ±20%
2	0.71	14.56	8,066	98.4	0.64	0.03	4.11E3	0.15	4.23	0.98 ±20%
3	0.95	14.65	10,730	98.9	0.85	0.04	5.78E3	0.35	3.37	1.04 ±14%
4	1.22	14.63	13,810	98.7	1.09	0.05	8.20E3	0.73	2.88	1.02 ±11%
5	1.44	14.61	16,100	98.3	1.28	0.06	1.13E4	1.14	2.91	1.02 ±9%
6	1.73	14.62	19,380	98.3	1.54	0.07	1.56E4	1.98	2.77	1.03 ±8%
7	1.95	14.61	21,760	98.2	1.73	0.08	1.88E4	2.67	2.64	0.98 ±7%
8	2.35	14.49	25,900	96.9	2.08	0.09	2.72E4	4.75	2.66	1.02 ±6%
9	2.18	14.51	24,020	96.8	1.93	0.09	2.37E4	3.80	2.69	1.02 ±6%
10	2.49	14.76	27,480	97.1	2.21	0.10	3.00E4	5.63	2.59	1.02 ±6%
11	2.99	14.83	32,770	97.0	2.63	0.12	4.17E4	9.64	2.52	1.04 ±5%
12	2.69	14.78	29,520	96.8	2.38	0.10	3.44E4	7.15	2.56	1.05 ±5%
13	0.98	28.66	21,080	188.5	0.87	0.04	1.16E4	0.65	3.31	0.96 ±12%
14	1.47	28.55	31,580	188.5	1.31	0.06	2.31E4	2.23	2.94	1.01 ±8%
15	1.95	28.81	41,870	189.2	1.73	0.08	3.80E4	5.11	2.75	1.02 ±6%

Run number 12 Sample type: tubes L/D = 84

200 mm long 2.375 mm diameter Entrance loss = 1.8 helium 94 Hz

Point	Xp (mm)	P (bar)	Re max	Re w	Ar	Mach#	ΔP (Pa)	pV (W)	Euler#	TDF
1	0.70	14.63	8,783	99.3	0.26	0.03	1.20E4	0.26	10.52	0.82 ±15%
2	0.95	14.63	11,860	98.9	0.36	0.04	1.72E4	0.63	8.24	0.85 ±11%
3	1.24	14.64	15,410	99.0	0.46	0.05	2.33E4	1.32	6.61	0.85 ±9%
4	1.46	14.55	17,980	98.5	0.54	0.06	2.90E4	2.14	6.01	0.87 ±8%
5	1.70	14.64	20,900	99.0	0.63	0.07	3.51E4	3.34	5.41	0.90 ±7%
6	1.97	14.74	24,220	99.5	0.72	0.08	4.09E4	4.79	4.71	0.86 ±7%
7	2.24	14.59	27,280	98.9	0.82	0.10	4.76E4	6.99	4.30	0.89 ±6%
8	2.51	14.67	30,400	98.8	0.91	0.11	5.43E4	9.63	3.94	0.89 ±6%
9	2.73	14.77	32,890	98.9	0.99	0.11	5.96E4	12.17	3.69	0.90 ±6%
10	2.89	14.79	34,640	98.8	1.04	0.12	6.16E4	14.47	3.43	0.93 ±6%
11	0.98	28.93	23,760	192.6	0.37	0.04	3.52E4	1.13	8.10	0.78 ±10%
12	1.48	28.85	35,530	193.1	0.55	0.06	5.66E4	3.90	5.86	0.88 ±7%
13	1.94	28.88	46,500	193.6	0.71	0.08	7.63E4	8.55	4.62	0.91 ±6%

Run number 13 Sample type: tubes L/D = 48

115 mm long 2.375 mm diameter Entrance loss = 1.8 helium 94 Hz

Point	Xp (mm)	P (bar)	Re max	Re w	Ar	Mach#	ΔP (Pa)	pV (W)	Euler#	TDF
1	0.71	15.75	8,892	105.8	0.43	0.03	7.08E3	0.18	6.42	0.86 ±17%
2	0.71	14.66	8,233	98.3	0.43	0.03	6.64E3	0.16	6.52	0.86 ±17%
3	0.71	14.48	8,181	97.0	0.44	0.03	6.68E3	0.17	6.56	0.87 ±17%
4	0.98	14.95	11,490	100.0	0.59	0.04	9.91E3	0.41	5.07	0.87 ±12%
5	1.20	15.16	14,270	101.3	0.73	0.05	1.25E4	0.75	4.22	0.87 ±10%
7	1.49	14.89	17,350	99.6	0.90	0.06	1.67E4	1.40	3.74	0.89 ±8%
8	1.70	14.55	19,290	97.0	1.03	0.07	1.94E4	2.06	3.42	0.91 ±7%
9	1.97	14.68	22,500	97.9	1.19	0.08	2.26E4	3.17	2.96	0.91 ±6%
10	2.19	15.03	25,390	99.8	1.31	0.09	2.54E4	4.30	2.65	0.90 ±6%
11	2.46	15.02	28,390	99.6	1.47	0.10	3.04E4	5.99	2.53	0.91 ±6%
12	2.73	14.51	30,370	96.3	1.63	0.11	3.65E4	8.04	2.57	0.94 ±5%
13	2.84	14.77	32,000	97.6	1.69	0.11	4.94E4	9.42	3.17	0.87 ±5%

Run number 14 Sample type: tubes L/D = 152

360 mm long 2.375 mm diameter Entrance loss = 1.8 nitrogen 30 Hz

Point	Xp (mm)	P (bar)	Re max	Re w	Ar	Mach#	ΔP (Pa)	pV (W)	Euler#	TDF
1	0.74	5.93	10,090	98.8	0.17	0.03	7.13E3	0.05	16.51	0.78 ±17%
2	0.97	6.07	13,280	100.8	0.22	0.04	9.12E3	0.10	12.41	0.78 ±14%
3	0.97	5.85	12,850	97.2	0.22	0.04	9.11E3	0.10	12.79	0.79 ±14%
4	1.25	5.93	16,550	98.3	0.28	0.05	1.13E4	0.20	9.63	0.77 ±12%
5	1.52	5.80	19,590	96.1	0.34	0.06	1.35E4	0.34	8.05	0.78 ±11%
6	1.77	5.98	23,020	98.8	0.38	0.07	1.60E4	0.52	7.09	0.80 ±10%
7	1.98	5.85	25,210	96.8	0.43	0.08	1.90E4	0.75	6.88	0.86 ±10%
8	2.26	5.93	28,590	97.6	0.48	0.09	2.26E4	1.11	6.39	0.90 ±10%
9	2.51	6.05	31,930	99.3	0.53	0.10	2.57E4	1.51	5.92	0.94 ±10%
10	2.77	5.88	33,930	96.1	0.58	0.11	2.89E4	1.97	5.71	0.96 ±10%
11	2.99	5.99	36,770	97.5	0.62	0.12	3.18E4	2.43	5.42	0.98 ±10%
12	3.99	6.02	47,080	96.8	0.80	0.15	4.60E4	5.17	4.71	1.01 ±12%
13	4.98	6.10	56,420	96.6	0.96	0.18	6.21E4	8.88	4.39	1.02 ±14%
14	6.04	5.91	63,140	91.7	1.14	0.21	8.20E4	14.01	4.36	1.04 ±17%

Run number 15 Sample type: tubes L/D = 152

360 mm long 2.375 mm diameter Entrance loss = 1.8 helium 30 Hz

Point	Xp (mm)	P (bar)	Re max	Re w	Ar	Mach#	ΔP (Pa)	pV (W)	Euler#	TDF
1	1.02	45.50	10,900	96.5	0.19	0.01	9.58E3	0.07	16.46	0.73 ±13%
2	1.51	45.64	16,230	96.9	0.28	0.02	1.29E4	0.21	10.01	0.74 ±9%
3	2.03	45.60	21,810	96.9	0.37	0.02	1.69E4	0.49	7.29	0.75 ±7%
4	2.54	45.65	27,310	96.9	0.46	0.03	2.10E4	1.02	5.76	0.84 ±5%
5	2.92	45.61	31,290	96.8	0.53	0.04	2.69E4	1.61	5.61	0.90 ±4%
6	3.98	45.67	42,590	96.7	0.73	0.05	5.04E4	4.11	5.67	0.95 ±3%
7	5.05	45.62	53,740	96.2	0.92	0.06	7.58E4	8.23	5.32	0.97 ±3%
8	5.52	45.60	58,430	95.8	1.01	0.07	8.76E4	10.61	5.17	0.98 ±3%

Run number 17 Sample type: tubes L/D = 126

300 mm long 2.375 mm diameter Entrance loss = 1.8 nitrogen 30 Hz

Point	Xp (mm)	P (bar)	Re max	Re w	Ar	Mach#	ΔP (Pa)	pV (W)	Euler#	TDF
1	1.03	6.15	13,870	103.4	0.27	0.04	8.10E3	0.09	10.42	0.75 ±14%
2	1.56	6.10	20,490	102.1	0.40	0.06	1.17E4	0.29	6.82	0.75 ±11%
3	1.98	5.96	25,130	99.5	0.50	0.08	1.62E4	0.60	6.07	0.83 ±10%
4	2.49	6.04	31,540	100.8	0.62	0.10	2.13E4	1.18	5.15	0.89 ±9%
5	3.02	6.05	37,810	100.7	0.74	0.12	2.67E4	2.04	4.49	0.92 ±9%
6	3.46	5.89	41,780	97.7	0.85	0.13	3.17E4	2.96	4.23	0.95 ±10%
7	3.99	5.94	47,890	98.5	0.96	0.15	3.79E4	4.32	3.87	0.96 ±10%
8	4.57	5.97	53,850	98.5	1.08	0.17	4.54E4	6.12	3.66	0.96 ±11%
9	5.06	5.95	58,530	97.9	1.18	0.19	5.31E4	7.93	3.60	0.97 ±12%
10	5.53	5.90	62,480	96.7	1.28	0.20	6.16E4	9.91	3.61	0.98 ±13%
12	6.54	5.95	71,070	96.2	1.46	0.23	7.98E4	14.72	3.58	0.98 ±15%
13	7.07	6.11	77,080	98.3	1.55	0.24	8.95E4	17.63	3.48	0.97 ±16%
14	1.05	11.89	26,300	193.6	0.27	0.04	1.67E4	0.19	11.06	0.85 ±11%
15	2.04	11.84	51,320	195.8	0.52	0.08	3.35E4	1.32	5.93	0.95 ±7%
16	3.00	11.67	73,010	193.0	0.75	0.12	5.15E4	3.84	4.43	0.98 ±7%
17	3.98	11.80	95,410	194.6	0.97	0.15	7.39E4	8.29	3.75	1.00 ±8%
18	4.55	11.97	108,200	196.4	1.09	0.17	8.81E4	11.70	3.51	1.00 ±9%

Run number 18 Sample type: tubes L/D = 102

241.3 mm long 2.375 mm diameter Entrance loss = 1.8 nitrogen 30 Hz

Point	Xp (mm)	P (bar)	Re max	Re w	Ar	Mach#	ΔP (Pa)	pV (W)	Euler#	TDF
1	1.04	11.86	25,500	196.0	0.32	0.04	1.57E4	0.15	11.24	0.88 ±11%
2	2.05	12.07	50,780	200.1	0.62	0.08	2.85E4	1.12	5.26	0.99 ±7%
3	2.96	12.14	72,590	200.8	0.89	0.11	4.21E4	3.16	3.81	1.01 ±6%
4	3.99	11.88	93,720	195.7	1.18	0.15	6.07E4	7.15	3.21	1.04 ±7%
5	4.56	11.91	105,800	195.4	1.33	0.17	7.68E4	10.26	3.17	1.05 ±8%
6	4.98	11.86	113,700	193.8	1.44	0.18	8.95E4	12.96	3.18	1.05 ±9%
7	1.02	6.20	13,290	103.8	0.32	0.04	7.31E3	0.07	10.27	0.78 ±15%
8	2.01	6.08	25,160	101.0	0.61	0.08	1.44E4	0.55	5.48	0.91 ±10%
9	3.07	6.00	37,120	99.5	0.92	0.12	2.31E4	1.85	3.97	0.99 ±9%
10	3.99	6.08	47,640	100.2	1.17	0.15	3.21E4	3.81	3.37	1.01 ±9%
11	5.06	6.03	58,280	98.9	1.45	0.18	4.87E4	7.10	3.36	1.02 ±11%
12	6.05	6.13	68,390	99.5	1.69	0.22	6.61E4	11.26	3.32	1.03 ±12%
13	7.06	6.14	77,430	98.9	1.93	0.24	8.48E4	16.43	3.29	1.03 ±14%

Run number 19 Sample type: tubes L/D = 84

200 mm long 2.375 mm diameter Entrance loss = 1.8 nitrogen 30 Hz

Point	Xp (mm)	P (bar)	Re max	Re w	Ar	Mach#	ΔP (Pa)	pV (W)	Euler#	TDF
1	1.03	12.18	25,540	203.9	0.37	0.04	1.47E4	0.12	11.00	0.80 ±11%
2	2.08	12.16	50,890	202.8	0.74	0.08	2.42E4	0.93	4.52	0.93 ±7%
3	2.96	11.93	70,430	198.5	1.05	0.11	3.42E4	2.54	3.26	0.96 ±6%
4	4.05	12.00	95,250	199.2	1.42	0.15	5.35E4	6.12	2.79	0.97 ±6%
5	5.05	12.07	117,300	199.7	1.74	0.18	7.91E4	11.21	2.73	0.98 ±7%
6	5.54	11.89	125,400	196.0	1.90	0.20	9.31E4	14.45	2.75	0.99 ±8%
7	1.05	6.23	13,460	105.1	0.38	0.04	6.76E3	0.06	9.40	0.73 ±16%
8	1.96	6.19	24,510	103.8	0.70	0.07	1.15E4	0.40	4.76	0.85 ±10%
9	3.03	5.90	35,740	98.7	1.08	0.11	1.82E4	1.42	3.36	0.93 ±9%
10	4.02	6.25	48,920	103.7	1.40	0.15	2.80E4	3.17	2.89	0.93 ±8%
11	4.97	6.06	57,650	100.0	1.71	0.18	4.06E4	5.66	2.90	0.95 ±9%
12	5.96	5.97	66,810	98.3	2.02	0.21	5.58E4	9.20	2.91	0.98 ±11%
13	7.05	6.11	78,430	99.8	2.33	0.25	7.43E4	14.24	2.85	0.97 ±13%
14	8.01	6.24	88,550	101.3	2.60	0.27	9.05E4	19.54	2.76	0.96 ±14%

Run number 79 Sample type: tubes L/D = 152

360 mm long 2.375 mm diameter Entrance loss = 1.05 helium 82 Hz

Point	Xp (mm)	P (bar)	Re max	Re w	Ar	Mach#	ΔP (Pa)	pV (W)	Euler#	TDF
1	1.07	16.85	13,580	99.3	0.23	0.04	2.73E4	0.73	11.44	0.69 ±10%
2	1.98	16.89	24,660	99.1	0.41	0.08	5.20E4	3.99	6.59	0.69 ±8%
3	3.05	16.95	36,890	98.0	0.62	0.11	9.31E4	15.65	5.18	0.87 ±9%
4	1.02	33.85	25,640	198.0	0.21	0.04	4.99E4	1.13	11.66	0.70 ±10%
5	1.70	33.85	42,310	197.9	0.35	0.06	9.12E4	5.65	7.82	0.88 ±8%
6	0.98	50.60	36,160	293.1	0.20	0.04	7.55E4	1.57	13.09	0.81 ±11%
7	1.18	50.55	43,850	294.5	0.25	0.04	9.10E4	2.78	10.80	0.86 ±10%

Run number 82 Sample type: tubes L/D = 5

12.7 mm long 2.375 mm diameter Entrance loss = 1.05 helium 82 Hz

Point	Xp (mm)	P (bar)	Re max	Re w	Ar	Mach#	ΔP (Pa)	pV (W)	Euler#	TDF
1	1.07	16.85	12,030	103.2	5.45	0.04	1.36E3	0.10	0.77	0.69 ±43%
2	2.08	16.90	23,330	103.2	10.57	0.07	5.42E3	0.69	0.81	0.66 ±13%
3	4.00	16.94	44,860	103.1	20.33	0.13	1.80E4	4.61	0.73	0.64 ±5%
4	5.99	17.02	67,260	103.4	30.40	0.20	3.81E4	14.54	0.69	0.61 ±4%
5	8.00	16.39	86,180	99.3	40.58	0.26	6.56E4	33.31	0.69	0.61 ±4%
6	1.07	33.72	23,510	201.6	5.45	0.04	2.93E3	0.18	0.84	0.65 ±24%
7	1.98	34.02	43,960	204.1	10.07	0.07	9.05E3	1.09	0.75	0.62 ±9%
8	3.98	33.91	87,530	202.5	20.21	0.13	3.14E4	7.87	0.65	0.57 ±4%
9	5.94	33.92	130,600	202.6	30.13	0.20	6.76E4	25.46	0.63	0.56 ±3%
10	6.88	33.93	148,600	199.3	34.86	0.22	9.07E4	39.30	0.64	0.57 ±3%
11	1.03	50.57	33,500	299.6	5.23	0.03	3.90E3	0.23	0.81	0.63 ±20%
12	2.00	50.68	65,490	301.2	10.17	0.07	1.22E4	1.54	0.67	0.59 ±7%
13	3.92	50.78	127,900	300.4	19.91	0.13	4.34E4	10.70	0.62	0.55 ±3%
14	5.85	50.71	190,900	300.1	29.74	0.19	9.63E4	35.18	0.62	0.55 ±3%

Run number 83 Sample type: tubes L/D = 10

23.7 mm long 2.375 mm diameter Entrance loss = 1.05 helium 82 Hz

Point	Xp (mm)	P (bar)	Re max	Re w	Ar	Mach#	ΔP (Pa)	pV (W)	Euler#	TDF
1	1.04	16.79	11,710	103.4	2.84	0.03	1.88E3	0.11	1.13	0.75 ±33%
2	1.99	16.81	22,420	103.2	5.45	0.07	6.24E3	0.76	1.01	0.75 ±12%
3	3.95	16.90	44,440	103.2	10.79	0.13	2.32E4	5.73	0.96	0.75 ±5%
4	6.00	16.97	67,450	103.4	16.35	0.20	5.18E4	19.55	0.93	0.75 ±4%
5	7.86	16.58	84,240	98.9	21.35	0.26	8.66E4	43.07	0.94	0.77 ±5%
6	1.00	33.68	22,370	205.2	2.73	0.03	3.56E3	0.18	1.15	0.71 ±21%
7	2.04	33.66	45,490	204.2	5.58	0.07	1.27E4	1.51	0.99	0.72 ±7%
8	5.76	33.77	127,900	204.0	15.70	0.19	9.06E4	32.81	0.89	0.73 ±3%
9	1.00	50.22	32,950	301.0	2.74	0.03	5.29E3	0.27	1.15	0.72 ±16%
10	2.01	50.46	66,340	302.7	5.49	0.07	1.79E4	2.14	0.97	0.73 ±6%
11	4.10	50.47	135,200	302.2	11.21	0.14	6.83E4	17.45	0.88	0.72 ±3%
12	4.79	50.64	158,100	303.0	13.08	0.16	9.14E4	27.37	0.87	0.72 ±3%

Run number 86 Sample type: tubes L/D = 5

12.7 mm long 2.375 mm diameter Entrance loss = 1.5 helium 82 Hz

Point	Xp (mm)	P (bar)	Re max	Re w	Ar	Mach#	ΔP (Pa)	pV (W)	Euler#	TDF
1	1.03	16.84	11,530	102.3	5.27	0.03	2.01E3	0.12	1.22	0.69 ±34%
2	2.03	17.06	22,860	103.4	10.34	0.07	7.41E3	0.92	1.15	0.69 ±11%
3	4.04	16.97	44,990	102.4	20.54	0.13	2.85E4	7.21	1.13	0.70 ±4%
4	5.95	16.90	65,310	101.4	30.11	0.20	6.10E4	22.81	1.14	0.72 ±4%
5	7.07	16.90	76,160	99.9	35.65	0.23	8.43E4	37.67	1.13	0.72 ±5%
6	1.01	33.69	22,210	201.8	5.15	0.03	3.64E3	0.21	1.17	0.67 ±21%
7	2.02	33.82	44,500	201.8	10.31	0.07	1.38E4	1.72	1.10	0.67 ±7%
8	3.90	33.95	85,370	201.4	19.81	0.13	5.08E4	12.36	1.10	0.69 ±3%
9	5.04	33.97	108,700	199.2	25.51	0.16	8.59E4	26.87	1.13	0.71 ±3%
10	1.03	50.55	33,490	299.6	5.23	0.03	5.53E3	0.33	1.15	0.67 ±16%
11	2.00	50.59	64,950	298.1	10.19	0.07	1.99E4	2.46	1.09	0.67 ±6%
12	4.07	50.73	131,500	297.7	20.65	0.13	8.08E4	20.86	1.08	0.69 ±3%

Run number 87 Sample type: tubes L/D = 10

23.7 mm long 2.375 mm diameter Entrance loss = 1.5 helium 82 Hz

Point	Xp (mm)	P (bar)	Re max	Re w	Ar	Mach#	ΔP (Pa)	pV (W)	Euler#	TDF
1	1.01	16.84	11,200	101.4	2.77	0.03	2.24E3	0.13	1.42	0.71 ±30%
2	2.02	16.97	22,500	101.8	5.54	0.07	8.66E3	1.02	1.37	0.72 ±10%
3	4.05	16.87	44,600	101.0	11.06	0.13	3.21E4	8.11	1.28	0.74 ±4%
4	6.06	16.86	66,230	100.6	16.48	0.20	6.81E4	26.29	1.22	0.74 ±4%
5	6.73	16.82	72,800	100.0	18.23	0.22	8.18E4	35.55	1.21	0.74 ±5%
6	1.02	33.84	22,450	200.5	2.81	0.03	4.48E3	0.24	1.39	0.67 ±18%
7	2.04	33.87	44,850	201.0	5.59	0.07	1.56E4	1.91	1.21	0.68 ±7%
8	3.99	33.89	86,770	199.5	10.90	0.13	5.83E4	14.41	1.20	0.71 ±3%
9	4.97	33.95	108,500	200.6	13.55	0.16	8.76E4	27.25	1.16	0.70 ±3%
10	1.02	50.67	33,200	298.2	2.79	0.03	6.48E3	0.35	1.36	0.66 ±15%
11	1.97	50.61	64,210	298.3	5.39	0.06	2.15E4	2.54	1.21	0.68 ±6%
12	4.10	50.68	133,300	298.3	11.19	0.13	8.62E4	22.64	1.13	0.69 ±3%

Run number 91 Sample type: tubes L/D = 10

23.7 mm long 2.375 mm diameter Entrance loss = 1.5 helium 82 Hz

Point	Xp (mm)	P (bar)	Re max	Re w	Ar	Mach#	ΔP (Pa)	pV (W)	Euler#	TDF
1	1.00	16.83	11,180	102.0	2.74	0.03	2.47E3	0.12	1.59	0.69 ±30%
2	2.00	16.83	22,270	101.7	5.49	0.07	8.23E3	0.96	1.33	0.70 ±10%
3	2.06	16.90	22,850	101.7	5.63	0.07	8.63E3	1.03	1.32	0.69 ±10%
4	2.01	16.91	22,240	101.4	5.50	0.07	8.26E3	0.96	1.33	0.70 ±10%
5	4.05	17.02	44,730	101.4	11.05	0.13	3.04E4	7.74	1.21	0.70 ±4%
6	6.01	17.06	65,880	101.3	16.29	0.20	6.50E4	24.82	1.18	0.71 ±4%
7	6.94	17.15	74,970	100.2	18.74	0.23	8.54E4	37.46	1.18	0.71 ±5%
8	1.04	33.83	22,700	199.5	2.85	0.03	4.72E3	0.26	1.42	0.68 ±17%
9	1.92	33.88	41,910	199.9	5.25	0.06	1.45E4	1.59	1.28	0.68 ±7%
10	4.01	34.02	87,310	199.9	10.94	0.13	5.78E4	14.41	1.18	0.69 ±3%
11	5.13	34.12	110,900	199.1	13.95	0.17	9.19E4	29.58	1.15	0.69 ±3%
12	1.01	50.73	32,860	296.6	2.78	0.03	6.99E3	0.35	1.49	0.66 ±15%
14	3.98	50.93	129,000	297.7	10.85	0.13	8.32E4	20.59	1.16	0.69 ±3%

Run number 92 Sample type: tubes L/D = 25

59.38 mm long 2.375 mm diameter Entrance loss = 1.5 helium 82 Hz

Point	Xp (mm)	P (bar)	Re max	Re w	Ar	Mach#	ΔP (Pa)	pV (W)	Euler#	TDF
1	0.96	16.99	11,070	103.7	1.07	0.03	5.39E3	0.20	3.60	0.95 ±17%
2	2.04	16.94	23,300	103.2	2.26	0.07	1.57E4	1.85	2.35	1.00 ±7%
3	4.01	17.18	45,810	103.8	4.41	0.13	5.21E4	13.35	2.03	1.01 ±4%
4	5.66	17.21	62,770	101.9	6.16	0.19	9.79E4	36.05	1.97	1.03 ±5%
5	1.01	33.89	22,820	204.1	1.12	0.03	9.70E3	0.42	2.99	0.92 ±12%
6	2.02	33.88	45,630	203.9	2.24	0.07	2.89E4	3.29	2.23	0.96 ±6%
7	3.71	33.95	82,640	202.5	4.08	0.12	8.45E4	19.76	1.96	1.00 ±4%

Run number 96 Sample type: tubes L/D = 25

59.38 mm long 2.375 mm diameter Entrance loss = 1.5 helium 82 Hz

Point	Xp (mm)	P (bar)	Re max	Re w	Ar	Mach#	ΔP (Pa)	pV (W)	Euler#	TDF
1	0.73	49.66	24,380	301.3	0.81	0.02	1.25E4	0.23	4.98	0.89 ±16%
2	1.09	50.08	36,910	304.0	1.21	0.04	1.53E4	0.76	2.69	0.91 ±11%
3	1.39	50.13	46,790	303.2	1.54	0.05	2.11E4	1.56	2.31	0.93 ±8%
4	1.69	50.34	57,090	304.1	1.88	0.06	2.94E4	2.78	2.16	0.93 ±7%
5	2.05	50.51	69,100	304.2	2.27	0.07	4.09E4	4.89	2.05	0.94 ±5%
6	2.37	50.88	80,260	305.7	2.63	0.08	5.25E4	7.60	1.96	0.95 ±5%
7	2.59	51.00	87,030	303.9	2.86	0.09	6.18E4	9.90	1.94	0.96 ±4%
8	2.66	51.26	89,780	305.8	2.94	0.09	6.47E4	10.64	1.92	0.95 ±4%
9	2.97	51.20	99,610	303.5	3.28	0.10	8.01E4	14.88	1.91	0.97 ±4%
10	3.16	51.42	105,900	303.6	3.49	0.11	8.97E4	18.03	1.89	0.98 ±4%
11	1.27	33.87	28,630	202.8	1.41	0.04	1.25E4	0.83	2.42	0.93 ±10%
12	1.69	34.05	38,210	203.5	1.88	0.06	2.02E4	1.91	2.21	0.93 ±7%
13	2.18	34.01	48,590	201.7	2.41	0.07	3.10E4	4.02	2.07	0.95 ±5%
14	2.61	34.21	58,570	202.6	2.89	0.09	4.34E4	6.91	2.00	0.95 ±5%
15	2.63	34.40	59,100	203.2	2.91	0.09	4.42E4	7.05	2.00	0.95 ±5%
16	3.03	34.79	68,070	203.6	3.34	0.10	5.75E4	10.79	1.96	0.96 ±4%
17	3.62	35.11	81,180	203.5	3.99	0.12	8.06E4	18.34	1.92	0.97 ±4%
18	3.99	34.87	87,610	199.6	4.39	0.13	9.65E4	24.36	1.93	0.99 ±4%

Run number 97 Sample type: tubes L/D = 25

59.38 mm long 2.375 mm diameter Entrance loss = 1.5 helium 82 Hz

Point	Xp (mm)	P (bar)	Re max	Re w	Ar	Mach#	ΔP (Pa)	pV (W)	Euler#	TDF
1	0.89	17.78	10,240	103.2	0.99	0.03	4.85E3	0.16	3.70	0.91 ±19%
2	1.64	17.90	18,890	103.9	1.82	0.05	1.04E4	0.94	2.34	0.93 ±9%
3	1.72	17.88	19,740	103.4	1.91	0.06	1.14E4	1.08	2.33	0.92 ±9%
4	2.55	18.04	29,410	104.3	2.82	0.08	2.22E4	3.41	2.07	0.93 ±6%
5	3.48	17.85	39,420	102.7	3.84	0.12	4.05E4	8.73	2.06	0.97 ±4%
6	4.43	18.35	50,620	104.0	4.87	0.15	6.17E4	17.53	1.92	0.96 ±4%
7	5.37	18.29	59,650	101.8	5.86	0.17	8.79E4	30.41	1.91	0.98 ±5%

Run number 101 Sample type: tubes L/D = 50

118.7 mm long 2.375 mm diameter Entrance loss = 1.5 helium 82 Hz

Point	Xp (mm)	P (bar)	Re max	Re w	Ar	Mach#	ΔP (Pa)	pV (W)	Euler#	TDF
1	0.95	17.19	11,060	102.6	0.54	0.03	7.95E3	0.26	5.22	0.90 ±14%
2	1.86	17.39	21,700	103.2	1.05	0.06	1.87E4	1.88	3.20	0.95 ±7%
3	2.66	17.23	30,520	101.7	1.50	0.09	3.45E4	5.37	2.94	0.99 ±5%
4	3.37	17.55	38,920	102.8	1.89	0.11	5.17E4	11.08	2.73	1.01 ±5%
5	3.51	17.55	40,550	102.8	1.97	0.12	5.46E4	12.23	2.65	1.01 ±5%
6	4.36	17.87	50,470	103.4	2.44	0.15	8.01E4	23.03	2.51	1.02 ±5%
7	4.39	17.93	50,800	103.7	2.45	0.15	8.09E4	23.39	2.51	1.02 ±5%
8	0.94	52.93	33,000	308.7	0.53	0.03	2.66E4	0.71	5.85	0.94 ±11%
9	1.15	52.59	40,260	307.3	0.65	0.04	3.13E4	1.29	4.60	0.96 ±9%
10	1.47	52.57	51,380	307.2	0.84	0.05	3.83E4	2.67	3.46	0.98 ±7%
11	1.72	52.58	59,750	306.8	0.97	0.06	4.91E4	4.17	3.27	0.98 ±6%
12	1.71	52.50	59,100	305.3	0.97	0.06	4.72E4	4.13	3.20	0.99 ±6%
13	2.06	52.68	71,560	306.8	1.17	0.07	6.36E4	7.14	2.95	1.00 ±5%
14	2.06	52.72	71,280	305.8	1.17	0.07	6.41E4	7.10	2.99	1.00 ±5%
15	2.33	52.85	80,780	306.9	1.32	0.08	7.79E4	10.19	2.84	1.01 ±5%
16	2.62	52.94	90,910	306.6	1.48	0.09	9.39E4	14.50	2.69	1.01 ±4%
17	0.93	35.68	21,770	205.4	0.53	0.03	1.59E4	0.47	5.32	0.92 ±12%
18	1.32	35.93	30,900	206.7	0.75	0.04	2.33E4	1.33	3.89	0.95 ±8%
19	1.72	35.91	40,490	207.3	0.98	0.06	3.51E4	2.93	3.43	0.97 ±6%
20	2.14	35.75	49,930	206.0	1.21	0.07	4.83E4	5.51	3.08	0.98 ±5%
21	2.59	35.76	60,290	205.8	1.47	0.09	6.48E4	9.64	2.83	1.00 ±5%

Run number 102 Sample type: tubes L/D = 150

356.3 mm long 2.375 mm diameter Entrance loss = 1.5 helium 82 Hz

Point	Xp (mm)	P (bar)	Re max	Re w	Ar	Mach#	ΔP (Pa)	pV (W)	Euler#	TDF
1	1.28	16.81	16,340	100.9	0.27	0.05	2.66E4	1.57	7.89	0.82 ±10%
2	1.34	16.86	17,130	101.0	0.28	0.05	2.84E4	1.81	7.66	0.83 ±9%
3	2.09	16.74	25,740	98.9	0.43	0.08	6.05E4	6.82	7.04	0.92 ±9%
4	2.87	17.00	34,650	98.8	0.58	0.11	1.02E5	17.00	6.47	0.97 ±9%
5	0.73	34.27	19,010	202.5	0.16	0.03	4.17E4	0.53	18.19	0.73 ±14%
6	1.15	33.95	29,300	200.6	0.24	0.04	6.71E4	2.21	12.22	0.89 ±10%
7	1.57	34.09	39,680	200.4	0.33	0.06	9.28E4	5.52	9.19	0.96 ±9%
8	0.79	51.02	30,310	301.3	0.17	0.03	6.86E4	1.05	17.54	0.86 ±13%
9	1.04	51.40	39,720	299.8	0.22	0.04	8.95E4	2.49	13.18	0.96 ±11%

Run number 103 Sample type: tubes L/D = 150

356.3 mm long 2.375 mm diameter Entrance loss = 1.05 helium 82 Hz

Point	Xp (mm)	P (bar)	Re max	Re w	Ar	Mach#	ΔP (Pa)	pV (W)	Euler#	TDF
1	0.75	16.73	9,617	99.4	0.16	0.03	2.00E4	0.28	16.84	0.69 ±14%
2	1.56	16.93	19,790	99.9	0.33	0.06	4.06E4	2.05	8.06	0.68 ±8%
3	2.36	16.92	29,120	98.9	0.49	0.09	7.03E4	7.42	6.36	0.81 ±8%
4	3.19	16.92	38,380	97.3	0.66	0.12	9.89E4	18.16	5.04	0.89 ±9%
5	0.69	34.79	17,600	201.3	0.15	0.03	3.74E4	0.36	18.79	0.66 ±15%
6	1.56	34.35	39,350	199.0	0.33	0.06	8.90E4	4.52	8.85	0.86 ±8%
7	1.17	34.52	29,630	200.5	0.25	0.04	6.62E4	1.85	11.69	0.78 ±10%
8	1.01	52.05	38,490	301.5	0.21	0.04	8.70E4	1.80	13.68	0.82 ±11%
9	0.75	52.22	28,830	302.6	0.16	0.03	6.61E4	0.74	18.61	0.75 ±14%

Run number 104 Sample type: tubes L/D = 100

237.5 mm long 2.375 mm diameter Entrance loss = 1.05 helium 82 Hz

Point	Xp (mm)	P (bar)	Re max	Re w	Ar	Mach#	ΔP (Pa)	pV (W)	Euler#	TDF
1	0.80	17.23	9,809	100.9	0.24	0.03	2.24E4	0.27	18.23	0.83 ±13%
2	2.44	17.21	29,240	100.4	0.73	0.09	5.31E4	6.43	4.83	1.00 ±6%
3	3.33	17.23	39,190	99.6	0.98	0.12	7.50E4	15.97	3.75	1.06 ±7%
4	4.05	17.42	47,410	99.8	1.19	0.14	9.29E4	27.60	3.17	1.07 ±7%
5	4.33	17.35	49,940	98.7	1.27	0.15	9.91E4	32.72	3.01	1.07 ±7%
6	2.42	17.31	28,950	100.0	0.72	0.09	5.33E4	6.16	4.91	0.97 ±6%
7	0.94	34.24	22,340	197.5	0.28	0.03	4.85E4	0.71	14.81	0.83 ±12%
8	0.87	34.34	20,840	198.5	0.26	0.03	4.42E4	0.58	15.60	0.86 ±12%
9	1.66	34.34	39,550	198.4	0.50	0.06	6.91E4	3.78	6.77	0.97 ±7%
10	1.24	34.46	29,550	199.1	0.37	0.04	5.64E4	1.57	9.92	0.91 ±9%
11	2.10	34.46	49,830	198.9	0.63	0.08	8.40E4	7.44	5.20	1.01 ±6%
12	2.50	34.46	59,190	198.4	0.75	0.09	9.96E4	12.56	4.35	1.04 ±6%
13	1.65	52.03	59,500	301.5	0.49	0.06	1.01E5	5.22	6.64	0.98 ±7%
14	1.39	52.13	50,210	301.8	0.42	0.05	9.02E4	3.16	8.35	0.95 ±8%
15	1.10	52.05	39,370	300.3	0.33	0.04	7.72E4	1.58	11.54	0.91 ±10%

Run number 106 Sample type: tubes L/D = 25

59.38 mm long 2.375 mm diameter Entrance loss = 1.05 helium 82 Hz

Point	Xp (mm)	P (bar)	Re max	Re w	Ar	Mach#	ΔP (Pa)	pV (W)	Euler#	TDF
1	0.93	16.65	10,590	101.9	1.04	0.03	4.28E3	0.14	3.07	0.88 ±19%
2	1.83	16.70	20,700	101.6	2.04	0.06	9.50E3	0.93	1.78	0.86 ±9%
3	2.53	16.80	28,630	102.0	2.81	0.09	1.58E4	2.45	1.55	0.89 ±6%
4	3.55	16.80	39,900	101.5	3.93	0.12	2.96E4	6.68	1.48	0.92 ±5%
5	4.54	16.90	50,830	101.5	5.01	0.15	4.75E4	13.53	1.47	0.92 ±4%
6	5.41	16.83	59,940	100.6	5.96	0.18	6.37E4	22.73	1.40	0.93 ±4%
7	6.39	17.15	71,240	101.6	7.01	0.21	8.89E4	36.75	1.39	0.93 ±5%
8	0.89	34.45	20,330	205.1	0.99	0.03	8.86E3	0.21	3.44	0.81 ±14%
9	1.34	34.13	30,500	204.2	1.49	0.05	1.12E4	0.70	1.92	0.84 ±10%
10	2.23	34.11	50,380	203.2	2.48	0.08	2.49E4	3.14	1.56	0.87 ±5%
11	1.84	34.12	41,430	203.0	2.04	0.06	1.82E4	1.76	1.68	0.86 ±7%
12	2.56	34.18	57,620	202.9	2.84	0.09	3.12E4	4.71	1.49	0.88 ±5%
13	2.73	34.41	61,880	204.1	3.03	0.09	3.48E4	5.71	1.45	0.87 ±4%
14	3.06	34.45	69,000	203.6	3.39	0.10	4.26E4	7.96	1.42	0.88 ±4%
15	4.04	34.24	89,910	201.4	4.46	0.13	7.08E4	17.91	1.37	0.89 ±3%
16	4.54	34.29	100,400	200.4	5.01	0.15	9.17E4	25.56	1.41	0.91 ±3%
17	3.61	34.14	81,090	202.4	4.01	0.12	5.81E4	13.08	1.40	0.89 ±4%
18	0.88	51.31	29,630	301.9	0.98	0.03	1.29E4	0.28	3.46	0.80 ±13%
19	0.95	51.16	31,650	300.8	1.05	0.03	1.32E4	0.35	3.09	0.80 ±12%
20	1.22	51.26	40,850	300.6	1.36	0.04	1.52E4	0.75	2.13	0.83 ±10%

Run number 107 Sample type: tubes L/D = 25

59.38 mm long 2.375 mm diameter Entrance loss = 1.05 helium 82 Hz

Point	Xp (mm)	P (bar)	Re max	Re w	Ar	Mach#	ΔP (Pa)	pV (W)	Euler#	TDF
1	1.48	51.19	49,330	300.7	1.64	0.05	1.90E4	1.34	1.82	0.85 ±8%
2	1.79	51.23	59,490	300.3	1.98	0.06	2.51E4	2.33	1.65	0.86 ±6%
3	2.44	51.21	80,970	299.5	2.70	0.08	4.02E4	5.79	1.42	0.86 ±5%
4	2.11	51.28	70,140	300.1	2.34	0.07	3.12E4	3.77	1.48	0.86 ±5%
5	2.77	51.44	92,120	300.3	3.07	0.09	5.08E4	8.42	1.40	0.87 ±4%
6	3.08	51.35	101,700	298.2	3.41	0.10	6.08E4	11.51	1.36	0.87 ±4%
7	3.68	51.72	121,400	298.7	4.06	0.12	8.58E4	19.46	1.34	0.88 ±3%

Run number 108 Sample type: tubes L/D = 50

118.7 mm long 2.375 mm diameter Entrance loss = 1.05 helium 82 Hz

Point	Xp (mm)	P (bar)	Re max	Re w	Ar	Mach#	ΔP (Pa)	pV (W)	Euler#	TDF
1	0.86	16.16	9,817	99.4	0.49	0.03	6.98E3	0.15	5.70	0.79 ±15%
2	1.73	16.23	19,570	99.5	0.98	0.06	1.35E4	1.08	2.77	0.82 ±8%
3	2.61	16.33	29,430	99.5	1.48	0.09	2.61E4	3.80	2.37	0.90 ±5%
4	3.57	16.39	40,100	99.4	2.02	0.12	4.55E4	9.61	2.21	0.93 ±5%
5	4.39	16.43	48,550	98.3	2.47	0.15	6.24E4	17.62	2.04	0.96 ±5%
6	5.19	17.24	59,330	101.8	2.91	0.18	8.58E4	29.15	1.94	0.95 ±5%
7	1.04	32.92	23,610	199.0	0.59	0.04	1.61E4	0.45	4.52	0.79 ±11%
8	1.32	32.71	29,700	197.3	0.75	0.05	2.03E4	0.95	3.58	0.85 ±8%
9	1.83	32.83	41,000	197.6	1.04	0.06	2.85E4	2.49	2.63	0.89 ±6%
10	2.25	33.06	50,830	198.7	1.28	0.08	4.04E4	4.61	2.44	0.89 ±5%
11	2.60	33.34	58,890	199.6	1.48	0.09	5.03E4	7.10	2.27	0.91 ±5%
12	3.04	33.55	69,000	200.3	1.72	0.10	6.05E4	11.32	1.99	0.92 ±4%
13	3.44	33.59	77,440	199.2	1.94	0.12	7.60E4	16.16	1.97	0.93 ±4%
14	4.00	33.70	90,000	199.1	2.26	0.14	9.94E4	24.41	1.90	0.92 ±4%
15	0.87	50.36	29,570	300.0	0.49	0.03	2.21E4	0.40	5.94	0.82 ±12%
16	1.22	50.47	41,510	299.7	0.69	0.04	2.90E4	1.10	3.93	0.86 ±9%
17	1.48	50.45	50,200	299.4	0.84	0.05	3.48E4	1.93	3.23	0.87 ±7%
18	1.70	50.57	57,970	299.9	0.97	0.06	3.14E4	3.00	2.19	0.89 ±6%
19	2.06	50.61	70,010	300.0	1.17	0.07	4.93E4	5.10	2.36	0.89 ±5%
20	2.98	50.71	100,800	299.1	1.69	0.10	8.95E4	14.81	2.05	0.90 ±4%
21	2.37	50.46	80,010	298.1	1.34	0.08	6.27E4	7.62	2.28	0.89 ±5%

Run number 117 Sample type: tubes L/D = 100

237.5 mm long 2.375 mm diameter Entrance loss = 1.5 helium 82 Hz

Point	Xp (mm)	P (bar)	Re max	Re w	Ar	Mach#	ΔP (Pa)	pV (W)	Euler#	TDF
1	0.83	16.44	10,080	100.1	0.25	0.03	1.95E4	0.27	15.15	0.75 ±13%
2	1.64	16.59	19,710	100.6	0.49	0.06	3.28E4	1.90	6.69	0.81 ±8%
3	2.53	16.60	29,850	99.5	0.75	0.09	5.14E4	7.00	4.50	0.90 ±6%
4	3.24	17.05	38,290	100.4	0.95	0.12	6.74E4	14.75	3.60	0.96 ±6%
5	3.35	17.06	39,610	100.6	0.98	0.12	7.26E4	16.02	3.63	0.94 ±7%
6	3.95	17.31	46,500	100.9	1.15	0.14	8.86E4	25.77	3.20	0.96 ±7%
7	0.90	33.85	21,730	201.8	0.27	0.03	4.32E4	0.66	14.45	0.81 ±12%
8	1.24	33.82	29,850	201.5	0.37	0.04	5.22E4	1.71	9.24	0.90 ±9%
9	2.05	33.84	49,310	201.3	0.61	0.07	7.64E4	7.48	4.95	0.95 ±6%
10	2.39	33.86	57,070	200.7	0.71	0.09	8.66E4	11.68	4.16	0.97 ±6%
11	1.66	34.23	40,340	203.2	0.50	0.06	6.38E4	4.07	6.22	0.93 ±7%
12	0.93	51.29	33,600	302.9	0.28	0.03	6.62E4	1.06	13.84	0.85 ±11%
13	1.38	51.21	50,190	303.5	0.41	0.05	8.33E4	3.40	7.84	0.93 ±8%
14	1.13	51.18	40,990	302.9	0.34	0.04	7.31E4	1.90	10.28	0.90 ±10%

Run number 119 Sample type: tubes L/D = 150

356.3 mm long 2.375 mm diameter Entrance loss = 1.5 helium 82 Hz

Point	Xp (mm)	P (bar)	Re max	Re w	Ar	Mach#	ΔP (Pa)	pV (W)	Euler#	TDF
1	1.58	16.41	19,640	98.5	0.33	0.06	4.06E4	2.48	8.13	0.76 ±8%
2	2.50	16.65	30,150	97.5	0.52	0.09	7.68E4	10.48	6.39	0.93 ±9%
3	3.45	16.63	39,540	94.9	0.69	0.12	1.02E5	25.27	4.75	1.00 ±10%
4	1.22	33.80	30,460	197.5	0.26	0.05	6.76E4	2.58	11.17	0.91 ±10%
5	1.65	33.89	40,940	197.7	0.35	0.06	9.49E4	6.31	8.67	0.98 ±8%
6	0.51	51.23	19,490	297.2	0.11	0.02	4.12E4	0.28	24.93	0.78 ±19%
8	1.07	51.09	40,280	298.4	0.22	0.04	8.81E4	2.60	12.58	0.96 ±10%

Run number 114 Stacked Screens Correlation used: See Table 7.2-1

12.7 mm long 68.0 % porous Wire diameter (μm) 41 helium 90 Hz

Point	Xp (mm)	P (bar)	Re max	Re w	Ar	Mach#	ΔP (Pa)	pV (W)	Euler#	TDF
2	1.06	16.81	10.6	0.15	0.12	8.7E-4	2.23E3	0.19	2097	1.44 ±27%
3	1.83	16.82	18.3	0.15	0.21	1.5E-3	4.20E3	0.62	1310	1.19 ±15%
4	2.11	17.25	21.5	0.15	0.24	1.7E-3	4.99E3	0.85	1151	1.14 ±13%
5	3.04	17.33	31.0	0.15	0.35	2.5E-3	8.33E3	1.94	922	1.04 ±8%
6	4.44	17.99	46.7	0.15	0.51	3.6E-3	1.40E4	4.68	703	0.97 ±6%
7	5.26	18.04	55.3	0.15	0.61	4.3E-3	1.78E4	7.01	636	0.95 ±5%
8	0.98	34.44	19.8	0.29	0.11	8.1E-4	2.31E3	0.18	1236	1.17 ±27%
9	2.04	34.63	41.3	0.30	0.24	1.7E-3	6.22E3	0.96	770	1.00 ±11%
10	2.48	34.97	50.5	0.30	0.29	2.0E-3	8.23E3	1.53	681	0.97 ±9%
11	3.07	35.34	63.0	0.30	0.36	2.5E-3	1.12E4	2.56	600	0.95 ±7%
12	3.42	35.53	70.2	0.30	0.40	2.8E-3	1.31E4	3.33	564	0.94 ±6%
13	5.08	35.91	105.2	0.30	0.59	4.2E-3	2.37E4	8.84	460	0.93 ±4%
14	6.12	36.53	128.4	0.31	0.71	5.0E-3	3.19E4	14.29	419	0.94 ±3%
15	1.31	53.32	40.0	0.45	0.15	1.1E-3	3.76E3	0.40	740	1.00 ±17%
16	2.05	53.15	62.6	0.45	0.24	1.7E-3	7.51E3	1.14	605	0.95 ±10%
17	2.69	53.44	82.2	0.45	0.31	2.2E-3	1.13E4	2.23	525	0.94 ±7%
18	3.24	53.88	99.0	0.45	0.38	2.6E-3	1.48E4	3.55	475	0.94 ±5%
19	4.18	54.40	128.5	0.45	0.48	3.4E-3	2.21E4	6.73	422	0.94 ±4%
21	6.10	55.64	190.8	0.46	0.71	5.0E-3	4.04E4	17.85	356	0.96 ±3%

Run number 116 Stacked Screens Correlation used: See Table 7.2-1

12.7 mm long 68.0 % porous Wire diameter (μm) 41 nitrogen 90 Hz

Point	Xp (mm)	P (bar)	Re max	Re w	Ar	Mach#	ΔP (Pa)	pV (W)	Euler#	TDF
1	1.01	2.17	10.1	0.15	0.12	2.4E-3	1.86E3	0.15	2194	1.47 ±39%
2	2.03	2.22	20.4	0.15	0.23	4.7E-3	4.07E3	0.65	1181	1.13 ±26%
3	3.08	2.26	31.1	0.15	0.35	7.1E-3	6.65E3	1.61	838	1.00 ±23%
4	4.16	2.33	42.6	0.15	0.47	9.5E-3	1.00E4	3.16	682	0.93 ±21%
5	5.00	2.39	51.9	0.16	0.56	1.1E-2	1.28E4	4.81	592	0.89 ±21%
6	1.07	4.74	22.8	0.31	0.12	2.5E-3	2.37E3	0.20	1126	1.14 ±28%
7	1.93	4.76	41.0	0.31	0.22	4.5E-3	4.97E3	0.77	729	1.00 ±16%
8	2.80	4.82	59.5	0.31	0.32	6.5E-3	8.61E3	1.81	602	0.95 ±13%
9	3.68	4.95	79.8	0.32	0.42	8.5E-3	1.26E4	3.47	503	0.91 ±11%
10	4.70	5.08	102.5	0.32	0.54	1.1E-2	1.80E4	6.27	435	0.89 ±11%
11	5.68	5.25	126.8	0.33	0.65	1.3E-2	2.34E4	10.01	378	0.88 ±11%
12	6.31	5.25	140.3	0.33	0.72	1.4E-2	2.70E4	12.76	356	0.87 ±11%
13	0.96	6.98	30.2	0.46	0.11	2.3E-3	2.31E3	0.18	922	1.08 ±28%
14	1.95	7.11	61.9	0.47	0.23	4.6E-3	6.34E3	0.93	610	0.97 ±13%
15	2.89	7.12	91.0	0.46	0.33	6.7E-3	1.11E4	2.37	490	0.94 ±10%
16	3.69	7.31	118.2	0.47	0.42	8.5E-3	1.59E4	4.35	423	0.93 ±9%
17	4.86	7.58	156.8	0.48	0.56	1.1E-2	2.38E4	8.65	361	0.92 ±8%
18	6.31	8.01	212.0	0.50	0.72	1.4E-2	3.63E4	16.79	313	0.92 ±8%
19	6.49	8.03	218.0	0.50	0.74	1.5E-2	3.79E4	17.98	308	0.92 ±8%
20	3.74	8.02	125.6	0.50	0.43	8.6E-3	1.74E4	4.74	422	0.94 ±8%

Run number 122 Metex Knit Wire Correlation used: See Table 7.2-1

12.7 mm long 80.0 % porous Wire diameter (μm) 89 helium 90 Hz

Point	Xp (mm)	P (bar)	Re max	Re w	Ar	Mach#	ΔP (Pa)	pV (W)	Euler#	TDF
7	4.52	17.42	157.0	2.47	0.45	3.1E-3	1.48E3	0.53	104	0.99 ±38%
8	5.26	17.88	184.3	2.49	0.52	3.6E-3	1.90E3	0.80	97	0.98 ±30%
9	5.30	18.30	188.7	2.53	0.52	3.7E-3	1.93E3	0.82	95	0.98 ±29%
10	5.88	18.22	206.8	2.50	0.58	4.0E-3	2.28E3	1.08	92	0.98 ±25%
11	6.52	18.18	226.8	2.47	0.64	4.5E-3	2.70E3	1.41	90	0.98 ±21%
12	7.25	18.24	251.2	2.46	0.71	5.0E-3	3.63E3	1.87	98	0.99 ±18%
15	3.01	36.34	213.2	5.03	0.30	2.1E-3	1.18E3	0.28	91	0.96 ±48%
16	3.43	36.30	240.6	4.99	0.34	2.4E-3	1.45E3	0.39	87	0.97 ±39%
17	4.37	36.42	308.2	5.01	0.43	3.0E-3	2.16E3	0.75	79	0.97 ±26%
18	5.32	36.64	376.6	5.03	0.52	3.7E-3	3.40E3	1.27	84	0.98 ±19%
19	6.31	36.53	444.2	5.00	0.62	4.3E-3	4.57E3	2.03	80	1.00 ±14%

Run number 123 Metex Knit Wire Correlation used: See Table 7.2-1

12.7 mm long 80.0 % porous Wire diameter (μm) 89 helium 90 Hz

Point	Xp (mm)	P (bar)	Re max	Re w	Ar	Mach#	ΔP (Pa)	pV (W)	Euler#	TDF
3	2.76	52.83	285.5	7.36	0.27	1.9E-3	1.30E3	0.28	82	0.96 ±44%
4	3.59	52.88	371.1	7.35	0.35	2.5E-3	2.00E3	0.57	74	0.97 ±28%
5	4.55	53.68	475.8	7.43	0.45	3.1E-3	3.40E3	1.08	78	0.99 ±19%
6	5.48	53.63	572.3	7.42	0.54	3.8E-3	4.70E3	1.80	74	1.01 ±14%
7	6.04	53.77	629.2	7.40	0.60	4.2E-3	5.55E3	2.39	72	1.04 ±11%

Run number 124 Brunswick Felt Metal Correlation used: See Table 7.2-1

12.85 mm long 84.0 % porous Wire diameter (μm) 13 helium 90 Hz

Point	Xp (mm)	P (bar)	Re max	Re w	Ar	Mach#	ΔP (Pa)	pV (W)	Euler#	TDF
1	0.97	16.77	6.1	0.09	0.09	6.5E-4	5.43E3	0.43	9184	1.29 ±16%
2	1.45	16.74	9.0	0.09	0.13	9.7E-4	8.28E3	0.96	6375	1.16 ±11%
3	2.41	17.68	15.5	0.09	0.22	1.6E-3	1.50E4	2.83	4000	1.01 ±7%
4	2.97	18.49	19.7	0.09	0.27	2.0E-3	1.93E4	4.46	3262	0.96 ±6%
5	4.30	19.69	29.9	0.10	0.40	2.8E-3	3.05E4	10.11	2327	0.89 ±5%
6	5.44	21.21	39.9	0.10	0.50	3.6E-3	4.15E4	17.26	1861	0.85 ±4%
7	6.62	22.85	51.8	0.11	0.61	4.3E-3	5.39E4	27.34	1527	0.83 ±4%
8	7.70	24.99	64.3	0.12	0.71	5.0E-3	6.79E4	39.73	1317	0.82 ±4%
9	8.03	25.11	66.7	0.12	0.74	5.2E-3	7.15E4	43.79	1277	0.81 ±4%
10	1.48	34.91	18.4	0.17	0.14	9.8E-4	9.56E3	1.14	3436	1.00 ±10%
11	1.39	34.78	17.1	0.17	0.13	9.2E-4	8.80E3	0.98	3627	1.00 ±10%
12	2.92	35.69	36.6	0.18	0.27	1.9E-3	2.27E4	5.07	2085	0.90 ±5%
13	3.54	36.56	45.1	0.18	0.33	2.3E-3	2.94E4	7.90	1799	0.89 ±4%
14	3.99	38.52	53.7	0.19	0.37	2.6E-3	3.52E4	10.59	1604	0.88 ±4%
15	4.97	40.35	69.2	0.19	0.46	3.3E-3	4.81E4	17.91	1356	0.87 ±3%
16	5.96	42.64	87.1	0.20	0.55	3.9E-3	6.27E4	27.92	1169	0.87 ±3%
17	6.74	44.52	101.3	0.21	0.62	4.4E-3	7.53E4	37.97	1061	0.87 ±3%
18	7.56	46.77	118.7	0.22	0.70	4.9E-3	8.92E4	50.87	953	0.88 ±3%

Run number 125 Brunswick Felt Metal Correlation used: See Table 7.2-1

12.85 mm long 84.0 % porous Wire diameter (μm) 13 helium 90 Hz

Point	Xp (mm)	P (bar)	Re max	Re w	Ar	Mach#	ΔP (Pa)	pV (W)	Euler#	TDF
1	1.11	54.18	21.0	0.27	0.10	7.3E-4	7.33E3	0.65	3067	0.97 ±12%
2	2.60	55.92	50.6	0.27	0.24	1.7E-3	2.29E4	4.49	1691	0.89 ±5%
3	3.19	57.12	62.7	0.28	0.30	2.1E-3	3.02E4	7.27	1469	0.89 ±4%
4	4.05	58.74	81.7	0.28	0.38	2.6E-3	4.24E4	12.98	1239	0.90 ±3%
5	5.06	61.22	105.3	0.29	0.47	3.3E-3	5.87E4	22.45	1063	0.91 ±3%
6	6.08	64.11	131.7	0.30	0.56	4.0E-3	7.84E4	35.84	940	0.93 ±3%
7	6.77	66.98	151.6	0.31	0.63	4.4E-3	9.30E4	47.19	869	0.93 ±3%

Run number 126 Stacked Screens Correlation used: See Table 7.2-1

25.4 mm long 66.5 % porous Wire diameter (μm) 191 helium 90 Hz

Point	Xp (mm)	P (bar)	Re max	Re w	Ar	Mach#	ΔP (Pa)	pV (W)	Euler#	TDF
3	2.59	17.50	116.7	2.83	0.15	2.2E-3	1.76E3	0.36	257	0.92 ±33%
4	3.62	17.63	162.8	2.83	0.21	3.0E-3	2.95E3	0.85	221	0.88 ±20%
5	4.19	17.70	188.4	2.82	0.25	3.5E-3	4.16E3	1.26	232	0.87 ±15%
6	5.08	18.07	231.5	2.86	0.30	4.2E-3	5.78E3	2.09	216	0.85 ±11%
7	6.34	18.31	289.0	2.86	0.38	5.3E-3	8.42E3	3.80	200	0.84 ±8%
8	7.19	18.36	326.5	2.85	0.43	5.9E-3	1.04E4	5.32	193	0.84 ±7%
9	7.92	18.60	359.3	2.85	0.47	6.5E-3	1.24E4	6.94	189	0.84 ±6%
11	2.05	35.70	185.0	5.66	0.12	1.7E-3	1.81E3	0.30	209	0.86 ±32%
12	3.43	36.06	308.8	5.66	0.20	2.8E-3	4.75E3	1.15	196	0.83 ±14%
13	4.33	36.13	390.5	5.66	0.26	3.6E-3	7.09E3	2.16	183	0.83 ±9%
14	5.23	36.45	474.5	5.70	0.31	4.3E-3	9.89E3	3.62	174	0.83 ±7%
15	6.09	36.57	553.2	5.70	0.36	5.0E-3	1.30E4	5.53	168	0.84 ±5%
16	7.06	37.24	647.2	5.76	0.42	5.8E-3	1.69E4	8.37	161	0.84 ±4%
17	8.15	37.31	747.7	5.76	0.48	6.7E-3	2.19E4	12.50	156	0.85 ±4%

Run number 127 Stacked Screens Correlation used: See Table 7.2-1

25.4 mm long 66.5 % porous Wire diameter (μm) 191 helium 90 Hz

Point	Xp (mm)	P (bar)	Re max	Re w	Ar	Mach#	ΔP (Pa)	pV (W)	Euler#	TDF
2	1.88	54.02	252.9	8.46	0.11	1.6E-3	2.02E3	0.30	186	0.83 ±29%
3	3.35	54.37	452.7	8.48	0.20	2.8E-3	6.10E3	1.43	175	0.83 ±11%
4	4.34	54.43	586.2	8.48	0.26	3.6E-3	9.62E3	2.91	165	0.84 ±7%
5	5.16	54.57	696.1	8.47	0.31	4.3E-3	1.31E4	4.70	159	0.85 ±5%
6	6.45	54.62	867.6	8.45	0.38	5.3E-3	1.96E4	8.76	153	0.86 ±4%

Run number 130 Stacked Screens Correlation used: See Table 7.2-1

12.7 mm long 66.3 % porous Wire diameter (μm) 94 helium 90 Hz

Point	Xp (mm)	P (bar)	Re max	Re w	Ar	Mach#	ΔP (Pa)	pV (W)	Euler#	TDF
2	1.96	17.74	43.1	0.67	0.23	1.6E-3	1.46E3	0.23	371	0.96 ±39%
3	3.05	17.69	66.5	0.67	0.36	2.5E-3	2.72E3	0.67	286	0.89 ±21%
4	4.26	18.35	95.6	0.69	0.51	3.5E-3	4.91E3	1.53	257	0.84 ±13%
5	5.03	18.23	111.5	0.68	0.60	4.2E-3	6.32E3	2.32	240	0.83 ±10%
6	5.79	18.33	128.4	0.68	0.69	4.8E-3	7.90E3	3.32	225	0.83 ±8%
7	6.48	18.77	145.5	0.69	0.77	5.4E-3	9.53E3	4.46	213	0.82 ±7%
8	7.05	19.01	157.1	0.68	0.84	5.8E-3	1.09E4	5.57	206	0.82 ±6%
9	7.60	19.46	170.5	0.69	0.90	6.2E-3	1.22E4	6.92	196	0.83 ±6%
12	3.95	36.95	174.7	1.35	0.47	3.3E-3	6.46E3	1.83	198	0.81 ±10%
13	4.92	37.28	217.9	1.36	0.59	4.1E-3	9.29E3	3.27	182	0.82 ±7%
14	5.66	37.76	251.2	1.36	0.67	4.6E-3	1.17E4	4.76	173	0.83 ±6%
15	6.98	38.27	310.3	1.36	0.83	5.7E-3	1.69E4	8.41	163	0.84 ±4%
17	2.02	55.44	133.4	2.02	0.24	1.7E-3	2.52E3	0.41	197	0.81 ±23%
18	3.74	55.68	247.0	2.02	0.44	3.1E-3	7.67E3	2.04	174	0.82 ±9%
19	5.27	57.23	352.1	2.05	0.63	4.3E-3	1.39E4	5.16	156	0.84 ±5%
20	6.91	57.63	459.8	2.04	0.82	5.6E-3	2.19E4	10.80	144	0.87 ±3%

Run number 131 Stacked Screens Correlation used: See Table 7.2-1

12.7 mm long 66.5 % porous Wire diameter (μm) 53 helium 90 Hz

Point	Xp (mm)	P (bar)	Re max	Re w	Ar	Mach#	ΔP (Pa)	pV (W)	Euler#	TDF
3	1.29	17.28	16.0	0.22	0.15	1.1E-3	2.47E3	0.26	1483	1.31 ±25%
4	1.92	17.53	23.8	0.22	0.23	1.6E-3	3.98E3	0.61	1077	1.15 ±15%
5	2.89	17.77	35.9	0.22	0.34	2.4E-3	7.17E3	1.57	846	1.04 ±10%
6	4.47	18.18	55.7	0.22	0.53	3.7E-3	1.31E4	4.41	641	0.96 ±6%
7	5.47	18.24	67.3	0.22	0.65	4.5E-3	1.75E4	7.15	575	0.94 ±5%
8	6.12	18.58	75.6	0.22	0.72	5.0E-3	2.08E4	9.43	539	0.93 ±4%
9	6.53	18.92	81.2	0.22	0.77	5.3E-3	2.31E4	11.14	520	0.92 ±4%
10	1.19	35.22	29.7	0.44	0.14	9.9E-4	2.63E3	0.25	911	1.09 ±23%
11	1.15	35.16	28.6	0.44	0.14	9.6E-4	2.51E3	0.23	939	1.10 ±24%
12	1.82	35.34	45.0	0.43	0.22	1.5E-3	4.62E3	0.68	690	1.00 ±14%
13	3.02	35.88	74.7	0.43	0.36	2.5E-3	1.03E4	2.29	555	0.94 ±7%
14	4.27	36.34	105.5	0.43	0.51	3.5E-3	1.74E4	5.42	467	0.93 ±5%
15	5.17	37.06	127.9	0.44	0.61	4.2E-3	2.36E4	8.83	428	0.93 ±4%
16	6.36	37.23	157.9	0.44	0.75	5.2E-3	3.21E4	14.96	383	0.93 ±3%
17	6.25	37.32	154.9	0.44	0.74	5.1E-3	3.12E4	14.28	386	0.93 ±3%
18	7.63	37.57	189.5	0.44	0.91	6.2E-3	4.33E4	23.88	358	0.93 ±3%

Run number 132 Stacked Screens Correlation used: See Table 7.2-1

12.7 mm long 66.5 % porous Wire diameter (μm) 53 helium 90 Hz

Point	Xp (mm)	P (bar)	Re max	Re w	Ar	Mach#	ΔP (Pa)	pV (W)	Euler#	TDF
1	0.75	53.99	27.9	0.65	0.09	6.2E-4	1.65E3	0.10	953	1.10 ±37%
2	0.73	54.05	27.1	0.65	0.09	6.0E-4	1.59E3	0.09	973	1.11 ±39%
3	1.65	54.60	61.3	0.65	0.20	1.4E-3	5.17E3	0.63	617	0.96 ±14%
4	2.74	55.55	101.6	0.65	0.32	2.2E-3	1.11E4	2.21	477	0.93 ±7%
5	3.87	56.76	143.8	0.65	0.46	3.1E-3	1.91E4	5.37	409	0.94 ±4%
6	4.80	57.14	177.8	0.65	0.57	3.9E-3	2.70E4	9.38	376	0.95 ±3%
7	6.23	58.24	232.4	0.66	0.74	5.0E-3	4.07E4	18.62	332	0.97 ±3%

Run number 133 Stacked Screens Correlation used: See Table 7.2-1

25.4 mm long 66.3 % porous Wire diameter (μm) 94 helium 90 Hz

Point	Xp (mm)	P (bar)	Re max	Re w	Ar	Mach#	ΔP (Pa)	pV (W)	Euler#	TDF
1	1.12	17.39	24.2	0.66	0.07	9.4E-4	1.62E3	0.15	1277	1.31 ±36%
2	1.67	18.06	36.3	0.66	0.10	1.4E-3	2.79E3	0.38	972	1.18 ±21%
3	1.75	18.58	38.5	0.67	0.10	1.4E-3	2.98E3	0.42	934	1.16 ±20%
4	2.30	18.49	49.9	0.66	0.14	1.9E-3	4.79E3	0.81	873	1.10 ±14%
5	2.92	18.78	63.3	0.66	0.17	2.4E-3	6.82E3	1.46	768	1.07 ±10%
6	3.60	19.06	78.0	0.66	0.21	2.9E-3	9.40E3	2.47	691	1.04 ±8%
7	4.22	19.30	90.9	0.66	0.25	3.4E-3	1.21E4	3.71	646	1.03 ±6%
8	5.01	19.61	108.0	0.66	0.29	4.0E-3	1.57E4	5.72	591	1.01 ±5%
9	5.92	20.11	128.5	0.67	0.35	4.7E-3	2.06E4	8.81	549	1.00 ±5%
10	6.01	20.27	130.2	0.66	0.35	4.8E-3	2.12E4	9.19	546	1.00 ±5%
11	1.07	38.01	46.8	1.34	0.06	8.7E-4	1.92E3	0.16	799	1.07 ±31%
13	1.40	38.07	61.0	1.34	0.08	1.1E-3	2.81E3	0.32	684	1.02 ±22%
14	2.50	38.31	109.1	1.33	0.15	2.0E-3	7.35E3	1.34	557	0.96 ±10%
15	3.47	38.68	149.6	1.32	0.20	2.8E-3	1.24E4	3.12	490	0.95 ±6%
16	4.37	39.70	188.9	1.32	0.26	3.5E-3	1.83E4	5.70	449	0.95 ±5%
17	4.98	40.40	215.3	1.33	0.29	4.0E-3	2.24E4	8.08	421	0.95 ±4%
18	5.73	41.59	249.6	1.34	0.34	4.6E-3	2.90E4	11.83	405	0.96 ±3%
19	6.67	41.73	289.9	1.33	0.39	5.3E-3	3.72E4	17.64	384	0.96 ±3%
20	7.23	42.18	315.0	1.34	0.42	5.7E-3	4.26E4	21.80	371	0.96 ±3%

Run number 134 Stacked Screens Correlation used: See Table 7.2-1

25.4 mm long 66.3 % porous Wire diameter (μm) 94 helium 90 Hz

Point	Xp (mm)	P (bar)	Re max	Re w	Ar	Mach#	ΔP (Pa)	pV (W)	Euler#	TDF
1	1.27	52.64	82.3	1.99	0.07	1.1E-3	2.74E3	0.28	563	0.95 ±22%
2	2.03	53.02	132.0	1.99	0.12	1.7E-3	6.30E3	0.92	500	0.92 ±11%
3	2.90	53.76	187.0	1.98	0.17	2.4E-3	1.12E4	2.32	435	0.92 ±7%
4	3.92	55.92	253.1	1.98	0.23	3.2E-3	1.91E4	5.22	400	0.93 ±5%
5	5.06	57.52	329.5	1.99	0.30	4.1E-3	2.92E4	10.38	361	0.94 ±3%
6	6.07	58.10	394.7	1.99	0.36	4.9E-3	3.97E4	17.03	340	0.96 ±3%
7	6.55	58.52	425.6	1.99	0.38	5.3E-3	4.40E4	21.10	323	0.98 ±3%

Run number 135 Sintered Screens Correlation used: See Table 7.2-1

25.7 mm long 61.4 % porous Wire diameter (μm) 41 helium 90 Hz

Point	Xp (mm)	P (bar)	Re max	Re w	Ar	Mach#	ΔP (Pa)	pV (W)	Euler#	TDF
1	1.44	18.08	10.9	0.08	0.08	1.2E-3	1.08E4	1.17	5300	1.00 ±11%
2	2.34	18.14	17.4	0.08	0.13	1.9E-3	1.83E4	3.33	3433	0.92 ±8%
3	2.75	18.80	20.3	0.08	0.16	2.2E-3	2.27E4	4.81	3043	0.91 ±8%
4	3.13	19.16	22.8	0.08	0.18	2.5E-3	2.66E4	6.39	2758	0.89 ±7%
5	4.21	19.39	30.6	0.08	0.24	3.3E-3	3.92E4	12.45	2238	0.86 ±7%
6	4.79	19.93	35.1	0.08	0.27	3.7E-3	4.61E4	16.73	2003	0.85 ±7%
7	5.62	20.18	41.0	0.08	0.32	4.3E-3	5.65E4	24.01	1786	0.84 ±7%
8	6.05	20.82	44.5	0.08	0.34	4.6E-3	6.15E4	28.66	1646	0.84 ±7%
9	6.92	20.90	50.1	0.08	0.39	5.3E-3	7.27E4	38.70	1498	0.82 ±7%
10	1.52	37.54	22.0	0.16	0.09	1.2E-3	1.37E4	1.54	3012	0.91 ±9%
11	3.07	38.44	44.9	0.16	0.18	2.4E-3	3.38E4	7.72	1805	0.89 ±5%
12	3.66	38.94	53.1	0.16	0.21	2.9E-3	4.32E4	11.75	1627	0.90 ±5%
13	4.71	39.97	68.4	0.16	0.27	3.7E-3	6.17E4	21.60	1385	0.91 ±5%
15	1.44	57.42	31.7	0.24	0.08	1.1E-3	1.46E4	1.53	2347	0.89 ±9%
16	3.04	57.52	66.4	0.24	0.17	2.4E-3	3.97E4	8.87	1445	0.92 ±5%
17	4.03	59.35	88.0	0.24	0.23	3.1E-3	6.05E4	17.81	1240	0.95 ±4%
18	5.23	60.51	112.9	0.24	0.30	4.0E-3	8.89E4	33.92	1082	0.98 ±4%

Run number 136 Sintered Screens Correlation used: See Equation 6.1-7

22.23 mm long 60.6 % porous Wire diameter (μm) 53 helium 90 Hz

Point	Xp (mm)	P (bar)	Re max	Re w	Ar	Mach#	ΔP (Pa)	pV (W)	Euler#	TDF
1	1.11	17.48	10.6	0.13	0.08	9.2E-4	3.27E3	0.29	2636	0.59 ±20%
2	1.90	18.12	18.5	0.13	0.13	1.6E-3	6.14E3	0.94	1650	0.67 ±11%
3	2.65	18.11	25.6	0.13	0.18	2.2E-3	9.79E3	1.98	1358	0.71 ±8%
4	3.62	18.14	34.5	0.13	0.25	3.0E-3	1.49E4	4.08	1118	0.74 ±6%
5	4.41	18.66	42.4	0.13	0.30	3.6E-3	1.98E4	6.53	983	0.75 ±5%
6	4.87	18.98	46.9	0.13	0.33	4.0E-3	2.31E4	8.34	934	0.76 ±5%
7	5.60	19.19	54.0	0.13	0.38	4.5E-3	2.91E4	11.76	884	0.77 ±5%
8	5.80	19.28	55.3	0.13	0.39	4.7E-3	3.10E4	12.89	883	0.78 ±5%
9	7.58	19.87	72.6	0.13	0.51	6.1E-3	4.60E4	25.27	758	0.81 ±5%
10	1.24	37.98	24.1	0.26	0.08	1.0E-3	4.57E3	0.46	1409	0.73 ±15%
11	2.21	38.06	42.9	0.26	0.15	1.8E-3	1.04E4	1.71	1010	0.78 ±8%
12	3.43	38.25	65.4	0.26	0.23	2.8E-3	1.93E4	4.88	788	0.80 ±5%
13	4.68	39.70	89.9	0.26	0.32	3.8E-3	3.30E4	10.76	711	0.82 ±4%
14	5.77	40.43	110.7	0.26	0.39	4.6E-3	4.54E4	18.75	639	0.86 ±3%
15	7.25	40.60	138.4	0.26	0.49	5.8E-3	6.50E4	33.28	580	0.86 ±3%
16	1.05	59.73	30.7	0.40	0.07	8.5E-4	4.18E3	0.35	1170	0.75 ±17%
17	3.07	59.65	89.3	0.40	0.21	2.5E-3	2.11E4	4.50	696	0.80 ±5%
18	4.34	59.97	124.6	0.39	0.29	3.5E-3	3.64E4	11.15	607	0.85 ±3%
19	5.74	61.01	164.9	0.39	0.39	4.6E-3	5.79E4	23.53	547	0.88 ±3%

Run number 137 Sintered Screens Correlation used: See Table 7.2-1

22.23 mm long 60.6 % porous Wire diameter (μm) 53 helium 90 Hz

Point	Xp (mm)	P (bar)	Re max	Re w	Ar	Mach#	ΔP (Pa)	pV (W)	Euler#	TDF
1	0.90	18.04	8.6	0.13	0.06	7.4E-4	2.65E3	0.19	3218	1.25 ±25%
2	2.26	18.19	21.8	0.13	0.15	1.9E-3	8.13E3	1.41	1547	0.95 ±9%
3	2.89	18.38	27.8	0.13	0.20	2.4E-3	1.09E4	2.41	1265	0.89 ±7%
4	3.66	18.67	35.2	0.13	0.25	3.0E-3	1.53E4	4.22	1103	0.86 ±6%
5	5.36	20.38	51.0	0.13	0.36	4.3E-3	2.77E4	10.76	905	0.83 ±5%
6	6.37	20.60	60.6	0.13	0.43	5.0E-3	3.60E4	16.46	830	0.83 ±4%
7	7.35	20.88	69.8	0.13	0.50	5.8E-3	4.43E4	23.34	763	0.82 ±4%
8	8.35	21.42	80.6	0.13	0.56	6.5E-3	5.35E4	32.03	701	0.81 ±4%

Run number 138 Sintered Screens Correlation used: See Table 7.2-1

22.23 mm long 60.6 % porous Wire diameter (μm) 53 helium 90 Hz

Point	Xp (mm)	P (bar)	Re max	Re w	Ar	Mach#	ΔP (Pa)	pV (W)	Euler#	TDF
1	0.90	37.91	17.5	0.26	0.06	7.4E-4	2.81E3	0.20	1647	0.94 ±23%
2	1.11	37.73	21.1	0.26	0.08	9.0E-4	3.51E3	0.31	1378	0.87 ±19%
3	1.99	38.39	38.2	0.26	0.14	1.6E-3	7.83E3	1.23	943	0.80 ±9%
4	3.25	38.62	62.3	0.26	0.22	2.6E-3	1.75E4	4.13	786	0.80 ±5%
5	4.68	39.63	89.4	0.26	0.32	3.8E-3	3.22E4	10.50	694	0.83 ±4%
6	5.75	39.94	108.7	0.26	0.39	4.6E-3	4.46E4	17.87	641	0.85 ±3%
7	6.63	40.44	126.1	0.26	0.45	5.3E-3	5.58E4	25.74	598	0.86 ±3%
8	7.58	41.61	144.8	0.26	0.51	6.0E-3	6.78E4	36.47	547	0.86 ±3%
9	1.32	59.55	38.0	0.39	0.09	1.1E-3	4.91E3	0.52	887	0.77 ±14%
10	2.33	59.74	67.3	0.39	0.16	1.9E-3	1.25E4	2.14	721	0.78 ±7%
11	3.71	60.51	106.1	0.39	0.25	3.0E-3	2.95E4	7.24	671	0.83 ±4%
12	5.05	61.51	144.6	0.39	0.34	4.0E-3	4.69E4	16.19	572	0.87 ±3%
13	5.94	62.49	170.6	0.39	0.40	4.7E-3	6.02E4	25.00	526	0.89 ±3%
14	6.66	62.77	190.5	0.39	0.45	5.3E-3	7.19E4	33.68	501	0.90 ±3%
15	7.63	63.41	218.9	0.39	0.52	6.0E-3	9.04E4	48.05	476	0.92 ±3%

Appendix C

Error Calculations for the Steady Flow Rig

Error analysis in the steady flow rig was much simpler than that required in the oscillating flow testing. There were three sources of measurement error: pressure drop, mass flow, and temperature. The calculated value subject to these errors was P_{ratio}. It was defined as

$$P_{ratio} = \frac{\Delta P_{measured}}{\dfrac{\left(f\dfrac{L}{D_h} + K_t\right)\dot{m}^2}{2\rho A^2}}$$

where

f is the Darcy friction factor (a weak function of Re, and thus mass flow),

L, D_h, and A are the length, hydraulic diameter, and flow areas of the sample,

K_t is the entrance/exit loss coefficient,

$\dot{m}$ is the mass flow rate, and

ρ is the density of the gas.

Geometrical errors were considered insignificant, as were errors in density, since that was determined by absolute temperature and pressure, both of which were subject to relatively small errors. That left

$$\left(f\frac{L}{D_h} + K_t\right)\dot{m}^2$$

as the only troublesome term, since errors in friction factor and mass flow are not independent of each other. However, since f is a function of Re with a negative exponent, the errors in f will counteract those in the $\dot{m}^2$ term. The relative error in P_{ratio} then reduces to

$$\mathrm{RSS}\left(\frac{\tilde{\Delta P}}{\Delta P},\ (2+\mathrm{Re\_power})\frac{\tilde{m}}{\dot{m}}\right)$$

where

Re_power is the value of the exponent on the Reynolds number in the friction factor correlation.

Manufacturer's specifications for the pressure transducer indicate that the error is less than 0.5% of the full scale pressure, which is determined by the diaphragm installed in the sensor. Calibrations with the 20 and 50 psi diaphragms confirmed that errors were generally under 0.5%, but the errors associated with the 5 psi diaphragm were higher - about 1.5% of full scale.

Manufacturer's specifications for the Hastings STH-750KGP mass flow sensor state that nonlinearities are less than $\pm$ 2% and that the calibration should be nearly independent of pressure. Inconsistent results in early testing raised some doubt about these, so the flowmeter was sent to NASA Lewis for calibration. NASA provided data at various pressures and mass flows of air and nitrogen, but no data on the repeatability of the measurements. Sunpower used a polynomial curve fit to NASA's data at 3.36 bar air and 18.26 bar nitrogen. The errors while running tests at these conditions were assumed to be $\pm$ the maximum discrepancy between NASA's data and the curve fit plus $\pm$ 0.5% repeatability. Tests were also run using 7 bar air. The calibration used was determined by finding the slopes of the best-fit lines for NASA's data using 3.36 and 18.26 bar air and then using a linear interpolation to 7 bar. The nonlinearity errors were assumed to be $\pm$ 1% for the 7-bar curve, to which was added the 0.5% repeatability error.

APPENDIX D

Appendix D - The Database

Data for the oscillating flow rig were stored in a database created with Reflex® for the Macintosh from Borland International. Two disks hold the oscillating flow data.

Table D.1 shows the structure of the oscillating flow database. Each data point is represented by one record in the file. The files are ASCII text, with fields separated by the tab (ASCII 9) character and records separated by return (ASCII 13) characters. The Fourier Series type is just 15 consecutive fields of the Real type. The first is the mean value, which is sometimes call the zeroth component. Each subsequent pair of fields are the cosine and sine coefficients of successive harmonics. To reconstruct the original signal magnitude at a phase angle θ, use the equation:

$$\text{Value} = \text{mean} + \text{cos1}[\cos(\theta)] + \text{sin1}[\sin(\theta)] + \text{cos2}[\cos(2\theta)] + \ldots + \text{sin7}[\sin(7\theta)]$$

Finally, the values of f_r and f_i are included in the database as variables Ffact_real and Ffact_imag. However, as explained in Section 2, these values are not reasonable due to the inability to determine the proper entrance and exit coefficient and due to the presence of higher harmonics in the measured data.

Table D.1 Structure of the Oscillating Flow Databases

Field	Type	Description [Units in brackets]
Run #	Integer	
Point #	Integer	
Time	Text	Month/Day/Year (two digit numbers)
Fluid	Text	helium or nitrogen
Position_err	Real	Error in the signal from the FLDT in meters
p_mean_err	Real	Error in the signal from the mean pressure transducer (Omega PX621) [Pa]
p_fast_err	Real	Error in the pressure drop transducer signal (Endevco 8510B) [Pa]
Entrance_loss_er	Real	Assumed error in the input entrance loss (usually 0.0, since the entrance loss was taken to be known from the steady flow correlations)
Hfilm_err	Real	Assumed error in the calculated film heat transfer coefficient [$W/m^2/°C$]
Piston_diameter	Real	Diameter of the piston [m]
Volume_mean	Real	Total volume in piston cylinder with piston at its midstroke position [m^3]
Seal_gap	Real	Clearance between piston and cylinder [m]
Seal_length	Real	Mean length of the clearance seal between piston and cylinder [m]
Fin_aspect	Real	For rectangular sample passages, the ratio of channel width to height (defined as ≤ 1)
hfilm	Real	Film heat transfer coefficient between the working fluid and the cylinder wall [$W/m^2/°C$]
cyl_mean_surface	Real	Total surface area exposed to working fluid in cylinder with piston at midstroke [m^2]
Sample_type	Text	Tubes, fins, screens, random, or generic
Length	Real	Length of sample [m]
Flow_area	Real	Cross-sectional flow area of the sample [m^2]
Hydraulic_diameter	Real	Hydraulic diameter of sample, defined as 4*area/perimeter [m]
Porosity	Real	For regenerator samples, the ratio of void volume to volume occupied by regenerator
Entrance_loss	Real	The assumed entrance loss coefficient

Temp_cyl_wall	Real	Temperature measured by thermocouple in cylinder wall [K]
Temp_sample_wall	Real	Measured temperature of sample wall [K]
Omega	Real	The angular velocity of the piston [rad/s]
p_mean	Real	the pressure as measured by the Omega PX-621 [Pa]
p_cos1		
p_sin1		
:	Fourier Series	The pressure wave measured by the Endevco 8510B pressure transducer [Pa]
p_cos7		
p_sin7		
xp_mean		
xp_cos1		
xp_sin1		
:	Fourier Series	The piston position from the FLDT [m]
xp_cos7		
xp_sin7		
Mean _density	Real	From ideal gas law [kg/m^3]
Velocity_ampl	Real	Maximum of the first harmonic of the velocity [m/s]
g_err	Real	Error in the mass flow [kg/m^2/s]
F_err	Real	Error in the shear force per unit volume [N/m^3]
C_osc	Real	Core dissipation factor (CDF)
C_osc_rel_err	Real	Relative error in CDF
Disp	Real	Total dissipation factor (TDF)
Disp_rel_err	Real	Relative error in TDF
Ffact_real	Real	The real component of the oscillating friction factor
Ffact_imag	Real	The imaginary component of the oscillating friction factor
Ffact_rel_err	Real	The relative error in Ffact
Re_max	Real	The Reynolds number at the maximum of the first harmonic of the mass flow
Re_omega	Real	The kinetic Reynolds, or Valensi number
pV_power	Real	The pV power obtained by integrating piston position and pressure over a cycle, calculated by the Turbo Pascal® program pV power [W]
tidal_ampl_ratio	Real	Tidal amplitude ratio

Mach#_peak	Real	Calculated at the maximum of the first harmonic of the mass flow
g_mean		
g_cos1		
g_sin1		
:	Fourier Series	Mass flow rate per unit area [kg/m^2/s]
g_cos7		
g_sin7		
F_mean		
F_cos1		
F_sin1		
:	Fourier Series	Shear force per unit volume in the sample being tested [N/m^3]
F_cos7		
F_sin7		
F_residual_mean		
F_residual_cos1		
F_residual_sin1		
:	Fourier Series	Difference between shear forces calculated from flow test and predicted by steady-state correlations [N/m^3]
F_residual_cos7		
F_residual_sin7		
F_stdypred_mean		
F_stdypred_cos1		
F_stdypred_sin1		
:	Fourier Series	Shear force per unit volume predicted by steady flow correlations at the mass flows in g_series [N/m^3]
F_stdypred_cos7		
F_stdypred_sin7		
DeltaP	Real	Peak pressure drop during the cycle (seven harmonics included), calculated by the program pV power [Pa]

☆U.S. GOVERNMENT PRINTING OFFICE:1990 -748 -158/00224

NASA
National Aeronautics and Space Administration

Report Documentation Page

1. Report No.: NASA CR-182288
2. Government Accession No.:
3. Recipient's Catalog No.:
4. Title and Subtitle: Oscillating Flow Loss Test Results in Stirling Engine Heat Exchangers
5. Report Date: May 1990
6. Performing Organization Code:

7. Author(s): G. Koester, S. Howell, G. Wood, E. Miller and D. Gedeon

8. Performing Organization Report No.: None

9. Performing Organization Name and Address:
Sunpower, Inc.
6 Byard St.
Athens, Ohio 45701

10. Work Unit No.: 586-01-11
11. Contract or Grant No.: NAS3-24879, Phase II SBIR
12. Sponsoring Agency Name and Address:
National Aeronautics and Space Administration
Lewis Research Center
Cleveland, Ohio 44135-3191
13. Type of Report and Period Covered: Contractor Report, Final
14. Sponsoring Agency Code:
15. Supplementary Notes: Project Manager, Lanny Thieme, Power Technology Division, NASA Lewis Research Center.

16. Abstract

ARE PRESENTED

This report presents the results of a test program designed to generate a database of oscillating flow loss information that is applicable to Stirling engine heat exchangers. The tests were performed on heater/cooler tubes of various lengths and entrance/exit configurations, on stacked and sintered screen regenerators of various wire diameters and on Brunswick & Metex random fiber regenerators. The tests results were performed over a range of oscillating flow parameters ~~(i.e., Re_{max}, Re_{ω} and A_r)~~ consistent with Stirling engine heat exchanger experience. The tests were performed on the Sunpower oscillating flow loss rig which is based on a variable stroke and variable frequency linear drive motor. In general, the results are presented by comparing the measured oscillating flow losses to the calculated flow losses. The calculated losses are based on the cycle integration of steady flow friction factors and entrance/exit loss coefficients.

17. Key Words (Suggested by Author(s)):
Stirling engine
Heat exchangers
Heat engine
Regenerators
Oscillating flow

18. Distribution Statement:
Date for general release May 1992.
Subject Category 20

19. Security Classif. (of this report)	20. Security Classif. (of this page)	21. No. of pages	22. Price*
Unclassified	Unclassified	296	A13